Neutrinos, cosmological phase transitions and the matter-antimatter asymmetry of the Universe

Rémi Faure

université
PARIS-SACLAY

Neutrinos, cosmological phase transitions and the matter-antimatter asymmetry of the Universe

Neutrinos, transitions de phase cosmologiques et asymétrie matière-antimatière de l'Univers

Thèse de doctorat de l'université Paris-Saclay

École doctorale n° 564, Physique en Île-de-France, EDPIF
Spécialité de doctorat : Physique
Graduate School : Physique. Référent : Faculté des Sciences d'Orsay

Thèse préparée à l'**Institut de Physique Théorique (CEA, Saclay)**, sous la direction de **Philippe BRAX**, Chargé de recherche, Institut de Physique Théorique (CEA, Saclay), et le co-encadrement de **Stéphane LAVIGNAC**, Directeur de recherche (CNRS), Institut de Physique Théorique (CEA, Saclay)

Thèse soutenue à Paris-Saclay, le 27 septembre 2024, par

Rémi FAURE

Composition du Jury

Membres du jury avec voix délibérative

Asmâa ABADA Professeure des universités, IJCLab, Université Paris-Saclay	Présidente
Thomas HAMBYE Directeur de recherche, Université libre de Bruxelles	Rapporteur & Examinateur
Pilar HERNANDEZ Professeure, Instituto de Física Corpuscular, València	Rapportrice & Examinatrice
Sacha DAVIDSON Directrice de recherche, LUPM, Université de Montpellier	Examinatrice
Aldo DEANDREA Professeur des universités, IP2I, Université Claude Bernard, Lyon	Examinateur

THESE DE DOCTORAT

NNT : 2024UPASP081

université PARIS-SACLAY

ÉCOLE DOCTORALE
Physique en Île-de-France (PIF)

Titre : Neutrinos, transitions de phase cosmologiques et asymétrie matière-antimatière de l'Univers

Mots clés : Neutrinos stériles, transitions de phase cosmologiques, leptogénèse résonante, leptogénèse ARS

Résumé : L'asymétrie entre matière et antimatière est un problème non résolu de la cosmologie. Une approche populaire pour l'expliquer est la leptogénèse avec des neutrinos stériles, qui sont des particules motivées expérimentalement pour expliquer les masses des neutrinos actifs du Modèle Standard. Il est possible d'inclure dans les scénarios de leptogénèse une transition de phase cosmologique qui donne leur masse aux neutrinos stériles. Cette idée est intéressante phénoménologiquement, car une transition de phase produit des ondes gravitationnelles pouvant être détectées.

À la température de la transition de phase T, les neutrinos stériles obtiennent une masse M. Deux mécanismes sont considérés.

Pour des neutrinos stériles non-relativistes M>T déviant de l'équilibre lors de la transition de phase, l'asymétrie leptonique est créée lors de leurs désintégrations. La rapidité de la transition permet d'avoir une population de neutrinos stériles initiale plus importante que dans le cas standard et améliore la création d'asymétrie. L'analyse numérique permet de décrire l'espace des paramètres où la leptogénèse est réussie. Pour des neutrinos stériles relativistes M<T, l'asymétrie est créée, lors de leur production, par des oscillations entre les différentes saveurs stériles. Selon les paramètres, ces oscillations, avec une transition de phase, peuvent être qualitativement différentes du cas standard. Les conditions pour que la transition de phase présente un avantage sont discutées et présentées numériquement et analytiquement.

Title : Neutrinos, cosmological phase transitions and the matter-antimatter asymmetry of the Universe

Keywords : Sterile neutrinos, cosmological phase transitions, resonant leptogenesis, ARS leptogenesis

Abstract : The baryon asymmetry in our Universe is an unsolved problem in cosmology. A popular approach for explaining it is leptogenesis with sterile neutrinos, which are particles motivated in order to explain the masses of active neutrinos in the Standard Model. It is possible to include in these scenarios a cosmological phase transition which gives rise to the sterile neutrino masses. This idea is phenomenologically interesting, as such a phase transition could produce detectable gravitational waves.

At the temperature T of the phase transition, sterile neutrinos acquire a mass M. Two mechanisms are considered.

For non-relativistic sterile neutrinos M>T, deviating from equilibrium due to the phase transition, they will quickly decay and produce a lepton asymmetry. The rapidity of the phase transition allows a larger sterile neutrino population than in usual scenarios and enhances the created asymmetry. Numerical analyses describe the successful regions in parameter space for leptogenesis. For relativistic sterile neutrinos M<T, the asymmetry is created by flavor oscillations in the sterile sector, as sterile neutrinos are being produced. Depending on the parameters, these oscillations, in the context of a phase transition, can be qualitatively different from the standard case. We discuss the parameter space where the phase transition presents an advantage, both analytically and numerically.

Remerciements

Je lis parfois des thèses où les remerciements commencent par une citation inspirante, poétique, épique ou drôle qui résume l'expérience de la thèse pour son auteur ou autrice. J'ai fait tourner mes méninges pour voir si je pouvais trouver moi aussi une telle citation, ou alors une réplique de film, une parole de chanson, qui décrirait au mieux ce que cette thèse représente pour moi. N'ayant rien trouvé, je me suis dit que c'était peut-être mieux : la façon dont je me sens maintenant n'a rien à voir avec celle des débuts de cette aventure, et ne sera sans doute pas comparable à ce que ressentira mon « moi » du futur qui relira (pour le plaisir, j'en suis sûr) ces quelques 170 pages. Beaucoup de choses ont traversé mon esprit ces trois dernières années, en rapport ou non avec les neutrinos, les transitions de phase et autres asymétries matière-antimatière, mais j'ai vécu là de beaux moments et je suis redevable à de nombreuses personnes pour cela.

A commencer par vous, déjà, lecteur, lectrice (anonyme, ou peut-être se connaît-on ?) que je remercie de prendre le temps de tourner ces pages. Même si l'histoire de l'ouvrage présent peut paraître fade (où sont les rebondissements et les scènes d'actions ?) et compliquée (que veulent dire tous ces symboles qui apparaissent au fil de la narration ?), je trouve déjà fascinant le pouvoir, que détient celui ou celle qui écrit, d'ouvrir des imaginaires à d'autres personnes par le simple intermédiaire d'une feuille de papier ou d'un écran. Merci, en lisant, de participer à cet échange de pensées qui littéralement voyagent à travers le temps et l'espace.

Merci à Stéphane de m'avoir autant échangé de pensées, justement. J'ai appris beaucoup de choses grâce à toi, sur la physique bien sûr, mais pas seulement. J'ai toujours pris plaisir à nos discussions, je savais qu'à chaque fois je sortirai avec une meilleure compréhension (ou une meilleure compréhension de mon incompréhension, ce qui est déjà pas mal) de ce que j'étais en train de faire, en train d'explorer. Merci de t'être rendu disponible, d'avoir descendu les escaliers je ne sais combien de fois pour venir me voir dans mon bureau. Merci pour ton encadrement et ta bienveillance.

Je dois aussi beaucoup aux membres du groupe B, Brando, Raffaele, Patrick, Florian, Gabriele, pour les séminaires et les repas ensemble, à Petter qui a bien plus amélioré son français que moi mon norvégien, à Dimitrios pour le partage de notre bureau et de nos ressentis sur la thèse, aux doctorant.es et postdocs Marcello, Nikola, Pablo, Louis, Emile, Corentin, Marc, Veronica, Duke, Anurag, Natalie, Siggi, Linnea, Maxence, et j'en oublie malheureusement, pour les séminaires pizzas et les sorties. Mention spéciale à Emile pour les super pâtisseries et l'organisation de la vie à l'IPhT en général !

De plus, le laboratoire ne tournerait pas bien rond sans l'équipe de soutien qui sait résoudre nos moindres soucis et égailler nos journées par leur bonne humeur. Merci donc à Laure, Camille, Justine, Laurent, Philippe, Emmanuelle pour votre aide au quotidien, bon courage pour la suite !

En dehors de l'IPhT, les repas de midi sur le plateau de Saclay ont été rendus agréables notamment grâce à Flore, toujours partante pour faire un volley ou m'expliquer plein de choses stylées, avec aussi Enguerrand qui passait par là quelques fois, ou encore Emma dans la dernière année, Maza dans les dernières semaines, bon appétit à vous et on remet ça quand vous voulez !

Aux colocs de Bourg-la-Reine, Marie, Ivan et l'inimitable Hibiscuit, pour m'avoir fait à manger quand je rentrais tard du volley et pour les soirées Phoenix Wright à crier « Objection ! », pour avoir animé les couloirs en courant toute la nuit (bon, j'avoue c'est surtout Hibiscuit ça), pour les chansons et les soirées jeux, pour tout ça, je vous dis merci.

J'ai aussi l'immense plaisir d'être entouré de belles personnes que je suis très heureux d'appeler mes ami.es, que je vois encore et qui viennent de partout. Sur Paris, j'ai pu me greffer aux Castors et aux Bisounours, merci beaucoup pour votre accueil et vos belles sorties. De Lyon, je garde en mémoire certaines de mes plus belles années, que ce soit grâce à la confrérie du bâtiment E, le BDE, la classe Sciences De la Matière, la team IPT, mes colocs, mes nakamas (coucou Kani et Quentin) et toutes les personnes qui rendaient la vie drôle et bienveillante. Mention spéciale à Gauthier et Francis, pour avoir fait des soutenances de thèse du feu de dieu et m'avoir remonté le moral quand j'en avais besoin. De la prépa à Bordeaux, j'ai amassé un bon stock d'anecdotes sur l'internat et les loups-garous (et je crois qu'on faisait des maths parfois), merci à vous pour ces souvenirs, et je suis toujours content de vous voir pour boire un verre ou faire une escape game ! Du lycée des Graves, enfin, je garde la meilleure bande d'ami.es possible, et je demande un tonnerre d'applaudissements pour (*roulements de tambours*) Arthur A, Arthur E-J, Marion, Estelle, Nicolas, Antoine, Swann, Cécile, Juliette, Adrien, Yann, vous êtes mon socle, ma base et j'espère continuer à beaucoup vous voir et rigoler avec vous.

Merci aussi à ma belle-famille, aux Legrand, prénoms : Damien, Martine, Adrien, Guillaume, Marie, Solène, sans oublier Thuy-Thuy et Ivan, et tous les chats (Tatopani aura même vérifié de très près certains codes utilisés dans cette thèse), j'ai adoré vos grandes tablées le dimanche midi, les sorties en bateau, en canoë, en cheval, la liste est sans fin. Pour les vacances et la vie de tous les jours, il y a toujours de belles occasions de se voir.

Je voudrais saluer celles et ceux qui sont là depuis le tout début, la famille proche même si elle n'est pas du sang, les Canales et les Lespinasse, les Fogli et les Wolf, et puis la famille encore plus proche qui me soutient depuis toujours. Merci bien evidemment à ma Mamie pour sa douceur et ses histoires, je pourrais t'écouter sans fin (ça tombe bien que tu sois bavarde !). Merci à mes parents, merci Papa pour m'avoir transmis ton goût des sciences et le plaisir d'apprendre, merci Maman pour ta persévérance et ta droiture dans tout ce que tu fais, merci Théo pour nos délires et pour l'envie que tu mets dans tous les jeux que tu joues ou inventes. C'est grâce à vos médailles que je me motive à avancer et à devenir une meilleure personne.

Je conclurai enfin avec mes actuels colocs, à Montrouge : Reiko d'abord qui réconforte comme personne par ses ronronnements et sa présence dès qu'on passe le pas de la porte. Et bien sûr, merci à toi Solène d'être la personne extraordinaire que tu es, de me faire rire du matin au soir, et de m'avoir encouragé tout le long de ses trois années. On a passé plus d'un huitième de nos

vies ensemble, je n'aurais pas écrit le quart de ce manuscrit sans toi, c'est donc sûrement pour ça que tu es ma moitié et mon double. Merci du fond du cœur pour tout ce qui est derrière nous, et merci d'avance pour la suite.

Allez, bonne lecture à vous !

Résumé étendu en français

L'asymétrie entre matière et antimatière dans notre Univers est un problème non résolu de la cosmologie moderne. Cette constatation d'une asymétrie découle de l'absence d'observation d'antimatière aux grandes échelles, et l'asymétrie se quantifie alors par l'abondance de matière (baryonique). Les différentes observations donnent une contrainte sur le paramètre sans dimension

$$\eta \equiv \frac{n_b}{n_\gamma} \simeq \frac{n_b - \overline{n}_b}{n_\gamma} \ , \tag{1}$$

qui est le ratio de la densité de matière baryonique n_b sur la densité de photons n_γ et qu'on utilise comme estimation de l'asymétrie baryonique, donnée par la différence entre la densité de baryons n_b et d'anti-baryons $\overline{n}_b$. Cette quantité η est mesurée de deux façons, dans le fond diffus cosmologique et dans l'abondance des éléments légers, qui dépendent de ce paramètre. La valeur trouvée est compatible dans les deux cas et vaut, d'après les données du fond diffus cosmologique,

$$\eta = (6.13 \pm 0.04) \times 10^{-10} \ . \tag{2}$$

Une approche populaire pour expliquer ce nombre est appelée la leptogénèse. La leptogénèse est un ensemble de modèles où l'asymétrie n'est pas directement créée entre baryons et anti-baryons, mais d'abord entre leptons et anti-leptons. Cette asymétrie leptonique est ensuite convertie en asymétrie baryonique par les processus de sphalérons du Modèle Standard, qui sont des processus conservant $B-L$ mais violant $B+L$ (avec B le nombre baryonique, L le nombre leptonique). La popularité de la leptogénèse peut se comprendre par le besoin d'expliquer un autre problème de la physique moderne, en physique des particules cette fois, à savoir les oscillations des neutrinos actifs, dans le secteur leptonique. Les neutrinos actifs peuvent notamment acquérir une masse (qu'ils n'ont pas dans le Modèle Standard) grâce au mécanisme dit du "Seesaw" incluant des particules supplémentaires, les neutrinos dits stériles car n'étant soumis à aucune des forces du Modèle Standard. Dans ce cas, ces neutrinos stériles possèdent une masse de Majorana et ont des interactions de Yukawa (qui violent la symétrie Charge-Parité) avec le Modèle Standard. Les neutrinos stériles peuvent alors reproduire l'asymétrie baryonique observée dans l'Univers lors de leur évolution cosmologique. L'espace des paramètres est cependant assez important puisque la leptogénèse peut tout autant fonctionner avec des masses de neutrinos stériles de l'ordre du GeV qu'avec des masses de l'ordre de 10^{12} GeV.

Deux exemples de leptogénèse sont pertinents pour cette thèse. D'un côté, la leptogénèse dite "thermale" dans laquelle les neutrinos stériles (typiquement lourds avec des masses $M \sim 10^{10}$ Gev) initialement à l'équilibre dévient de cet équilibre à cause de l'expansion de l'Univers et de la réduction de température, deviennent instables et tendent à se désintégrer en leptons et particules de Higgs. Les processus de désintégration ont des probabilités différentes pour les leptons et les anti-leptons, ce qui génère l'asymétrie. D'un autre côté, la leptogénèse dite "ARS" (pour Akhmedov, Rubakov et Smirnov) s'intéresse à la production des neutrinos stériles (typiquement légers avec des masses $M \sim 1$ GeV) et à leurs oscillations entre différents états propres de masse alors qu'ils se rapprochent de l'équilibre. Ces oscillations induisent une asymétrie en hélicité chez les neutrinos stériles, qui se convertit en asymétrie leptonique par leurs interactions.

Récemment, des études de leptogénèse avec des neutrinos stériles ont inclus dans leur scénario une transition de phase cosmologique, induite par un champ scalaire, qui donne leur masse aux neutrinos stériles. L'idée peut être motivée théoriquement, dans des théories de grande unification où un champ scalaire non standard interagit avec les neutrinos stériles, comme c'est le cas dans des théories basées sur le groupe $SU(5)$ ou $SO(10)$. Le lagrangien de notre théorie est alors

$$\mathcal{L} = \mathcal{L}_{\rm SM} + \left[\frac{i}{2}\overline{N}_{RI}\partial\!\!\!/ N_{RI} - \frac{1}{2}\lambda_I S\overline{N}_{RI}N^c_{LI} - Y_{Ia}\overline{N}_{RI}\tilde{\phi}^\dagger l_a + \text{h.c.}\right] \tag{3}$$

où N_I sont les neutrinos stériles, l le champ leptonique, ϕ le champ de Higgs et S est le champ scalaire qui subit la transition de phase. Cette idée est intéressante phénoménologiquement, car une transition de phase aurait pu produire des ondes gravitationnelles. Grâce aux détections par les expériences LISA Virgo, l'époque et l'intensité d'une telle transition de phase pourraient être contraintes. Il devient alors intéressant d'étudier une connexion entre leptogénèse et transition de phase, en cherchant des corrélations entre la masse ou les couplages des neutrinos stériles et les propriétés de la transition de phase qui peuvent chacun être contraints indépendamment.

Cette thèse se propose de décrire la leptogénèse lorsqu'une transition de phase est incluse dans le modèle. Nous incluons dans notre étude la dynamique des neutrinos stériles durant la période de la transition de phase. Pour des transitions de phase du premier ordre, que nous considèrerons ici, le changement de vide se fait par l'expansion de bulles de vraie vide, à l'intérieur desquelles la valeur moyenne du champ scalaire, et donc la masse des neutrinos stériles, est non-nulle. Une bonne approximation du profil du mur de ces bulles peut être donnée par

$$v_S(t) = \frac{v_S^0}{2}\left(1 + \tanh\left(\frac{v_w}{L_w}(t - t_{\rm nucl})\right)\right) \ , \ M_I(t) = \lambda_I v_S(t) \ , \tag{4}$$

où v_w est la vitesse du mur, L_w son épaisseur et v_S est la valeur moyenne du champ, nulle en dehors de la bulle, non-nulle égale à v_S^0 à l'intérieur. La nucléation de ces bulles survient à un certain temps donné par $t_{\rm nucl}$, l'âge de l'Univers lorsque la température T_n de nucléation est atteinte. Les bulles grandissent à des vitesses pouvant avoisiner celle de la lumière, pour de fortes transitions de phase, donc nous prendrons $v_w \simeq 1$ (en unités naturelles). L_w dépend des propriétés de la transition de phase ; son estimation peut être compliquée mais est reliée à la température T_n. Cela implique donc que la bulle se propage sur un temps caractéristique $\approx T_n^{-1}$. Cela peut être comparé au temps de Hubble, à température T_n qui caractérise l'expansion de l'Univers $t_n \equiv t_H(T_n) \propto \frac{M_{\rm Pl}}{T_n}T_n^{-1} \gg T_n^{-1}$ pour des températures typiques en leptogénèse qui sont bien plus basses que l'échelle de Planck $M_{\rm Pl} \simeq 1.22 \times 10^{19}$ GeV.

L'étude de ce profil de masse dépendante du temps conduit à des effets supplémentaires dans la dynamique des neutrinos stériles. Notamment, en négligeant pour l'instant ses interactions avec le reste du plasma, les oscillations particule-antiparticule dans le vide du champ de neutrinos stériles conduisent à une production de particules. Cet effet peut être calculé analytiquement, et permet d'obtenir quelle densité d'espace des phases pour les neutrinos stériles est produite après la transition de phase. Sur la Figure 1, on peut estimer cette production dans deux cas

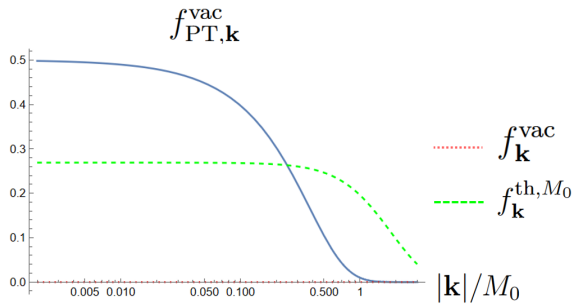

(a) Conditions initiales nulles

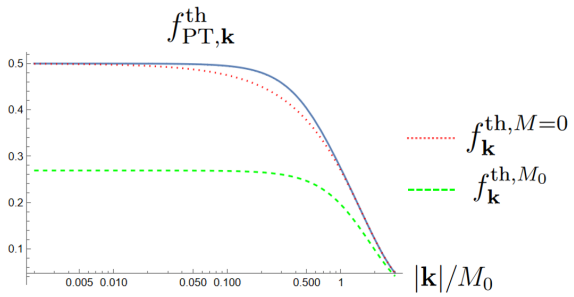

(b) Condition initiale thermique

Figure 1: La distribution $f_{{\rm PT},\mathbf{k}}$ créée lors de la transition de phase est tracée en bleu. On a choisi $M_0 \equiv \lambda v_S^0 = \frac{v_w}{L_w}$, pour simplifier. La distribution initiale est tracée en pointillés rouges, la distribution thermale après la transition de phase en tirets verts.

intéressants physiquement: soit une distribution initiale nulle (Fig. 1a), soit une distribution initiale à l'équilibre thermique (de masse nulle, avant la transition de phase, Fig. 1b). Dans les deux graphiques, on constate que la distribution finale après la transition de phase est plus importante que celle de départ, on a donc bien produit des neutrinos stériles. De plus, cette distribution créée dévie fortement de l'équilibre thermique (de masse non nulle), ce qui est un ingrédient désirable pour la production d'asymétrie leptonique. On note également que cette production lors de la transition de phase existe en l'absence d'interactions.

En ajoutant les interactions, l'étude physique est plus complexe mais peut être approchée en utilisant la théorie des champs hors équilibre. Le formalisme utilisé dans cette thèse est celui dit du "Closed-Time Path", qui considère un contour fermé dans le plan complexe pour la variable temporelle dont dépendent les propagateurs. L'avantage de ce formalisme est de considérer des champs quantiques dont seule la condition initiale est connue, ce qui est nécessaire pour des situations hors d'équilibre. Cela se fait au prix de l'introduction de deux propagateurs, appelés fonctions de Wightmann et notés $S^<$ et $S^>$, au lieu d'un seul. Il est alors possible de dériver des équations, appelées équations de Kadanoff-Baym, pour ces deux propagateurs, avec l'inclusion d'interactions sous la forme d'énergies propres $\Sigma^<$ et $\Sigma^>$. Ces équations sont non-locales en temps et par conséquent seraient très difficiles à résoudre numériquement. Certaines approximations sont donc nécessaires, pour réduire cette complexité numérique.

La principale approximation utilisée dans les travaux de cette thèse est celle dite de la "local approximation" dans laquelle les effets non locaux de la théorie des champs sont contrôlés et la propagation des neutrinos stériles peut être décrite par des équations locales avec une masse explicitement dépendante du temps. Ces équations peuvent alors être résolues numériquement en un temps raisonnable. Cette approximation existait déjà dans la littérature, mais elle est adaptée dans cette thèse au problème de neutrinos stériles lors d'une transition de phase. Nous obtenons alors des équations cinétiques, dépendantes de l'impulsion, pour le secteur des neutrinos stériles, couplés à une asymétrie leptonique. Par la suite, nous nous intéresserons à différents régimes de masse pour les neutrinos stériles, relativistes ou non relativistes, avec un

possible changement de régime durant la dynamique, étant donné que la masse dépend du temps. Il s'avère que l'énergie propre, nécessaire pour calculer les termes d'interactions, ne peut se calculer explicitement pour une masse arbitraire. Ce problème est résolu par un *ansatz*, introduit récemment dans la littérature pour la leptogénèse standard, pour l'énergie propre qui approxime raisonnablement sa valeur pour tous les régimes de masse. Ce point distingue notre approche de précédents travaux avec une transition de phase qui n'étudient qu'un seul régime. L'étude numérique de nos équations a porté sur deux scénarios distincts, correspondant à deux façons différentes de produire l'asymétrie baryonique.

Le premier scénario, nommé "Mass Gain" dans la littérature, s'intéresse à des neutrinos stériles

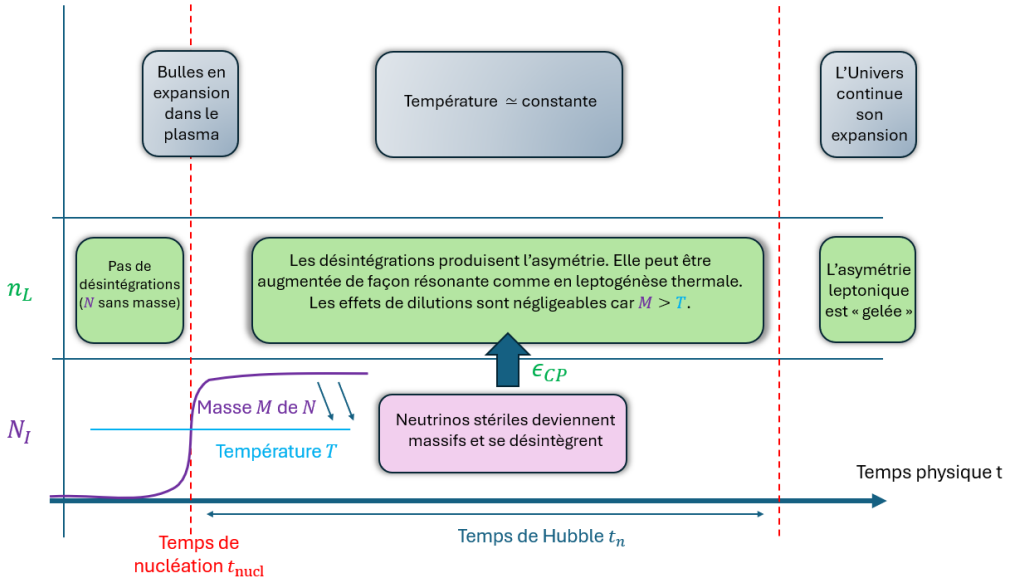

Figure 2: Schéma du scénario "Mass Gain". Le temps de nucléation $t_{\rm nucl}$ correspond à l'âge de l'Univers au moment de la nucléation et l'expansion des bulles. Le temps de Hubble t_n est le temps typique d'expansion de l'Univers, et donc d'évolution de la température.

dont la masse devient très large comparée à la température à la transition de phase ($M > T_n$) et qui ont tendance à se désintégrer rapidement. Une explication schématique de ce scénario est donnée dans la Figure 2. Les désintégrations, comme dans la leptogénèse thermale, produisent une différente quantité de particules que d'antiparticules, conduisant à une asymétrie. L'étude numérique montre que l'asymétrie est efficacement créée pour une masse de neutrino stérile un ordre de grandeur supérieur à la température de la transition de phase, $M > 10\ T_n$. Cela s'explique par le fait que les processus de dilution, tendant à réduire l'asymétrie, sont supprimés par un facteur de Boltzmann $\exp(-M/T_n)$. De plus, la dégénérescence en masse des neutrinos stériles joue un rôle sur la quantité d'asymétrie produite: pour des neutrinos stériles hiérarchiques, leurs masses doivent être suffisamment importantes $M > 10^9$ GeV pour que la leptogénèse fonctionne, tandis que des neutrinos stériles dégénérés autorisent des valeurs plus faibles en masse. Cela s'interprète par une résonance dans l'asymétrie CP $\epsilon_{\rm CP}$ pour les désintégrations. Nous trouvons une excellente corrélation entre l'asymétrie produite et cette asymétrie CP.

Le second scénario considère la création d'une asymétrie lors de la production des neutrinos

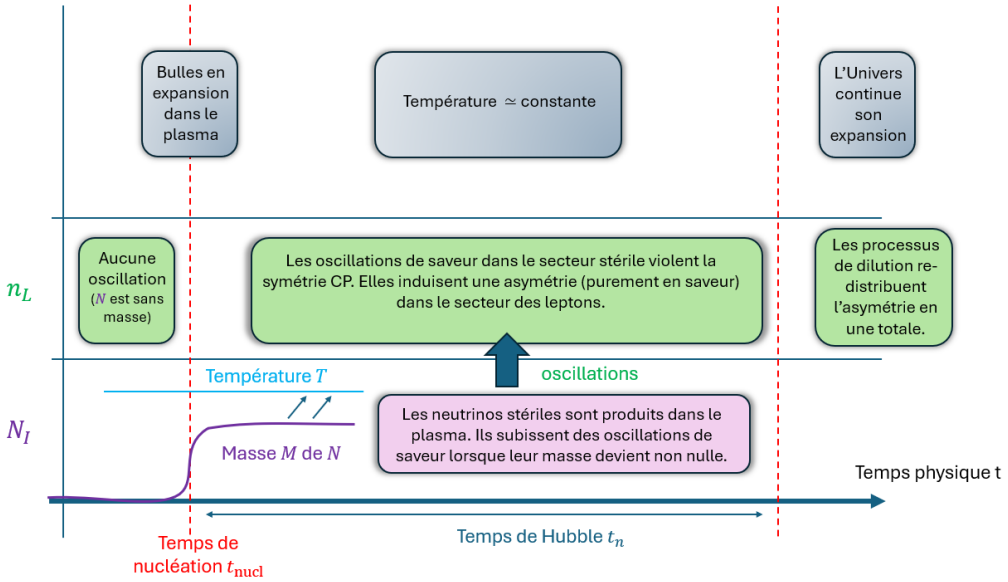

Figure 3: Schéma du scénario "type ARS". Le temps de nucléation $t_{\rm nucl}$ correspond à l'âge de l'Univers au moment de la nucléation et l'expansion des bulles. Le temps de Hubble t_n est le temps typique d'expansion de l'Univers, et donc d'évolution de la température.

stériles qui restent relativistes même après la transition de phase ($M < T_n$). Dans la leptogénèse ARS habituelle, les oscillations entre les différents états propres de masse des neutrinos stériles sont cruciales pour créer une asymétrie. Ces oscillations ne sont possibles qu'en présence d'une masse dans le vide pour les neutrinos stériles; elles sont donc frustrées avant la transition de phase et peuvent se produire très rapidement juste après la transition de phase, quand la masse dans le vide est restaurée. Cela conduit à une asymétrie produite quantitativement différente. Des estimations analytiques peuvent être faites, et reproduisent la dépendance de l'asymétrie produite en les paramètres. La leptogénèse est réussie pour des valeurs de masse autour de 1 GeV, une dégénérescence de masse de l'ordre de $\Delta M \sim 10^{-5} M$ et une transition de phase survenant à une température $T_n \sim 10$ TeV. Pour des valeurs de températures de nucléation plus basses, le risque est de ne pas produire assez d'asymétrie leptonique avant le découplage des sphalérons à $T_{\rm sph} = 150$ GeV, tandis que une température de nucléation plus grande implique une transition de phase trop précoce, qui ne "frustre" pas assez les oscillations.

En conclusion, notre étude a porté sur la formalisation du problème de la leptogénèse incluant une transition de phase durant laquelle la masse des neutrinos stériles devient dépendante du temps. Cette thèse décrit comment inclure cette variation rapide de la masse dans des équations cinétique pour les neutrinos stériles et comment cela impacte l'asymétrie leptonique. En particulier, ces équations incluent à la fois la dynamique des neutrinos stériles durant la transition de phase (qui produisent des neutrinos stériles, même en l'absence d'autres interactions) et à la fois l'impact sur les scénarios de leptogénèse standard (où les interactions avec le Modèle Standard jouent un rôle important). L'espace des paramètres où la leptogénèse est

réussie est modifié dans certains cas à cause de la transition de phase, et une comparaison des différents scénarios, basée sur des estimations analytiques, permet de comprendre dans quels circonstances une transition de phase favorise la création d'une asymétrie.

En définitive, la leptogénèse durant une transition de phase peut être décrite à l'aide d'équations cinétiques qui modélisent le comportement des neutrinos stériles durant la transition de phase, notamment avec la création de particules due au changement de vide du champ scalaire, et après la transition, avec la création d'une asymétrie leptonique. Cela peut être fait de différentes façons et cette thèse décrit le cas du "Mass Gain" (neutrinos stériles qui se désintègrent) et d'un cas "type ARS" (neutrinos stériles qui oscillent). L'étude numérique faite ici permet de trouver les régimes où la leptogénèse est réussie. Cette étude pourrait être améliorée en incluant le champ scalaire comme dynamique et considérer son impact sur la production d'asymétrie. Enfin, ces travaux pourraient être complétés en établissant le lien avec la phénoménologie des ondes gravitationnelles, pour connecter les propriétés de la transition de phase (par exemple la température à laquelle elle intervient, et sa magnitude) utilisées pour la leptogénèse avec le spectre en fréquence attendu pour les ondes gravitationnelles pouvant être détectées dans les expériences présentes ou futures.

This thesis is partially based on an article to be published shortly.

Notations and conventions

Throughout the manuscript, we use Einstein convention for summation of repeated indices, unless stated otherwise.

We are working in units where $\hbar = c = k_B = 1$. Our signature for Minkowski space-time is $(+ - - -)$.

Contents

Chapter 1

Introduction

When Paul Dirac predicted in 1928 the existence of an anti-particle for the electron, the positron, he opened the doors to a whole new world, a world that was a "mirror" version of ours as we knew it. Since his prediction, the positron was discovered in 1932 by Anderson, and later on, so were all the other particles' anti-partners. These "mirror" particles are now deeply connected to our understanding of spinors and quantum fields. It is still pretty astonishing that it took us so long to find antimatter, and that the Universe, or at least the majority of our environment, seems to be only made out of matter, despite the relatively similar properties of antimatter. This everyday experience that we are made of carbon atoms and not anti-carbon atoms, breath dioxygen and not anti-dioxygen, is actually not totally well understood and is part of a puzzle in modern physics.

These interrogations have been particularly important thanks to the recent improvement of observations by telescopes and satellites in the past decades, and the question "why is there more matter than anti-matter?" can now be made more precise. We want to compare the density of baryons n_b (making out most of the observable matter) to the density of anti-baryons $n_{\bar{b}}$. It is convenient to define a dimensionless asymmetry η, given by the difference $n_b - n_{\bar{b}}$ normalized by the density of photons n_γ in the Universe,

$$\eta \equiv \frac{n_b - n_{\bar{b}}}{n_\gamma} \simeq \frac{n_b}{n_\gamma} \ . \tag{1.1}$$

η is the Baryon Asymmetry of the Universe (BAU). Assuming the anti-baryons represent a negligible quantity of baryonic matter in the observed Universe $n_{\bar{b}} \ll n_b$, we can estimate the asymmetry η by the measurement of the baryon-to-photon ratio n_b/n_γ only. Fortunately, in the celebrated Λ-Cold Dark Matter (Λ-CDM) model [1, 2], the cosmological evolution of the Universe is described by a set of six parameters, among which we find the ratio $\Omega_b h^2 \equiv \frac{\rho_b}{\rho_c} h^2 = \frac{m_b n_b}{\rho_c} h^2 = \frac{m_b n_\gamma h^2}{\rho_c} \eta$. The mass m_b of the baryons is the mass of the nucleons (protons and neutrons) which constitute most of the baryonic matter. $h \equiv H/100$ km.Mpc^{-1}.sec^{-1} is given by the present value of the Hubble parameter, while ρ_b is the energy density of baryons and is compared to the critical density $\rho_c \equiv 1.88 \times 10^{-29}\ h^2$ g.cm^{-3}.

The BAU η can then be deduced from $\Omega_b h^2$, which itself is measured from the Cosmic Microwave Background (CMB) and its value [3] leads to

$$\eta = (6.13 \pm 0.04) \times 10^{-10} \ . \tag{1.2}$$

The study of Big Bang Nucleosynthesis (BBN) [4] confirms this value is consistent with the abundance of most light elements (except for a tension for the ^{7}Li abundance [5,6]). The value of η may seem small, but we should compare it to a naive estimate: in a perfectly symmetric Universe, with no initial asymmetry between matter and anti-matter, not all baryon and anti-baryons annihilate (see for example [7,8]), and leave a residual abundance

$$\frac{n_b}{n_\gamma} = \frac{n_{\bar{b}}}{n_\gamma} = 10^{-20} \ . \tag{1.3}$$

The observed value (1.2) is therefore different by 10 orders of magnitude! Trying to start with an initially asymmetric Universe runs into another issue: inflation [9] (our current best explanation of the so-called horizon problem) assumes an exponential expansion of the Universe during its early stages, which would dilute any pre-existing baryon asymmetry. Manifestly, there is a need for a more detailed explanation. Such an explanation by the dynamical production of the asymmetry η is called **baryogenesis**. Our understanding of its origin is primordial in order to make sense of our observations and collect information about the first instants of our Universe.

The baryon asymmetry is not only an important quantity in our cosmological models, it may also determine the viability (or not) of local theories that we use. If we have a new particle physics model in mind, we can ask ourselves if it allows successful baryogenesis. This would not be a direct test (through measurements at colliders for example) of new interactions or new particles, but rather an indirect challenge for our theory. At the same time, the baryon asymmetry motivates new models that can be ruled out or tested at colliders. The interplay between cosmological observations, model-building and particle experiments is at the heart of current attempts to explain the baryon asymmetry, but also dark matter, dark energy, etc. Concerning baryogenesis, Andreï Sakharov described in 1967 a set of conditions, known as Sakharov conditions [10], that a theory needs in order to create the Baryon Asymmetry of the Universe (BAU):

- (1) Violation of the baryon (or lepton) number,
- (2) C and CP violation,
- (3) Out of equilibrium evolution at some point in the Universe.

The first condition is needed to have a process able to create a baryon asymmetry. Note that it could also be a process violating lepton number which would be converted in a baryon asymmetry by the so-called sphalerons processes; in that case, we speak of **leptogenesis** [11], creating a lepton asymmetry. In any case, once such processes are available, C-violation is necessary

for distinguishing particles and anti-particles, and CP-violation is also needed, otherwise CP-conjugated processes would cancel each other's contribution to the baryon asymmetry, once integrated over phase space. Finally, the last condition is needed because at thermal equilibrium, any process creating an asymmetry would be counter-balanced by its inverse process, canceling the asymmetry. It can be understood if we think of thermal equilibrium as a state where time translation symmetry is respected, which in virtue of the CPT theorem [12] allows no CP violation, even if they are terms in the theory that could potentially have violated it.

A popular way of satisfying these Sakharov conditions is by using **Majorana sterile neutrinos**. They are hypothetical particles that are good candidates for explaining another puzzle in the Standard Model, the active neutrino masses. These masses for the active neutrinos are not predicted by the Standard Model, but are now well-established from oscillations experiments, first evidenced in 1998 for atmospheric neutrinos by the Super-Kamiokande experiment [13] and in 2001 for solar neutrinos by the Sudbury Neutrino Observatory [14]. By interacting with active neutrinos, sterile neutrinos can solve this issue, adding lepton number violation and CP-violation to the Standard Model, hence satisfying the first two Sakharov conditions. While it is an elegant solution to the neutrino oscillation problem, it barely constrains the sterile neutrino properties [15]. The sterile neutrino mass scale M, for example, can range from the $M \sim 1$ eV scale to up to much larger scales $M \sim 10^{15}$ GeV, representing a range of more than 20 orders of magnitude! Requiring that they help reproduce the baryon asymmetry can constrain the parameter space more, and could be (mainly for low-scale sterile neutrinos) a guide for direct searches.

While the sterile neutrinos help us satisfy the first two Sakharov conditions from particle physics considerations alone, the way they deviate from equilibrium (to satisfy the third Sakharov condition) depends on the specific leptogenesis scenario we consider. The original leptogenesis scenario [11], sometimes referred to as **thermal leptogenesis**, relies on the expansion of the Universe bringing the sterile neutrino distribution out of equilibrium, once the temperature drops below the mass scale (with masses typically $M \gtrsim 10^5$ GeV), making the sterile neutrinos decay. Another scenario, proposed by Akhmedov, Rubakov and Smirnov (ARS) and dubbed **ARS leptogenesis**, considers instead the production and oscillations of lighter sterile neutrinos (of masses $M \sim 1 - 100$ GeV).

A quite recent and popular approach involves yet another out-of-equilibrium phenomenon: **cosmological phase transitions**. These transitions are interesting cosmological phenomena that typically correspond to a rather rapid change in a physical quantity, like for example the vacuum expectation value (*vev*) of a scalar field. They are of phenomenological interest for many reasons. First of all, standard cosmology and the Standard Model of particle physics already predict two phase transitions: the electroweak phase transition in which the Higgs field obtains a non-zero *vev* and the QCD phase transition for the confinement of quarks. Secondly, several scenarios of new physics beyond the Standard Model involve the phase transition of a scalar field. We can mention Grand Unification Theories like $SU(5)$ or $SO(10)$ [16, 17], in which the extra gauge symmetries are spontaneously broken, or also conformal models [18–21]. Finally, the recent detection, in 2015, of Gravitational Waves (GW) by the LIGO-Virgo collab-

oration [22] opened up the possibility of constraining violent phenomena such as cosmological phase transitions by searching for their GW signature. New generation of detectors like the Einstein telescope, Cosmic Explorer (for ground-based detectors, already in early design phase) or LISA, TianQin (for detectors in space, programmed to be launched around 2035) will be looking for such signatures. Any detection (or non-detection) will tell us more about the early Universe and what could have happened in it.

A cosmological phase transitions is then an original context to work with, worth considering also phenomenologically speaking. We wish to study its role and possible impact in the context of leptogenesis with sterile neutrinos, and ask the following questions: does it make the creation of an asymmetry easier or more complicated? Are there any advantages compared to standard leptogenesis scenarios? If so, what are the properties and characteristics of such a phase transition? This thesis tries to address these points.

There have already been studies on leptogenesis with a phase transition. In the majority of them (see [23–25] for different approaches), sterile neutrinos are coupled to a new scalar field in such a way that it gives them a mass. As the phase transition happens, their mass is then changing: this is the out-of-equilibrium ingredient we were looking for. A common setup for this phase transition is to have the scalar field experience a *first-order* phase transition (which induces stronger deviation from equilibrium than a second-order one) at some high, new physics scale. While it is not the only way to proceed (for instance, [26] relied on a second-order phase transition, and [27] studied an extension of the electroweak phase transition), we will focus now on previous works of leptogenesis which considered such a first-order phase transition in a new scalar sector. We can separate them into two categories, depending on how the sterile neutrinos react to the phase transition and produce the asymmetry.

Out-of-equilibrium decays In the studies [28–31], the phase transition was used to provoke a large deviation from equilibrium by making the sterile neutrinos suddenly very massive and likely to decay. This situation resembles thermal leptogenesis, in that decays are producing the lepton asymmetry. We will call this scenario *"Mass Gain"* in reference to a study [32] (conducted in baryogenesis instead of leptogenesis) which used this idea under that name.

Out-of-equilibrium production The production of sterile neutrinos can be affected by an extra scalar and a phase transition, especially for low-scale sterile neutrinos. The situation is then more similar to ARS leptogenesis; we will often refer to it as *"ARS-like"* leptogenesis. Some studies [33–36] have considered the effect of an extra scalar field on standard ARS leptogenesis, including new decays and interactions, while other works [37–39] included the phase transition of this new scalar into the dynamics.

In both cases (decays and production), the phase transition was assumed to be mostly instantaneous, which is an assumption that can be refined. Moreover, in the Mass Gain scenario (with non-relativistic sterile neutrinos), a larger parameter scan is lacking, for instance the

dependence on the mass degeneracy is not fully described ([29, 30] consider degenerate sterile neutrinos, [28, 31] consider hierarchical ones). In the ARS-like regime, while numerical studies were performed, more detailed analytical results and descriptions of the physical processes leading to an asymmetry in the case of a phase transition could be helpful.

We therefore have two objectives in this thesis. Firstly, we would like to include the dynamics of the sterile neutrinos during the (relatively short) period of the phase transition, and estimate the physical effect of their mass change. Secondly, we would like to describe both relativistic and non-relativistic sterile neutrinos within the same framework, in order to analyze the Mass Gain and ARS-like cases, and perform a larger scan of the parameters for each scenario. This includes resonant and non-resonant regimes in the case of the Mass Gain, and a physical description of oscillations in the case of ARS leptogenesis.

Structure of this thesis This work can be decomposed into three main parts: first an introduction to leptogenesis and cosmology in general, then the description of the formalism needed for adding a phase transition in the context of leptogenesis, and finally our numerical and analytical results as well as our discussions. We detail how each of these parts is itself decomposed in chapters.

The first two chapters are introductory and remind the reader of the dynamics of the particle plasma in the early Universe, few seconds after the Big Bang and inflation. Chapter 2 is a general description of the Universe's expansion and the phenomena that can occur in a cosmological history, most importantly phase transitions which are the focus of this work. Chapter 3 focuses on the specific case of leptogenesis, using sterile neutrinos and introduces the main scenarios of interest for this work.

Once these concepts are set, we delve into the dynamics of a particle during a first-order phase transition. This particle obtains a time-dependent mass due to the nucleation and expansion of bubbles. We show in chapter 4 that a distribution of particles is created during the phase transition, in a simplified single-flavor approach. A more complete treatment of interacting fields requires the machinery of out-of-equilibrium Quantum Field Theory, presented in chapter 5. We arrive at a set of equations for the sterile neutrinos and the lepton asymmetry.

Using these equations, we are able to explore the possibilities opened up by the phase transition. We consider two different mechanisms of lepton asymmetry production. For relatively heavy sterile neutrinos, deviating from equilibrium due to the phase transition, they will decay and we recover the Mass Gain (MG) regime in chapter 6. We describe it with kinetic equations, allowing us to scan over a large portion of parameter space, considering hierarchical or degenerate masses for the sterile neutrinos; we discuss and compare our results to previous studies. In chapter 7, we investigate, both numerically and analytically, the production of sterile neutrinos in the context of a phase transition. A baryon asymmetry gets produced through oscillations, which resembles ARS leptogenesis, but with a parameter dependence that can be qualitatively different. We then make a general conclusion of our observations, in both regimes.

Part I

Baryogenesis in the early Universe

This first part is introductory and aims at presenting the general context of our study. We start with a review of the early Universe in Chapter 2, exposing the tools to describe the expansion of the Universe, the kinematics of interacting particles and cosmological phase transitions. All these concepts are relevant for baryogenesis, which we present before moving on to the more specific case of leptogenesis in Chapter 3. In there we present how leptogenesis can explain the baryon asymmetry of the Universe, in particular involving sterile neutrinos. Two main popular scenarios involve either non-relativistic sterile neutrinos (in the so-called thermal and resonant leptogenesis) or relativistic ones (in the so-called ARS leptogenesis).

Chapter 2

A guide of the early Universe

Cosmology is interested in the Universe as a physical system, and not only the arena in which phenomena take place. Increasingly precise observations have allowed to establish the basis of modern cosmology. First, the expansion of the Universe, first evidenced by galaxy surveys in the late 1920's, has lead to the deduction that at earlier times, the Universe must have been denser, and hotter. This revolutionary measurement, together with the contemporary theoretical revolution that was general relativity, paved the way to a description of the Universe as a dynamical object that expands as time goes. Its exact evolution is determined by its matter and energy content, which then in return are affected by the expansion of the Universe.

This chapter is meant as a presentation of the most relevant aspects of cosmology for our study. We start by reviewing how the expansion of the Universe is determined, before focusing on the radiation domination period which will be of interest to us. Once the arena is understood, we can let the players in, and we detail how the dynamics of fields in the early Universe is described using kinetic Boltzmann equations. This provides the context and tools for phenomena like baryogenesis and cosmological phase transitions that we present in section 2.5 and 2.4 respectively.

2.1 Expansion of the Universe

At cosmological scales, galaxies in every direction are red-shifting away from the Earth, and the further they are, the faster they move away from us. This is the Hubble-Lemaître law, predicted by Georges Lemaître in 1927 and discovered by Edwin Hubble in 1929. The simplest explanation for this observation is that space-time itself is expanding, in an approximate spatially homogeneous and isotropic way. This leads to the postulate that the metric of the Universe was given, not by the flat Minkowski space-time, but by the Friedmann-Lemaître-Robertson-Walker (FLRW) metric

$$\mathrm{d}s^2 = \mathrm{d}t^2 - a(t)^2 \mathrm{d}\mathbf{x}^2 \ , \tag{2.1}$$

where $a(t)$ is the scale factor. Its evolution rate gives the Hubble parameter

$$H \equiv \frac{\mathrm{d}a/\mathrm{d}t}{a} \tag{2.2}$$

whose value today is precisely the parameter of the Hubble-Lemaître law, that tells us how further galaxies seem to move faster away from us.

The evolution in time of the scale factor determines how the Universe expanded and will expand. It is quite remarkable that this simple metric can help us ask and (partially) answer questions such as "how was the Universe born?" and "what will be his fate?". The energy and matter content of the Universe influence its evolution through the Einstein equations applied to the FLRW metric, leading to the well-known Friedmann equations [8]. The first Friedmann equation gives us (neglecting the spatial curvature of the Universe, suggested to be zero by observations)

$$H^2 = \frac{8\pi G}{3}\rho \ . \tag{2.3}$$

Here, ρ is the energy density of all the content of the Universe, approximated to be a fluid once we average over large (cosmological) scales. This quantity is also dependent on the scale factor, as it can undergo dilution from the expansion of the Universe. The evolution of ρ is constrained by the conservation of energy, that imposes a continuity equation

$$\frac{\mathrm{d}\rho}{\mathrm{d}t} = -3H\left(\rho + p\right) \ , \tag{2.4}$$

with p the pressure of the fluid. The pressure can be related to the energy density by an equation of state, which depends on the nature of the fluid's content. A fluid made of radiation satisfies

$$p_{\mathrm{rad}} = \frac{\rho_{\mathrm{rad}}}{3} \ , \tag{2.5}$$

a matter fluid

$$p_{\mathrm{mat}} = 0 \ , \tag{2.6}$$

while the cosmological constant, with its negative pressure, satisfies the (more exotic) relation

$$p_\Lambda = -\rho_\Lambda \ . \tag{2.7}$$

For each type of fluid, the continuity equation (2.4) tells us how the energy density of the fluid scales with $a(t)$,

$$\rho_{\mathrm{rad}} = \rho^0_{\mathrm{rad}}\left(\frac{a(t)}{a_0}\right)^{-4} \ , \ \rho_{\mathrm{mat}} = \rho^0_{\mathrm{mat}}\left(\frac{a(t)}{a_0}\right)^{-3} \ , \ \rho_\Lambda = \rho^0_\Lambda \ , \tag{2.8}$$

where $a_0 = a(t_0)$ is the scale factor today, with $t_0 \simeq 13.8$ Gyr the age of the Universe. The first Friedmann equation becomes a closed equation for a, with the densities present in our present Universe ρ^0_X as parameters,

$$H^2 = \left(\frac{\mathrm{d}a/\mathrm{d}t}{a}\right)^2 = \frac{8\pi G}{3}\left[\rho^0_{\mathrm{rad}}\left(\frac{a(t)}{a_0}\right)^{-4} + \rho^0_{\mathrm{mat}}\left(\frac{a(t)}{a_0}\right)^{-3} + \rho^0_\Lambda\right] \ . \tag{2.9}$$

The constants ρ_X^0 are then parameters fixed by the best match to observations. The very good agreement to CMB and BBN (Big Bang Nucleosynthesis) data and the relative simplicity of the cosmological fluids make this model a remarkable tool for navigating in various epochs of the Universe's history. Going back in time, constraints from observations are robust roughly from now until the BBN epoch corresponding to around a minute after the Big Bang, for temperatures around 20-100 keV.

2.2 Radiation domination

From the different a-dependence in the equation (2.9), one can note that for early times, when the scale factor was small, mostly the contribution from $\rho_{\rm rad} \propto a^{-4}$ will dominate. The epoch where $\rho_{\rm rad}$ is the largest contribution to the total energy density is called radiation domination. In our Universe, from our current observations, it is expected to have happened until about 47 000 years after inflation, before the matter contribution started to be predominant.

In the radiation-dominated era, $\rho \simeq \rho_{\rm rad}$, and

$$H \simeq \sqrt{\frac{8\pi G}{3}} \left(\rho_{\rm rad}\right)^{1/2} \propto a^{-2} \;\Leftrightarrow\; a(t) \propto t^{1/2} \,. \tag{2.10}$$

More can be said about the content of the Universe; in principle, all particles of the Standard Model can be present after being produced at reheating. In the early Universe, if the Universe is hot enough, the Higgs field is experiencing an effective potential (due to thermal corrections) that only allows a null vacuum expectation value (*vev*). In particular, all particles in the Standard Model should be massless, and therefore count as radiation. The 'soup' of SM radiation will be called the SM plasma.

2.2.1 Thermal equilibrium

Interactions among particles (in particular between fermions and gauge bosons, or gauge bosons amongst themselves) bring the particle distributions to a thermal state, of common temperature T. At this temperature T, the energy density of the SM plasma is computed by integrating over the energies of the particles in the plasma. For bosons and fermions in thermal equilibrium, their phase space distribution is given by the Bose-Einstein and the Fermi-Dirac distributions respectively

$$f_{\rm eq}(E) = \begin{cases} f_{BE}(E) \equiv \dfrac{1}{e^{E/T}-1} & \text{bosons,} \\ f_{FD}(E) \equiv \dfrac{1}{e^{E/T}+1} & \text{fermions.} \end{cases} \tag{2.11}$$

For massless bosons and fermions, the individual energies are simply $E = |\mathbf{k}|$, such that one can obtain expressions for the number densities

$$N_{\text{boson}} \equiv \int \frac{\mathrm{d}^3\mathbf{k}}{(2\pi)^3} \frac{1}{e^{|\mathbf{k}|/T} - 1} = \frac{\zeta(3)}{\pi^2} T^3 \ , \tag{2.12}$$

$$N_{\text{fermion}} \equiv \int \frac{\mathrm{d}^3\mathbf{k}}{(2\pi)^3} \frac{1}{e^{|\mathbf{k}|/T} - 1} = \frac{3\zeta(3)}{4\pi^2} T^3 \ , \tag{2.13}$$

as well as for the energy densities

$$\rho_{\text{boson}} = \int \frac{\mathrm{d}^3\mathbf{k}}{(2\pi)^3} \frac{|\mathbf{k}|}{e^{|\mathbf{k}|/T} - 1} = \frac{\pi^2}{30} T^4 \ , \tag{2.14}$$

$$\rho_{\text{fermion}} = \int \frac{\mathrm{d}^3\mathbf{k}}{(2\pi)^3} \frac{|\mathbf{k}|}{e^{|\mathbf{k}|/T} + 1} = \frac{7\pi^2}{240} = \frac{7}{8}\frac{\pi^2}{30} T^4 \ . \tag{2.15}$$

The total energy density of the SM plasma is the sum over all SM species

$$\rho_{\text{rad}} = \rho_{\text{SM}} = \frac{\pi^2}{30} g_* T^4 \ , \tag{2.16}$$

where g_* is the number of effectively massless degrees of freedom, given by the formula

$$g_* = \sum_{\text{boson } i} g_b^i + \frac{7}{8} \sum_{\text{fermion } i} g_f^i \ . \tag{2.17}$$

We sum over all species i that individually correspond to $g_{b/f}^i$ degrees of freedom. In the SM, at high enough energy such that all particles are considered massless and at the same temperature, we have $g_* = 106.75$.

Another important thermodynamic quantity to consider is the entropy S of the system. It obeys the first law of thermodynamics $T\mathrm{d}S = \mathrm{d}E + p\mathrm{d}V$, within a volume V. For the entropy density $s \equiv S/V$, using the fact that S and E are extensive quantities, one obtains a relation between s and the pressure and energy density

$$s \equiv \frac{\rho + p}{T} \ . \tag{2.18}$$

Considering the SM plasma made of radiation (whose equation of state we recall is $p = \rho/3$), the entropy density s is

$$s = \frac{2\pi^2}{45} g_{*,S} T^3 \ . \tag{2.19}$$

where

$$g_{*,S} = \sum_{\text{boson } i} g_b^i \left(\frac{T_i}{T}\right)^3 + \frac{7}{8} \sum_{\text{fermion } i} g_f^i \left(\frac{T_i}{T}\right)^3 \ . \tag{2.20}$$

In principle, $g_{*,S}$ can be different from g_* if certain species in the SM are not at thermal equilibrium with the rest of the plasma, *i.e.* $T_i \neq T$. In our study, however, we will always assume $g_{*,S} = g_*$.

The thermal equilibrium condition allows us to express all quantities of interest (number density, energy density, entropy density) in terms of the temperature T only.

2.2.2 Time-temperature relation

The properties of the particles are not the only quantities that can be determined from the temperature. The scale factor a can also be related to T. We expect the temperature to be greater when the Universe was denser, *i.e.* a should be a decreasing function of T. A precise relation can be given in the case where all particles are at thermal equilibrium, such that the total entropy in a volume $a(t)^3$ is conserved

$$\frac{\mathrm{d}S}{\mathrm{d}t} = 0 = \frac{\mathrm{d}\left(a^3(t)s(t)\right)}{\mathrm{d}t}. \tag{2.21}$$

We know that for radiation, $s \propto T^3$. The conservation of entropy (2.21) during the Universe's expansion is thus only possible if

$$a \propto T^{-1} \ . \tag{2.22}$$

This reproduces the intuitive reasoning that the plasma is hotter when the Universe is denser.

Using the expression (2.16), the Hubble parameter is given by the Friedmann equation in terms of the temperature,

$$H = \sqrt{\frac{8\pi G}{3}}\sqrt{\frac{\pi^2}{30}g_* T^4} \equiv \frac{T^2}{a_R} \ , \ a_R \equiv \sqrt{\frac{45}{4\pi^3 g_*}}\frac{1}{\sqrt{G}} = \sqrt{\frac{45}{4\pi^3 g_*}}M_{\mathrm{Pl}} \ , \tag{2.23}$$

where $M_{\mathrm{Pl}} = 1/\sqrt{G} \simeq 1.2\times10^{19}$ GeV, in natural units. Recall how we concluded that $a(t) \propto t^{1/2}$ in a radiation-dominated Universe. This implies

$$H = \frac{\mathrm{d}a/\mathrm{d}t}{a} = \frac{1}{2t} = \frac{T^2}{a_R} \tag{2.24}$$

leading to a relation between time and temperature

$$T(t) = \left(\frac{a_R}{2}\right)^{1/2} t^{-1/2} \ . \tag{2.25}$$

In the early Universe, the temperature is thus directly related to time, and we will see that it can be convenient to jump from one to the other in our study, especially considering explicitly time-dependent processes such as phase transitions.

2.3 Boltzmann equations from every angle

In cosmology, we are typically concerned with (average) densities of different kinds of fields interacting as the Universe expands. In principle, one should work with Quantum Field Theory (QFT) in a thermal bath (the SM plasma, with potential additional species) in a curved space-time (the FLRW metric) to compute the dynamics of each field. It is however not always useful in practice; numerical resolutions usually become very involved because equations for

correlation functions are non local, and the nature of the physical processes can get obscured by the formalism. A more transparent approach is based on kinetic Boltzmann equations. They describe the evolution of (on-shell) particle densities in phase space $f_i(\mathbf{x}, \mathbf{k}, t)$ in the plasma, where i labels the species.

2.3.1 Kinetic Boltzmann equations

A kinetic Boltzmann equation has the form

$$\frac{\mathrm{d}f_i}{\mathrm{d}t} = \frac{\partial f_i}{\partial t} + \mathbf{v} \cdot \boldsymbol{\nabla}_{\mathbf{x}} f_i + \frac{\partial \mathbf{k}}{\partial t} \cdot \boldsymbol{\nabla}_{\mathbf{k}} f_i = \mathcal{C}_{\mathrm{col}}[f_i; f_j] \ , \tag{2.26}$$

where $\boldsymbol{\nabla}_{\mathbf{x}} = \left(\frac{\partial}{\partial x}, \frac{\partial}{\partial y}, \frac{\partial}{\partial z}\right)^T$, $\boldsymbol{\nabla}_{\mathbf{k}} = \left(\frac{\partial}{\partial k_x}, \frac{\partial}{\partial k_y}, \frac{\partial}{\partial k_z}\right)^T$. The left-handed side of the equation is the homogeneous equation, describing the phase space density along the flow of particles which is moving at velocity $\mathbf{v}$ and whose momenta are changing at a rate $\partial\mathbf{k}/\partial t$. $\mathcal{C}_{\mathrm{col}}[f]$ is a collision term that depends on the interactions of the particle we describe with itself and the rest of the system. The collision term can describe exchange of momenta (scattering) or a change in the number of particles (decays, production). It is usually computed from zero- or finite-temperature QFT amplitudes and plugged into the kinetic Boltzmann equations. This includes the quantum processes of the theory inside these more classical equations.

The effect of the space-time background will also be taken into account. Indeed, considering the FLRW metric, we first notice that it is spatially homogeneous and isotropic. We will therefore only consider phase space densities independent of space and only dependent on the norm of the momentum $\mathbf{k}$. The homogeneous part of the kinetic Boltzmann equations becomes

$$\frac{\mathrm{d}}{\mathrm{d}t} f_i(|\mathbf{k}|, t) = \frac{\partial f_i}{\partial t} + \frac{\partial |\mathbf{k}|}{\partial t} \frac{\partial f_i}{\partial |\mathbf{k}|} \ . \tag{2.27}$$

In the FLRW metric, space is expanding with a scale factor $a(t)$, and momentum is red-shifting $\mathbf{k} \propto a^{-1}$. Therefore,

$$\frac{\partial |\mathbf{k}|}{\partial t} = -\frac{\mathrm{d}a/\mathrm{d}t}{a} |\mathbf{k}| = -H|\mathbf{k}| \ . \tag{2.28}$$

The Boltzmann equations are then

$$\frac{\partial f_i}{\partial t} - H|\mathbf{k}| \frac{\partial f_i}{\partial |\mathbf{k}|} = \mathcal{C}_{\mathrm{col}}[f_i; f_j] \ . \tag{2.29}$$

These equations are partial differential equations for the f_i's, containing the main ingredients for cosmology, the expansion of the Universe with the H factor, and the quantum processes in $\mathcal{C}_{\mathrm{col}}$.

Cosmological observables, for example the ratio η, are sensitive to number densities $N_i(t)$,

once we integrate over momentum. It is therefore usual to write Boltzmann equations (which are no longer "kinetic") for the N_i's, integrating (2.29) over $\mathbf{k}$,

$$\frac{\mathrm{d}N_i}{\mathrm{d}t} + 3HN_i = \int \frac{\mathrm{d}^3\mathbf{k}}{(2\pi)^3}\mathcal{C}_{\mathrm{col}}[f_i; f_j] \ , \tag{2.30}$$

$$N_i = \int \frac{\mathrm{d}^3\mathbf{k}}{(2\pi)^3} f_i \ . \tag{2.31}$$

We will see examples of such Boltzmann equations applied to leptogenesis in Chapter 3. In Chapter 5, we will see how a first-principle QFT approach can lead to kinetic Boltzmann equations (or a quantum analog of it), and how the collision parts are computed from the particle physics model.

2.3.2 Comoving and rescaled quantities

Contrary to the collision term in the Boltzmann equations which is non generic and depends on the model, the dilution term $-H|\mathbf{k}|\frac{\partial f_i}{\partial|\mathbf{k}|}$ or $3HN_i$ is always the same once $a(t)$ is determined. It is common to absorb this dilution by a change of variable, including automatically the red-shifting of momentum for example. We present here two equivalent ways this can be realized; the first one is more frequently used in the literature while the second is convenient for our work, so we explain here the connection between both. The first one uses *comoving* quantities. It introduces a comoving momentum

$$\mathbf{k}_{\mathrm{com}} \equiv a(t)\mathbf{k} \ . \tag{2.32}$$

This quantity is fixed for a given particle, as the Universe expands. The phase space density appearing in the kinetic Boltzmann equations can be changed to be a function of comoving momentum,

$$f_i^{\mathrm{com}}(|\mathbf{k}_{\mathrm{com}}|, t) \equiv f_i(|\mathbf{k}|, t) = f_i(a(t)^{-1}|\mathbf{k}_{\mathrm{com}}|, t) \ , \tag{2.33}$$

such that

$$\frac{\mathrm{d}f_i^{\mathrm{com}}}{\mathrm{d}t} = \frac{\partial f_i^{\mathrm{com}}}{\partial t} = \frac{\partial}{\partial t} f_i(|\mathbf{k}|, t) - |\mathbf{k}|H\frac{\partial}{\partial|\mathbf{k}|} f_i(|\mathbf{k}|, t) = \mathcal{C}_{\mathrm{col}}\left[f_i^{\mathrm{com}}; f_j^{\mathrm{com}}\right] \ . \tag{2.34}$$

There is no dilution term for f_i^{com}, which is no surprise as the comoving momentum doesn't get red-shifted any more. We can then integrate over comoving momentum to get a comoving number density

$$N_i^{\mathrm{com}} \equiv \int \frac{\mathrm{d}^3\mathbf{k}_{\mathrm{com}}}{(2\pi)^3} f_i^{\mathrm{com}} = a(t)^3 N_i \ , \tag{2.35}$$

satisfying

$$\frac{\mathrm{d}N_i^{\mathrm{com}}}{\mathrm{d}t} = \int \frac{\mathrm{d}^3\mathbf{k}_{\mathrm{com}}}{(2\pi)^3}\mathcal{C}_{\mathrm{col}}[f_i^{\mathrm{com}}; f_j^{\mathrm{com}}] \ . \tag{2.36}$$

Again, the dilution term disappeared from the equation.

A second, equivalent way of dealing with this is to recall the relation between $a \propto T^{-1}$ in a radiation-dominated Universe. Therefore, instead of comoving quantity, we can define *rescaled* quantities

$$\boldsymbol{\kappa} \equiv \frac{\mathbf{k}}{T} \ , \tag{2.37}$$

$$f_i^{\rm resc}(|\boldsymbol{\kappa}|, t) \equiv f_i(|\mathbf{k}|, t) \ , \tag{2.38}$$

$$n_i(t) \equiv \frac{N_i(t)}{T^3} \ . \tag{2.39}$$

They are proportional to the comoving quantities, so the physical argument is the same for getting rid of the dilution. However, we find it more useful in this work as temperature is relevant for the phase transition, and the ratio $|\mathbf{k}|/T$ naturally appears in collision terms, as we will see.

It is also common to define a yield Y_i as the ratio of the number density with the entropy of the plasma $s \equiv \frac{2\pi^2}{45} g_* T^3$. As $s \propto T^3$, the yield is proportional to the rescaled quantity,

$$Y_i \equiv \frac{N_i}{s} = \frac{45}{2\pi^2 g_*} n_i \ . \tag{2.40}$$

2.3.3 Time and inverse temperature

So far, we worked with time as the variable, but it might not always be the most relevant. In particular, we have a direct relation (2.25) between time t and temperature T, that we recall here

$$T(t) = \left(\frac{a_R}{2}\right)^{1/2} t^{-1/2} \ . \tag{2.41}$$

It is common to change variables from t to a variable

$$z \equiv \frac{T_{\rm ref}}{T} = T_{\rm ref} \left(\frac{2}{a_R}\right)^{1/2} t^{1/2} \ , \tag{2.42}$$

where $T_{\rm ref}$ is a fixed reference temperature. It is usually taken to be a main scale of interest, for example the mass of a sterile neutrino in thermal leptogenesis as we will see, or the electroweak scale. In terms of the variable z,

$$\frac{\mathrm{d}}{\mathrm{d}t} = \frac{\mathrm{d}z}{\mathrm{d}t}\frac{\mathrm{d}}{\mathrm{d}z} = \frac{T_{\rm ref}}{a_R} T \frac{\mathrm{d}}{\mathrm{d}z} = zH \frac{\mathrm{d}}{\mathrm{d}z} \ . \tag{2.43}$$

The homogeneous part of the Boltzmann equations can therefore be written in several equivalent ways,

$$\frac{\partial f_i}{\partial t} - H|\mathbf{k}|\frac{\partial f_i}{\partial |\mathbf{k}|} = \frac{\partial f_i^{\rm com}}{\partial t} = \frac{\partial f_i^{\rm resc}}{\partial t} = zH \frac{\partial f_i^{\rm resc}}{\partial z} \ , \tag{2.44}$$

$$\frac{\mathrm{d}N_i}{\mathrm{d}t} + 3HN_i = \frac{1}{a(t)^3}\frac{\mathrm{d}N_i^{\rm com}}{\mathrm{d}t} = T(t)^3 \frac{\mathrm{d}n_i}{\mathrm{d}t} = T_{\rm ref}^3 \frac{H}{z^2}\frac{\mathrm{d}n_i}{\mathrm{d}z} = sHz\frac{\mathrm{d}Y_i}{\mathrm{d}z} \ . \tag{2.45}$$

Depending on the context, one or the other formulation can be more enlightening. In our study, we will alternate at some point between the t and the z variables, because different time scales will be involved. Indeed, z is related to the temperature and evolves significantly only over cosmological times, *i.e.* when the Universe expands, while t and variation Δt around a given time are more adequate for processes faster than the Universe expansion. In particular, we will be interested in phase transitions that have relatively short time scales, as we describe in the next section.

2.4 Cosmological phase transitions

Phase transitions are an interesting physical phenomenon to be considered in cosmology. In a very large sense, they correspond to the change of a physical quantity over time. A common example is a scalar field changing its vacuum expectation value (*vev*). These phase transitions imply an explicit time dependence (there is a *before* and an *after* the phase transition) in a way that can differ radically with the expansion of the Universe, in that they can be non adiabatic and happen over different time scales. Such an explicit time dependence can lead to deviation from thermal equilibrium, which is desirable for creating the BAU from the Sakharov conditions.

Two such cosmological phase transitions occur in the Standard Model: the QCD phase transition [40–42] and the electroweak phase transition [43–45]. The QCD cosmological phase transition happens for temperatures around 100 MeV [46, 47], when the quarks are low-energetic enough such that they confine into hadrons. It is unclear whether or not it would be a first-order phase transition, as the phase diagram is difficult to draw for QCD. While it can be relevant for observations [48, 49] and could influence what happens at BBN, the QCD cosmological phase transition is not directly related to an observable of the present universe, and has thus received relatively less attention than its older sister, the electroweak phase transition.

The ElectroWeak Phase Transition (EWPT) is of greater interest to us here, mainly because it relates directly to baryogenesis and leptogenesis, and shares similarities with the work done in this thesis. During the EWPT, happening around $T_{\text{EW}} \simeq 130$ GeV, the *vev* of the Higgs field becomes non zero. It is then only after the EWPT that all particles in the SM obtain vacuum masses. This is why it provides a good context for baryogenesis, as it leads the quark sector out of equilibrium while the non zero *vev* induces CP-violating Dirac masses for those same quarks. We will say more about this later, in section 2.5.

Phase transitions also occur in extensions of the Standard Model with new scalar fields, like for example in Grand Unified Theories such as $SU(5)$ or $SO(10)$ [16, 17]. The spontaneous breaking of the additional gauge symmetries is typically achieved through such phase transitions. It is therefore a phenomenon present in many particle physics models and that is of great cosmological interest.

We start by presenting a toy model of a phase transition in order to introduce notations and concepts. We explain how a cosmological phase transition can create bubbles (regions of the Universe with different properties) and how one can compute their properties. These bubbles will be of interest in the present work for bringing the plasma out-of-equilibrium. Cosmological phase transitions can also be constrained by cosmological observations and we say a few words on their phenomenology.

2.4.1 A toy model

For concreteness, let us consider a (real) scalar field S, interacting with the SM plasma at temperature T. It has a certain potential that can be decomposed into vacuum and thermal parts,

$$V_S(S,T) = V_0(S) + V_{\rm th}(S,T) \ . \tag{2.46}$$

The vacuum potential V_0 comes from the mass and self-interactions of S in vacuum, while the thermal potential $V_{\rm th}$ is derived from its interactions with the plasma of temperature T. In this section, we consider a toy model where we take

$$V_0(S) = -\frac{\mu^2}{2}S^2 + \frac{\lambda}{4}S^4 \ , \ \mu^2 > 0 \ , \ \lambda > 0 \ , \tag{2.47}$$

$$V_{\rm th}(S,T) = \frac{\alpha T^2}{2}S^2 - \frac{\beta T}{3}S^3 \ , \ \alpha > 0 \ . \tag{2.48}$$

The vacuum parameters μ^2 and λ determine the behaviour of S in the vacuum limit. Indeed, for $T \to 0$, the minimum of the potential would be achieved for $\langle S \rangle = \pm \left(\mu^2/\lambda\right)^{1/2}$. However, at finite temperature, the thermal potential modifies its extremum condition

$$\frac{\partial}{\partial S}V_S = \left(\alpha T^2 - \mu^2\right) S - \beta T S^2 + \lambda S^3 = 0 \ . \tag{2.49}$$

This equation has three solutions, provided

$$\beta^2 T^2 + 4\lambda\left(\mu^2 - \alpha T^2\right) > 0 \ . \tag{2.50}$$

One of these solutions corresponds to a local minimum, different from the one in $\langle S \rangle = 0$, located at

$$\langle S \rangle = v_S(T) = \frac{\beta T}{2\lambda}\left(1 + \sqrt{1 + \frac{4\left(\mu^2 - \alpha T^2\right)}{\beta^2 T^2}}\right) \ . \tag{2.51}$$

This minimum at $v_S(T)$ will be degenerate with the one in $\langle S \rangle = 0$ for

$$T = \sqrt{\frac{\mu^2}{\alpha}}\left(1 - \frac{2\beta^2}{9\alpha\lambda}\right)^{-1/2} \equiv T_c \ , \tag{2.52}$$

provided $9\alpha\lambda > 2\beta^2$.

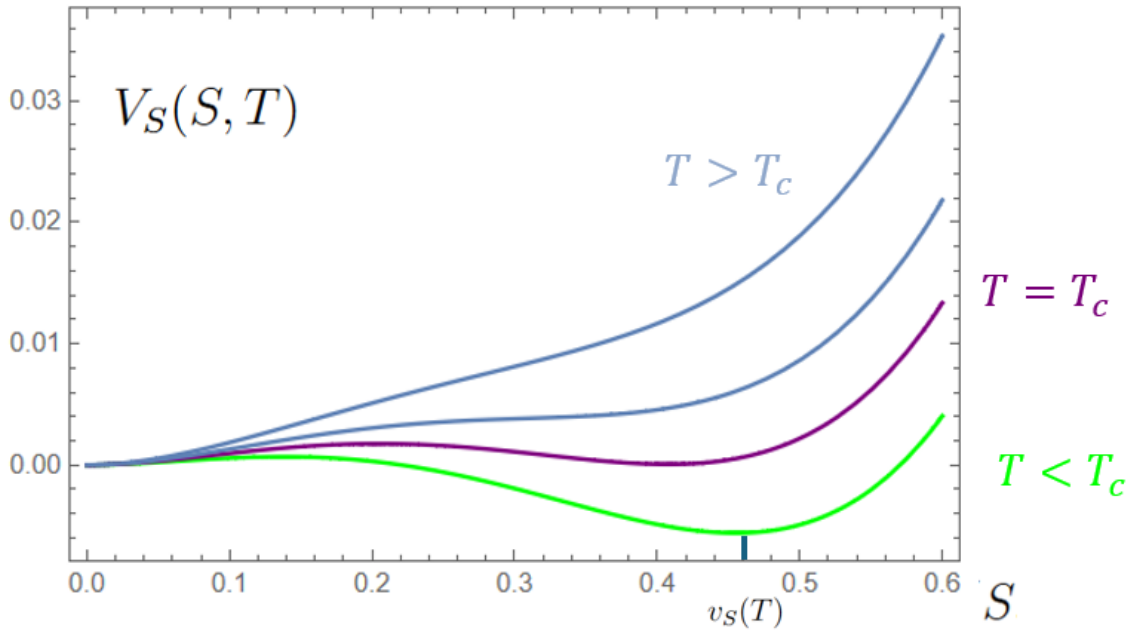

Figure 2.1: Evolution of the potential as a function of S for different values of T. We fixed $\alpha = 2$, $\mu^2 = 1$, $\beta = 3$ and $\lambda = 4$ for concreteness, giving $T_c = \sqrt{2/3}$.

We show in Figure 2.1 the potential profile at different temperatures. As temperature decreases, another non zero value of the scalar field becomes a local minimum. The critical temperature T_c corresponds to the temperature for which the value of the potential at the local minima $\langle S \rangle = v_S(T_c) \neq 0$ is exactly 0, therefore degenerate with $\langle S \rangle = 0$. The potential at temperature T_c, in our toy model, takes a nice factorized form

$$V_S(S, T_c) = \frac{\lambda}{4} S^2 \left(S - v_S(T_c)\right)^2 \ . \tag{2.53}$$

As soon as $T < T_c$ the global minimum jumps from 0 to $v_S(T) > 0$ in a discontinuous way, which makes this transition a First-Order Phase Transition (FOPT). Characterizing the transition a bit more, the FOPT can be called a *strong* FOPT [50, 51] iff

$$v_S(T_c) > T_c \ . \tag{2.54}$$

The gap between the two minima in 0 and v_S is larger in this case, which corresponds to a stronger discontinuity. This notion is very important for studies of baryogenesis with a phase transition; most scenarios require a strong FOPT, as we will see. In our toy model, the condition (2.54) is given in terms of the parameters of the model,

$$\frac{v_S(T_c)}{T_c} = \frac{2\beta}{3\lambda} > 1 \ . \tag{2.55}$$

Once the temperature is low enough, the preferred vacuum is changed and the phase transition starts. The way it then develops is through the nucleation of bubbles [1].

2.4.2 Nucleation of bubbles

The same way bubbles of gas form inside the water as it boils, a FOPT usually proceeds by **nucleation of bubbles**. These bubbles correspond to a region of space where the field is in its global minimum $\langle S \rangle = v_S(T)$, called *true vacuum*. Outside the bubble, the field is still in its local (but non global) minimum $\langle S \rangle = 0$, called *false vacuum*. The phase transition is complete when the bubbles have expanded enough to cover all the space, *i.e.* when all the water has boiled and turned to gas, in the boiling water analogy.

The bubble nucleation is interpreted as the decay from the vacuum in $\langle S \rangle = 0$ which becomes the false vacuum, into the newly formed true vacuum in $\langle S \rangle = v_S$. Due to the metastability of the false vacuum, thermal fluctuations are needed in order to exit the minimum in $\langle S \rangle = 0$. Taking those corrections into account, the probability (per unit volume $\mathcal{V}$ per unit time δt) of false vacuum decay at finite temperature [2] can be estimated [54–56]

$$\Gamma_{\text{bub}} \simeq T^4 \left(\frac{S_3(T)}{2\pi T} \right)^{3/2} \exp\left(-S_3(T)/T\right) , \tag{2.56}$$

where S_3 is the so-called "bounce" action in three spatial dimensions. It is defined as

$$S_3(T) = \int \mathrm{d}^3\mathbf{x} \left[\frac{1}{2} \left(\boldsymbol{\nabla} S_{b,T} \right)^2 + V_S(S_{b,T}(\mathbf{x}), T) \right] , \tag{2.57}$$

where $S_{b,T}$ is a static, $O(3)$-symmetric "bounce" solution. We will also refer to it as "static bubble", as it corresponds to the field configuration that will be allowed to form during the nucleation. It obeys the equation of motion

$$\nabla^2 S_{b,T} = \frac{\partial V_S}{\partial S}(S_{b,T}(\mathbf{x}), T) . \tag{2.58}$$

$\boldsymbol{\nabla} \equiv (\partial_x, \partial_y, \partial_z)$ is the nabla-differential operator in 3-dimensional space and $\boldsymbol{\nabla}^2$ gives the Laplacian. Note that $S_{b,T}$ depends on the temperature *via* the potential V_S. In a spherical symmetric space, the bounce solution depends only on $r \equiv |\mathbf{x}|$ (at fixed temperature). The equation of motion can be written in terms of derivatives with respect to r,

$$\frac{\mathrm{d}^2 S_{b,T}}{\mathrm{d}r^2} + \frac{2}{r} \frac{\mathrm{d}S_{b,T}}{\mathrm{d}r} = \frac{\partial V_S}{\partial S}(S_{b,T}(r), T) . \tag{2.59}$$

[1] There exist some subtleties about this statement, and in some cases a FOPT could complete without nucleating bubbles (see [52] for example). We consider that nucleation does happen in our case.

[2] At $T = 0$, without thermal fluctuations, the decay rate is given y quantum tunneling, which is related to $O(4)$-symmetric bounces instead of the $O(3)$-symmetric ones mentioned in the text in the thermal case, see for instance [53].

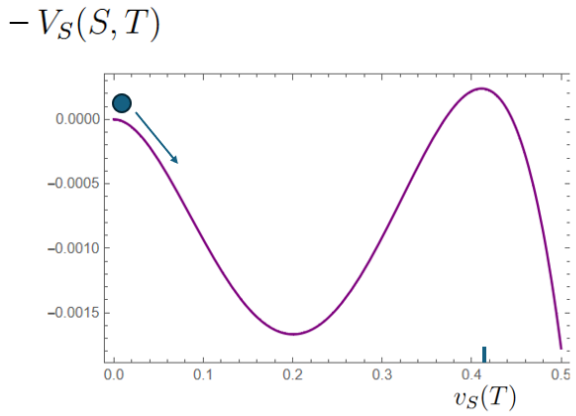

(a) Upturned potential $-V_S(S,T)$ for a temperature $T \lesssim T_c$ such that $V_S(0,T) \gtrsim V_S(v_S(T),T)$. We fixed $\alpha = 2$, $\mu^2 = 1$, $\beta = 3$ and $\lambda = 4$. The temperature is $T = 0.815 \lesssim T_c = \sqrt{2/3}$.

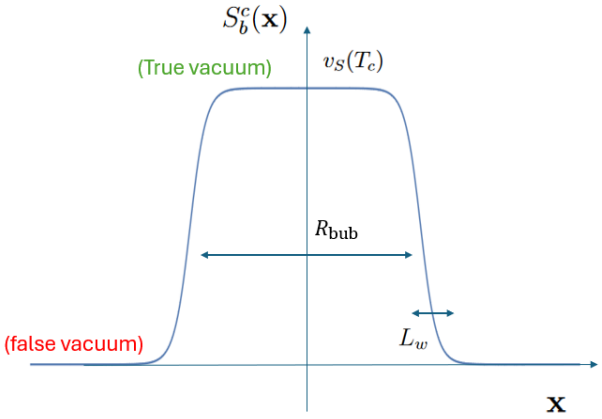

(b) Sketch of the "bounce" (or static bubble) solution S_b^c, reaching the false vacuum for $|\mathbf{x}| \to \infty$ and bouncing off the true vacuum in $|\mathbf{x}| = 0$. We sketched two physical length, the radius R_{bub} of the static bubble and the thickness of the wall L_w.

The mechanical analog of this equation is a particle at "position" $S_{b,T}$ evolving through "time" r, falling in an upturned potential $-V_S$ (see Figure 2.2a). The additional term $\frac{2}{r}\frac{\mathrm{d}S_{b,T}}{\mathrm{d}r}$ plays the role of friction. The bounce solution is assumed to be at rest in the center of our coordinate system

$$\frac{\mathrm{d}}{\mathrm{d}r} S_{b,T}(r=0) = 0 \tag{2.60}$$

and it should reach the false vacuum ($\langle S \rangle = 0$) at infinity and remain at rest there,

$$S_{b,T}(r \to \infty) = 0 \ , \ \frac{\mathrm{d}}{\mathrm{d}r} S_{b,T}(r \to \infty) = 0 \ . \tag{2.61}$$

In order to understand these equations a bit better, let us consider our toy model for the scalar potential. We recall that, close to the critical temperature $T \simeq T_c$, we had

$$V_S(S,T_c) = \frac{\lambda}{4} S^2 \left(S - v_S(T_c)\right)^2 \ . \tag{2.62}$$

The equation for $S_{b,T_c} \equiv S_b^c$ is then

$$\frac{\mathrm{d}^2 S_b^c}{\mathrm{d}r^2} + \frac{2}{r}\frac{\mathrm{d}S_b^c}{\mathrm{d}r} = \frac{\lambda}{2} S_b^c \left(S_b^c - v_S(T_c)\right)\left(2S_b^c - v_S(T_c)\right) \ , \tag{2.63}$$

which actually has an approximate analytical solution (see for example [57]),

$$S_b^c(r) = \frac{v_S(T_c)}{2}\left[1 - \tanh\left(\frac{r - R_{\text{bub}}}{L_w}\right)\right] \ , \tag{2.64}$$

where

$$L_w \equiv \left(\alpha T_c^2 - \mu^2\right)^{-1/2} \tag{2.65}$$

is fixed by the parameters of the potential, and where $R_{\rm bub}$ is an arbitrary constant as long as it satisfies

$$R_{\rm bub} \gg L_w \ . \tag{2.66}$$

Both quantities can be interpreted for this profile, $R_{\rm bub}$ as the radius of the static bubble, and L_w as the thickness of the wall of this bubble. The condition $R_{\rm bub} \gg L_w$ is therefore usually referred to as the "thin wall approximation" in the literature. We draw the profile S_b^c in Figure 2.2b.

Looking at the profile $S_b^c(\mathbf{x})$, we understand why such solutions are called "bounces". Along a certain spatial direction, the field configuration starts from the false vacuum, gets up to the true vacuum, and gets back down to the false vacuum. It "bounces" off the "bump" of true vacuum in $\mathbf{x} = \mathbf{0}$. The region around $|\mathbf{x}| = 0$ is understood as a **static bubble** of true vacuum, of radius $R_{\rm bub}$ and wall thickness L_w, inside a space filled with false vacuum.

More generally, these bounce solutions depend on the potential $V_S(S_{b,T}, T)$, and therefore on temperature. Given a certain potential V_S, finding the rate $\Gamma_{\rm bub}$ requires to solve numerically for $S_{b,T}$ and plug it back in S_3 for computing the bounce action. Publicly available codes [58–60] can be used for these purposes.

Once the rate $\Gamma_{\rm bub}$ is computed, it is used to define the *nucleation* temperature T_n, which is the temperature at which one bubble is created per Hubble volume, satisfying the condition [61, 62]

$$1 = \int_{t_c}^{t_{\rm nucl}} {\rm d}t \ \Gamma_{\rm bub} H^{-3} = \int_{T_n}^{T_c} {\rm d}T \ \frac{\Gamma_{\rm bub}(T)}{T H(T)^4} \ . \tag{2.67}$$

$t_{\rm nucl}$ and t_c are the cosmological times corresponding to the temperatures T_n and T_c, respectively (using the relation $t = 1/(2H(T)) = a_R/(2T^2)$). From the expression of the rate 2.56, we only need to determine the bounce action in order to get the nucleation temperature of our phase transition. Depending on the temperature dependence of the potential, T_n can be more or less separated from T_c. Phase transitions for which the actual nucleation happens long after the critical temperature are characterized as **supercooled**. In such supercooled phase transitions, the metastable false vacuum survives longer than in standard phase transitions, and $T_n \ll T_c$. It can be explicitly realized for example with a large potential barrier between the false and the true vacua, such that thermal fluctuations are not sufficient (at first) to go over it. We will come back to this point; we should keep in mind that the nucleation temperature T_n can be well below the critical temperature T_c.

2.4.3 Dynamics of the bubbles

Let us go now to bubbles. We described how to obtain the decay rate $\Gamma_{\rm bub}$ of the false vacuum. We computed this decay of false vacuum by finding static solutions $S_{b,T}$ to the equations of motions. Once the false vacuum decays, we obtain field configurations, that we call bubbles, that satisfy similar conditions than $S_{b,T}$ (the static bubble): spatially, they correspond to false

vacuum at infinity and true vacuum at some point in space which will be the center of the bubble, of certain radius $R_{\rm bub}$. The main difference, however, is that the bubbles are not static, but dynamical. It can be easily understood why it has to be so; the true vacuum is energetically favorable, so the energy density is lower inside the bubble than outside. This leads to a pressure difference that tends to expand and accelerate the bubble.

The radius $R_{\rm bub} = R_{\rm bub}(t)$ of the bubble is then time-dependent. There is a vast literature on determining what the velocity of the bubble is; here is a (non-exhaustive) list of studies [63–66]. Because of friction between the wall and the plasma, the bubble wall is expected to reach a terminal velocity that we note v_w. Its precise determination depends on the hydrodynamics of the fluid in front of the wall, as well as on the energy difference between the false and true vacuum. In particular, for supercooled phase transitions, the energy release is important, the bubbles are accelerated [52,67–69] and quickly reach velocities close to the speed of light $v_w \simeq 1$. We can for now simply take v_w as a parameter; if it is constant, the radius of a typical bubble expanding at the time of nucleation then evolves like

$$R_{\rm bub}(t) \simeq v_w \left((t - t_{\rm nucl}\right) \equiv v_w \Delta t \ , \tag{2.68}$$

where $t_{\rm nucl}$ is the cosmological time at which the nucleation happens. In the case where the potential is given by our toy model, using the expression for the bounce solution leads to a profile of the field (at the critical temperature)

$$S(t,r) \equiv S_b^c(r)\Big|_{R_{\rm bub}=R_{\rm bub}(t)} = \frac{v_S(T_c)}{2}\left(1 + \tanh\left(\frac{v_w \Delta t - r}{L_w}\right)\right) \ , \tag{2.69}$$

where v_w is the velocity of the wall and L_w is its spatial thickness. At a fixed position x, the *vev* of the scalar field is evolving at a certain rate in time γ given by

$$\gamma = \frac{v_w}{L_w}. \tag{2.70}$$

The time rate $\gamma = v_w/L_w$ is calculated from the thickness of the wall and its velocity.

2.4.4 Phenomenology

If a phase transitions did indeed happen in the history of our Universe, we would like to test this hypothesis. The phenomenology of cosmological phase transitions is very interesting, mainly for two reasons. We know there should be "something", as the SM already predicts the electroweak and the QCD phase transitions, and at the same time we can constrain models of new physics involving new fields undergoing a phase transition, for example. Ideally, we would like to constraint the temperature T_n of bubble nucleation, in order to know when exactly in the early Universe it occurred. However, another important parameter that determines if a phase transition will be observable or not is its strength α_n defined by

$$\alpha_n \equiv \frac{\Delta V_S(T_n)}{\rho_{\rm SM}(T_n)} \ . \tag{2.71}$$

$\Delta V_S(T_n)$ is the potential energy difference between the false and true vacuum, at the temperature of nucleation. It represents the amount of energy released from the false vacuum decay, through the nucleation of bubbles. The strength α_n compares it to the energy already present in the plasma, $\rho_{\rm SM}(T_n)$. A crucial effect of this energy release is *reheating*. The vacuum energy ΔV_S is converted into thermal energy in the plasma, increasing the temperature to a reheating temperature $T_{\rm reh}$, by conservation of energy

$$\rho_{\rm plasma}(T_{\rm reh}) \simeq \rho_{\rm plasma}(T_n) + \Delta V_S(T_n) \ . \tag{2.72}$$

If the plasma is dominated by Standard Model radiation, given that $\rho_{\rm plasma}(T) = \rho_{\rm SM}(T) \propto T^4$ in that case, we obtain

$$\left(\frac{T_{\rm reh}}{T_n}\right)^4 = 1 + \alpha_n \ . \tag{2.73}$$

For a given nucleation temperature, the stronger the phase transition (the larger α_n, that is), the more impact it has on observables.

Several cosmological observables can be considered in order to constrain the properties of the phase transition. In particular, a relatively strong (α_n around 1) FOPT modifies the temperature evolution of photons, leptons, neutrinos in the bath, due to reheating. For nucleation temperatures $T_n \sim$ MeV, this can affect Big Bang Nucleosynthesis (BBN), in modifying the freeze-out temperature of various quantities like the neutron fraction. It can also modify the effective relativistic degrees of freedom $N_{\rm eff}$ obtained from the Cosmic Microwave Background (CMB), which depends on the freeze-out temperatures of neutrinos and photons. Combined analysis of these constraints give [70] reheating temperature of a FOPT with $\alpha_n = 1$ to be $T_{\rm reh} > 3$ MeV, equivalently $T_n > 2^{-1/4}3$ MeV ≈ 2.5 MeV.

Another popular avenue for constraining cosmological phase transitions, and in particular (strongly) first-order ones, is the detection of primordial gravitational waves. Indeed, the vacuum energy stored in the scalar sector gets released during the phase transition and can produce gravitational waves. Experiments like LIGO, Virgo or in the future LISA can then detect these waves. Such waves are typically described as being part of a Stochastic Gravitational Wave Background (SWBG). It corresponds to the superposition of GW coming from different sources across the Universe and from the past, like binary systems, primordial fluctuations, cosmic strings or cosmological phase transitions (see [71] for a review). This background has recently been detected, in 2023, by the NANOGrav collaboration [72]. By surveying pulsars, they were able to find perturbations of their frequencies that were due to nano-Hertz GW passing by. The preferred explanation of these waves is the superposition of massive binary systems.

Future experiments with higher sensitivity and wider frequency range might be able to tell us more about the SGWB. In this thesis, we consider first-order phase transitions; their gravitational wave signature has been well studied in order to predict, for a given phase transition, the frequency range and amplitude of the emitted GW. We will not attempt a comprehensive review of how the GW spectrum is established from the parameters of a cosmological phase

transition; we refer the reader to reviews on this topic such as [71,73,74]. In short, what we can say is that there are three main sources that are expected to produce GW during a first-order cosmological phase transition [75–77]: collisions between bubbles, sound waves in the plasma, and turbulence in the plasma.

For each of these phenomena, a peak frequency f_{peak} and a shape of the GW spectrum $\Omega_{\text{GW}}h^2$ can be estimated from the parameters of the phase transition (see discussion in [76, 77] for example). Once (and if) the SGWB is detected, more details about phase transitions could then be constrained from the profile of the frequency spectrum. For instance, with the projected sensitivity of LISA [78] of GW frequencies around the mHz range, it was estimated [79] that a rather strong phase transition ($\alpha_n = 1$) happening at temperatures up to $T = 10^6$ GeV could emit a detectable GW spectrum. This would allow GW detection to be a great test of new physics phenomena happening at high energies. In this thesis, we will focus on such phase transitions involving new physics, in order to explain the baryon asymmetry of the Universe.

2.5 Baryogenesis and CP violation

One of the goals of this thesis is to explain the Baryon Asymmetry of the Universe (BAU). We recall the Sakharov conditions, necessary for the creation of a BAU:

- (1) Violation of the baryon or lepton number,
- (2) C and CP violation,
- (3) Out of equilibrium evolution at some point in the Universe.

One may now ask if such conditions are already met in the Standard Model. The answer is actually yes, these conditions are satisfied with the current theory that we have, without needing to introduce any new physics:

- (1) $B + L$ (and B) is anomalous in the SM,
- (2) The CKM matrix and the weak interactions violate C and CP,
- (3) The ElectroWeak Phase Transition (EWPT) drives the system out of equilibrium.

However, it was shown (see for example [80] or reviews [81–83]) that the amount of CP violation in the SM is actually too small to reproduce the BAU, and that the EWPT should be strongly first-order, which it is not in the SM [84, 85]. It is instructive to say a few words on this last point. First of all, the B-violating processes in the SM are the so-called sphalerons. We will say more about them at the beginning of next section; what we will say here is that they are topological processes, connecting different vacua of the theory, which have different baryon numbers B. At zero temperature, they are suppressed by potential barriers between the vacua,

but at finite temperature they can be efficient at violating B. For weak sphalerons (associated to the gauge group $SU(2)_L$ of the SM), their energy $E_{\rm sph}(T)$ is related to $\langle\phi\rangle(T)$, the *vev* of the Higgs field. Without detailing all the calculation (see for example [83]), one can compute the rate $\Gamma_{\rm sph}$ of these spalerons at finite temperature and obtain

$$\Gamma_{\rm sph} \propto e^{-E_{\rm sph}(T)/T} \ , \ E_{\rm sph}(T) \propto \langle\phi\rangle(T) \ . \tag{2.74}$$

Due to the third Sakharov condition, sphalerons should be out-of-equilibrium [86] at the critical temperature $T_c = T_{\rm sph} \simeq 130$ GeV of the EWPT. This means their rate $\Gamma_{\rm sph}$ should be smaller than the Hubble rate (at $T = T_c$)

$$\Gamma_{\rm sph}(T_c) \lesssim H(T_c) \ . \tag{2.75}$$

This leads to a lower bound on $E_{\rm sph}(T_c)/T_c$ which can be written in terms of the *vev* [83],

$$\frac{\langle\phi\rangle(T_c)}{T_c} \gtrsim 1 \ . \tag{2.76}$$

This is simply the condition (2.54) for having a strong first-order phase transition! This tells us that, if sphalerons are the only B-violating process and we wish to reproduce the baryon asymmetry, the EWPT should be a strongly first-order phase transition.

In order to see if this is realized or not in the SM, we need to study the Higgs potential. In the SM, the scalar potential for the Higgs field has a vacuum part (related to its mass and self-coupling) and a thermal part coming from the dense early Universe plasma at temperature T. The computation of the total potential, at high temperatures, can be computed using thermal field theory [87] and we obtain a well-known form [88–91]

$$V_\phi(\phi, T) = \frac{\alpha T^2 - \mu^2}{2}\phi^2 - \frac{\beta T}{3}\phi^3 + \frac{\lambda}{4}\phi^4 \ , \tag{2.77}$$

where α and β are related to the particles interacting with the Higgs, namely the W and Z bosons and the top-quark,

$$\alpha = \frac{2m_W^2 + m_Z^2 + 2m_t^2}{8v^2} \ , \tag{2.78}$$

$$\beta = \frac{6m_W^3 + 3m_Z^3}{4\pi v^3} \ . \tag{2.79}$$

This is the potential we studied in our toy-model in section 2.4. Recall we derived that a strongly first-order phase transition should satisfy

$$\frac{v_S(T_c)}{T_c} = \frac{2\beta}{3\lambda} = \frac{4\beta v^2}{3m_h^2} > 1 \ . \tag{2.80}$$

We related λ to the Higgs mass $m_h^2 = 2\lambda v^2$. Numerically, taking $m_W = 80$ GeV, $m_Z = 91$ GeV and $v = 246$ GeV the condition above gives

$$m_h^2 < (48 \text{ GeV})^2 \ , \tag{2.81}$$

which we know is incorrect since the measure in 2012 of a Higgs particle at a mass around $m_h \simeq 125$ GeV. This failure of the SM makes the BAU a new physics observable, and has motivated numerous extensions of the particle content.

Arguably, there are two main popular ways of explaining the baryon asymmetry. One of them is electroweak baryogenesis [43] whose main idea is to modify the EWPT to make baryogenesis successful, usually by adding new scalars that are SM singlets [92–95]. This qualitative change allows a stronger departure from equilibrium. The B-violating processes are the sphalerons, and an extra source of CP-violation is needed compared to the SM. The baryon asymmetry is then generated by the dynamics of quarks during the phase transition.

Another alternative is leptogenesis [11]. Instead of considering the baryonic sector of the Standard Model, this approach focuses on the lepton part. The lepton sector is extended with new sources of CP- and L-violation, such that a lepton asymmetry can be created. Leptogenesis relies on the $B+L$-violating sphaleron processes to convert the lepton asymmetry into a baryon one. We will detail how this works in the next section.

Chapter 3

Leptogenesis and sterile neutrinos

A popular approach for explaining the BAU is leptogenesis, and in particular leptogenesis involving right-handed (or sterile) neutrinos. These new particles have Yukawa interactions with the Higgs and lepton fields, adding CP-violating terms that can create an asymmetry between leptons and anti-leptons. This asymmetry can then be converted into a baryon asymmetry through the so-called sphaleron processes. Sterile neutrinos are also motivated from particle physics experiments for explaining the masses of active neutrinos in the SM.

In this chapter, we review some of the basics of leptogenesis and general properties of sterile neutrinos. We start by explaining how a lepton asymmetry gets converted into a baryon asymmetry in section 3.1. We detail in section 3.2 why sterile neutrinos are good candidates for an extension of the SM, and introduce the type-I Seesaw mechanism, which connects the masses of the sterile neutrinos to the masses of the active neutrinos. Finally, we present in section 3.5 a scalar extension in which the sterile neutrino masses are given from the interaction with a scalar field.

3.1 Sphalerons and spectator effects

The asymmetry observed from the CMB and light-element abundances is really an asymmetry in the baryonic sector, so we start by explaining how a lepton asymmetry can help create a baryon asymmetry, through sphalerons.

Sphalerons (from the Greek $\sigma\phi\alpha\lambda\epsilon\rho o\zeta$, "ready to fall") are described as potential barriers [96] that separate different vacua of non-abelian gauge theories [97,98] (in the SM, we are concerned with $SU(2)$ and $SU(3)$). Indeed, certain charges (the baryon number B and the lepton number in each flavor $L_{e/\mu/\tau}$) are preserved classically in the SM, but are anomalous in the sense that quantum fluctuations can violate this conservation. In particular, while $B-L$ is still preserved, $B+L$ is anomalous and is violated by sphalerons. This violation is however topological (it depends on the topology of the gauge groups) and corresponds to integer changes in the charges,

between different vacua (defined by the values of the charges in them). Because they connect vacua of different lepton and baryon number, we can also picture them as processes that change the value of $B + L$.

Sphaleron processes are non-perturbative and are exponentially suppressed at zero temperature, however, in a cosmological context, thermal fluctuations activate them at higher temperature. There thus exists a finite temperature T_{sph} above which the SM allows to change the values of B and L, and under which these processes are exponentially suppressed.

This phenomenon is crucial for baryogenesis through leptogenesis. For temperatures above T_{sph}, if we start with $B = 0$ and $L \neq 0$ (we suppose we created a lepton asymmetry), sphalerons can modify the value of L and convert it into $B \neq 0$, because we need to conserve $B - L$ in the process. As a conclusion, a model that can create a non-zero lepton number $L \neq 0$ at temperatures above T_{sph} can also explain a non-zero baryon asymmetry.

It is convenient, for species near thermal equilibrium like the ones in the SM, to consider their chemical potential. For a species X, the chemical potential μ_X is defined from the distributions of the particle f_X and of the anti-particle $f_{\overline{X}}$,

$$f_X(E) = f_{\text{eq}}\left(E - \mu_X\right) \ , \ f_{\overline{X}}(E) = f_{\text{eq}}\left(E + \mu_X\right) \ , \tag{3.1}$$

where f_{eq} is either the Fermi-Dirac $f_{FD}(E) = \left(\exp\left(E/T\right) + 1\right)^{-1}$ distribution for fermions or the Bose-Einstein distribution $f_{BE} = \left(\exp\left(E/T\right) - 1\right)^{-1}$ for bosons. We are interested in asymmetries between particles and anti-particles, which for small chemical potential give

$$f_X - f_{\overline{X}} \simeq -\mu_X \ f'_{\text{eq}}(E) = \frac{\mu_X}{T} \left| \begin{array}{ll} f_{FD}\left(1 - f_{FD}\right) & \text{for fermions,} \\ f_{BE}\left(1 + f_{BE}\right) & \text{for bosons.} \end{array} \right. \tag{3.2}$$

Integrating over momentum, we obtain a relation for the asymmetry in the number densities, expressed either with physical N_X or rescaled $n_X \equiv N_X/T^3$ number densities,

$$N_X \equiv 2 g_X \int \frac{\mathrm{d}^3\mathbf{k}}{(2\pi)^3} \ f_X \ , \tag{3.3}$$

$$N_X - N_{\overline{X}} \simeq \frac{g_X T^3}{6} \frac{\mu_X}{T} \times \left| \begin{array}{ll} 1 & \text{for massless fermions,} \\ 2 & \text{for massless bosons,} \end{array} \right. \tag{3.4}$$

$$n_X - n_{\overline{X}} \simeq \frac{g_X}{6} \frac{\mu_X}{T} \times \left| \begin{array}{ll} 1 & \text{for massless fermions,} \\ 2 & \text{for massless bosons,} \end{array} \right. \tag{3.5}$$

where g_X is the number of (non-spinorial) degrees of freedom of particle X.

While the particle distributions can be deviating from equilibrium due to these chemical potentials, interactions between different species can be fast enough to connect the chemical potentials to each other. For each interaction at equilibrium, there exists a relation between the chemical potentials of the various SM species subject to this interaction. These SM interactions are often referred to as spectator effects in leptogenesis.

Gauge interactions When the gauge interactions are at thermal equilibrium, this implies that all gauge bosons chemical potential are zero and that all fermions in a same $SU(3)$ or $SU(2)$ multiplet should have the same chemical potential. We then consider μ_{Q_a}, μ_{u_a}, μ_{d_a}, indexed on flavor, in the quark sector and μ_{l_a}, μ_{e_a} in the lepton sector. The SM plasma should also be neutral under hypercharge,

$$\sum_a (\mu_{Q_a} + 2\mu_{u_a} - \mu_{d_a} - \mu_{l_a} - \mu_{e_a}) + 2\mu_\phi = 0 \ . \tag{3.6}$$

Yukawa interactions In the SM, the left-handed $SU(2)$-doublets l_a and Q_a also interact with the Higgs and right-handed fields through Yukawa couplings. If these interactions are at equilibrium,

$$\mu_{Q_a} - \mu_{u_a} + \mu_\phi = 0 \ , \tag{3.7}$$

$$\mu_{Q_a} - \mu_{d_a} - \mu_\phi = 0 \ , \tag{3.8}$$

$$\mu_{l_a} - \mu_{e_a} - \mu_\phi = 0 \ . \tag{3.9}$$

Sphalerons They are two types of sphalerons processes in the SM corresponding to the two (non-abelian) gauge groups $SU(2)$ for weak interactions and $SU(3)$ for strong interactions. Accordingly, we have strong QCD sphalerons [99, 100], which at equilibrium impose

$$\sum_a (2\mu_{Q_a} - \mu_{u_a} - \mu_{d_a}) = 0 \ , \tag{3.10}$$

while weak sphalerons [96, 101] at equilibrium give

$$\sum_a (3\mu_{Q_a} + \mu_{l_a}) = 0 \ . \tag{3.11}$$

We insist that all these relations are only true if the corresponding process is at thermal equilibrium. The equilibrium condition of a certain process is usually estimated by comparing, at a given temperature T, the rate $\Gamma(T)$ of the process to the Hubble rate $H(T)$. We need the process to be faster than the expansion of the Universe, *i.e.* $\Gamma(T) > H(T)$, in order to consider it at thermal equilibrium. As the Universe expands and the temperature evolves, processes will arrive or depart from equilibrium, and which relations among chemical potentials we can use depends on the temperature.

In a study of baryogenesis and leptogenesis, the relevant combination of chemical potentials describing the baryon B and lepton L numbers are

$$\mu_B \equiv \sum_a (2\mu_{Q_a} + \mu_{u_a} + \mu_{d_a}) = \sum_a \mu_{B_a} \ , \tag{3.12}$$

$$\mu_L \equiv \sum_a (2\mu_{l_a} + \mu_{e_a}) = \sum_a \mu_{L_a} \ . \tag{3.13}$$

From the previous relations, as long as weak sphalerons and Yukawa interactions are at equilibrium, one has

$$\mu_B = 4\sum_a \mu_{Q_a} \equiv 4\mu_Q \ , \tag{3.14}$$

$$\mu_L = \sum_a (2\mu_{l_a} + \mu_{e_a}) = 3\mu_\phi + 3\sum_a \mu_{l_a} = 3\mu_\phi - 9\mu_Q \ . \tag{3.15}$$

Moreover, the hypercharge neutrality implies

$$\begin{aligned} 2\mu_\phi &= -\sum_a (\mu_{Q_a} + 2\mu_{u_a} - \mu_{d_a} - \mu_{l_a} - \mu_{e_a}) \\ &= -\sum_a (2\mu_{Q_a} + 3\mu_\phi - 2\mu_{l_a} + \mu_\phi) \\ &= -12\mu_\phi - 8\mu_Q \end{aligned} \tag{3.16}$$

such that $7\mu_\phi = 4\mu_Q$ and ultimately

$$\mu_L = -\frac{51}{7}\mu_Q \ , \tag{3.17}$$

$$\mu_{B-L} = \frac{79}{7}\mu_Q \ . \tag{3.18}$$

One can recover the well-known [44, 102] relation

$$\mu_B = \frac{28}{79}\mu_{B-L} \ . \tag{3.19}$$

This last equation is fundamental for leptogenesis. It explains how a $B-L$ (or simply L) asymmetry is converted into the desired baryon asymmetry. Note that this holds only before the weak sphalerons decouple at $T_{\rm sph} \simeq 130$ GeV [86]; any leptogenesis scenario, trying to explain the baryon asymmetry from the lepton sector, should be realized at higher temperatures $T > T_{\rm sph}$.

It will also be useful later to relate the (flavored) $\Delta_a \equiv n_{B/3} - n_{L_a}$ asymmetry to other chemical potentials. In particular, leptogenesis will be concerned with sterile neutrinos interacting (*via* Yukawa couplings) to the lepton and Higgs fields. We therefore look for relations between μ_{l_a}, μ_ϕ and Δ_a,

$$\frac{\mu_{l_a}}{T} = \sum_b C^l_{ab}\Delta_b \ , \ \ \frac{\mu_\phi}{T} = \frac{1}{2}\sum_b C^\phi_b \Delta_b \ , \tag{3.20}$$

$$\frac{\mu_{l_a} + \mu_\phi}{T} = \sum_b \left(C^l_{ab} + C^\phi_b/2\right)\Delta_b \equiv \sum_b \mathcal{A}_{ab}\Delta_b \ , \tag{3.21}$$

where Δ_a is the (rescaled) number density associated to the $B/3 - L_a$ number, related to the chemical potentials in the SM by

$$\Delta_a = \frac{1}{6}\frac{\mu_{\Delta_a}}{T} = \frac{1}{6}\left[\sum_b \frac{1}{3}(2\mu_{Q_b} + \mu_{u_b} + \mu_{d_b}) - (2\mu_{l_a} + \mu_{e_a})\right] \ . \tag{3.22}$$

The matrices C^l and C^ϕ are determined (after some algebra) from the equilibrium conditions described above (see for example [103–105]). They also only make sense for the flavors that are close to thermal equilibrium and are entitled to have a chemical potential. In the lepton sector, the τ is the first to equilibrate around $T \sim 10^{12}$ GeV, followed by the muon μ at $T \sim 10^{10}$ GeV, and finally the electron e has the smallest Yukawa couplings in the SM and equilibrates around $T \sim 10^6$ GeV (for a more detailed study of equilibration rates, see [106]). This determines four ranges of temperature in which 0, 1, 2 or 3 lepton flavors are defined. In this study, we will only be concerned with temperatures below $T < 10^{12}$ GeV, so let us only mention the three other range of temperatures. We give the different set of matrices taken from [103] summarized in Table 3.1. The boundaries are not exact and could be refined by considering the equilibration temperature of each Yukawa interaction more carefully; we will however fix them like this in this study.

10^{12} GeV $> T > 10^{10}$ GeV	10^{10} GeV $> T > 10^6$ GeV	10^6 GeV $> T$
$C^l = \frac{1}{460}\begin{pmatrix} -196 & 24 \\ 9 & -156 \end{pmatrix}$	$C^l = \frac{1}{2148}\begin{pmatrix} -906 & 120 & 120 \\ 75 & -688 & 28 \\ 75 & 28 & -688 \end{pmatrix}$	$C^l = \frac{1}{711}\begin{pmatrix} -221 & 16 & 16 \\ 16 & -221 & 16 \\ 16 & 16 & -221 \end{pmatrix}$
$C^H = -\frac{1}{230}(41\ 56)$	$C^H = -\frac{1}{358}(37\ 52\ 52)$	$C^H = -\frac{8}{79}(1\ 1\ 1)$
$\mathcal{A} = \frac{-1}{460}\begin{pmatrix} 237 & 32 \\ 32 & 212 \end{pmatrix}$	$\mathcal{A} = \frac{-1}{2148}\begin{pmatrix} 1017 & 36 & 36 \\ 36 & 844 & 128 \\ 36 & 128 & 844 \end{pmatrix}$	$\mathcal{A} = \frac{-1}{711}\begin{pmatrix} 257 & 20 & 20 \\ 20 & 257 & 20 \\ 20 & 20 & 257 \end{pmatrix}$

Table 3.1: Relevant matrices for different range of temperatures.

3.2 Sterile neutrinos and the type-I Seesaw

As we just showed, a theory that can produce a lepton asymmetry could explain the Baryon Asymmetry of the Universe (BAU). Leptogenesis describes the set of theories that aim at producing a lepton asymmetry in the SM, for example by extending it with additional particles, interacting with the lepton sector. To do so, sterile neutrinos, also referred to as right-handed neutrinos, are interesting candidates; they are already considered for a physical problem that is not related to the BAU, namely explaining the masses of active neutrinos.

Indeed, active neutrinos in the SM are the only fermions for which we have only detected a left-handed particle (and right-handed antiparticle). In particular, in the SM, they have no Yukawa interactions with the Higgs field and are therefore predicted to be massless. This prediction has been contradicted for over 20 years now by observations of neutrino oscillations, that is, the fact that a neutrino in a given flavor can be later measured in another flavor. They

were first evidenced with atmospheric neutrinos by Super-Kamiokande [13] in 1998 and not long after with solar neutrinos by the Sudbury Neutrino Observatory (SNO) [14] in 2001-2002. These oscillations were verified in numerous experiments and in various contexts since then, and these achievements were acknowledged by the 2015 Nobel Prize awarded to Takaaki Kajita and Arthur B. McDonald. Let us briefly explain why oscillations imply that neutrinos have a mass. Consider for instance a situation with two flavors of neutrinos, say the electron neutrino $|\nu_e\rangle$ and the muon neutrino $|\nu_\mu\rangle$. They form a two-dimensional Hilbert space. Consider the emission of an electron neutrino at a time $t = 0$, in a given experiment. It corresponds to a flavor eigenstate (an eigenstate of weak interactions) that does not necessarily coincide with the mass eigenstates $(|\nu_1\rangle, |\nu_2\rangle)$ that diagonalize the Hamiltonian. The emitted electron neutrino is then a linear combination of the mass eigenstates,

$$|\nu(t=0)\rangle = |\nu_e\rangle = \cos(\theta)\,|\nu_1\rangle + \sin(\theta)\,|\nu_2\rangle \ . \tag{3.23}$$

Considering a spatial momentum $\mathbf{k}$ for the neutrino, each eigenstate ν_i of the Hamiltonian has a definite energy $E_i = \sqrt{|\mathbf{k}|^2 + m_i^2} \simeq |\mathbf{k}| + m_i^2/(2|\mathbf{k}|)$ in the relativistic case (where the m_i's are the masses, but could be zero). As they propagate, the energy eigenstates evolve with a phase e^{-iE_it} such that

$$|\nu(t)\rangle = \cos(\theta)e^{-iE_1t}\,|\nu_1\rangle + \sin(\theta)e^{-iE_2t}\,|\nu_2\rangle \ . \tag{3.24}$$

The "survival" probability that our emitted neutrino remained an electron neutrino after travelling a distance $L = ct$ is given by the projection on $|\nu_e\rangle$ of the state at time t,

$$\begin{aligned} P_{\nu_e\to\nu_e}(t) \equiv |\langle\nu_e|\,\nu(t)\rangle|^2 &= 1 - \sin^2(2\theta)\sin^2\left(\frac{E_2 - E_1}{2}t\right) \\ &= 1 - \sin^2(2\theta)\sin^2\left(\frac{m_2^2 - m_1^2}{4|\mathbf{k}|}t\right) \ . \end{aligned} \tag{3.25}$$

Here comes the crucial observation: if the masses were degenerate $m_1 = m_2$, the probability $P_{\nu_e\to\nu_e}$ is constant equal to 1 at all times, and no oscillations should occur. The fact that we observe oscillations contradicts this and means that the two masses m_1 and m_2 are different. In particular, one of the two masses (at least) should be non-zero.

In the Standard Model we have three neutrino flavors, so we consider three mass eigenstates m_1, m_2 and m_3. In neutrino oscillations, m_2^2 is measured to be greater than m_1^2 from solar neutrinos, while the difference $m_3^2 - m_1^2$ is only known in absolute value from atmospheric neutrinos. Therefore, m_3^2 could be greater or smaller than the two other masses. These two options are not yet fully differentiated by experiments and observations. The ordered choice $m_1 < m_2 < m_3$ is called Normal Ordering (NO), while the second choice $m_3 < m_1 < m_2$ is called Inverse Ordering (IO). Moreover, experimentally, $\Delta m_{21}^2 \ll |\Delta m_{31}^2| \simeq |\Delta m_{32}^2|$. This means we have two non-zero and distinct mass gaps, and therefore at least two non-zero masses. The recent NuFIT 5.3 (2024) [107] gives the best fit for the squared mass differences,

$$\Delta m_{21}^2 = (7.41 \pm 0.61) \times 10^{-5}\ \text{eV}^2 \ , \tag{3.26}$$

$$\Delta m_{31}^2 = (2.505 \pm 0.08) \times 10^{-3}\ \text{eV}^2\ [\text{NO}] \ , \ \Delta m_{32}^2 = -(2.487 \pm 0.08) \times 10^{-3}\ \text{eV}^2\ [\text{IO}] \ , \tag{3.27}$$

where uncertainties were given at the 3σ confidence level. The squared mass gap Δm^2_{21} measured from solar neutrinos is fitted to the same value in both ordering, while the squared mass gap Δm^2_{3l} from atmospheric neutrinos depends on the ordering, $\Delta m^2_{3l} = \Delta m^2_{31} > 0$ for NO, $\Delta m^2_{3l} = \Delta m^2_{32} < 0$ for NO.

A simple way to explain these oscillations is to allow the neutrinos to have a Yukawa interaction with a right-handed partner (which remains to be detected). The neutrino masses would then be given by the Higgs mechanism, in the same way as all the other fermion masses in the SM. Oscillation experiments then tell us what value the mass differences between different mass eigenstates should be in order to reproduce the oscillations.

But even if we introduce right-handed partners to the neutrinos, it still remains mysterious why their masses are so light. While neutrino oscillations don't fix the absolute value of the masses and only the squared mass differences, they give an idea of the neutrino mass scale, which without strong fine-tuning would be expected to be below the eV scale. Moreover, cosmological constraints independently provide an upper bound on the sum of the neutrino masses [3]

$$\sum_i m_i < 0.12 \text{ eV } (95\% \text{ C.L.}) \ . \tag{3.28}$$

Taking neutrinos of masses around 0.1 eV leaves a gap of 6 orders of magnitude with the lightest particle in the SM, the electron, with its mass of 511 keV. This large separation of scales between neutrinos and the rest of the SM calls for an explanation. A way to explain this is called the Seesaw mechanism.

Seesaw mechanism There exists different types of Seesaw mechanisms. The first kind to have been proposed and that was named "Seesaw" by Yanagida in 1979 is the type-I Seesaw [108–111]. It involves massive Majorana sterile neutrinos which, in the original version of the type-I Seesaw, are very heavy such that it acts as a "seesaw", precisely, and makes the active neutrinos light. There also exists two other types of seesaw mechanisms, the type-II [112–115] which involves a scalar electroweak triplet, and the type-III [116, 117] which involves fermionic electroweak triplets. The type-I Seesaw is by far the most popular and is the one we work with in this thesis.

We mentioned that right-handed neutrinos (which are chiral fermions) would allow a Dirac mass for the active neutrinos. For the type-I Seesaw, we actually need Majorana fermions. A Majorana particle is described by a spinor $N \in \mathbb{C}^4$ that satisfies

$$N^c = N \ , \ N^c \equiv C\overline{N}^T \ . \tag{3.29}$$

The index c denotes the charge conjugation of the spinor, with C the charge conjugation matrix. In the chiral representation, we make a choice for γ^μ and C

$$\gamma^0 = \begin{pmatrix} 0 & \mathbb{I} \\ \mathbb{I} & 0 \end{pmatrix} \ , \ \gamma^i = \begin{pmatrix} 0 & \sigma_i \\ -\sigma_i & 0 \end{pmatrix} \ , \ C \equiv i\gamma^0\gamma^2 \ , \tag{3.30}$$

σ_i being the Pauli matrices. This is the mathematical formulation of a particle being its own anti-particle. We note that a Majorana particle can't carry any conserved quantum charge, because the complex conjugation inverts the sign of the charge, so the reality condition imposes the charge to be zero. In particular, in our model, Majorana neutrinos will be singlets under the SM gauge group, henceforth called "sterile". For a spinor satisfying (3.29), we can write a Lorentz invariant mass term

$$\mathcal{L}_M = -\frac{1}{2} M \overline{N}^c N \ . \tag{3.31}$$

The Majorana spinor N is often written in terms of a right-handed Weyl spinor N_R such that

$$N \equiv N_R + i\sigma_2 N_R^* \equiv N_R + N_L^c \ , \tag{3.32}$$

where the reality condition (3.29) is automatically satisfied for N. It is the sum of a right-handed Weyl spinor, and its charge conjugate. This is why we refer to a Majorana neutrino sometimes as "right-handed" neutrino, even if *per se* it has no chirality: we assimilate it to the N_R defined above. In the following, we will note N_R the right-handed Weyl spinor from which we construct the physical Majorana sterile neutrino N.

In order to explain the masses of the active neutrinos, we need more than one sterile neutrino. Let us consider n_R neutrinos, that we label with the indices $I, J = 1, ..., n_R$, each of them with Majorana mass M_I. The Lagrangian of the theory in this model is

$$\mathcal{L} = \mathcal{L}_{SM} + \left[\frac{i}{2} \overline{N}_{RI} \not{\partial} N_{RI} - \frac{1}{2} \overline{N}_{RI} M_I N_{LI}^c - Y_{Ia} \overline{N}_{RI} \tilde{\phi}^\dagger l_a + \text{h.c.} \right] \ , \tag{3.33}$$

where $\mathcal{L}_{SM}$ is the Lagrangian of the SM, to which we added massive right-handed neutrinos N_{RI}, and Yukawa couplings Y_{Ia} mixing them with the active charged leptons. After symmetry-breaking, the Higgs field ϕ takes a non-zero *vev* that we define as $\frac{v}{\sqrt{2}}$, where $v = 246$ GeV. We can then regroup the terms mixing left- and right-handed neutrinos,

$$\begin{aligned} \mathcal{L} \ni & -\left(\frac{1}{2} \overline{N}_{RI} M_I N_{LI}^c + \frac{v}{\sqrt{2}} Y_{Ia} \overline{N}_{RI} \nu_{La} + \ \text{h.c.} \right) \\ & = -\frac{1}{2} \begin{pmatrix} \overline{\nu}_{Ra}^c & \overline{N}_{RI} \end{pmatrix} \overbrace{\begin{pmatrix} 0 & m_{DJa} \\ m_{DIa} & M_I \delta_{IJ} \end{pmatrix}}^{\mathcal{M}} \begin{pmatrix} \nu_{La} \\ N_{LJ}^c \end{pmatrix} + \ \text{h.c.} \end{aligned} \tag{3.34}$$

We introduced the Dirac mass matrix $(m_D)_{Ia} \equiv Y_{Ia} \frac{v}{\sqrt{2}}$. The final mass eigenstates are found by diagonalizing block-wise the above matrix $\mathcal{M}$. This can be done perturbatively if we consider the masses M_I to be large compared to (the eigenvalues of) m_D . In the end, one obtains

$$\mathcal{M} \to \mathcal{M}^{\text{block}} \approx \begin{pmatrix} -m_D^T M_N^{-1} m_D & 0 \\ 0 & M_N \end{pmatrix} \equiv \begin{pmatrix} m_\nu & 0 \\ 0 & M_N \end{pmatrix} \ . \tag{3.35}$$

We have thus obtained two families of neutrinos, one that is "heavy" with mass matrix $(M_N)_{IJ} \equiv M_I \delta_{IJ}$, and one that is "light" of mass matrix $m_\nu \propto M_N^{-1}$. Note that m_ν may still be non-diagonal. We define the Pontecorvo-Maki-Nakagawa-Sakata (PMNS) [118–120]

matrix U to be the unitary matrix between the eigenstates of flavor and the eigenstates of mass for the light neutrinos, such that

$$\left(U^T\right)_{ia} (m_\nu)_{ab} U_{bj} = m_i \delta_{ij} \equiv (D_\nu)_{ij} \ , \tag{3.36}$$

with m_i's being the masses of the light neutrinos. The PMNS matrix is similar to the CKM matrix in the quark sector, and tells us about the mixing between different generations of fermions. It is a three-by-three unitary matrix that can be written as the product of 3 rotation matrices together with 6 phases. Not all of these phases are physical due to the possible redefinition of the fields. If active neutrinos are Dirac particles, only one phase remains physical (like in the CKM matrix) and is called δ. If they are Majorana fermions, the Majorana condition forbids certain redefinitions, and 3 phases remain physical, the phase δ and two additional ones that are called "Majorana" phases, noted α_1 and α_2. δ is related to CP-violation in neutrino oscillations, while the Majorana phases are only involved in lepton number violating process such as neutrinoless beta decay. Keeping the Majorana phases for generality, we can decompose the PMNS matrix as

$$U \equiv \begin{pmatrix} 1 & 0 & 0 \\ 0 & c_{23} & s_{23} \\ 0 & -s_{23} & c_{23} \end{pmatrix} \begin{pmatrix} c_{13} & 0 & s_{13} e^{-i\delta} \\ 0 & 1 & 0 \\ -s_{13} e^{i\delta} & 0 & c_{13} \end{pmatrix} \begin{pmatrix} c_{12} & s_{12} & 0 \\ -s_{12} & c_{12} & 0 \\ 0 & 0 & 1 \end{pmatrix} P \ , \tag{3.37}$$

with $P = \mathrm{diag}\left(e^{i\alpha_1/2}, e^{i\alpha_2/2}, 1\right)$. We defined the compact notations $c_{ij} \equiv \cos(\theta)_{ij}$, $s_{ij} \equiv \sin(\theta)_{ij}$. θ_{12}, θ_{13} and θ_{23} are the different mixing angles. Various oscillations experiments are sensitive to different parts of the PMNS matrix. θ_{12} turns out to be best constrained by measurements of solar neutrino oscillations, θ_{23} is best constrained by atmospheric neutrinos, and θ_{13} is best constrained in experiments with reactors. Their values given by NuFIT 5.3 (2024) [107], with uncertainties at the 3σ level, are

$$\theta_{12} = (33.67 \pm 2.07)^\circ \ , \tag{3.38a}$$
$$\theta_{13} = (\ 8.54 \pm 0.35)^\circ \ , \tag{3.38b}$$
$$\theta_{23} = (\ 49.2 \pm\ 9.6)^\circ \ , \tag{3.38c}$$

We note that θ_{13} and θ_{12} have lower relative uncertainties than θ_{23}. This is due to the fact that θ_{23} is close to $\pi/4$, such that $\sin^2(2\theta_{23})$ (which is the actual quantity determined in oscillation experiments) is flat around this value. It is thus not known which octant ($\theta_{23} < \pi/4$ or $\theta_{23} > \pi/4$) is more favorable.

Concerning the phases, the Majorana phases are not yet measured and would only be involved in lepton-number-violating processes, for which we have no evidence yet. The δ phase is CP-violating ($\delta \neq 0, \pi$) to a good confidence level (90%).

The Casas-Ibarra parametrization The Seesaw mechanism explains why the masses m_i can be small; the heavy Majorana masses M_I suppress them. The model is constrained to reproduce neutrino oscillations data, *i.e.* the correct masses of left-handed neutrinos and their

mixing angles. Indeed, using the definition of m_ν and condition (3.36), we get

$$U^T m_D^T M_N^{-1} m_D U = -\frac{v^2}{2} U^T Y^T M_N^{-\frac{1}{2}} M_N^{-\frac{1}{2}} Y U = -\frac{v^2}{2} \left(M_N^{-\frac{1}{2}} Y U\right)^T M_N^{-\frac{1}{2}} Y U = D_\nu \ . \tag{3.39}$$

We used the fact that M_N is symmetric and positive in order to take its square root. We can now note that, up to an orthogonal matrix, $M_N^{-\frac{1}{2}} Y U$ is the square root of $-\frac{2}{v^2} D_\nu$. Therefore, we define

$$M_N^{-\frac{1}{2}} Y U \equiv i\frac{\sqrt{2}}{v} R D_\nu^{\frac{1}{2}} \rightarrow \frac{v^2}{2i^2} \left(M_N^{-\frac{1}{2}} Y U\right)^T M_N^{-\frac{1}{2}} Y U = D_\nu^{\frac{1}{2}} \left(R^T R\right) D_\nu^{\frac{1}{2}} = D_\nu \ . \tag{3.40}$$

R is an orthogonal matrix (that can be complex *a priori*) satisfying $R^T R = \mathbb{I}$. Thus, we recover the good light neutrino masses and their mixing angles by parametrizing our Yukawa coupling matrix

$$Y \equiv i\frac{\sqrt{2}}{v} M_N^{\frac{1}{2}} R D_\nu^{\frac{1}{2}} U^\dagger \ . \tag{3.41}$$

This is known as the Casas-Ibarra (CI) parametrization [121]. In this equation, U and D_ν are quantities related to the neutrino oscillation experiments. $(M_N)_{IJ} = M_I \delta_{IJ}$ is the matrix of the masses of the right-handed neutrinos, that we choose for our theory. R is an orthogonal complex matrix that is not measurable in oscillations and mixing experiments; it is an additional parameter in our theory. Its size will depend on the number n_R of right-handed neutrinos that we add.

A simple and yet useful case is for $n_R = 2$. We have only two right-handed neutrinos, two Majorana masses, and the complex matrix R is 2 by 3. Two sterile neutrinos can only account for two massive active neutrinos, so in this case, one of the masses m_i of the left-handed neutrinos is exactly zero (*i.e.* one of the entries in D_ν is zero). We recall the two possibilities compatible with neutrino oscillations: $m_1 < m_2 < m_3$ (Normal Ordering (NO)), or $m_3 < m_1 < m_2$ (Inverse Ordering (IO)). In the case where we set the lightest mass to zero, it corresponds to $m_1 = 0$ for NO, and $m_3 = 0$ for IO.

The complex orthogonal matrix R is then fixed to be a rotation matrix (up to a discrete reflection) with one complex angle $z_R = z_r + i z_i$,

$$R = \begin{pmatrix} 0 & \cos z_R & -\sin z_R \\ 0 & \sin z_R & \cos z_R \end{pmatrix} \ [\text{NO}] \ , \ R = \begin{pmatrix} \cos z_R & -\sin z_R & 0 \\ \sin z_R & \cos z_R & 0 \end{pmatrix} \ [\text{IO}] \ . \tag{3.42}$$

Even though it might be interesting to study the complete dependence of the problem on this complex angle $z_R = z_r + i z_i$, we will make an assumption and fix the real part of this angle. It can be realized that the amount of CP-violation in the Yukawa sector, quantified by

$$a_{CP} \equiv \text{Im}\left[\left(Y Y^\dagger\right)^2_{12}\right] \ , \tag{3.43}$$

is maximized (in absolute value) for $z_r \equiv \frac{\pi}{4} \left[\frac{\pi}{2}\right]$, all other parameters being fixed. We will fix $z_r = \text{Re}(z) = 3\pi/4$ in the following.

Counting the degrees of freedom in the sterile sector for two sterile neutrinos, we have two parameters for the complex angle (only one left if we fix z_r) and two masses M_1 and M_2. It is convenient to define the average mass scale M and the degeneracy ΔM

$$M \equiv \frac{M_1 + M_2}{2} \ , \ \Delta M \equiv M_2 - M_1 \ . \tag{3.44}$$

We therefore have 4 parameters to work with and scan over in the sterile neutrino sector. In addition to these parameters coming from the hidden sterile sector, some of the constants of the PMNS matrix, related to SM neutrinos, are measured, but uncertainty bars can be large. This is the case for the CP-violating phase δ, where it is not even clear yet if there is CP-violation at all (*i.e.* δ could be 0 or π). Combined fits [122] of various experiments seem to favor a value of $\delta \approx \frac{3\pi}{2}$ which violates CP. Additionally, two Majorana phases α_1, α_2 are allowed but are not measured yet. For the sake of simplicity, we will fix them,

$$\delta = \frac{3\pi}{2} \ , \ \alpha_1 = \alpha_2 = 0 \ . \tag{3.45}$$

The rest of the parameters, that is, the neutrino masses and the mixing angles in the PMNS matrix, were taken from NuFIT 5.2 (2022) [122], assuming Normal Ordering and $m_1 = 0$ (only two sterile neutrinos). The central values and uncertainties of these parameters are summarized in a table presented in Appendix A.

3.3 Thermal and resonant leptogenesis

The first attempt to explain the baryon asymmetry with sterile neutrinos can be traced back to 1986, with the work of Fukugita and Yanagida [11]. In this scenario, sterile neutrinos are driven away from thermal equilibrium when their interaction rate $\Gamma(T)$ with the SM plasma becomes smaller than the Hubble rate $H(T)$. The condition

$$\Gamma(T) < H(T) \tag{3.46}$$

is the out-of-equilibrium condition. Once they are out-of-equilibrium and overpopulated, they will decay into leptons and anti-leptons in a non-symmetric way, characterized by a decay CP-asymmetry $\epsilon^I_{\rm CP}$ for each sterile neutrino flavor,

$$\epsilon^I_{\rm CP} \equiv \frac{\Gamma(N_I \to l\phi) - \Gamma(N_I \to \bar{l}\phi^*)}{\Gamma(N_I \to l\phi) + \Gamma(N_I \to \bar{l}\phi^*)} \ . \tag{3.47}$$

This model is called *thermal leptogenesis*. The dynamics of decays (and inverse decays) is captured by Boltzmann equations [123, 124] (see [105, 125] for reviews on their derivation), describing the evolution of a number density N_{N_I} of sterile neutrinos, coupled to a lepton asymmetry N_L,

$$\frac{{\rm d}N_{N_I}}{{\rm d}t} + 3HN_I = -\gamma_I \left(\frac{N_{N_I}}{N^{\rm eq}_{N_I}} - 1 \right) \tag{3.48}$$

$$\frac{\mathrm{d}N_L}{\mathrm{d}t} + 3HN_L = -\sum_I \left[\gamma_I \frac{N_L}{2N_l^{\rm eq}} - \epsilon^I_{\rm CP}\gamma_I \left(\frac{N_{N_I}}{N_I^{\rm eq}} - 1\right)\right] \ . \tag{3.49}$$

The lepton asymmetry $N_L \equiv N_l - N_{\bar{l}}$ is the difference between the lepton and the anti-lepton number densities. We also defined the equilibrium densities

$$N_l^{\rm eq} = g_W \int \frac{\mathrm{d}^3\mathbf{k}}{(2\pi)^3}\, e^{-|\mathbf{k}|/T} = \frac{g_W T^3}{\pi^2} \ , \tag{3.50}$$

$$N_{N_I}^{\rm eq} = g_N \int \frac{\mathrm{d}^3\mathbf{k}}{(2\pi)^3}\, e^{-(|\mathbf{k}|^2+M_I^2)^{1/2}/T} = g_N \frac{M_I^2 T}{2\pi^2}\mathcal{K}_2(M/T) \ , \tag{3.51}$$

with $g_W = 2$ the $SU(2)$ degrees of freedom of the lepton doublet and $g_N = 2$ are the helicity degrees of freedom of the Majorana sterile neutrinos.

The first equation (3.48) describes how the population of sterile neutrinos is approaching equilibrium. For $N_{N_I} > N_{N_I}^{\rm eq}$, the right-hand term is negative and reduces the population with a decay rate γ_I. The second equation (3.49) describes the evolution of the lepton asymmetry. It is reduced by inverse decays washing out the asymmetry, while it receives a source term coming from the sterile neutrino decays characterized by a CP-asymmetry $\epsilon^I_{\rm CP}$.

We must stress that these equations only describe the dominant processes which are decays and inverse decays $N_I \leftrightarrow l\phi$. They can be refined by including scatterings and diffusion (see [105, 125] for reviews additional processes). Moreover, we worked in the one-flavor approximation for simplicity, meaning that we neglected any flavor effect in the lepton asymmetry. This can be fully justified only for temperatures $T > 10^{12}$ GeV [106], when all leptons are out of equilibrium, as mentioned earlier. Below that temperature, lepton flavors are differentiated and flavor effects should be taken into account [104, 126–129].

The Boltzmann equations can be obtained from particle physics amplitudes, integrated over momentum. The integration is done by assuming *kinetic equilibrium*, meaning that the phase space distribution is taken proportional to the number density, for instance

$$f_I(E) = \frac{N_{N_I}}{N_{N_I}^{\rm eq}} f_I^{\rm eq}(E) \ . \tag{3.52}$$

Neglecting spin-statistics, the equilibrium phase space distribution is the Maxwell-Boltzmann $f_I^{\rm eq}(E) = e^{-E/T}$. Various quantities can then be calculated as averages over momentum,

$$\gamma_I = 2\Gamma_I \int \frac{\mathrm{d}^3\mathbf{k}}{(2\pi)^3} \frac{M_I}{(|\mathbf{k}|^2 + M_I^2)^{1/2}} e^{-(|\mathbf{k}|^2+M_I^2)^{1/2}/T} = N_{N_I}^{\rm eq}\Gamma_I \frac{\mathcal{K}_1(M_I/T)}{\mathcal{K}_2(M_I/T)} \ , \tag{3.53}$$

where $\mathcal{K}_1$ and $\mathcal{K}_2$ are modified Bessel functions of the second kind. $\Gamma_I = \Gamma(N_I \to l\phi) + \Gamma(N_I \to \bar{l}\phi^*)$ is the (CP-even) total decay rate.

The crucial element of these equations is the CP-asymmetry $\epsilon^I_{\rm CP}$. Successful leptogenesis requires a sufficiently large value of this parameter, which depends on the Yukawa couplings

and the masses of the sterile neutrinos. Calculating the decay amplitudes at zero temperature [125, 130–133], we obtain two contributions to ϵ^I_{CP},

$$\epsilon^I_{\text{CP}} = \epsilon^I_{\text{CP},V} + \epsilon^I_{\text{CP,wave}} \ , \tag{3.54}$$

where

$$\epsilon^I_{\text{CP},V} = \frac{1}{8\pi} \sum_J \frac{\text{Im}\left[\left(YY^\dagger\right)^2_{IJ}\right]}{\left(YY^\dagger\right)_{II}} f\left(\frac{M_J^2}{M_I^2}\right) \ , \tag{3.55}$$

with $f(x) = \sqrt{x}\left[1 - (1+x)\ln\left(\frac{1+x}{x}\right)\right]$, and

$$\epsilon^I_{\text{CP,wave}} = \frac{1}{8\pi} \sum_J \frac{\text{Im}\left[\left(YY^\dagger\right)^2_{IJ}\right]}{\left(YY^\dagger\right)_{II}} \frac{M_I M_J}{M_J^2 - M_I^2} \ , \tag{3.56}$$

$\epsilon^I_{\text{CP},V}$ is a vertex contribution, corresponding to loop-correction to the vertex $N_I \to l\phi$, while $\epsilon^I_{\text{CP,wave}}$ is a wave-function contribution corresponding to flavor mixing during the propagation of sterile neutrinos $N_I \to N_J$.

When the sterile neutrinos are hierarchical (for two sterile neutrinos, $M_1 \ll M_2$), the two contributions are of the same order. The CP-asymmetry in decays is then important only for large Yukawa couplings, which imposes that the sterile neutrino masses are large. If we want to reproduce enough baryon asymmetry, this then sets a lower bound on the mass M_1, known as the Davidson-Ibarra bound [134]. The exact bound can depend on the initial sterile neutrino population as was shown in [135], but the bound roughly says we need $M_1 > 10^9$ GeV for thermal leptogenesis to work.

Such high masses make a direct detection of sterile neutrinos impossible in any foreseeable future. The bound can however be circumvented by abandoning the assumption of hierarchical sterile neutrinos. Indeed, ϵ^I_{CP} can be made large for degenerate sterile neutrinos $M_2 - M_1 \ll M_1, M_2$, which enhance the wave-function contribution. Such a degeneracy allows successful thermal leptogenesis for masses well below the Davidson-Ibarra bound. This regime is known as *resonant leptogenesis*.

3.4 ARS leptogenesis

Another option for generating a lepton asymmetry with sterile neutrinos was proposed by Akhmedov, Rubakov and Smirnov (ARS) in 1998 [136]. It is a scenario based, not on decays, but on flavor oscillations in the sterile neutrino sector, which are CP-violating. We will call this mechanism ARS leptogenesis; it can also be referred to as leptogenesis with sterile neutrino oscillations in the literature. Contrary to thermal and resonant leptogenesis, the sterile neutrinos are relativistic during most of the period of interest, with masses around the GeV scale. Moreover, they are assumed to be absent of the plasma initially, not at thermal equilibrium.

The lepton asymmetry is then created as sterile neutrinos are being produced; this can be called the *freeze-in* scenario.

In ARS leptogenesis, a crucial ingredient is flavor mixing, correlation between sterile neutrino flavors, that oscillates as the sterile neutrinos propagate. The dynamics of these oscillations is then best described by considering the (rescaled) sterile neutrino density matrix (for each helicity h), which is a matrix in the space of sterile neutrino flavors

$$n_h = \delta n_h + n_{\rm eq}\mathbb{I} \ , \tag{3.57}$$

with $n_{\rm eq} \equiv 3\zeta(3)/(4\pi^2)$ the rescaled equilibrium distribution (for a single helicity) of a relativistic (effectively massless) fermion. The sterile neutrino density matrix n_h and its deviation from equilibrium δn_h are hermitian matrices. Sterile neutrinos couple to the (rescaled) asymmetry $\Delta_a \equiv n_{B/3} - n_{L_a}$, a combination of the baryon and flavored lepton asymmetries. It is a convenient quantity to consider, because $\sum_a \Delta_a = n_{B-L}$ is the density of $B-L$ asymmetry, which is preserved in the SM. Note that we are working with the rescaled number densities (see the definition (2.39)) where we divide by T^3, including the dilution from the expansion of the Universe. These quantities obey the equations [136–138]

$$\frac{{\rm d}\delta n_h}{{\rm d}t} = -i\left[\langle H_0\rangle + \left\langle H^h_{\rm th}\right\rangle, \delta n_h\right] - \frac{1}{2}\left\{\langle\Gamma_h\rangle, \delta n_h\right\} + n_{\rm eq}\sum_a \left\langle\tilde{\Gamma}_{h,a}\right\rangle \frac{\mu_a+\mu_\phi}{T} \ , \tag{3.58}$$

$$\frac{{\rm d}\Delta_a}{{\rm d}t} = {\rm Tr}\left[\langle\Gamma_a\rangle\right]\frac{\mu_a+\mu_\phi}{T} - \sum_{I,J,h}\left\langle\tilde{\Gamma}_{h,a}\right\rangle_{JI}(\delta n_h)_{IJ} \ . \tag{3.59}$$

The sterile neutrino density matrix δn_h is coupled to the lepton asymmetry *via* the chemical potentials μ_a of the lepton flavor a and μ_ϕ of the Higgs field. The latter are directly related by the relation (3.21) to Δ_a from our discussions in the previous section. For two sterile neutrinos, the diagonal terms $\delta n_{h,11/22}$ correspond to the deviation from equilibrium of the population in each flavor. The off-diagonal term $\delta n_{h,12}$ corresponds to quantum flavor mixing.

Equation (3.59) describes the evolution of the asymmetry, which is washed out by inverse processes $\propto (\mu_a+\mu_\phi)/T$ that tend to bring the asymmetry back to zero. It is in competition with a source term $\propto \delta n_h$ coming from the interactions with the sterile neutrinos.

Equation (3.58) is a matrix equation with several terms involving matrices with flavor indices. First, the commutator with the Hamiltonian describes oscillations, as we will see soon. The Hamiltonian contains two contributions: a vacuum Hamiltonian H_0 given by the energy in the mass eigenbasis,

$$(H_0)_{IJ} = \delta_{IJ}\left(|\mathbf{k}|^2 + M_I^2\right)^{1/2} \ , \tag{3.60}$$

and a thermal Hamiltonian $\left\langle H^h_{\rm th}\right\rangle$, corresponding to thermal masses, given by the Yukawa couplings

$$\left\langle H^+_{\rm th}\right\rangle \simeq O(10^{-1})\ T\left(YY^\dagger\right) \ , \ \left\langle H^-_{\rm th}\right\rangle \simeq O(10^{-1})\ T\left(Y^*Y^T\right) \ . \tag{3.61}$$

We detail in a later section (section 7.2) how the pre-factors are obtained, and how the thermal average $\langle\ \rangle$ is taken. The important point we want to make here is that the thermal Hamiltonian is given by a matrix ($YY^\dagger$ or Y^*Y^T) that is non-diagonal in the mass eigenbasis. It also

differentiates between the two helicities.

In addition, we have several collision terms in (3.58): the bracket with $\langle\Gamma_h\rangle$ corresponds to production of sterile neutrinos, bringing them closer to equilibrium, while the term $\left\langle\tilde{\Gamma}_{h,a}\right\rangle$ couples them to the lepton asymmetry in the flavor a. Both are given by the Yukawa couplings, with terms of the form

$$\langle\Gamma_+\rangle \simeq O(10^{-2})\ T\left(YY^\dagger\right)\ ,\ \langle\Gamma_-\rangle_{IJ} \simeq O(10^{-2})\ T\left(Y^*Y^T\right)\ , \tag{3.62}$$

$$2\left\langle\tilde{\Gamma}_{+,a}\right\rangle \simeq \langle\Gamma_{+,a}\rangle \simeq O(10^{-2})\ T\left(Y_{\cdot a}Y_{a\cdot}^\dagger\right)\ ,\ -2\left\langle\tilde{\Gamma}_{-,a}\right\rangle \simeq \langle\Gamma_{-,a}\rangle \simeq O(10^{-2})\ T\left(Y_{\cdot a}^*Y_{a\cdot}^T\right)\ . \tag{3.63}$$

In the second line, we extracted the contribution to flavor a from the Yukawa matrices, $\left(Y_{\cdot a}Y_{a\cdot}^\dagger\right)_{IJ} \equiv Y_{Ia}Y_{Ja}^*$. We make the same observation as before that these are (complex) matrices corresponding to a different basis than the mass eigenbasis. In particular, the production rate contains induces flavor mixing, due to off-diagonal elements $\langle\Gamma_h\rangle_{12}$, for two flavors for example. This off-diagonal production, together with oscillations, is a crucial ingredient for successful leptogenesis. Simultaneously, the collision term also reduces the diagonal elements $\delta n_{h,11/22}$, which means bringing the population of each sterile neutrino flavor towards equilibrium.

We now explain how the oscillations occur. The commutator with the vacuum Hamiltonian H_0 describes flavor oscillations coming from the vacuum masses. The Hamiltonian coming from thermal masses can be neglected for our discussion here. For a given momentum $\mathbf{k}$, H_0 is a diagonal matrix

$$(H_0)_{IJ} = \delta_{IJ}\left(|\mathbf{k}|^2 + M_I^2\right)^{1/2} \simeq \delta_{IJ}\left(|\mathbf{k}| + \frac{M_I^2}{2|\mathbf{k}|}\right)\ , \tag{3.64}$$

where we used the relativistic approximation in the second equality. In the equation for δn_h, it contributes as an oscillation term

$$\frac{\mathrm{d}\delta n_{h,IJ}}{\mathrm{d}t} = -i\left\langle\frac{1}{2|\mathbf{k}|}\right\rangle\left(M_I^2 - M_J^2\right)\delta n_{h,IJ} + ... \tag{3.65}$$

In particular, for two sterile neutrinos, only the off-diagonal term $\delta n_{h,12}$ oscillates, at a typical rate

$$\left\langle\frac{M_2^2 - M_1^2}{2|\mathbf{k}|}\right\rangle \sim \frac{M_2^2 - M_1^2}{2T} \equiv \omega_{12}(T)\ . \tag{3.66}$$

We used the fact that the (thermal) average of momentum is of the same order as the temperature. Temperature is however evolving along with the expansion of the Universe, so that the frequency ω_{12} grows with time. Using the correspondence (2.45), we can better describe the evolution in terms of $z = T_{\rm ref}/T$,

$$\frac{\mathrm{d}\delta n_{h,12}}{\mathrm{d}z} \sim -i\frac{a_R}{T_{\rm ref}}\frac{M_2^2 - M_1^2}{2T^2}\delta n_{h,12} + ... = -i\frac{a_R\left(M_2^2 - M_1^2\right)}{2T_{\rm ref}^3}z^2\delta n_{h,12} + ... \tag{3.67}$$

If vacuum oscillations were all there was, the off-diagonal term would be oscillating like

$$\delta n_{h,12}(z) \sim \delta n_{h,12}^{\rm in}\ \exp\left(-i\frac{a_R\left(M_2^2 - M_1^2\right)}{6T_{\rm ref}^3}z^3\right)\ . \tag{3.68}$$

This determines the typical value of z over which oscillations occur, defined by [137]

$$z_{\rm osc}^{\rm ARS} \equiv \left[\frac{T_{\rm ref}^3}{a_R\left(M_2^2 - M_1^2\right)}\right]^{1/3} , \tag{3.69}$$

or equivalently a temperature of oscillation

$$T_{\rm osc}^{\rm ARS} \equiv \left[a_R\left(M_2^2 - M_1^2\right)\right]^{1/3} . \tag{3.70}$$

Note that the power 1/3 came from integrating the temperature-dependent frequency ω_{12}. This temperature scale will be important later for discussions in the case with a phase transition.

Of course, oscillations are only possible if $\delta n_{h,12}$ is produced in the first place, *i.e.* we want to have $\delta n_{h,12}^{\rm in} \neq 0$ in the oscillation (3.68). This is why the (off-diagonal) production by the $\langle\Gamma_h\rangle$ term is important. The sterile neutrinos are therefore produced from the plasma, trying to reach thermal equilibrium. They are produced in the interaction basis, given by the Yukawa couplings $YY^\dagger/Y^*Y^T$ in the $\langle\Gamma_\pm\rangle$ term. This basis is misaligned with the mass eigenbasis, where vacuum masses drive the oscillations. This misalignment is essential to have CP-violating oscillations. In addition, the rate of creation of $\delta n_{h,12}$ is different for the two helicities, which leads to an asymmetry $\delta n_{+,12} - \delta n_{-,12} \neq 0$ between them.

The final step in ARS leptogenesis is the conversion of the helicity asymmetry into a lepton asymmetry. This can be understood quite easily by looking at the right-hand term of the equation (3.59). The source term depends on the helicity asymmetry,

$$\begin{aligned}\sum_{I,J,h}\left\langle\tilde{\Gamma}_{h,a}\right\rangle_{IJ}\delta n_{h,JI} &\sim O(10^{-2})\ T\ {\rm Re}\left[Y_{2a}Y_{1a}^*\delta n_{+,12} - Y_{2a}^*Y_{1a}\delta n_{-,12}\right] \\ &\sim O(10^{-2})\ T\left({\rm Re}\left[Y_{2a}Y_{1a}^*\right]{\rm Re}\left[\delta n_{+,12} - \delta n_{-,12}\right] - {\rm Im}\left[Y_{Ia}^*Y_{Ja}\right]{\rm Im}\left[\delta n_{+,12} + \delta n_{-,12}\right]\right) .\end{aligned} \tag{3.71}$$

A lepton asymmetry can then be produced from the helicity asymmetry; at this stage, flavor effects are still very important and more could be said. We will however leave this discussion for later in chapter 7, and refer the reader to the review [137] for more details. As a summary, we will say that ARS leptogenesis relies on the simultaneity of production and oscillation of sterile neutrinos. The basis in which they are produced (given by $\langle\Gamma_h\rangle$) is misaligned, in a CP-violating way (with the complex Yukawa couplings), compared to the basis in which they oscillate (given by the vacuum Hamiltonian H_0). This produces an helicity asymmetry that sources the lepton asymmetry.

As a final note, it was shown quite recently [139] that ARS leptogenesis and resonant leptogenesis can be seen as two sides of the same coin, two solutions of the same equations. As was already pointed at by previous studies [132, 135, 140–143], one can recover resonant leptogenesis from the equations of ARS leptogenesis. The mixing contribution to $\epsilon_{\rm CP}$ in resonant leptogenesis is captured by the off-diagonal term $\delta n_{h,12}$ in the sterile neutrino density matrix. Integrating it out of the dynamics leads to effective classical Boltzmann equations with mixing

included in $\epsilon_{\rm CP}$. The two scenarios therefore share a common ground and both rely on mixing between the sterile neutrino flavors. They differ however in how sterile neutrinos deviate from equilibrium when the asymmetry is created; in resonant leptogenesis, they drop out of thermal equilibrium because the thermal distribution becomes Boltzmann-suppressed, while in ARS leptogenesis, their density is zero initially. This leads to different physical mechanisms: out-of-equilibrium decays (*freeze-out*) for resonant leptogenesis, out-of-equilibrium production (*freeze-in*) for ARS leptogenesis.

In the present work, we will also recover both regimes from the same equations, but they will be slightly modified as we consider sterile neutrinos affected by a phase transition.

3.5 Scalar extension and FOPT

We detailed how massive sterile neutrinos could produce a lepton asymmetry, either *via* their decays or *via* their flavor oscillations. We introduce in this section a different approach, used in this thesis, in which a new scalar interacts with the sterile neutrinos, replacing the mass term

$$-\frac{1}{2}\overline{N}_I^c M_I N_I \rightarrow -\frac{1}{2}\lambda_I S \overline{N}_I^c N_I \ . \tag{3.72}$$

Note that the constants λ_I are dimensionless. The sterile neutrinos are therefore massless, unless S takes a non-zero *vev*. There exists a vast range of scenarios in which the scalar field experiences a phase transition to acquire this *vev*. This is the case for example in Grand Unified Theories, where S is associated to the breaking of a $B-L$ gauge theory [144–147], or in conformal models [18–21] through the Gildener-Weinberg mechanism [148]. In all these cases, the sterile neutrinos then obtain their Majorana masses needed to explain the neutrino oscillations experiments.

We will assume the scalar field S undergoes a First-Order Phase Transition (FOPT), like the ones described in section 2.4, at a certain nucleation temperature T_n. As the FOPT goes on, regions of space are converted into true vacuum, forming bubbles of true vacuum inside the rest of the space in a false vacuum state. The bubbles expand, sweeping through the plasma of particles and end up covering all the space (see Figure 3.1).

In this work, we will remain agnostic on how the FOPT happens exactly, as long as it produces expanding bubbles of true vacuum, and we will focus only on the dynamics of sterile neutrinos in this context. There are numerous phenomenological constraints on the parameters of the scalar potential and its interactions with the SM [149], *e.g.* scalar mixing with the Higgs field. For simplicity, we will take a scalar field totally decoupled from the SM.

The main parameters from the scalar sector of interest for our study will be the nucleation temperature T_n at which bubbles form, and the *vev* v_S taken by the scalar field once the FOPT

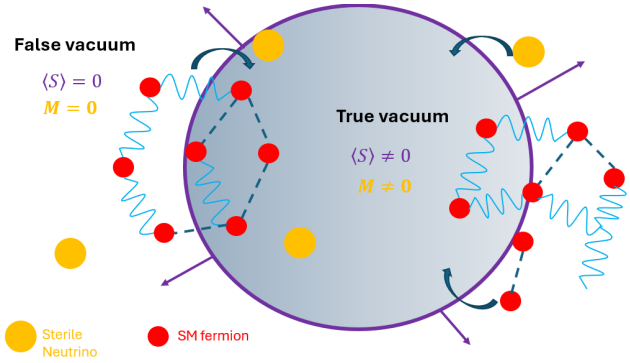

Figure 3.1: Schematic representation of the bubbles expanding during a FOPT. The *vev* of the scalar field fixes the mass of the sterile neutrinos, which then varies with time.

is completed. In the true vacuum, the masses of the sterile neutrinos will be given by

$$M_{I0} = \lambda_I v_S \ . \tag{3.73}$$

3.5.1 Time-dependent masses

During a FOPT, we described in section 2.4 how bubbles can nucleate, forming an expanding region of true vacuum (where the *vev* of the scalar field is v_S). For our toy model, we found that the profile of the field during the expansion of a critical bubble was given by

$$S(t,r) = \frac{v_S}{2}\left(1+\tanh\left(\frac{v_w\Delta t - r}{L_w}\right)\right) = \frac{v_S}{2}\left(1+\tanh\left(\frac{v_w(t-t_{\rm nucl}-r/v_w)}{L_w}\right)\right) \ . \tag{3.74}$$

r is the radial position with respect to the center of the bubble. v_w is the velocity of the bubble wall and L_w is its spatial thickness. The sterile neutrino mass is proportional to the value of the field, such that

$$M_I(t,r) = \lambda_I S(t,r) = \frac{M_{I0}}{2}\left(1+\tanh\left(\frac{v_w(t-t_{\rm nucl}-r/v_w)}{L_w}\right)\right) \ . \tag{3.75}$$

At a fixed position in space r, the mass evolves at a certain rate in time γ given by

$$\gamma = \frac{v_w}{L_w}. \tag{3.76}$$

We now make some assumptions to simplify the space-time dependence of the mass. First of all, in supercooled FOPT, as was considered in the original Mass Gain scenario [32], the bubbles are typically expanding at velocities close to the speed of light, so $v_w \simeq 1$ and $\gamma \simeq L_w^{-1}$. It was also argued in [32, 64] that for relativistic walls, all particles in the plasma enter the bubble without reflection. We will assume this is the case in our work, *i.e.* bubbles expand fast enough so that all particles enter the bubble and no reflection occurs. Roughly speaking, the transition corresponds in this case to a "switching on" of the sterile neutrino masses.

Having this in mind, we will simplify our problem and consider only the time dependence of the mass profile

$$M_I(t,r) \simeq M_I(t) = M_{I0}\frac{1+\tanh(\gamma\Delta t)}{2} \ , \quad \text{with } \Delta t = t - t_{\text{nucl}} \ . \tag{3.77}$$

This is an approximation, but it describes well the fact that, at a time $t = t_{\text{nucl}}$, the sterile neutrinos all start feeling a mass at the same time, as the fast expanding bubbles sweep through the plasma. It will allow us to describe the transition explicitly with the analytical profile (3.77).

Let us say a few words on the determination of the time rate γ_w. The connection between $\gamma \simeq L_w^{-1}$ and the other parameters of the FOPT has been discussed in the literature in the context of the electroweak phase transition [63, 150], and no exact relation has been derived. The typical scale of the bubble expansion has only be estimated and is dependent on the scalar sector and how the bubbles develop, but it is related to the transition happening at the scale T_n. As an estimate, in order to reduce the complexity of our analysis, we take this parameter to be *equal* to the temperature at the time of nucleation,

$$\gamma = T_n \ . \tag{3.78}$$

We will keep this assumption in our numerical study. Consideration of more realistic profiles would require more attentive work and a full numerical resolution the bubble profile at any temperature.

3.5.2 Vacuum expectation value and critical temperature

The FOPT actually starts at a certain critical temperature T_c when the global minimum of the scalar potential changes, and bubbles of true vacuum are created at the nucleation temperature $T_n \leq T_c$. In general, these temperatures should be different. In the dynamics we study, we are interested in the passage of the bubble, so on what happens at temperature T_n. The masses of the sterile neutrinos, however, are given by the *vev* v_S of the scalar field that usually closely relates to the critical temperature. For a strongly first-order FOPT, as mentioned in section 2.4, we typically have $v_S \gtrsim T_c$. It is also possible to make $T_c \gg T_n$ in a supercooled FOPT. This would allow us to obtain masses well above the nucleation temperature T_n, even though the coupling λ of sterile neutrinos to the scalar field is of order one, as

$$\frac{M_{I0}}{T_n} = \frac{\lambda_I v_S}{T_n} \gtrsim \lambda_I \frac{T_c}{T_n} \ . \tag{3.79}$$

A priori, T_c/T_n can be as large as $O(10)$ for a supercooled FOPT. This means the ratio M/T_n can be made large even if the coupling λ_I to S should remain smaller than order 1. In this work, because we remain agnostic about the details of the FOPT, T_c, T_n and λ_I are independent parameters that we should scan over. However, the physics we are interested in are mostly sensitive to the mass M and the temperature of the bubble nucleation T_n. We will therefore consider M and T_n as the relevant independent parameters, using T_c/T_n to create a hierarchy between λ_I and M/T_n when we would like to consider $M/T_n > 1$.

3.5.3 Additional effects: thermal masses

In addition to experimenting a phase transition, the scalar field can have other effects on the sterile neutrinos, that we mention briefly here.

One effect that we will take into account in the final chapter is the thermal masses induced for the sterile neutrinos from their interaction with the scalar field. Given the coupling term $-\frac{1}{2}\lambda_I S\overline{N}_I^c N_I$, if the field S has thermalized to a temperature T, it will induce a thermal mass for the sterile neutrinos given by [37, 39]

$$\left(M^S_{\mathrm{th},I}\right)^2 = \frac{\lambda_I^2}{12}T^2 \ . \tag{3.80}$$

This term is only relevant if S has thermalized with the SM plasma. We assumed earlier for simplicity that the scalar S is decoupled from the SM. If this is the case, its only coupling to the fields of interest is the coupling to the sterile neutrinos, which might themselves not be in thermal equilibrium. For the rest of the study, we will then assume that S is absent from the plasma, and will only come back to this assumption later, in chapter 7.

Other than the thermal masses, we will neglect all other effects of adding the scalar field, in this study. In principle, the coupling term $-\frac{1}{2}\lambda_I S\overline{N}_I^c N_I$ opens up annihilation and production channels for the sterile neutrinos. Indeed, either the scalar decays into sterile neutrinos $S \to N\overline{N}$, or the sterile neutrinos annihilate into the scalar field $N\overline{N} \to S$. The first process could be relevant for light sterile neutrinos, but would be suppressed if the scalar was not present in the plasma, as we assumed. The annihilation processes can be made negligible if we consider a large mass for the scalar field, for example. We refer the reader to studies [33, 35, 39] of the impact of an extra scalar field on sterile neutrinos for a more detailed discussion.

3.6 Summary and relevant temperature scales

We conclude these introductory chapters on the early Universe and leptogenesis by a short summary of the epochs of interest and how they compare to each others. On Figure 3.2, we put the temperature (and time) scales of relevance to our work. After inflation, the Universe is radiation dominated. As we saw, leptogenesis can happen at different scales; at large scales (around $T \sim 10^9$ GeV), thermal leptogenesis ("therm. lepto." on the sketch) is relevant, while at lower temperatures (around $T \sim 10^3$ GeV) the so-called ARS leptogenesis ("ARS lepto.") is relevant. Two phase transitions are expected to have happened in the SM, the ElectroWeak Phase Transition ("EWPT" on the sketch) and the QCD Phase Transition ("QCD PT"). Current constraints on First-order Phase Transitions (FOPT) come mainly from Big Bang Nucleosynthesis (BBN) and the Cosmic Microwave Background (CMB), and fix $T_n \gtrsim 1$ MeV for a FOPT of strength $\alpha_n = 1$. Projection can be made for future GW detectors which will test higher temperatures, T_n up to 10^6 GeV for a phase transition of strength $\alpha_n = 1$. In this work, we will consider a new phase transition, driven by an extra scalar S. It will affect sterile

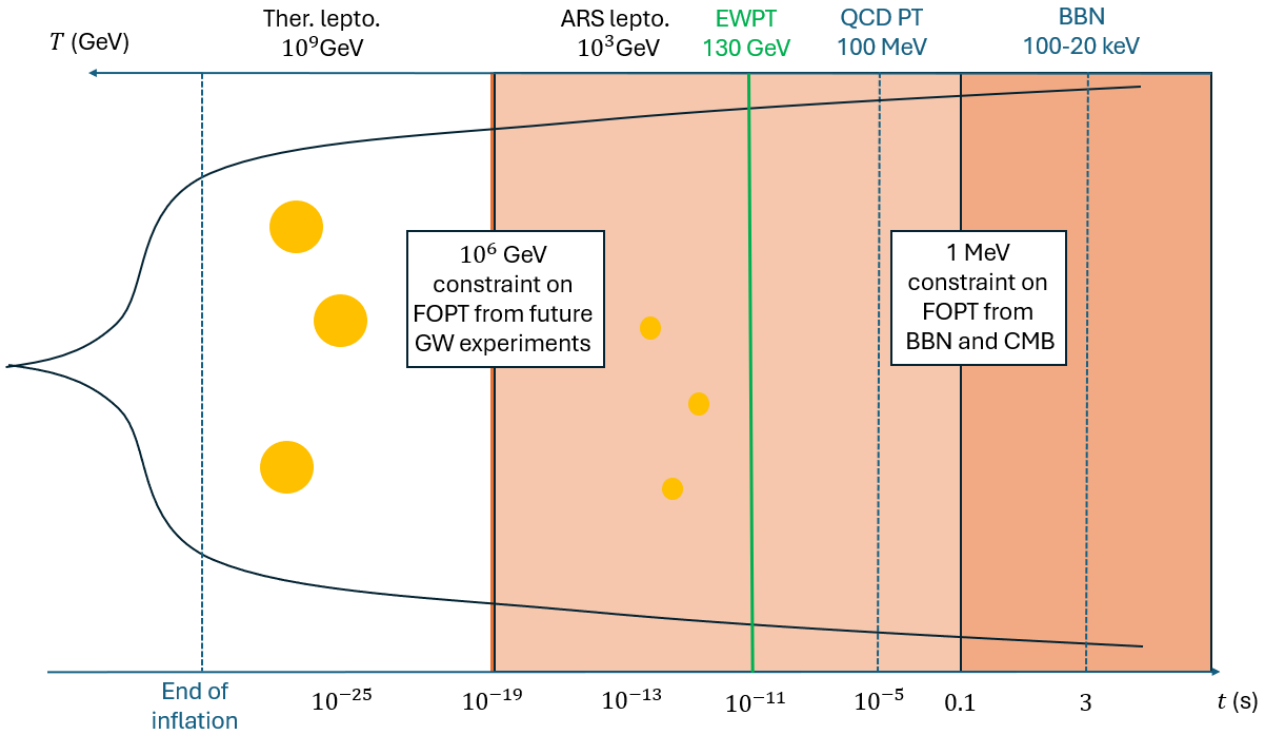

Figure 3.2: Schematic picture of the early Universe. Time is growing from left to right, temperature from right to left. The dark-red area corresponds to the excluded region for a FOPT of fixed strength $\alpha_n = 1$, while the light-red area is a projected exclusion region from future GW experiments, for the same strength. Scales on the axis are *not* respected and the various points are only indicative of the typical time (or temperature) scales.

neutrinos, during their dynamics for the production of a lepton asymmetry. From the timeline in Figure 3.2, a phase transition happening at the scales of leptogenesis could actually be constrained by future GW experiments, and a theory of leptogenesis during a cosmological phase transition is of phenomenological interest, relating GW detection, cosmological observations (the BAU η) and particle physics searches (direct or indirect detection of sterile neutrinos).

Part II

Dynamics during a cosmological phase transition

This second part is more technical and develops the formalism for understanding the dynamics of the fields of interest in the context of a phase transition. First, we address the effect of the transition itself on a sterile neutrino distribution in Chapter 4. We then move on, in Chapter 5, to a more general description of the interacting fields in an expanding Universe, using the Closed-Time-Path formalism for out-of-equilibrium fields.

Chapter 4

Particle production of sterile neutrinos for a time-dependent mass

The FOPT induces a time-dependent mass for the sterile neutrino, as the bubble sweeps through the plasma. This has implications for the evolution of the field, and even for the definition of the particle states. Indeed, the evolution of the mass modifies what we mean by states of well-defined energies. This implies a change in the definition of creation and annihilation operators for the sterile neutrinos, by a so-called Bogoliubov transformation. A direct consequence is that a vacuum state before the FOPT will not appear empty anymore, after the FOPT. Sterile neutrinos will get produced, as a consequence of the fact that the phase transition is injecting energy in the plasma to produce a time-varying background, the time-varying mass.

Particle production from a time-dependent background occurs in other contexts, such as gravitational contexts, where space-time is curved. It has been studied extensively in the context of inflation [151–153], dark matter production [154–156], and also the generation of a baryon asymmetry in the so-called gravitational leptogenesis scenario [157, 158].

For now, we are only concerned with the time dependence coming from the passage of bubbles in the plasma. In particular, we will neglect the expansion of the Universe, in this chapter. This is justified, if we recall the profile of the sterile neutrino masses during the FOPT

$$M_I(t) = M_{I0}\frac{1+\tanh\left(\gamma\Delta t\right)}{2}\ , \tag{4.1}$$

with $\gamma = T_n$ the temperature of the phase transition. It evolves over typical time scales $\Delta t \sim T_n^{-1}$, much shorter than the Hubble time $H^{-1}(T_n) = \frac{a_R}{T_n}T_n^{-1} \gg T_n^{-1}$. The dynamics of the passage of the bubble is well separated from the expansion of the Universe, that we will neglect here.

In this chapter, we will show how sterile neutrinos behave for a time-dependent mass, by solving analytically the Dirac equation similarly to what was done in [159]. Note that this work itself followed the steps of [160] which studied a space-dependent mass. We will then

deduce how the number density of sterile neutrinos gets changed before and after the phase transition. This first approach is conducted without interactions (only the time-varying mass). A more complete description of interactions and flavor will be given in the next chapter.

4.1 Decomposition of the sterile neutrino field into momentum modes

We are interested in the evolution of the sterile neutrino field during a phase transition, when its mass is time-dependent. Because we neglect interactions for now, we consider only one sterile neutrino flavor that we denote N, of mass M.

The most general decomposition into spatial momentum modes, in a spatially homogeneous and isotropic Universe, of a single sterile Majorana neutrino field is given by

$$N(\mathbf{x},t) = \sum_h \int_{\mathbf{k}} \left[e^{i\mathbf{k}\cdot\mathbf{x}} \begin{pmatrix} L_h(t,|\mathbf{k}|) \\ R_h(t,|\mathbf{k}|) \end{pmatrix} \otimes \xi_h^{\mathbf{k}} \hat{a}_{h,\mathbf{k}} + e^{-i\mathbf{k}\cdot\mathbf{x}} \begin{pmatrix} -hR_h^*(t,|\mathbf{k}|) \\ hL_h^*(t,|\mathbf{k}|) \end{pmatrix} \otimes \xi_{-h}^{\mathbf{k}} \hat{a}_{h,\mathbf{k}}^\dagger \right] . \tag{4.2}$$

Because initially (before the FOPT), the field is massless, we expand it in terms of $\hat{a}_{h,\mathbf{k}}$ / $\hat{a}_{h,\mathbf{k}}^\dagger$, the annihilation/creation operators for a massless sterile Majorana neutrino, spatial momentum $\mathbf{k}$ and helicity $h/2$. N is a spinor in $\mathbb{C}^4$, where we used the tensor product $\otimes$ to write it in terms of $\mathbb{C}^2$ vectors. L_h/R_h are (yet) arbitrary complex numbers, functions of time and momentum, corresponding to the left- and right-handed parts of the field. The $\xi_h^{\mathbf{k}}$'s are helicity eigenvectors, satisfying the eigenvector equation

$$\frac{\mathbf{k}\cdot\boldsymbol{\sigma}}{|\mathbf{k}|}\xi_h^{\mathbf{k}} = h\xi_h^{\mathbf{k}} \ , \text{ with } \boldsymbol{\sigma} = (\sigma_1,\sigma_2,\sigma_3) \text{ the Pauli matrices.} \tag{4.3}$$

In order to ensure that the field (4.2) is a Majorana field, we imposed

$$\xi_+^{\mathbf{k}} = -i\sigma_2\xi_-^{\mathbf{k}*} \ , \ \xi_-^{\mathbf{k}} = i\sigma_2\xi_+^{\mathbf{k}*} \ . \tag{4.4}$$

Explicit formulas for the helicity eigenvectors are given in Appendix B, with a description of their properties.

4.2 Field equation

The Dirac equation for the field N is given by

$$i\partial\!\!\!/ N - M(t)N = 0 \ , \tag{4.5}$$

which can be rewritten, in terms of the complex functions L_h and R_h,

$$i\partial_t L_h + h|\mathbf{k}|L_h - M(t)R_h = 0 \ , \tag{4.6}$$

$$i\partial_t R_h - h|\mathbf{k}|R_h - M(t)L_h = 0 \ . \tag{4.7}$$

The left- and right-handed parts of the fields are coupled by the mass term in these first-order differential equations. This set of equations can be re-written as two decoupled second-order differential equations

$$\partial_t^2 L_h - \frac{\partial_t M}{M}\partial_t L_h + \left(|\mathbf{k}|^2 + M(t)^2 + ih|\mathbf{k}|\frac{\partial_t M}{M}\right) L_h = 0 \ , \tag{4.8}$$

$$\partial_t^2 R_h - \frac{\partial_t M}{M}\partial_t L_h + \left(|\mathbf{k}|^2 + M(t)^2 - ih|\mathbf{k}|\frac{\partial_t M}{M}\right) R_h = 0 \ . \tag{4.9}$$

Note that if the mass is constant ($\partial_t M = 0$), we recover the Klein-Gordon equation for the field mode of momentum $|\mathbf{k}|$. It may in general be very complicated to solve these equations for an arbitrary function $M(t)$. However, as was shown in [159], analytical results can be derived for the mass profile

$$M(t) = M_0 \frac{1 + \tanh(\gamma t)}{2} \ . \tag{4.10}$$

Later on, for the study of the FOPT we will replace t by $\Delta t = t - t_{\rm nucl}$. The equations for the modes L_h and R_h can then be rewritten in terms of a better-suited variable Z,

$$Z \equiv \frac{1 + \tanh(\gamma t)}{2} \ , \ \partial_t = \frac{\mathrm{d}Z}{\mathrm{d}t}\partial_Z = 2\gamma Z(1-Z) \times \partial_Z \ , \tag{4.11}$$

$$\partial_t^2 = 2\gamma Z(1-Z)\partial_Z \left(2\gamma Z(1-Z)\partial_Z\right) = 4\gamma^2 Z(1-Z)\left[Z(1-Z)\partial_Z^2 + (1-2Z)\partial_Z\right] \ . \tag{4.12}$$

We will, in the following, note with a prime the derivatives with respect to Z, and use

$$\partial_t M = 2\gamma Z(1-Z)M' = 2\gamma Z(1-Z)M_0 = 2\gamma(1-Z)M(Z) \ . \tag{4.13}$$

The equations (4.6), (4.7) become

$$2i\gamma Z(1-Z)L_h' + h|\mathbf{k}|L_h - M_0 Z R_h = 0 \ , \tag{4.14}$$

$$2i\gamma Z(1-Z)R_h' - h|\mathbf{k}|R_h - M_0 Z L_h = 0 \ . \tag{4.15}$$

It turns out that a solution is better found in terms of the sum and difference of those two functions, defining

$$u_{h\pm} \equiv \frac{1}{2}\left(L_h \pm R_h\right) \ , \tag{4.16}$$

$$2i\gamma Z(1-Z)u_{h\pm}' + h|\mathbf{k}|u_{h\mp} \mp M_0 Z u_{h\pm} = 0 \ . \tag{4.17}$$

Acting with ∂_Z on the two coupled first-order differential equations (4.17), we obtain two independent second-order differential equations for u_{h+} and u_{h-}

$$4\gamma^2 Z(1-Z)\left[Z(1-Z)\partial_Z^2 + (1-2Z)\partial_Z\right]u_{h\pm} + \left(|\mathbf{k}|^2 + M_0^2 Z^2 \pm 2i\gamma M_0 Z(1-Z)\right)u_{h\pm} = 0 \tag{4.18}$$

or equivalently

$$Z(1-Z)u_{h\pm}'' + (1-2Z)u_{h\pm}' + \left[\frac{|\mathbf{k}|^2 + M_0^2 Z^2}{4\gamma^2 Z(1-Z)} \pm i\frac{M_0}{2\gamma}\right]u_{h\pm} = 0 \ . \tag{4.19}$$

Following [159], we use a parametrization to factor out of the u functions certain (yet undetermined) powers of Z and $1-Z$,

$$u_{h\pm}(Z) \equiv Z^{\alpha}(1-Z)^{\beta}\chi_{h\pm}(Z) \ . \tag{4.20}$$

The derivatives give

$$\begin{aligned} u'_{h\pm} &= \left[\alpha Z^{\alpha-1}(1-Z)^{\beta}\chi_{h\pm} - \beta Z^{\alpha}(1-Z)^{\beta-1}\chi_{h\pm} + Z^{\alpha}(1-Z)^{\beta}\chi'_{h\pm}\right] \\ &= \left[\left(\frac{\alpha}{Z} - \frac{\beta}{1-Z}\right)\chi_{h\pm} + \chi'_{h\pm}\right] Z^{\alpha}(1-Z)^{\beta} \ , \end{aligned} \tag{4.21}$$

$$\begin{aligned} u''_{h\pm} = &\left[\alpha(\alpha-1)Z^{\alpha-2}(1-Z)^{\beta}\chi_{h\pm} - 2\alpha\beta Z^{\alpha-1}(1-Z)^{\beta-1}\chi_{h\pm} + \beta(\beta-1)Z^{\alpha}(1-Z)^{\beta-2}\chi_{h\pm}\right. \\ &\left. +2\left(\alpha Z^{\alpha-1}(1-Z)^{\beta} - \beta Z^{\alpha}(1-Z)^{\beta-1}\right)\chi'_{h\pm} + Z^{\alpha}(1-Z)^{\beta}\chi''_{h\pm}\right] \\ = &\left[\left(\frac{\alpha(\alpha-1)}{Z^2} - \frac{2\alpha\beta}{Z(1-Z)} + \frac{\beta(\beta-1)}{(1-Z)^2}\right)\chi_{h\pm} + 2\left(\frac{\alpha}{Z} - \frac{\beta}{1-Z}\right)\chi'_{h\pm} + \chi''_{h\pm}\right] Z^{\alpha}(1-Z)^{\beta} \ . \end{aligned} \tag{4.22}$$

The equation (4.19) becomes one for $\chi_{h\pm}$, where we have not yet fixed the values of α and β,

$$\begin{aligned} &Z(1-Z)\chi''_{h\pm} + (1+2\alpha-2(\alpha+\beta+1)Z)\,\chi'_{h\pm} \\ &+\left[\frac{\alpha^2+\frac{|\mathbf{k}|^2}{4\gamma^2}}{Z} + \frac{\beta^2+\frac{|\mathbf{k}|^2+M_0^2}{4\gamma^2}}{(1-Z)} - 2\alpha\beta - \alpha(\alpha+1) - \beta(\beta+1) \pm i\frac{M_0}{2\gamma} - \frac{M_0^2}{4\gamma^2}\right]\chi_{h\pm} = 0 \ , \end{aligned} \tag{4.23}$$

where we used the simple-element decomposition $\frac{1}{Z(1-Z)} = \frac{1}{Z} + \frac{1}{1-Z}$ to regroup terms into $1/Z$ and $1/(1-Z)$ poles. We will now fix the α and β such that these poles disappear from our equation. Therefore, we impose

$$\beta^2 + \frac{|\mathbf{k}|^2 + (M^0)^2}{4\gamma^2} = 0 \ , \ \alpha^2 + \frac{|\mathbf{k}|^2}{4\gamma^2} = 0 \ , \tag{4.24}$$

giving

$$\beta = \pm i\frac{\sqrt{|\mathbf{k}|^2 + (M^0)^2}}{2\gamma} \equiv \pm i\frac{\omega_0}{2\gamma} \ , \ \alpha = \pm\frac{i|\mathbf{k}|}{2\gamma} \ . \tag{4.25}$$

Choosing $\beta = -i\frac{\omega_0}{2\gamma}$ and $\alpha = -\frac{i|\mathbf{k}|}{2\gamma}$, the equation for $\chi_{h\pm}$ can be put in the form

$$Z(1-Z)\chi''_{h\pm} + [1+2\alpha-(2\alpha+2\beta+2)Z]\,\chi'_{h\pm} - \left[1+\alpha+\beta \pm i\frac{M_0}{2\gamma}\right]\left[\alpha+\beta \mp i\frac{M_0}{2\gamma}\right]\chi_{h\pm} = 0 \tag{4.26}$$

which of the form

$$Z(1-Z)\chi''_{h\pm}(Z) + (c-(a_\pm+b_\pm+1)Z)\chi'_{h\pm}(Z) - a_\pm b_\pm\ \chi_{h\pm}(Z) = 0 \ , \tag{4.27}$$

where we recover a known equation, the Gaussian hypergeometric equation. The numbers $a_\pm$, $b_\pm$ and c are given in terms of α, β and M_0,

$$c = 1 + 2\alpha = 1 - \frac{i|\mathbf{k}|}{\gamma} \ , \tag{4.28}$$

$$a_\pm = 1 + \alpha + \beta \pm i\frac{M_0}{2\gamma} = 1 - i\frac{\omega_0 + |\mathbf{k}| \mp M_0}{2\gamma} \ , \ b_\pm = \alpha + \beta \mp i\frac{M_0}{2\gamma} = -i\frac{\omega_0 + |\mathbf{k}| \pm M_0}{2\gamma} \ . \tag{4.29}$$

The solutions of (4.27) are the linear combinations of hypergeometric functions ${}_2F_1$,

$$\chi_{h\pm}(Z) = A_{h\pm}\ {}_2F_1(a_\pm, b_\pm, c, Z) + B_{h\pm}\ Z^{1-c}\,{}_2F_1(a_\pm + 1 - c, b_\pm + 1 - c, 2 - c, Z) \ , \tag{4.30}$$

$$u_{h\pm}(Z) = A_{h\pm}\ Z^\alpha(1-Z)^\beta\,{}_2F_1(a_\pm, b_\pm, c, Z) + B_{h\pm}\ Z^{\alpha+1-c}(1-Z)^\beta\,{}_2F_1(a_\pm+1-c, b_\pm+1-c, 2-c, Z) \ . \tag{4.31}$$

where $A_{h\pm}$ and $B_{h\pm}$ are constants that we determine in the following.

4.3 Initial conditions and normalization

The constants appearing in $u_{h\pm}$ can be constrained by initial conditions, and by the relation (4.17) between u_{h+} and u_{h-}. At early times, $\Delta t \to -\infty$ before the FOPT, the field is massless so we need to impose that

$$L_- = R_+ = e^{-i|\mathbf{k}|t} \ , \ L_+ = R_- = 0 \ , \tag{4.32}$$

implying

$$u_{h\pm} \propto e^{-i|\mathbf{k}|t} \ . \tag{4.33}$$

In particular, because $Z(t) \approx e^{2\gamma t}$ as $t \to -\infty$,

$$Z^\alpha \approx e^{-i|\mathbf{k}|t} \ , \ Z^{\alpha+1-c} \approx e^{+i|\mathbf{k}|t} \ , \tag{4.34}$$

in equation (4.31) we can only keep the solution proportional to Z^α,

$$B_{h\pm} = 0 \ , \tag{4.35}$$

$$u_{h\pm}(Z) = A_{h\pm}\ Z^\alpha(1-Z)^\beta\,{}_2F_1(a_\pm, b_\pm, c, Z) \ . \tag{4.36}$$

There exists a relation between the normalization constants $A_\pm$, as the functions $u_{h\pm}$ are related by (4.17). Moreover, normalization of the modes can be imposed,

$$|L_h|^2 + |R_h|^2 = 1 = 2\left(|u_{h+}|^2 + |u_{h-}|^2\right) \tag{4.37}$$

which finally fixes the constants $A_{h\pm}$. The full procedure is rather involved and requires to use different formulas for the hypergeometric functions. It is detailed in Appendix C, and we only give the final results, which is the determination of the constants, $A_{h+} = \frac{1}{2}$, $A_{h-} = -\frac{h}{2}$, such that

$$u_{h+} = \frac{1}{2}Z^\alpha(1-Z)^\beta\,{}_2F_1(a_+, b_+, c, Z) \ , \ u_{h-} = -\frac{h}{2}Z^\alpha(1-Z)^\beta\,{}_2F_1(a_-, b_-, c, Z) \ , \tag{4.38}$$

$$L_h = \frac{1}{2}Z^\alpha(1-Z)^\beta\left[{}_2F_1(a_+, b_+, c, Z) - h\,{}_2F_1(a_-, b_-, c, Z)\right] \ , \ R_h = L_{-h} \ . \tag{4.39}$$

4.4 Bogoliubov transformation and particle production

Now that we determined the expression of the field as a function of time for a time-dependent mass, we can compute observables from it, notably the number of particles. We will see that the number density is time-dependent, even though our field was so far considered without interactions. It can be understood by a change in the definition of what a particle is. Because the mass is explicitly evolving, the way to count modes of definite energy changes and this can be seen from the Hamiltonian of the field. For a massive Majorana field N, the Hamiltonian (in the flat Minkowski time direction) is given by

$$H = \int \mathrm{d}^3\mathbf{x}\, \frac{1}{2}\left[i\overline{N}\boldsymbol{\gamma}\cdot\boldsymbol{\nabla}N + M(t)\overline{N}^c N\right] \ . \tag{4.40}$$

Focusing on the field decomposition (4.2), at a fixed momentum $\mathbf{k}$ and helicity $h/2$, it is convenient to consider

$$N_{h\mathbf{k}} \equiv e^{i\mathbf{k}\cdot\mathbf{x}}\begin{pmatrix} L_h \\ R_h\end{pmatrix}\otimes\xi^{\mathbf{k}}_h\hat{a}_{h,\mathbf{k}} + e^{-i\mathbf{k}\cdot\mathbf{x}}\begin{pmatrix} -hR^*_h \\ hL^*_h\end{pmatrix}\otimes\xi^{\mathbf{k}}_{-h}\hat{a}^\dagger_{h,\mathbf{k}} \ , \tag{4.41}$$

$$\gamma^0 N_{h\mathbf{k}} \equiv e^{i\mathbf{k}\cdot\mathbf{x}}\begin{pmatrix} R_h \\ L_h\end{pmatrix}\otimes\xi^{\mathbf{k}}_h\hat{a}_{h,\mathbf{k}} + e^{-i\mathbf{k}\cdot\mathbf{x}}\begin{pmatrix} hL^*_h \\ -hR^*_h\end{pmatrix}\otimes\xi^{\mathbf{k}}_{-h}\hat{a}^\dagger_{h,\mathbf{k}} \ , \tag{4.42}$$

$$N^\dagger_{h\mathbf{k}} = e^{-i\mathbf{k}\cdot\mathbf{x}}\begin{pmatrix} L^*_h \\ R^*_h\end{pmatrix}^T\otimes\xi^{\mathbf{k}\dagger}_h\hat{a}^\dagger_{h,\mathbf{k}} + e^{i\mathbf{k}\cdot\mathbf{x}}\begin{pmatrix} -hR_h \\ hL_h\end{pmatrix}^T\otimes\xi^{\mathbf{k}\dagger}_{-h}\hat{a}_{h,\mathbf{k}} \ , \tag{4.43}$$

and compute its contribution to the Hamiltonian. The spatial derivative acts only on the complex exponential,

$$i\gamma^0\boldsymbol{\gamma}\cdot\boldsymbol{\nabla}N_{h\mathbf{k}} = h|\mathbf{k}|\left[e^{i\mathbf{k}\cdot\mathbf{x}}\begin{pmatrix} L_h \\ -R_h\end{pmatrix}\otimes\xi^{\mathbf{k}}_h\hat{a}_{h,\mathbf{k}} - e^{-i\mathbf{k}\cdot\mathbf{x}}\begin{pmatrix} hR^*_h \\ hL^*_h\end{pmatrix}\otimes\xi^{\mathbf{k}}_{-h}\hat{a}^\dagger_{h,\mathbf{k}}\right] \ . \tag{4.44}$$

We recall we work in the chiral basis for the γ-matrices. Our helicity eigenvectors are given explicitly in Appendix B; in particular, they satisfy

$$\xi^{\mathbf{k}\dagger}_h\cdot\xi^{\mathbf{k}}_h = 1 \ , \ \xi^{\mathbf{k}\dagger}_{-h}\cdot\xi^{\mathbf{k}}_h = 0 \ , \tag{4.45}$$

$$\xi^{-\mathbf{k}}_h = e^{ih\varphi_{\mathbf{k}}}\xi^{\mathbf{k}}_{-h}, \tag{4.46}$$

where $\varphi_{\mathbf{k}}$ is the azimuth angle of the vector $\mathbf{k}$ in the coordinate system we choose to write our helicity eigenvectors. Using these relations, after taking the scalar product with $N^\dagger_{h\mathbf{k}}$, we obtain

$$i\overline{N}_{h\mathbf{k}}\boldsymbol{\gamma}\cdot\boldsymbol{\nabla}N_{h\mathbf{k}} = h|\mathbf{k}|\left(|L_h|^2 - |R_h|^2\right)\left(\hat{a}^\dagger_{h,\mathbf{k}}\hat{a}_{h,\mathbf{k}} - \hat{a}_{h,\mathbf{k}}\hat{a}^\dagger_{h,\mathbf{k}}\right) \ , \tag{4.47}$$

$$i\overline{N}_{h-\mathbf{k}}\boldsymbol{\gamma}\cdot\boldsymbol{\nabla}N_{h\mathbf{k}} = 2|\mathbf{k}|L_hR_he^{-ih\varphi_{\mathbf{k}}}\hat{a}_{h,-\mathbf{k}}\hat{a}_{h,\mathbf{k}} - 2|\mathbf{k}|L^*_hR^*_he^{+ih\varphi_{\mathbf{k}}}\hat{a}^\dagger_{h,-\mathbf{k}}\hat{a}^\dagger_{h,\mathbf{k}} \ . \tag{4.48}$$

The mass term corresponds simply to the scalar product

$$N^\dagger_{h\mathbf{k}}\gamma^0 N_{h\mathbf{k}} = 2\mathrm{Re}\left[L_hR^*_h\right]\left[\hat{a}^\dagger_{h,\mathbf{k}}\hat{a}_{h,\mathbf{k}} - \hat{a}_{h,\mathbf{k}}\hat{a}^\dagger_{h,\mathbf{k}}\right] \ , \tag{4.49}$$

$$N^\dagger_{h-\mathbf{k}}\gamma^0 N_{h\mathbf{k}} = h\left(L_h^2 - R_h^2\right)e^{-ih\varphi_\mathbf{k}}\hat{a}_{h,-\mathbf{k}}\hat{a}_{h,\mathbf{k}} - h\left((L_h^*)^2 - (R_h^*)^2\right)e^{+ih\varphi_\mathbf{k}}\hat{a}^\dagger_{h,-\mathbf{k}}\hat{a}^\dagger_{h,\mathbf{k}} \ . \tag{4.50}$$

Integrating over momenta, the (free) Hamiltonian is (see [152, 161, 162]),

$$H = \int \frac{\mathrm{d}^3\mathbf{k}}{(2\pi)^3}\frac{1}{2}\sum_h \left[\Omega^h_\mathbf{k}\left(\hat{a}^\dagger_{h,\mathbf{k}}\hat{a}_{h,\mathbf{k}} - \hat{a}_{h,\mathbf{k}}\hat{a}^\dagger_{h,\mathbf{k}}\right) + \left(\Lambda^h_\mathbf{k}e^{-ih\varphi_\mathbf{k}}\ \hat{a}_{h,-\mathbf{k}}\hat{a}_{h,\mathbf{k}} + \text{h.c.}\right)\right] \ , \tag{4.51}$$

with

$$\Omega^h_\mathbf{k} = h|\mathbf{k}|\left(|L_h|^2 - |R_h|^2\right) + 2M\mathrm{Re}\left[L_h R_h^*\right] \ , \ \Lambda^h_\mathbf{k} = 2|\mathbf{k}|L_h R_h + hM\left(L_h^2 - R_h^2\right) \ . \tag{4.52}$$

Note that in a free theory for a Majorana neutrino with constant mass, we would expect a diagonal Hamiltonian. Because the modes L_h/R_h are complicated functions, it is no longer the case in general. The Hamiltonian can be diagonalized in a new basis by a Bogoliubov transformation [163, 164]. The eigenvalues, found in the diagonal basis, will correspond to the physical particle number, multiplied by the individual energies.

The explicit Bogoliubov transformation to new creation and annihilation operators $\hat{A}^\dagger_{h,\mathbf{k}}/\hat{A}_{h,\mathbf{k}}$ is

$$\hat{A}_{h,\mathbf{k}} \equiv \alpha_{h,\mathbf{k}}\hat{a}_{h,\mathbf{k}} + \beta_{h,\mathbf{k}}e^{ih\varphi_\mathbf{k}}\hat{a}^\dagger_{h,-\mathbf{k}} \ , \tag{4.53a}$$

$$\hat{A}^\dagger_{h,\mathbf{k}} \equiv \alpha^*_{h,\mathbf{k}}\hat{a}^\dagger_{h,\mathbf{k}} + \beta^*_{h,\mathbf{k}}e^{-ih\varphi_\mathbf{k}}\hat{a}_{h,-\mathbf{k}} \ . \tag{4.53b}$$

It preserves the anti-commutation relation under the condition

$$|\alpha_{h,\mathbf{k}}|^2 + |\beta_{h,\mathbf{k}}|^2 = 1 \ . \tag{4.54}$$

We can then diagonalize the Hamiltonian (4.51) using

$$\begin{aligned}\hat{A}^\dagger_{h,\mathbf{k}}\hat{A}_{h,\mathbf{k}} = |\alpha_{h,\mathbf{k}}|^2\,\hat{a}^\dagger_{h,\mathbf{k}}\hat{a}_{h,\mathbf{k}} + |\beta_{h,\mathbf{k}}|^2\,\hat{a}_{h,-\mathbf{k}}\hat{a}^\dagger_{h,-\mathbf{k}} \\ + \left(\alpha_{h,\mathbf{k}}\beta^*_{h,\mathbf{k}}e^{-ih\varphi_\mathbf{k}}\hat{a}_{h,-\mathbf{k}}\hat{a}_{h,\mathbf{k}} + \text{h.c.}\right) \ ,\end{aligned} \tag{4.55}$$

which, for the expressions

$$|\alpha_{h,\mathbf{k}}|^2 = \frac{1}{2} - \frac{\Omega^h_\mathbf{k}}{2\omega_\mathbf{k}} \ , \ |\beta_{h,\mathbf{k}}|^2 = \frac{1}{2} + \frac{\Omega^h_\mathbf{k}}{2\omega_\mathbf{k}} \ , \tag{4.56}$$

$$\alpha_{h,\mathbf{k}}\beta^*_{h,\mathbf{k}} = \frac{\Lambda^h_\mathbf{k}}{2\omega_\mathbf{k}} \tag{4.57}$$

leads to

$$H = \int \frac{\mathrm{d}^3\mathbf{k}}{(2\pi)^3}\sum_h \omega_\mathbf{k}\left[\hat{A}^\dagger_{h,\mathbf{k}}\hat{A}_{h,\mathbf{k}} - \frac{1}{2}\right] \ . \tag{4.58}$$

In this basis, the Hamiltonian is simply the sum of the individual energies $\omega_\mathbf{k} = \sqrt{|\mathbf{k}|^2 + M(t)^2}$ times the number operator $\hat{A}^\dagger_{h,\mathbf{k}}\hat{A}_{h,\mathbf{k}}$, counting the (quasi)-particles. Note the familiar $\omega_\mathbf{k}/2$

vacuum energy. For completeness, we give the expressions (defined up to a global phase) for $\alpha_{h,\mathbf{k}}$ and $\beta_{h,\mathbf{k}}$,

$$\alpha_{h,\mathbf{k}} = \frac{1}{\sqrt{2}}\left[\left(1-\frac{h|\mathbf{k}|}{\omega_{\mathbf{k}}}\right)^{1/2} L_h - \left(1+\frac{h|\mathbf{k}|}{\omega_{\mathbf{k}}}\right)^{1/2} R_h\right] , \tag{4.59a}$$

$$\beta_{h,\mathbf{k}} = \frac{h}{\sqrt{2}}\left[\left(1+\frac{h|\mathbf{k}|}{\omega_{\mathbf{k}}}\right)^{1/2} L_h^* + \left(1-\frac{h|\mathbf{k}|}{\omega_{\mathbf{k}}}\right)^{1/2} R_h^*\right] . \tag{4.59b}$$

We mentioned at the beginning of this section that the phase transition creates particles. This is because the Bogoliubov transformation forces us to change our creation and annihilation operators; if we had started initially (before the phase transition) in a vacuum state $|0\rangle$ for which $\hat{a}_{h,\mathbf{k}}|0\rangle = 0$, the number of particles would have been zero,

$$\langle 0|\hat{a}^\dagger_{h,\mathbf{k}}\hat{a}_{h,\mathbf{k}}|0\rangle = 0 . \tag{4.60}$$

However, after the FOPT, the new number operator, counting the particles of definite energy, gives

$$\langle 0|\hat{A}^\dagger_{h,\mathbf{k}}\hat{A}_{h,\mathbf{k}}|0\rangle = |\beta_{h,\mathbf{k}}|^2 = \frac{1}{2} - \frac{\Omega^h_{\mathbf{k}}}{2\omega_{\mathbf{k}}} \neq 0 . \tag{4.61}$$

We can generalize it to any value of the initial number density $\langle \text{ini}|\hat{a}^\dagger_{h,\mathbf{k}}\hat{a}_{h,\mathbf{k}}|\text{ini}\rangle \equiv f_{0\mathbf{k}}$. Using the expression of $\Omega^h_{\mathbf{k}}$, similarly to [159, 162] we can define an instantaneous phase space distribution

$$f_{h\mathbf{k}}(t) = \frac{1}{2} + \frac{1-2f_{0\mathbf{k}}}{2\sqrt{|\mathbf{k}|^2+M^2(t)}}\left[h|\mathbf{k}|\left(|L_h|^2-|R_h|^2\right) + 2M(t)\mathrm{Re}\left[L_h R_h^*\right]\right] . \tag{4.62}$$

Note how $f_{h\mathbf{k}}$ is actually independent of helicity, as $R_h = L_{-h}$. At early times, when $M = 0$, we recover the initial distribution $f_{0\mathbf{k}}$, while at later times, once $M \to M_0$, it converges to a different value that we will call $f_{\text{PT},\mathbf{k}}$. We plot in Figure 4.1 these final distributions as a function of momentum for vacuum initial conditions (Figure 4.1a) and for vacuum initial conditions (Figure 4.1b).

What we realize is that the FOPT is not harmless and modifies the particle distribution for sterile neutrinos. Starting from vacuum, we have a net creation of particles, that is still very different from the thermal distribution. Note that the lowest momenta are the ones that are the most produced. Starting from a thermal distribution, the production is in proportion less significant, but we see that not all momenta are equally affected, and the profile deviates from an equilibrium one. What remains true is that the thermal distribution for the massive particle has lower values than the massless one, which creates a stronger deviation from equilibrium. The distribution is however symmetric in helicity, which is expected as no CP-violation was included.

In order to create an asymmetry, we want to include the Yukawa interactions, which are CP-violating. One can try to repeat the same procedure as the one presented in this section, considering different sterile neutrino flavors N_I; we detail some attempts and discussions in

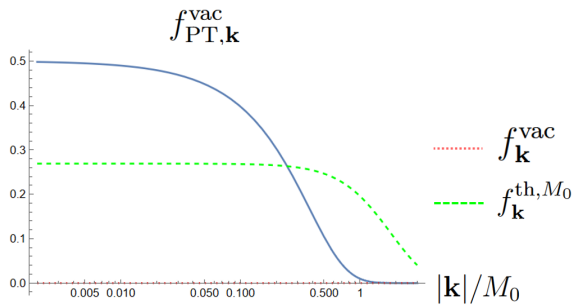

(a) Particle distribution after the FOPT starting from an initial vacuum distribution.

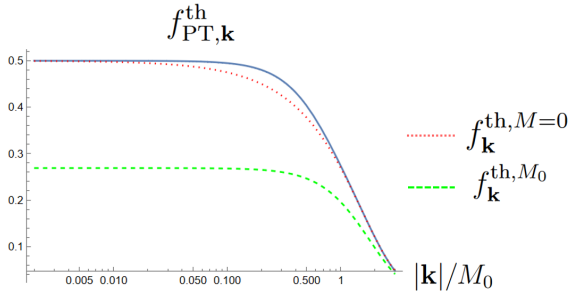

(b) Particle distribution after the FOPT starting from an initial thermal distribution, with zero mass.

Figure 4.1: We plot (in blue) the particle distribution created by the time-varying mass as a function of momentum (in units of the mass of the particle). We took $M_0/\gamma = 1$, for simplicity. We compare, in both graphs, the produced distribution with the initial distribution (dotted-red) which is either *vacuum* ((a)) or *massless thermal equilibrium* ((b)). We also plot the *massive* thermal distribution (dashed-green) in both cases. The deviation from equilibrium after the FOPT is given by the difference between the blue and the dashed-green curves.

Appendix D. We realized however that the description in terms of fields N_I is not well suited for considering interactions with the SM plasma, and also doesn't take into account the effect on the distribution of lepton and anti-leptons, which we want to describe in leptogenesis. A more accurate approach involves instead the two-point functions of the field and the propagator $S_{IJ} \sim \langle N_I \overline{N}_J \rangle$. We should use techniques from Quantum Field Theory, as presented in the next chapter.

Chapter 5

Out-of-equilibrium QFT with a time-dependent mass

In the previous chapter, we were able to describe accurately the dynamics of sterile neutrino during the phase transition when they have no other interactions. If we turn Yukawa interactions back on, sterile neutrinos will experience a time-dependent mass while also interacting with the ambient SM plasma. A common playground to capture all these dynamics is out-of-equilibrium Quantum Field Theory (QFT) which can describe how an initial set of correlation functions evolves, with parameters that are explicitly time-dependent.

This chapter aims at deriving equations that include all relevant aspects for leptogenesis during a cosmological phase transition. We want to be able to describe sterile neutrinos that

- are out-of-equilibrium,
- have a time-dependent mass,
- can be relativistic or non-relativistic.

Following previous studies, we are able to deal with all these points using

- the Closed-Time Path (CTP) formalism [165, 166] for out-of-equilibrium fields,
- the so-called Local Approximation (LA) [167, 168] for a time-dependent mass,
- an estimate of the sterile neutrino self-energy [139] describing all regimes of masses.

The structure of this chapter follows this list, first starting in sections 5.1 and 5.2 with the CTP formalism leading to equations known as Kadanoff-Baym (KB) equations. We then use the LA in section 5.3 which reduces the complexity of the KB equations and allows to treat a time-dependent mass. The self-energy appearing in the equations is described in section 5.4 by an estimate reproducing closely all regimes of sterile neutrino masses. Finally, our final equations are given in section 5.5.

5.1 The Closed-Time Path approach

Due to the third Sakharov conditions, in the study of the matter-antimatter asymmetry of the Universe, we are interested in quantum fields that are out-of-equilibrium. This implies some technical changes in the way we treat propagators and amplitudes, compared to QFT in vacuum. Indeed, in most situations, we only know the initial (quantum) state of our particles. We therefore do not know the asymptotic states for out-going particles, contrarily to scattering theory for example. Quantum expectation values can be computed for initial states (so-called "in" states), but we do not know before hand what quantum states are accessible in the future, at late time (so-called "out" states). The out-of-equilibrium formalism is sometimes called "in-in" formalism, in contrast with the "in-out" formalism of scattering theory. We give here an overview (which is by no means complete) of how this formalism is developed, and refer the reader to general reviews [169,170] and to [142,171] for its use in baryogenesis and leptogenesis.

What we are interested in are correlators of our fields. Let us consider for now simply a real scalar field operator $\hat{\phi}(x)$. It is a function of space and time, and we will assume we know its state (described by a density matrix ρ) at an initial time t_i. We want to know what happens to the field at later times, and in particular we want to compute correlation functions. A common object for dealing with n-point functions is the generating functional $Z[J]$, also called partition function,

$$\mathcal{Z}[J] \equiv \mathrm{Tr}\left[\rho(t_i)\mathcal{T}_{\mathcal{C}} \exp\left(i\int_{\mathcal{C}} \mathrm{d}^4x\ J(x)\hat{\phi}(x)\right)\right] \ , \tag{5.1}$$

$$\text{with } \int_{\mathcal{C}} \mathrm{d}^4x \equiv \int_{\mathbb{R}^3} \mathrm{d}^3\mathbf{x} \int_{\mathcal{C}} \mathrm{d}t \ . \tag{5.2}$$

The integral in the exponential is over a path $\mathcal{C}$ which we will say more about later; $\mathcal{T}_{\mathcal{C}}$ defines the ordering on this path. $\mathcal{Z}[J]$ is a function of an external current J that is usually not a physical current, but a tool for conveniently computing n-point functions as derivatives of $\mathcal{Z}$ with respect to J. For instance, the time-ordered two-point function

$$\left\langle \mathcal{T}_{\mathcal{C}}\left(\hat{\phi}(x_1)\hat{\phi}(x_2)\right)\right\rangle \equiv \mathrm{Tr}\left[\rho(t_i)\ \mathcal{T}_{\mathcal{C}}\left(\hat{\phi}(x_1)\hat{\phi}(x_2)\right)\right] = \left.\frac{\delta^2\mathcal{Z}}{i\delta J(x_1) i\delta J(x_2)}\right|_{J=0} \ . \tag{5.3}$$

The trace in the partition function (5.1) can be replaced by a functional integral,

$$\mathcal{Z} = \int \mathcal{D}\phi^{(1)}(\mathbf{x})\mathcal{D}\phi^{(2)}(\mathbf{x})\ \left\langle\phi^{(1)}\right|\rho(t_i)\left|\phi^{(2)}\right\rangle \times \left\langle\phi^{(2)}\right|\mathcal{T}_{\mathcal{C}} \exp\left(i\int_{\mathcal{C}} \mathrm{d}^4x\ J(x)\hat{\phi}(x)\right)\left|\phi^{(1)}\right\rangle \ . \tag{5.4}$$

We are integrating over two spatial field configurations $\phi^{(1)}(\mathbf{x})$ and $\phi^{(2)}(\mathbf{x})$, which should be understood as possible values of the field at $t = t_i$. The first factor $\left\langle\phi^{(1)}\right|\rho(t_i)\left|\phi^{(2)}\right\rangle$ corresponds to the initial condition for the system, while the second term with the exponential is a transition amplitude, encoding the quantum dynamics. Note that the initial condition is evaluated at t_i only. In this approach, we only know our quantum state, over which we average, at this initial time.

The idea of the Closed-Time Path emerges from this last observation. In order to use standard QFT techniques, and in particular, the Feynman path integral method, the quantum evolution should bring the states back to the initial time where they are evaluated on $\rho(t_i)$. It can be achieved by choosing the path $\mathcal{C}$ in the definition (5.1) to be *closed* in time, like in Figure 5.1. It starts from t_i and turns around at a certain time t_f. The transition amplitude can now be

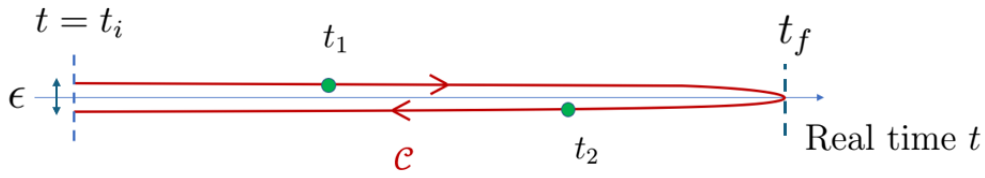

Figure 5.1: Complex contour used in the CTP formalism. The contour (in the time variable) is close to the real axis and loops back to its initial time t_i.

expressed in terms of a standard Feynman path integral,

$$\left\langle \phi^{(2)} \right| \mathcal{T}_{\mathcal{C}} \exp\left(i \int_{\mathcal{C}} \mathrm{d}^4x \; J(x)\hat{\phi}(x) \right) \left| \phi^{(1)} \right\rangle = \int_{\varphi(t_i^-,\mathbf{x})=\phi^{(2)}(\mathbf{x})}^{\varphi(t_i^+,\mathbf{x})=\phi^{(1)}(\mathbf{x})} \mathcal{D}\varphi(x) \; \exp\left(iS[\varphi] + i \int_{\mathcal{C}} \mathrm{d}^4x \; J(x)\varphi(x) \right) . \tag{5.5}$$

We see that we have managed to evaluate the boundary conditions at the initial time t_i. The path $\mathcal{C}$ can be decomposed into an upper branch $\mathcal{C}_+$ and a lower branch $\mathcal{C}_-$, where all times in the lower branch happen later, on the path $\mathcal{C}$, than the times on the upper one. Integration over the path can be seen as an integration forwards from t_i to t_f on the $\mathcal{C}_+$-branch and then backwards on the $\mathcal{C}_-$-branch,

$$\int_{\mathcal{C}} \mathrm{d}^4x \equiv \int_{\mathbb{R}^3} \mathrm{d}^3\mathbf{x} \int_{\mathcal{C}} \mathrm{d}t = \int_{\mathbb{R}^3} \mathrm{d}^3\mathbf{x} \left[\int_{t_i^+}^{t_f} \mathrm{d}t - \int_{t_i^-}^{t_f} \mathrm{d}t \right] . \tag{5.6}$$

The action defined with the Lagrangian of the theory, along the Closed-Time Path, can then also be decomposed

$$S[\varphi] \equiv \int_{\mathcal{C}} \mathrm{d}^4x \; \mathcal{L}[\varphi] = \int_{\mathbb{R}^3} \mathrm{d}^3\mathbf{x} \left[\int_{t_i^+}^{t_f} \mathrm{d}t \; \mathcal{L}[\varphi_+] - \int_{t_i^-}^{t_f} \mathrm{d}t \; \mathcal{L}[\varphi_-] \right] \equiv S_+[\varphi_+] - S_-[\varphi_-] \; . \tag{5.7}$$

The total action along the whole path has been separated into two actions, one for each branch. The values of the function φ are not necessarily the same on each branch, so we should really distinguish the function φ_+ appearing in S_+ from φ_- appearing in S_-. The same should be

done to the source term in (5.5), such that

$$\begin{aligned}
&\left\langle \phi^{(2)} \right| \mathcal{T}_{\mathcal{C}} \exp\left(i \int_{\mathcal{C}} \mathrm{d}^4 x \; J(x) \hat{\phi}(x) \right) \left| \phi^{(1)} \right\rangle \\
&= \int\limits_{\substack{\varphi_+(t_i^+,\mathbf{x})=\phi^{(1)}(\mathbf{x}) \\ \varphi_-(t_i^-,\mathbf{x})=\phi^{(2)}(\mathbf{x})}} \mathcal{D}\varphi_+(\mathbf{x}) \mathcal{D}\varphi_-(\mathbf{x}) \\
&\qquad \times \exp\left(i \left(S_+[\varphi_+] - S_-[\varphi_-] + \int_{\mathbb{R}^3} \mathrm{d}^3\mathbf{x} \int_{t_i}^{t_f} \mathrm{d}t \; \left[J_+(x)\varphi_+(x) - J_-(x)\varphi_-(x) \right] \right) \right) .
\end{aligned} \tag{5.8}$$

Note that the time integral is now over the real segment $[t_i, t_f]$, not along the Closed-Time Path anymore. t_f can be taken arbitrarily large, so we will put it to $+\infty$ in the following. We now see the price to pay for using the path-integral method in the out-of-equilibrium case: the system has virtually been doubled in its dynamics. For any real time t, there is a $t^+ \equiv t + i\epsilon$ point on the CTP with field value ϕ^+ and a $t^- \equiv t - i\epsilon$ point on the CTP with field value ϕ^-. The real time t should be considered the physical one at which one wants to compute correlation functions, while t^+ and t^- are artifacts introduced to describe non-equilibrium cases with standard techniques.

Calculating 2-point functions $\left\langle \mathcal{T}_{\mathcal{C}} \left(\hat{\phi}(t_1, \mathbf{x}_1) \hat{\phi}(t_2, \mathbf{x}_2) \right) \right\rangle$, we should then consider all possibilities for the t's, lying either on the upper or the lower branch. They are obtained by deriving with respect to J_+ or J_-,

$$iG^{ss'} \equiv \left\langle \mathcal{T}_{\mathcal{C}} \left(\hat{\phi}(t_1^s, \mathbf{x}_1) \hat{\phi}(t_2^{s'}, \mathbf{x}_2) \right) \right\rangle = \left. \frac{\delta^2 \mathcal{Z}}{i\delta J_s(x_1) i\delta J_{s'}(x_2)} \right|_{J_+ = J_- = 0} , \; s, s' = \pm . \tag{5.9}$$

The time ordering on the path then puts all upper-branch points before the lower-branch ones and is just the time ordering (respectively, anti-time ordering) $\mathcal{T}$ (respectively, $\overline{\mathcal{T}}$) for two points lying on the upper (respectively, lower) branch,

$$iG^{+-}(x_1, x_2) \equiv iG^{<}(x_1, x_2) = \left\langle \hat{\phi}(t_2, \mathbf{x}_2) \hat{\phi}(t_1, \mathbf{x}_1) \right\rangle , \tag{5.10a}$$

$$iG^{-+}(x_1, x_2) \equiv iG^{>}(x_1, x_2) = \left\langle \hat{\phi}(t_1, \mathbf{x}_1) \hat{\phi}(t_2, \mathbf{x}_2) \right\rangle , \tag{5.10b}$$

$$iG^{++}(x_1, x_2) = \left\langle \mathcal{T} \left(\hat{\phi}(t_1, \mathbf{x}_1) \hat{\phi}(t_2, \mathbf{x}_2) \right) \right\rangle , \tag{5.10c}$$

$$iG^{--}(x_1, x_2) = \left\langle \overline{\mathcal{T}} \left(\hat{\phi}(t_1, \mathbf{x}_1) \hat{\phi}(t_2, \mathbf{x}_2) \right) \right\rangle . \tag{5.10d}$$

G^{++} describes a field propagating from the upper (+) branch to the upper branch (+), G^{+-} describes the propagation from the upper (+) to the lower (-) branch, etc. $G^{\lessgtr}$ are called the Wightman functions, and the time-ordered propagator G^{++} corresponds to the Feynman propagator one would usually consider in ordinary QFT.

For a complex scalar field (relevant for the Higgs field in the Standard Model), we give

$$i\Delta^{+-}(x_1,x_2) \equiv i\Delta^{<}(x_1,x_2) = \left\langle \hat{\phi}^\dagger(t_2,\mathbf{x}_2)\hat{\phi}(t_1,\mathbf{x}_1)\right\rangle \ , \tag{5.11a}$$

$$i\Delta^{-+}(x_1,x_2) \equiv i\Delta^{>}(x_1,x_2) = \left\langle \hat{\phi}(t_1,\mathbf{x}_1)\hat{\phi}^\dagger(t_2,\mathbf{x}_2)\right\rangle \ , \tag{5.11b}$$

$$i\Delta^{++}(x_1,x_2) = \left\langle \mathcal{T}\left(\hat{\phi}(t_1,\mathbf{x}_1)\hat{\phi}^\dagger(t_2,\mathbf{x}_2)\right)\right\rangle \ , \tag{5.11c}$$

$$i\Delta^{--}(x_1,x_2) = \left\langle \overline{\mathcal{T}}\left(\hat{\phi}(t_1,\mathbf{x}_1)\hat{\phi}^\dagger(t_2,\mathbf{x}_2)\right)\right\rangle \ . \tag{5.11d}$$

Similar definitions apply as well to a fermionic field ψ, with the extra care that the time ordering can induce an additional minus sign from the anti-commutation properties of fermions, and that we should consider spinor indices α, β

$$iS^{+-}_{\alpha\beta}(x_1,x_2) \equiv iS^{<}_{\alpha\beta}(x_1,x_2) = -\left\langle \overline{\psi}_\beta(t_2,\mathbf{x}_2)\psi_\alpha(t_1,\mathbf{x}_1)\right\rangle \ , \tag{5.12a}$$

$$iS^{-+}_{\alpha\beta}(x_1,x_2) \equiv iS^{>}_{\alpha\beta}(x_1,x_2) = \left\langle \psi_\alpha(t_1,\mathbf{x}_1)\overline{\psi}_\beta(t_2,\mathbf{x}_2)\right\rangle \ , \tag{5.12b}$$

$$iS^{++}_{\alpha\beta}(x_1,x_2) = \left\langle \mathcal{T}\left(\psi_\alpha(t_1,\mathbf{x}_1)\overline{\psi}_\beta(t_2,\mathbf{x}_2)\right)\right\rangle \ , \tag{5.12c}$$

$$iS^{--}_{\alpha\beta}(x_1,x_2) = \left\langle \overline{\mathcal{T}}\left(\psi_\alpha(t_1,\mathbf{x}_1)\overline{\psi}_\beta(t_2,\mathbf{x}_2)\right)\right\rangle \ . \tag{5.12d}$$

Among the four propagators for each field, only two are linearly independent, for example

$$X^{++}(x_1,x_2) = \theta(t_1-t_2)X^{>}(x_1,x_2) + \theta(t_2-t_1)X^{<}(x_1,x_2) \ , \tag{5.13}$$

$$X^{--}(x_1,x_2) = \theta(t_1-t_2)X^{<}(x_1,x_2) + \theta(t_2-t_1)X^{>}(x_1,x_2) \ , \tag{5.14}$$

with θ the Heaviside function, for $X = G, \Delta, S$. It is then sufficient to consider only two of the propagators as independent. In the present study, we will focus on the Wightman functions $S^{\lessgtr}$. In the following section, we describe the evolution equations they satisfy, known as the Kadanoff-Baym equations.

5.2 Kadanoff-Baym equations

We apply the CTP formalism to leptogenesis, involving fermionic fields. We use the assumption of spatial homogeneity to arrive at compact equations (5.47) that will be the starting point of the local approximation in section 5.3.

5.2.1 Propagators and kinetic equations

Given a fermionic field ψ, we introduced the two Wightman functions

$$iS^{<}_{\alpha\beta}(x_1,x_2) \equiv -\left\langle \overline{\psi}_\beta(x_2)\psi_\alpha(x_1)\right\rangle \ , \tag{5.15a}$$

$$iS^{>}_{\alpha\beta}(x_1,x_2) \equiv \left\langle \psi_\alpha(x_1)\overline{\psi}_\beta(x_2)\right\rangle \ . \tag{5.15b}$$

We use the most commonly used notation with a minus sign for $S^<$, but note that in [167, 168, 172], which we follow for the Local Approximation later, the opposite sign is taken. Physically, ψ could either be a SM fermion, specifically the $SU(2)$ lepton doublet l_a we will be interested in for leptogenesis, or a Majorana neutrino N. Some linear combinations of $S^>$ and $S^<$ are of physical interest. It is common to introduce the spectral S^ρ and the statistical S^F correlation functions

$$S^\rho \equiv \frac{i}{2}\left(S^> - S^<\right) \ , \ S^F \equiv \frac{1}{2}\left(S^> + S^<\right) \ . \tag{5.16}$$

We will also need to introduce the retarded and advanced propagators S^R and S^A defined as

$$S^R \equiv -2i\ \theta(t_1 - t_2)S^\rho \ , \ S^A \equiv 2i\ \theta(t_2 - t_1)S^\rho \ . \tag{5.17}$$

They contain the information of the spectral propagator S_ρ on the two regions $t_1 < t_2$ and $t_1 > t_2$. Further more, we can take the hermitian and anti-hermitian parts of these propagators,

$$S^{\mathcal{H}} \equiv \frac{1}{2}\left(S^R + S^A\right) \ , \ S^\rho = \frac{i}{2}\left(S^R - S^A\right) \ . \tag{5.18}$$

In the Closed-Time-Path (CTP) formalism, one is interested in a path that is formally a loop in time, such that we consider, roughly speaking, the propagation from x_1 to x_2 and the propagation backwards. We can consider the propagator

$$S(x_1, x_2) \equiv \theta_{\mathcal{C}}(t_1 - t_2)S^>(x_1, x_2) + \theta_{\mathcal{C}}(t_2 - t_1)S^<(x_1, x_2) \ . \tag{5.19}$$

The times t_1 and t_2 can either lie on the upper or on the lower branch of the CTP. They are ordered by $\theta_{\mathcal{C}}(t_1 - t_2)$ on the complex path, with $\theta_{\mathcal{C}}(t_1 - t_2) = 1$ if t_2 is before t_1 on the path, 0 otherwise. The self-energy Σ of the field is defined as the correction, due to interactions, of the dressed propagator S compared to the propagator of the free theory (or bare propagator) S_0. Explicitly, it is defined by the Schwinger-Dyson equation [173]

$$S^{-1}(x_1, x_2) = S_0^{-1}(x_1, x_2) - \Sigma(x_1, x_2) \ . \tag{5.20}$$

This equation summarizes how the interactions modify the free propagator. S_0 is given by the purely kinetic part of the theory; for a massless $SU(2)$ doublet l_a and a heavy neutrino, respectively, the free propagators are

$$\left(S_{0,l_a}\right)^{-1} = i\delta^{(4)}_{\mathcal{C}}(x_1 - x_2)P_L\partial\!\!\!/_1 \ , \ \left(S_{0,N}\right)^{-1} = \delta^{(4)}_{\mathcal{C}}(x_1 - x_2)\left(i\partial\!\!\!/_1 - M_N(x_1)\right) \ . \tag{5.21}$$

The partial derivative acts on the x_1 variable, we write $\partial_1 \equiv \left(\frac{\partial}{\partial x_1^\mu}\right)$. Note that the mass matrix M_N is a matrix in the space of neutrino flavors, but is proportional to identity in spinorial space. It is space-time dependent, as we will consider the evolution of sterile neutrinos during a FOPT. We also define the contributions of the self-energy to the forward and backward propagation $\Sigma^{\lessgtr}$ in the same fashion as in Equation (5.19),

$$\Sigma \equiv \theta_{\mathcal{C}}(t_1 - t_2)\Sigma^>(x_1, x_2) + \theta_{\mathcal{C}}(t_2 - t_1)\Sigma^<(x_1, x_2) \ , \tag{5.22}$$

from which we derive the same linear relations as for $S^{\lessgtr}$, in order to define $\Sigma^{F/\rho}$, $\Sigma^{R/A}$, etc.

In the following, we focus only on the propagator for the neutrinos. Similar manipulations can be applied to the lepton correlation functions.

5.2.2 Derivation of the Kadanoff-Baym equation

A more convenient way to use Equation (5.20) is by first taking the convolution product *on the path* $\mathcal{C}$ on the right by S

$$S^{-1} *_{\mathcal{C}} S = S_0^{-1} *_{\mathcal{C}} S - \Sigma *_{\mathcal{C}} S \ , \tag{5.23}$$

where the $*_{\mathcal{C}}$ product is defined as

$$(F *_{\mathcal{C}} G)(x_1, x_2) \equiv \int_{\mathcal{C}} \mathrm{d}^4 x \ F(x_1, x) G(x, x_2) \ . \tag{5.24}$$

Using $(S^{-1} *_{\mathcal{C}} S)(x_1, x_2) = \delta_{\mathcal{C}}^{(4)}(x_1 - x_2)$ and the expression for S_0^{-1},

$$\delta_{\mathcal{C}}^{(4)}(x_1 - x_2) = \left(i\partial\!\!\!/_1 - M_N(x_1)\right) S(x_1, x_2) - \int_{\mathcal{C}} \mathrm{d}^4 x \ \Sigma(x_1, x) S(x, x_2) \ . \tag{5.25}$$

It is usually more convenient to work with the Wightman functions $S^{\lessgtr}$. Expressing the propagator S like in (5.19), the derivative term becomes

$$\begin{aligned} i\partial\!\!\!/_1 S &= \theta_{\mathcal{C}}(t_1 - t_2) i\partial\!\!\!/_1 S^{>} + \theta_{\mathcal{C}}(t_2 - t_1) i\partial\!\!\!/_1 S^{<} + i\delta_{\mathcal{C}}(t_1 - t_2)\gamma^0 S^{>} - i\delta_{\mathcal{C}}(t_2 - t_1)\gamma^0 S^{<} \\ &= \theta_{\mathcal{C}}(t_1 - t_2) i\partial\!\!\!/_1 S^{>} + \theta_{\mathcal{C}}(t_2 - t_1) i\partial\!\!\!/_1 S^{<} + 2\delta_{\mathcal{C}}(t_1 - t_2)\gamma^0 S^{\rho} \end{aligned} \tag{5.26}$$

We take the limit of equal time $t_1 \to t_2$ for the spectral propagator in factor of the Dirac δ function. Given the canonical anti-commutation relation between the field ψ and its conjugate field $\overline{\psi}$, we obtain

$$\lim_{t_1 \to t_2} i\gamma^0 S^{\rho}(x_1, x_2) = \gamma^0 \frac{1}{2} \left\langle \left\{ \psi(t_1, \mathbf{x}_1) \overline{\psi}(t_2, \mathbf{x}_2) \right\} \right\rangle = \frac{1}{2} \delta^{(3)}(\mathbf{x}_1 - \mathbf{x}_2) \ . \tag{5.27}$$

All together, we obtain a $\delta_{\mathcal{C}}^{(4)}(x_1 - x_2)$ from the derivative term that cancels out with the one on the left-hand side of (5.25). We still need to rewrite

$$\begin{aligned} \Sigma(x_1, x) S(x, x_2) &= \left[\theta_{\mathcal{C}}(t_1 - t)\Sigma^{>} + \theta_{\mathcal{C}}(t - t_1)\Sigma^{<}\right] \left[\theta_{\mathcal{C}}(t - t_2) S^{>} + \theta_{\mathcal{C}}(t_2 - t) S^{<}\right] \\ &= \left[\theta_{\mathcal{C}}(t_1 - t) \left(\Sigma^{>} - \Sigma^{<}\right) + \Sigma^{<}\right] \left[\theta_{\mathcal{C}}(t - t_2) \left(S^{>} - S^{<}\right) + S^{<}\right] \ , \end{aligned} \tag{5.28}$$

using $\theta_{\mathcal{C}}(-u) = 1 - \theta_{\mathcal{C}}(u)$. In order to regroup the terms, we need to remember that the integration in (5.25) is over the closed-path $\mathcal{C}$, such that

$$\int_{\mathcal{C}} \mathrm{d}^4 x \ \theta_{\mathcal{C}}(t_1 - t) \ [...] = \int_{t_i}^{t_1} \mathrm{d}t \int \mathrm{d}^3\mathbf{x} \ [...] = - \int_{\mathcal{C}} \mathrm{d}^4 x \ \theta_{\mathcal{C}}(t - t_1) \ [...] \ , \tag{5.29}$$

$$\int_{\mathcal{C}} \mathrm{d}^4 x \ \theta_{\mathcal{C}}(t_1 - t)\theta_{\mathcal{C}}(t - t_2) \ [...] = \theta_{\mathcal{C}}(t_1 - t_2) \int_{t_2}^{t_1} \mathrm{d}t \int \mathrm{d}^3\mathbf{x} \ [..] \ . \tag{5.30}$$

We can decompose the integral into terms proportional to either $\theta_{\mathcal{C}}(t_1 - t_2)$ or $\theta_{\mathcal{C}}(t_2 - t_1)$,

$$\begin{aligned}
\int_{\mathcal{C}} \mathrm{d}^4x\ \Sigma S &= \int_{t_i}^{t_2} 2i\Sigma^< S^\rho - \int_{t_i}^{t_1} 2i\Sigma^\rho S^< + \theta_{\mathcal{C}}(t_1 - t_2) \int_{t_2}^{t_1} (2i\Sigma^\rho)\,(2iS^\rho) \\
&= \theta_{\mathcal{C}}(t_1 - t_2) \left[\int_{t_2}^{t_1} (2i\Sigma^\rho)\,(2iS^\rho) + \int_{t_i}^{t_2} 2i\Sigma^< S^\rho - \int_{t_i}^{t_1} 2i\Sigma^\rho S^< \right] \\
&\quad + \theta_{\mathcal{C}}(t_2 - t_1) \left[\int_{t_i}^{t_2} 2i\Sigma^< S^\rho - \int_{t_i}^{t_1} 2i\Sigma^\rho S^< \right] \\
&= \theta_{\mathcal{C}}(t_1 - t_2) \left[\int_{t_i}^{t_2} 2i\Sigma^> S^\rho - \int_{t_i}^{t_1} 2i\Sigma^\rho S^> \right] \\
&\quad + \theta_{\mathcal{C}}(t_2 - t_1) \left[\int_{t_i}^{t_2} 2i\Sigma^< S^\rho - \int_{t_i}^{t_1} 2i\Sigma^\rho S^< \right] . \qquad (5.31)
\end{aligned}$$

Identifying the $\theta_{\mathcal{C}}$ components, we get the so-called Kadanoff-Baym equations for $S^{\lessgtr}$

$$\left(i\partial\!\!\!/_1 - M_N(x_1)\right) S^s(x_1, x_2) = \int_{t_i}^{t_2} 2i\Sigma^s S^\rho - \int_{t_i}^{t_1} 2i\Sigma^\rho S^s \ ,\ s = <, > \ . \qquad (5.32)$$

The equations involve an integral over the values of the (unknown) propagator at different times, making them non local. The boundaries of the integral depend on the argument t_1 and t_2. It is usually more convenient to rewrite the right-hand term as integrals over an infinite interval, using retarded and advanced functions (5.17),

$$\left(i\partial\!\!\!/_1 - M_N(x_1)\right) S^s(x_1, x_2) = \int_{t_i}^{+\infty} \Sigma^s S^A + \int_{t_i}^{+\infty} \Sigma^R S^s \ ,\ s = <, > \ . \qquad (5.33)$$

For all our purposes, the initial time at which we start our evolution can be considered far in the past compared to the typical time of the processes we will consider, $t_i \to -\infty$. We find that the Kadanoff-Baym equations can be written

$$\left(i\partial\!\!\!/_1 - M_N(x_1)\right) S^<(x_1, x_2) = \left(\Sigma^R * S^< + \Sigma^< * S^A\right)(x_1, x_2) \ . \qquad (5.34)$$

$$\left(i\partial\!\!\!/_1 - M_N(x_1)\right) S^>(x_1, x_2) = \left(\Sigma^R * S^> + \Sigma^> * S^A\right)(x_1, x_2) \ , \qquad (5.35)$$

with the $*$-product defined as the standard convolution product

$$(\Sigma * S)(x_1, x_2) = \int_{\mathbb{R}^4} \mathrm{d}^4x\ \Sigma(x_1, x) S(x, x_2) \ . \qquad (5.36)$$

These are the equations that describe the dynamics in full generality. If we know the quantum state of the field at some initial time, we get the initial conditions for the correlation functions. It is however hard to solve (5.34) and (5.35), mainly because they are *integro-differential* equations. Their right-hand terms, a convolution product between self-energies and the propagator, involve the value of the propagator (the unknown) at all values of space-time. This makes even a numerical approach very complex, not to mention analytical approaches. We will describe how to deal with this problem later.

5.2.3 Spatial homogeneity and isotropy

The equations (5.34),(5.35) contain information about correlation functions between any two points in space-time. Assuming the FOPT implies a mass that is only time-dependent (*i.e.* neglecting the spatial expansion of the bubble, at least on average), the Universe can be taken spatially homogeneous. This means the propagators should only depend on the spatial separation between the two arguments (and also still on the absolute values of time arguments). It is then convenient to work in momentum space, by taking the Fourier Transform (FT) of the propagators, defined by

$$S_{\mathbf{k}}(t_1,t_2) \equiv \int \mathrm{d}^3\mathbf{r}\ S((\mathbf{x}_1,t_1),(\mathbf{x}_1+\mathbf{r},t_2))e^{i\mathbf{k}\cdot\mathbf{r}} = \int \mathrm{d}^3\mathbf{r}\ S(\mathbf{r};t_1,t_2)e^{i\mathbf{k}\cdot\mathbf{r}}\ . \tag{5.37}$$

The FT replaces the convolution over space-time by convolution only over time,

$$(\Sigma * S)_{\mathbf{k}}(t_1,t_2) \equiv \int \mathrm{d}^3\mathbf{r}\ \ (\Sigma * S)(x_1,x_2)e^{i\mathbf{k}\cdot\mathbf{r}} = \int \mathrm{d}t\ \Sigma_{\mathbf{k}}(t_1,t)S_{\mathbf{k}}(t,t_2) = (\Sigma_{\mathbf{k}} * S_{\mathbf{k}})(t_1,t_2)\ . \tag{5.38}$$

For simplicity we will keep the same notations for the convolution product over space-time than the convolution only over time. It should be understood as the convolution over whatever space-time indices the functions depend on. Taking the FT of (5.34),(5.35), paying attention to the space-time derivatives, gives the following equations

$$\left(i\gamma^0\partial_{t_1} + \mathbf{k}\cdot\boldsymbol{\gamma} - M_N(t_1)\right) S^<_{\mathbf{k}}(t_1,t_2) = \left(\Sigma^R_{\mathbf{k}} * S^<_{\mathbf{k}} + \Sigma^<_{\mathbf{k}} * S^A_{\mathbf{k}}\right)(t_1,t_2)\ . \tag{5.39a}$$

$$\left(i\gamma^0\partial_{t_1} + \mathbf{k}\cdot\boldsymbol{\gamma} - M_N(t_1)\right) S^>_{\mathbf{k}}(t_1,t_2) = \left(\Sigma^R_{\mathbf{k}} * S^>_{\mathbf{k}} + \Sigma^>_{\mathbf{k}} * S^A_{\mathbf{k}}\right)(t_1,t_2)\ . \tag{5.39b}$$

5.2.4 Local evolution equations

Preparing the ground for the local approximation of the next section, we will focus on the equation for the local part of the propagators, *i.e.* the equal-time propagators $S^{</>}_{\mathbf{k}}(t,t)$. Its interest is that we have extra symmetries (see [138, 167]) of the propagators, notably

$$\left(i\gamma_0 S^{</>}_{\mathbf{k}}\right)^\dagger(t,t) = -i\gamma^0 S^{</>}_{\mathbf{k}}(t,t)\ , \tag{5.40}$$

$$\left(i\gamma_0 S^<_{\mathbf{k}} - i\gamma_0 S^>_{\mathbf{k}}\right)(t,t) = 2\gamma^0 S^\rho_{\mathbf{k}}(t,t) = \mathbb{I}\ . \tag{5.41}$$

Equation (5.41) is known as the spectral rule, or the sum rule. Equations (5.39a),(5.39b) can then be decomposed into hermitian and anti-hermitian parts, with the time derivative only appearing in the anti-hermitian part. The hermitian one is a constraint equation. We write both explicitly for $S^<(t,t)$ (a similar derivation applies for $S^>$), and we have

$$\left\{\left(M_N(t) - \mathbf{k}\cdot\boldsymbol{\gamma}\right)\gamma^0, \gamma^0 S^<_{\mathbf{k}}\right\} = \left(\Sigma^R_{\mathbf{k}} * S^<_{\mathbf{k}} + \Sigma^<_{\mathbf{k}} * S^A_{\mathbf{k}} + \text{h.c.}\right)(t,t)\ , \tag{5.42}$$

$$i\gamma^0\partial_t S^<_{\mathbf{k}}(t,t) - \left[\left(M_N(t) - \mathbf{k}\cdot\boldsymbol{\gamma}\right)\gamma^0, \gamma^0 S^<_{\mathbf{k}}\right] = \left(\Sigma^R_{\mathbf{k}} * S^<_{\mathbf{k}} + \Sigma^<_{\mathbf{k}} * S^A_{\mathbf{k}} - \text{h.c.}\right)(t,t)\ . \tag{5.43}$$

We should bear in mind that the time derivative acts on both arguments of $S^<_{\mathbf{k}}(t,t)$,

$$\partial_t S^<_{\mathbf{k}}(t,t) = \lim_{t_1 \to t_2} \left[\left(\partial_{t_1} + \partial_{t_2} \right) S^<_{\mathbf{k}}(t_1, t_2) \right] \ . \tag{5.44}$$

The first two terms of Equation (5.43) are reminiscent of a Schrödinger equation; the commutator with $\gamma^0 S^<_{\mathbf{k}}$ can be identified as a commutator with a Hamiltonian $\mathbf{H}_0$ given by

$$\mathbf{H}_0(t) \equiv \left(M_N(t) - \mathbf{k} \cdot \boldsymbol{\gamma} \right) \gamma^0 = M_N(t) \gamma^0 + \gamma^0 \mathbf{k} \cdot \boldsymbol{\gamma} \ . \tag{5.45}$$

Note that for more than one sterile neutrino flavor, $\mathbf{H}_0$ is a matrix in both the neutrino family space (in which we assume M to be diagonal) and the spinorial space. Defining $\mathcal{S} \equiv \gamma^0 S$, $\mathbf{\Sigma} \equiv \Sigma \gamma^0$ (for all propagator indices, $R, A, <, >$),

$$\left\{ \mathbf{H}_0, \mathcal{S}^<_{\mathbf{k}}(t,t) \right\} = \left(\mathbf{\Sigma}^R_{\mathbf{k}} * \mathcal{S}^<_{\mathbf{k}} + \mathbf{\Sigma}^<_{\mathbf{k}} * \mathcal{S}^A_{\mathbf{k}} + \text{h.c.} \right)(t,t) \ , \tag{5.46}$$

$$i \partial_t \mathcal{S}^<_{\mathbf{k}}(t,) - \left[\mathbf{H}_0, \mathcal{S}^<_{\mathbf{k}}(t,t) \right] = \left(\mathbf{\Sigma}^R_{\mathbf{k}} * \mathcal{S}^<_{\mathbf{k}} + \mathbf{\Sigma}^<_{\mathbf{k}} * \mathcal{S}^A_{\mathbf{k}} - \text{h.c.} \right)(t,t) \ . \tag{5.47}$$

These equations, while describing the evolution of the local part of the propagator, are still non local due to the convolutions on the right-hand side, that involve the propagators' values at all times. We will see how to deal with this issue in section 5.3. Let us first describe these equations in terms of convenient phase space distribution functions.

5.2.5 Mass- and coherence-shell distribution functions

In order to get a better physical understanding of the equation (5.47), it is useful to look at the simpler case of a free field, with only one flavor. The free part of the above equation is the equation obtained by putting all interactions to zero, *i.e.* all self-energies $\Sigma = 0$. The equation is just driven by the vacuum Hamiltonian

$$\partial_t \mathcal{S}^<_{\mathbf{k}} = -i \left[M \gamma^0 + \gamma^0 \boldsymbol{\gamma} \cdot \mathbf{k}, \mathcal{S}^<_{\mathbf{k}} \right] = -i \left[\mathbf{H}_0, \mathcal{S}^<_{\mathbf{k}} \right] \ . \tag{5.48}$$

One can define phase space distributions as the components (in a basis that we define further below) of the sterile neutrino propagator,

$$f_h^{s,s'}(t) \equiv -i \text{Tr} \left[\mathcal{P}_h^{ss'}(t) \mathcal{S}^<_{\mathbf{k}}(t,t) \right] \ , \ \mathcal{S}^<_{\mathbf{k}}(t,t) = i \sum_{h,s,s'} f_h^{s,s'}(t) \mathcal{P}_h^{ss'}(t) \ . \tag{5.49}$$

These functions describe how the propagator transports a particle of energy $s' \, \omega$ (where negative energies means we actually consider the anti-particle) to a particle of energy $s \, \omega$, with a given helicity h. These transitions can then be of two types, a particle-particle one preserving the sign of energy, and a particle-antiparticle one that changes the sign. Physically, we associate them to two separate kind of phase space distributions. The ones corresponding to particle-particle transitions (*i.e.* $s = s'$) are called mass-shell ($f_h^{m,s}$), and the ones for particle-antiparticle transitions (*i.e.* $s = -s'$) are called coherence-shell ($f_h^{c,s}$) ,

$$f_h^{m,s} \equiv f_h^{s,s} \ , \ f_h^{c,s} \equiv f_h^{s,-s} \ . \tag{5.50}$$

These distribution functions are found using projectors on eigenstates of $\mathbf{H}_0$. Note how $\mathbf{H}_0^2 = (M^2(t) + |\mathbf{k}|^2)\,\mathbb{I} \equiv \omega^2(t)\mathbb{I}$. The eigenvalues of the free Hamiltonian thus represent the energy states accessible to the particles (or anti-particles). They can be positive or negative,

$$E_s = s\sqrt{|\mathbf{k}|^2 + M^2(t)} = s\omega(t) \ , \ s = \pm \ . \tag{5.51}$$

Note the explicit time dependence of these energy eigenvalues. We use the Hamiltonian to define the projectors

$$\mathbf{P}^s(t) \equiv \frac{1}{2}\left(\mathbb{I} + s\frac{\mathbf{H}_0}{\omega(t)}\right) \ , \ \mathbf{P}^s\mathbf{H}_0 = s\omega\mathbf{P}^s \ . \tag{5.52}$$

Particles of a given energy can have different helicities $h = \pm$; defining a projector on helicity, we notice that it commutes with the projector on energy,

$$P_h \equiv \frac{1}{2}\left(\mathbb{I} + h\gamma^0\boldsymbol{\gamma}\cdot\hat{\mathbf{k}}\gamma^5\right) \ , \ [P_h, \mathbf{P}^s(t)] = 0 \ , \ \hat{\mathbf{k}} \equiv \frac{\mathbf{k}}{|\mathbf{k}|} \ . \tag{5.53}$$

It only depends on momentum direction, in particular it is not time dependent. We now have detailed enough the states described by our propagator. Given that the accessible energies are $\pm\omega$ with two possible helicities in both case, we can construct a basis of 8 linear independent matrices that are used in the definition (5.49),

$$\mathcal{P}_h^{ss'}(t) \equiv N^{ss'}(t)P_h\mathbf{P}^s(t)\gamma^0\mathbf{P}^{s'}(t) \ . \tag{5.54}$$

The factor $N^{ss'}(t)$ is a normalization factor. We define it as

$$N^{ss'}(t) \equiv \left[\mathrm{Tr}\left(P_h P\mathbf{P}_I^s(t)\gamma^0\mathbf{P}_J^{s'}(t)\gamma^0\right)\right]^{-1/2} = \sqrt{\frac{2\omega(t)^2}{\omega(t)^2 + ss'\left(M(t)^2 - |\mathbf{k}|^2\right)}} = \begin{vmatrix} \dfrac{\omega(t)}{M(t)} & \text{if } s = s' \\ \dfrac{\omega(t)}{|\mathbf{k}|} & \text{if } s = -s' \end{vmatrix} \ . \tag{5.55}$$

It doesn't depend on helicity, but it does depend on time.

The dynamics of each function, in the free theory, are derived from (5.48),

$$i\partial_t f_h^{m,s} = i\frac{|\mathbf{k}|}{2}\frac{\partial_t M}{\omega(t)^2}\left(f_h^{c,s} + f_h^{c,-s}\right) \ , \tag{5.56a}$$

$$i\partial_t f_h^{c,s} = 2s\omega f_h^{c,s} - i\frac{|\mathbf{k}|}{2}\frac{\partial_t M}{\omega(t)^2}\left(f_h^{m,s} + f_h^{m,-s}\right) \ . \tag{5.56b}$$

We made use of the properties of the projector $\mathbf{H}_0\mathcal{P}_h^{ss'} = s\omega\mathcal{P}_h^{ss'}$, $\mathcal{P}_h^{ss'}\mathbf{H}_0 = s'\omega\mathcal{P}_h^{ss'}$ to get the oscillation term $2s\omega f_h^{c,s}$. The other terms, appearing in both equations, and coupling the coherence- and mass-shell functions come from the time dependence of the projector, in the basis we chose to project our propagator on. The time derivatives of the projectors satisfy

$$\partial_t\mathcal{P}_h^{m,s} = \partial_t\mathcal{P}_h^{ss} = \frac{|\mathbf{k}|\partial_t M}{2\omega^2}\left(\mathcal{P}_h^{c,s} + \mathcal{P}_h^{c,-s}\right) \ , \tag{5.57}$$

$$\partial_t \mathcal{P}_h^{c,s} = \partial_t \mathcal{P}_h^{s,-s} = -\frac{|\mathbf{k}|\partial_t M}{2\omega^2}\left(\mathcal{P}_h^{m,s} + \mathcal{P}_h^{m,-s}\right) \ . \tag{5.58}$$

This leads to the coupling between mass- and coherence-shell functions in Equation (5.56).

The equations (5.56) illustrate the effect of an explicitly time-dependent mass. Indeed, the derivative of M implies an interaction between mass- and coherence-shell functions that is not present otherwise (if $\partial_t M = 0$). These non-trivial dynamics relate to the discussion in section 4 about particle production during the FOPT. Indeed, recalling the Dirac equation for a (free) Majorana field in terms of the modes L_h/R_h,

$$i\partial_t L_h + h|\mathbf{k}|L_h - M(t)R_h = 0 \ , \ i\partial_t R_h - h|\mathbf{k}|R_h - M(t)L_h = 0 \ , \tag{5.59}$$

it can be checked that

$$f_h^{m,s} \equiv \frac{s}{2} + \frac{1-2f_{0\mathbf{k}}}{2\sqrt{|\mathbf{k}|^2+M(t)^2}}\left[h|\mathbf{k}|\left(|L_h|^2 - |R_h|^2\right) + 2M(t)\mathrm{Re}\left[L_h R_h^*\right]\right] \ , \tag{5.60}$$

$$f_h^{c,s} \equiv -\frac{h\left(1-2f_{0\mathbf{k}}\right)}{2\sqrt{|\mathbf{k}|^2+M(t)^2}}\left[M(t)\left(|L_h|^2 - |R_h|^2\right) + 2h|\mathbf{k}|\mathrm{Re}\left[L_h R_h^*\right] - 2i\sqrt{|\mathbf{k}|^2+M(t)^2}\mathrm{Im}\left[L_h R_h^*\right]\right] \ , \tag{5.61}$$

are solutions of the system of equations (5.56). We recognize in $f_h^{m,+}$ the instantaneous particle distribution in momentum $f_{\mathbf{k}}$ that we calculated in Equation (4.62). It is no surprise that we find the same result, as the free propagator $\mathcal{S}_{\mathbf{k}}^<$ is constructed from the modes of a field that is a solution of the Dirac equation. What we conclude here is that the determination of the L_h/R_h functions not only gives us the particle number density, but also the whole propagator with a time-dependent mass, at the free level.

5.2.6 Flavored shell functions

The flavored version of the mass- and coherence-shell distribution functions are simply

$$f_{h,IJ}^{m,s} \equiv -i\mathrm{Tr}\left[\mathcal{P}_h^{ss}{}_{JI}\mathcal{S}_{\mathbf{k},IJ}^<(t,t)\right] \ , \ f_{h,IJ}^{c,s} \equiv -i\mathrm{Tr}\left[\mathcal{P}_h^{s-s}{}_{JI}\mathcal{S}_{\mathbf{k},IJ}^<(t,t)\right] \ . \tag{5.62}$$

The (free) Hamiltonian $\mathbf{H}_0$ was extended to be also a diagonal matrix in flavor space,

$$(\mathbf{H}_0)_{IJ} = \gamma^0 M_I \delta_{IJ} + \gamma^0 \boldsymbol{\gamma}\cdot\mathbf{k}\delta_{IJ} = \left(\gamma^0 M_I + \gamma^0\boldsymbol{\gamma}\cdot\mathbf{k}\right)\delta_{IJ} = \mathbf{H}_0^I\delta_{IJ} \ . \tag{5.63}$$

Similarly to before, we have defined the projectors on energy

$$\mathbf{P}_I^s \equiv \frac{1}{2}\left(\mathbb{I} + s\frac{\mathbf{H}_0^I}{\omega_I}\right) \ , \ \omega_I(t) \equiv \sqrt{|\mathbf{k}|^2 + M_I(t)^2} \ , \tag{5.64}$$

and the full projectors for our propagators

$$\mathcal{P}_{h,IJ}^{ss'} \equiv N_{IJ}^{ss'} P_h \mathbf{P}_I^s \gamma^0 \mathbf{P}_J^{s'} \ , \tag{5.65}$$

$$N_{IJ}^{ss'} \equiv \sqrt{\frac{2\omega_I(t)\omega_J(t)}{\omega_I(t)\omega_J(t) + ss'\left(M_I(t)M_J(t) - |\mathbf{k}|^2\right)}} \ . \tag{5.66}$$

The mass- and coherence-shell distributions can still be seen as describing the transition between a particle of energy $s'\ \omega$ and flavor J and a particle of energy $s\ \omega$ and flavor I. One of the main differences with the flavorless case is that we also have oscillations for the mass-shell function, from transitions between particles of different flavors. The typical frequency for the mass-shell distribution is given by the energy difference $\omega_I - \omega_J$. It is smaller (in absolute value) than the frequency for coherence-shell distributions, which goes as the sum $\omega_I + \omega_J$.

Because of the Majorana nature of the sterile neutrinos, these distribution functions satisfy symmetries. For a Majorana field, the symmetries of the (equal-time) propagator are explicitly written (see Appendix D in [167] for more details)

$$\left(\mathcal{S}^<_{\mathbf{k},IJ}\right)^\dagger(t,t) = \mathcal{S}^<_{\mathbf{k},JI}(t,t) \ , \tag{5.67}$$

$$\mathcal{S}^>_{\mathbf{k},IJ}(t,t) - \mathcal{S}^<_{\mathbf{k},IJ}(t,t) = \delta_{IJ}\mathbb{I} \ , \tag{5.68}$$

$$\left(\mathcal{S}^<_{\mathbf{k},IJ}\right)^T(t,t) = \gamma^0 C \mathcal{S}^>_{-\mathbf{k},JI}(t,t) C\gamma^0 \ . \tag{5.69}$$

The propagators used to define the mass- and coherence-shell function satisfy similar properties, namely

$$\left(\mathcal{P}^{ss'}_{\mathbf{k},IJ}\right)^T(t,t) = \gamma^0 C \mathcal{P}^{-s-s'}_{-\mathbf{k},JI}(t,t) C\gamma^0 \ . \tag{5.70}$$

In the end, all these relations inserted in the trace give us symmetries for the mass- and coherence-shell functions

$$f^{m,s}_{h,IJ} = 1 - f^{m,-s}_{h\ JI} = \left(f^{m,s}_{h,JI}\right)^* \ , \tag{5.71}$$

$$f^{c,s}_{h,IJ} = -\left(f^{c,-s}_{h\ JI}\right)^* = f^{c,s}_{h,JI} \ . \tag{5.72}$$

Both for mass- and coherence-shell functions, the distributions $s = +$ and $s = -$ are not independent. For two sterile neutrinos, the mass-shell matrix $f^{m,+}_{h,IJ}$ is a 2-by-2 hermitian matrix, with 4 independent components, while the coherence-shell matrix $f^{c,+}_{h,IJ}$ is a 2-by-2 symmetric complex matrix, with 6 independent components.

We have identified the scalar functions of interest that can be derived from the (equal-time) propagator $\mathcal{S}^<(t,t)$. Turning interactions back on, we need to deal with the non-local terms in the KB equation (5.47).

5.3 Local approximation and adiabatic background

The local approximation (LA), first defined in [167], is a method for reducing the complexity of the non local KB equations. The idea is to introduce a known adiabatic background containing the information about the non localities, and to only solve for the remaining local data. This

method allows us to keep quantum correlations while reducing the complexity.

The first step is to consider an adiabatic background that dominates the self-energy. In the leptogenesis picture, the thermal bath is the main contribution to the self-energy of the sterile neutrinos, while small deviation will arise from non-zero chemical potentials for the lepton and Higgs fields as an asymmetry gets created. We then *define* the deviations from the adiabatic background by

$$\mathbf{\Sigma}_{\mathbf{k}}(t_1,t_2) = \mathbf{\Sigma}_{\mathrm{ad},\mathbf{k}}(t_1,t_2) + \delta\mathbf{\Sigma}_{\mathbf{k}}(t_1,t_2)\ , \tag{5.73}$$

$$\mathcal{S}_{\mathbf{k}}(t_1,t_2) = \mathcal{S}_{\mathrm{ad},\mathbf{k}}(t_1,t_2) + \delta\mathcal{S}_{\mathbf{k}}(t_1,t_2)\ . \tag{5.74}$$

We will discuss later the choice of $\mathbf{\Sigma}_{\mathrm{ad}}$ and $\mathcal{S}_{\mathrm{ad}}$, but the important part is that they are known and fixed once and for all. We require that they form a stationary solution of our equations, meaning that the right-hand side of Equation (5.47) should vanish when replacing $\mathcal{S}_{\mathbf{k}}$ by $\mathcal{S}_{\mathrm{ad},\mathbf{k}}$ and $\mathbf{\Sigma}_{\mathbf{k}}$ by $\mathbf{\Sigma}_{\mathrm{ad},\mathbf{k}}$.

So far, we have done no approximation and this is merely a redefinition of what our unknowns are. The LA is the following step; instead of considering a generic deviation $\delta\mathcal{S}$, we assume that its non local values are given by propagating its local values using the (spectral function of the) adiabatic background. In other words, the LA is written

$$\delta\mathcal{S}^{<}_{\mathbf{k}}(t_1,t_2) = \left(2\mathcal{S}^{\rho}_{\mathrm{ad},\mathbf{k}}(t_1,t)\right)\delta\mathcal{S}^{<}_{\mathbf{k}}(t,t)\left(2\mathcal{S}^{\rho}_{\mathrm{ad},\mathbf{k}}(t,t_2)\right)\ . \tag{5.75}$$

It was noted in [167] that this condition implies that the retarded and advanced propagators can be taken purely adiabatic, $\mathcal{S}^{R/A} = \mathcal{S}^{R/A}_{\mathrm{ad}}$, and in particular $\delta\mathcal{S}^{R/A} = 0$. This result is exact in a free theory, so considering the retarded and advanced deviations from the adiabatic background would be of higher order in the couplings and we will not consider it here.

The argument t in Equation (5.75) is in principle arbitrary, and it will be useful, depending on how it gets convoluted, to put it to $t = t_2$, such that the LA (5.75) becomes $\delta\mathcal{S}_{\mathbf{k}}(t_1,t_2) = \left(2\mathcal{S}^{\rho}_{\mathrm{ad},\mathbf{k}}(t_1,t_2)\right)\delta\mathcal{S}_{\mathbf{k}}(t_2,t_2)$.

The convolutions are now calculated

$$\begin{aligned}\left(\mathbf{\Sigma} * \delta\mathcal{S}\right)_{\mathbf{k}}(t_1,t_2) &= \int \mathrm{d}t'\ \mathbf{\Sigma}_{\mathbf{k}}(t_1,t')2\mathcal{S}^{\rho}_{\mathrm{ad},\mathbf{k}}(t',t_2)\delta\mathcal{S}_{\mathbf{k}}(t_2,t_2)\\ &= \left(\mathbf{\Sigma} * 2\mathcal{S}^{\rho}_{\mathrm{ad}}\right)_{\mathbf{k}}(t_1,t_2)\delta\mathcal{S}_{\mathbf{k}}(t_2,t_2)\\ &\equiv \mathbf{\Sigma}^{\mathrm{eff}}_{\mathbf{k}}(t_1,t_2)\delta\mathcal{S}_{\mathbf{k}}(t_2,t_2)\ .\end{aligned} \tag{5.76}$$

The non localities have been packaged into a single object that we call an *effective* self-energy $\mathbf{\Sigma}^{\mathrm{eff}}_{\mathbf{k}}$, so that convolutions with the actual self-energy become simple products with the effective self-energy. Proceeding with this approximation, we can transform the non local equation (5.47) into a simpler equation for the local deformations of the propagator. In particular, most terms involving the adiabatic background will disappear as we assumed it is a stationary solution of the equation (5.47). As described in [167, 168], the equation becomes to leading-order in the

deviations $\delta\mathcal{S}_{\mathbf{k}}$, $\delta\mathbf{\Sigma}_{\mathbf{k}}$,

$$\begin{aligned}\partial_t\left(\delta\mathcal{S}^<_{\mathbf{k}}\right)(t,t) = &-i\left[\mathbf{H}_0, \delta\mathcal{S}^<_{\mathbf{k}}(t,t)\right] - \partial_t\mathcal{S}^<_{\mathrm{ad},\mathbf{k}} \\ &-i\left[\mathbf{\Sigma}^{\mathrm{eff},R}_{\mathrm{ad},\mathbf{k}}(t,t)\delta\mathcal{S}^<_{\mathbf{k}}(t,t) + \mathrm{h.c.}\right] \\ &-i\left[\left(\delta\mathbf{\Sigma}^R_{\mathbf{k}} * \mathcal{S}^<_{\mathrm{ad},\mathbf{k}} + \delta\mathbf{\Sigma}^<_{\mathbf{k}} * \mathcal{S}^A_{\mathrm{ad},\mathbf{k}}\right)(t,t) + \mathrm{h.c.}\right] \ . \end{aligned} \tag{5.77}$$

Note that the unknown $\delta\mathcal{S}$ is no longer involved in any convolution product. We recognize a commutator with a Hamiltonian (the free part of the equation). The adiabatic background acts as a source for the deviation through its time derivative. The second line corresponds to a collision term describing the interactions; it is computed from the (effective) self-energy at equilibrium. Finally, the deviation of the self-energy $\delta_a\mathbf{\Sigma}$ due to non-zero lepton chemical potential induces a backreaction from the asymmetry on the sterile neutrinos.

We now need to specify a certain adiabatic background in order to move on with these equations. The adiabatic background is best described in the so-called Wigner representation, for which we first give a definition.

5.3.1 Wigner representation and gradient expansion

While we switched to momentum space $\mathbf{k}$ for spatial coordinates, we kept the time dependence explicit in these equations to remind ourselves that our fields can be out-of-equilibrium and that dynamics are not time-translation invariant. It will be however be useful for later to consider also a momentum representation in the time coordinate, leading to a full 4-dimensional momentum space described by coordinates $k \equiv (k^0, \mathbf{k})$. For propagators such as $S_{\mathbf{k}}(t_1, t_2)$ with two time arguments, a 4-dimensional momentum representation is given by the so-called Wigner representation. In general, we define the Wigner transform as the Fourier transform with respect to the difference in the time arguments,

$$\tilde{S}(k,t) \equiv \int \mathrm{d}(t_2 - t_1)\ S_{\mathbf{k}}(t_1,t_2)e^{-ik^0(t_2-t_1)} = \int \mathrm{d}y\ S_{\mathbf{k}}\left(t - \frac{y}{2}, t + \frac{y}{2}\right)e^{-ik^0 y}\ , \tag{5.78}$$

$$y = t_2 - t_1\ ,\ t = \frac{t_1+t_2}{2}\ ,\ k = (k^0,\mathbf{k})\ . \tag{5.79}$$

This expression is particularly convenient when we have time-translation symmetry, like for fields in thermal equilibrium. In that case, the Wigner transform of an equilibrium propagator $S_{\mathbf{k},\mathrm{eq}}$ is only a function of 4-momentum, $\tilde{S}_{\mathrm{eq}}(k,t) = \tilde{S}_{\mathrm{eq}}(k)$. The inverse Wigner transform is given by

$$S_{\mathbf{k}}(t_1,t_2) \equiv \int \frac{\mathrm{d}k^0}{2\pi}\ \tilde{S}\left(k, \frac{t_1+t_2}{2}\right)e^{+ik^0(t_2-t_1)}\ . \tag{5.80}$$

The convolution product can be related to the Wigner transforms of the functions by a pretty complicated expression,

$$\begin{aligned}\left(\Sigma_{\mathbf{k}} * S_{\mathbf{k}}\right)(t_1,t_2) &= \int \mathrm{d}t'\ \Sigma_{\mathbf{k}}(t_1,t')S_{\mathbf{k}}(t',t_2) \\ &= \int \frac{\mathrm{d}k^0}{2\pi}\ e^{ik^0(t_2-t_1)}\left[\tilde{\Sigma}(k,t)e^{\frac{i}{2}\left(\overleftarrow{\partial_t}\overrightarrow{\partial_{k^0}}-\overleftarrow{\partial_{k^0}}\overrightarrow{\partial_t}\right)}\tilde{S}(k,t)\right]\Big|_{t=(t_1+t_2)/2} \\ &= \int \frac{\mathrm{d}k^0}{2\pi}\ e^{ik^0(t_2-t_1)} \diamond \left\{\tilde{\Sigma}(k,t),\tilde{S}(k,t)\right\}\Big|_{t=(t_1+t_2)/2} . \end{aligned} \tag{5.81}$$

The $\diamond$ product is the so-called Moyal product [174],

$$\begin{aligned}\diamond\left\{\tilde{F}(k,t),\tilde{G}(k,t)\right\} &\equiv \left[\tilde{F}(k,t)e^{\frac{i}{2}\left(\overleftarrow{\partial_t}\overrightarrow{\partial_{k^0}}-\overleftarrow{\partial_{k^0}}\overrightarrow{\partial_t}\right)}\tilde{G}(k,t)\right] \\ &= \tilde{F}(k,t)\tilde{G}(k,t) + \frac{i}{2}\left[\partial_t\tilde{F}\partial_{k^0}\tilde{G} - \partial_{k^0}\tilde{F}\partial_t\tilde{G}\right] + \dots , \end{aligned} \tag{5.82}$$

where $\overleftarrow{\partial}$ is only acting on the left function (here, $\tilde{F}$) while $\overrightarrow{\partial}$ only acts on the right one (here, $\tilde{G}$). It involves, because of the exponential, an infinite tower of derivatives of the functions. It may be quite impractical to manipulate; it is usually simplified, in out-of-equilibrium studies, by an approximation called the gradient expansion [175]. It consists in neglecting higher order derivatives coming from the Moyal product. We therefore require that the product of the derivatives is small is some sense, that is

$$(\partial_t\partial_{k^0}) \ll 1 . \tag{5.83}$$

This is usually assumed in standard leptogenesis scenarios, where the macroscopic time scales of evolution are related to the Hubble time $t_H \equiv H^{-1}$, which is typically large compared to the microscopic time scales. Indeed, the explicit time dependence, in standard leptogenesis scenarios, is related to the expansion of the Universe. The estimation of the time derivative gives

$$\partial_t \sim H = \frac{T^2}{a_R} , \tag{5.84}$$

while, for on-shell quantities, k^0 will be evaluated at the energy ω

$$\partial_{k^0} \sim \frac{1}{\omega} . \tag{5.85}$$

In the thermal bath, both for relativistic ($\omega \sim T$) and non-relativistic ($\omega \sim M$) sterile neutrinos, the product

$$(\partial_t\partial_{k^0}) \sim \frac{T}{\omega}\frac{T}{a_R} \ll 1 \tag{5.86}$$

is small and the gradient expansion is justified (for temperature well below the Planck scale, which is usually the case).

For the case of a phase transition, this may not be obvious, so let us say a few words

on how it can be justified. In the case of sterile neutrinos, of momentum $\mathbf{k}$, we will have $k^0 \sim \omega = (|\mathbf{k}|^2 + M(t)^2)^{1/2}$, where $M(t)$ is the time-dependent mass scale of the sterile neutrinos. The energy is then time dependent, because the mass is time dependent. If we estimate the derivatives as

$$\partial_{k^0} \sim \frac{1}{k^0} \sim \frac{1}{\omega} \ , \tag{5.87}$$

$$\partial_t = (\partial_t \omega)\, \partial_\omega \sim \frac{\partial_t \omega}{\omega} \tag{5.88}$$

then the gradient expansion is justified as long as

$$(\partial_t \partial_{k^0}) \sim \frac{\partial_t \omega}{\omega^2} = \frac{M \partial_t M}{\omega^3} \ll 1 \ . \tag{5.89}$$

For the sterile neutrino mass during a phase transition, recall that we took a profile

$$M(t) = M_0 \frac{1 + \tanh(\gamma \Delta t)}{2} \ , \tag{5.90}$$

where $\gamma = T_n$ is related to the temperature of the phase transition. The time derivative therefore brings out a factor T_n, and $\partial_t M \sim T_n M$. The condition (5.89) becomes a condition on

$$\frac{M \partial_t M}{\omega^3} \sim \frac{M^2 T_n}{\omega_3} \ . \tag{5.91}$$

Let us consider two extreme cases. For relativistic sterile neutrinos $M \ll T_n$, we have a typical energy $\omega \sim T_n$ and $\frac{M^2 T_n}{\omega_3} \sim \frac{M^2}{T_n^2} \ll 1$. In the other extreme, for non-relativistic sterile neutrinos, $M \gg T_n$, $\omega \sim M$ and $\frac{M^2 T_n}{\omega_3} \sim \frac{T_n}{M} \ll 1$. In both cases, the gradients are suppressed, and the gradient expansion can be justified. We will assume it holds for the rest of our study.

Expanding the Moyal product to zeroth order in gradients, the convolution product is written in terms of the Wigner transformations directly.

$$(\Sigma_{\mathbf{k}} * S_{\mathbf{k}})(t_1, t_2) \simeq \int \frac{\mathrm{d}k^0}{2\pi}\, e^{ik^0(t_2 - t_1)} \tilde{\Sigma}(k,t) \tilde{S}(k,t) \Big|_{t=(t_1+t_2)/2} \ . \tag{5.92}$$

5.3.2 Choice of the adiabatic background

In principle, there is some freedom to choose the adiabatic background. For the self-energy, as it is given by the lepton and Higgs fields, a natural choice is to decompose into the equilibrium part and the deviation from the chemical potentials. As presented for example in [138], both the lepton (μ_a for each flavor) and the Higgs (μ_ϕ) chemical potentials have an effect on the sterile neutrinos. We can expand the self-energy in small $\mu_a, \mu_\phi / T$. The adiabatic background is then the equilibrium part, while the small deviations come from the chemical potentials,

$$\mathbf{\Sigma} \equiv \mathbf{\Sigma}_{\mathrm{eq}} + \sum_a \delta_a \mathbf{\Sigma} \ , \ \mathbf{\Sigma}_{\mathrm{ad}} = \mathbf{\Sigma}_{\mathrm{eq}} \ , \ \delta \mathbf{\Sigma} = \sum_a \delta_a \mathbf{\Sigma} \ . \tag{5.93}$$

We will say more about the expressions of $\mathbf{\Sigma}_{\rm eq}$ and $\delta_a\mathbf{\Sigma}$ in the next section 5.4. For the propagator $\mathcal{S}_{\rm ad}$, a particularly transparent choice, made in [167, 172], is to take the retarded and advanced propagators to be similar to the fermionic propagator with a mass taken at its instantaneous value at time t,

$$\tilde{S}^{A,R}_{\rm ad}(k,t) = \frac{1}{\not{k} - M_N(t) - \tilde{\Sigma}^{A,R}_{\rm eq}(k) \pm i\epsilon} \ , \tag{5.94}$$

and to use them to define the adiabatic Wightman functions

$$\tilde{S}^{<,>}_{\rm ad}(k,t) = \tilde{S}^{R}_{\rm ad}(k,t)\tilde{\Sigma}^{<,>}_{\rm eq}(k)\tilde{S}^{A}_{\rm ad}(k,t) \ . \tag{5.95}$$

Note that we defined the adiabatic propagator in Wigner representation, where it has a nicer form. The retarded adiabatic propagator $\tilde{S}^{A}_{\rm ad}$ (respectively, the advanced adiabatic propagator $\tilde{S}^{R}_{\rm ad}$) came with a $+i\epsilon$ (respectively, $-i\epsilon$) prescription for the poles, that will be important for computing residues later. The equilibrium self-energy $\tilde{\Sigma}^{<,>}_{\rm eq}(k)$ is, by definition, time-translation invariant, therefore it does not depend explicitly on time (in the Wigner representation). Moreover, it satisfies the Kubo-Martin-Schwinger (KMS) relation [176, 177]

$$\tilde{\Sigma}^{>}_{\rm eq}(k) = -e^{k^0/T}\tilde{\Sigma}^{<}_{\rm eq}(k) \ . \tag{5.96}$$

This relation carries on to the adiabatic Wightman functions,

$$\tilde{S}^{>}_{\rm ad}(k,t) = -e^{k^0/T}\tilde{S}^{<}_{\rm ad}(k,t) \ . \tag{5.97}$$

This is a central property for relating the different correlation functions among them, like for example

$$\begin{aligned}\tilde{S}^{<}_{\rm ad}(k,t) = f_{FD}(k^0)\left(\tilde{S}^{<}_{\rm ad}(k,t) - \tilde{S}^{>}_{\rm ad}(k,t)\right) &= 2if_{FD}(k^0)\tilde{S}^{\rho}_{\rm ad}(k,t) \\ &= f_{FD}(k^0)\left(\tilde{S}^{A}_{\rm ad} - \tilde{S}^{R}_{\rm ad}\right)(k,t) \ ,\end{aligned} \tag{5.98}$$

$$\tilde{S}^{>}_{\rm ad}(k,t) = -2i(1-f_{FD}(k^0))\tilde{S}^{\rho}_{\rm ad}(k,t) = -(1-f_{FD}(k^0))\left(\tilde{S}^{A}_{\rm ad} - \tilde{S}^{R}_{\rm ad}\right)(k,t) \ , \tag{5.99}$$

The Fermi-Dirac distribution appeared from the KMS relation, as $f_{FD}(k^0) \equiv (\exp{(k^0/T)}+1)^{-1}$. From these relations, using the adiabatic background (5.94) and going back to the two-time representation (performing an inverse Wigner transform), one obtains [167]

$$\begin{aligned}i\mathcal{S}^{<}_{{\rm ad},\mathbf{k},IJ}(t_1,t_2) &= \int \frac{{\rm d}k^0}{2\pi}\ f_{FD}(k^0)\gamma^0 i\left(\tilde{S}^{A}_{\rm ad} - \tilde{S}^{R}_{\rm ad}\right)_{IJ}(k,t)e^{ik^0(t_1-t_2)} \\ &\simeq -\delta_{IJ}\sum_{s=\pm} f_{FD}(s\omega_I(t))\frac{e^{-is\omega_I(t)(t_1-t_2)}}{2s\omega_I(t)}\gamma^0\left(s\omega_I(t)\gamma^0 + \boldsymbol{\gamma}\cdot\mathbf{k} + M_I(t)\right) \\ &= -\delta_{IJ}\sum_{s=\pm} f_{FD}(s\omega_I(t))e^{-is\omega_I(t)(t_1-t_2)}\mathbf{P}^s_I \ ,\end{aligned} \tag{5.100}$$

with $t = (t_1+t_2)/2$. The integral was calculated using complex analysis, taking the residues of the poles (in the k^0 variable) of $\tilde{S}^{R,A}_{\rm ad}$, which correspond to $k^0 \simeq \pm\sqrt{|\mathbf{k}|^2 + M_I(t)^2} \equiv \pm\omega_I(t)$.

In doing so, we neglected the deviation induced on the poles by $\Sigma^{R,A}_{\rm ad}$, which are of higher order in the Yukawa couplings.

Once we have an expression for the adiabatic propagator we can calculate the effective self-energy, by taking a convolution product with the self-energy. In particular, the effective self-energy can be expressed [167], at lowest order in the gradient expansion (5.92), in terms of the Wigner transforms

$$\begin{aligned}\mathbf{\Sigma}^{\rm eff}_{\mathbf{k},IJ}(t,t) = (\mathbf{\Sigma} * 2\mathcal{S}^{\rho}_{\rm ad})_{\mathbf{k},IJ} &\simeq \int \frac{{\rm d}k^0}{2\pi}\tilde{\mathbf{\Sigma}}_{IJ}(k,t) i\left(\tilde{\mathcal{S}}^R_{\rm ad} - \tilde{\mathcal{S}}^A_{\rm ad}\right)_{JJ}(k,t) \\ &\simeq \sum_{s=\pm} \tilde{\mathbf{\Sigma}}_{IJ}(s\omega_I(t),t)\mathbf{P}^s_J(t)\ . \end{aligned} \tag{5.101}$$

In the end, the effective self-energy is computed from the self-energies taken on-shell, with the energy component of the 4-momentum $k^0 = \pm\sqrt{\mathbf{k}^2 + M_I(t)^2}$.

Recalling back the equation (5.77), now the adiabatic propagator $\mathcal{S}_{{\rm ad},\mathbf{k}}$, the equilibrium $\mathbf{\Sigma}^{{\rm eff},R}_{{\rm eq},\mathbf{k}}$ and deviation $\delta_a\mathbf{\Sigma}_{\mathbf{k}}$ are fixed,

$$\begin{aligned}\partial_t\left(\delta\mathcal{S}^<_{\mathbf{k}}\right)(t,t) = &-i\left[\mathbf{H}_0, \delta\mathcal{S}^<_{\mathbf{k}}(t,t)\right] - \partial_t\mathcal{S}^<_{{\rm ad},\mathbf{k}} \\ &-i\left[\mathbf{\Sigma}^{{\rm eff},R}_{{\rm eq},\mathbf{k}}(t,t)\delta\mathcal{S}^<_{\mathbf{k}}(t,t) + {\rm h.c.}\right] \\ &-i\sum_a\left[\left(\delta_a\mathbf{\Sigma}^R_{\mathbf{k}} * \mathcal{S}^<_{{\rm ad},\mathbf{k}} + \delta_a\mathbf{\Sigma}^<_{\mathbf{k}} * \mathcal{S}^A_{{\rm ad},\mathbf{k}}\right)(t,t) + {\rm h.c.}\right]\ , \end{aligned} \tag{5.102}$$

with expressions for the self-energies given in the next section.

5.4 Sterile neutrino self-energies

We have derived the equations so far with a self-energy made of an equilibrium part $\Sigma_{\rm eq}$ and a small deviation $\delta\Sigma$. In the context of leptogenesis, they are given by the Yukawa interactions of the sterile neutrinos with the SM. We explicit in this section which expressions should be used.

Most self-energies in this section are best calculated in 4-dimensional momentum space, *i.e.* considering their Wigner transform (see section 5.2.3). We will therefore work with the 4-dimensional momentum $k \equiv (k^0, \mathbf{k})$, and we will drop the $\tilde{}$ notation for the whole section. It should be clear from their argument that the self-energies considered here are functions of 4-momentum. Computing the self-energies from the Lagrangian in the context of non-equilibrium QFT involves some subtleties and requires to use the so-called two-particle irreducible effective action method [178, 179]. It is not our goal here to review this technique; we refer the reader to [180] for a general description and to [143, 167] for its use in leptogenesis.

In leptogenesis, the Yukawa interactions couple the sterile neutrinos to the lepton and Higgs fields. We detail how expressions are computed at the one-loop level in sub-section 5.4.1. Higher order corrections can however be important when sterile neutrinos are relativistic. We will estimate these effects later in sub-section 5.4.2.

5.4.1 Sterile neutrino self-energy: one loop estimate

The sterile neutrino self-energy Σ, at the one-loop level, is computed as a sum of the diagram presented in Figure 5.2 involving the lepton and Higgs fields,

$$i\Sigma_{IJ}^{<,>}(k) = g_W \sum_a \int \frac{\mathrm{d}^4 p}{(2\pi)^4} \left[Y_{Ia} Y_{Ja}^* P_L i S_{l,a}^{<,>}(p) i\Delta_H^{<,>}(k-p) \right.$$
$$\left. + Y_{Ia}^* Y_{Ja} P_R C i S_{l,a}^{>,<}(-p)^T C^{-1} i\Delta_H^{>,<}(-k+p) \right] \ , \tag{5.103}$$

where $g_W = 2$ is the number of $SU(2)$ degrees of freedom. In order to compute this self-energy, we need to know what propagators to use for the lepton and Higgs fields. Because of their fast gauge interactions, they are assumed to be close to thermal equilibrium. In this case, we have expressions for their propagators. We first treat the case of exact thermal equilibrium, before introducing also deviations due to (small) chemical potentials.

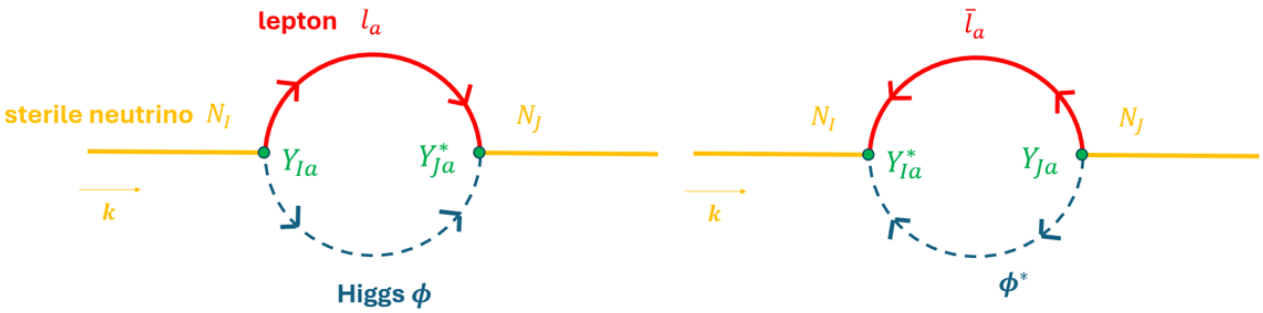

Figure 5.2: One-loop diagrams contributing to the sterile neutrino self-energy.

Propagators and self-energy in thermal equilibrium

At thermal equilibrium, propagators are time-translation invariant and the lepton and Higgs fields have a finite phase space distribution given by the Fermi-Dirac f_{FD} and the Bose-Einstein f_{BE} distributions, respectively. In that case, propagators are given by [143, 167, 181, 182]

$$iS_{l,a,\mathrm{eq}}^{<}(p) = P_L \left[iS_{\mathrm{eq}}^{<}(p) \right] = P_L \left[-2\pi\delta(p^2) \not{p}\, \mathrm{sign}(p^0) f_{FD}(p^0) \right] \ , \tag{5.104a}$$
$$iS_{l,a,\mathrm{eq}}^{>}(p) = P_L \left[iS_{\mathrm{eq}}^{>}(p) \right] = P_L \left[+2\pi\delta(p^2) \not{p}\, \mathrm{sign}(p^0) f_{FD}(-p^0) \right] \ , \tag{5.104b}$$

for the lepton field, introducing $S_{\rm eq}$ the thermal propagator for a Dirac fermion (and where sign is the sign function). Note that we neglected the lepton masses, such that the propagators are diagonal in lepton flavor. For the Higgs field, we have

$$i\Delta^{<}_{H,\rm eq}(q) = -2\pi\delta(q^2)\ \mathrm{sign}(q^0) f_{BE}(q^0)\ , \tag{5.105a}$$
$$i\Delta^{>}_{H,\rm eq}(q) = +2\pi\delta(q^2)\ \mathrm{sign}(q^0) f_{BE}(-q^0)\ . \tag{5.105b}$$

These propagators satisfy convenient symmetries, namely

$$C i S^{<}_{\rm eq}(-p)^T C^{-1} = i S^{>}_{\rm eq}(p)\ , \tag{5.106a}$$
$$i\Delta^{<}_{H,\rm eq}(-q) = i\Delta^{>}_{H,\rm eq}(q)\ . \tag{5.106b}$$

The equilibrium self-energies can then be rewritten

$$i\Sigma^{<,>}_{IJ,\rm eq}(k) = g_W \left[Y_{Ia} Y^*_{Ja} P_L + Y^*_{Ia} Y_{Ja} P_R\right] i\hat{\Sigma}^{<,>}_{\rm eq}(k)\ , \tag{5.107}$$

where $i\hat{\Sigma}^{<,>}_{\rm eq}$ doesn't carry any flavor index and can be computed using the expressions for the thermal propagators

$$\begin{aligned} i\hat{\Sigma}^{<}_{\rm eq} &= \int \frac{\mathrm{d}^4 p}{(2\pi)^4} S^{<}_{\rm eq}(p)\Delta^{<}_{H,\rm eq}(k-p) \\ &= \int \frac{\mathrm{d}^4 p}{(2\pi)^2}\ \delta(p^2)\delta((k-p)^2)\mathrm{sign}(p^0)\mathrm{sign}(k^0-p^0)\ \not{p} f_{FD}(p^0) f_{BE}(k^0-p^0)\ , \end{aligned} \tag{5.108}$$

$$\begin{aligned} i\hat{\Sigma}^{>}_{\rm eq} &= \int \frac{\mathrm{d}^4 p}{(2\pi)^4} S^{>}_{\rm eq}(p)\Delta^{>}_{H,\rm eq}(k-p) \\ &= \int \frac{\mathrm{d}^4 p}{(2\pi)^2}\ \delta(p^2)\delta((k-p)^2)\mathrm{sign}(p^0)\mathrm{sign}(k^0-p^0)\ \not{p} f_{FD}(-p^0) f_{BE}(p^0-k^0)) \\ &= -e^{\frac{k^0}{T}} i\hat{\Sigma}^{<}_{\rm eq}\ . \end{aligned} \tag{5.109}$$

In the last line, we recovered the KMS relation (5.96), using the fact that $f_{FD}(-p^0) = e^{p^0/T} f_{FD}(p^0)$ and $f_{BE}(-q^0) = -e^{q^0/T} f_{BE}(q^0)$. We will focus on the spectral (equilibrium) self-energy. The computation of the one-loop diagram gives

$$\begin{aligned} 2\hat{\Sigma}^{\rho}_{\rm eq} &\equiv i\hat{\Sigma}^{>}_{\rm eq} - i\hat{\Sigma}^{<}_{\rm eq} \\ &= \int \frac{\mathrm{d}^4 p}{(2\pi)^2}\ \delta(p^2)\delta((k-p)^2)\mathrm{sign}(p^0)\mathrm{sign}(k^0-p^0)\ \not{p}\left[f_{FD}(-p^0) + f_{BE}(k^0-p^0)\right]\ . \end{aligned} \tag{5.110}$$

Note that its spinorial structure is simply the Dirac slash of a 4-vector (whose components are given by integrals over p).

Deviations from chemical potentials

In our study, lepton and Higgs fields could deviate from equilibrium due to a (small) chemical potential. The propagators can be modified to include them,

$$i S^{<}_{l,a}(p) = P_L\left[-2\pi\delta(p^2)\ \not{p}\ \mathrm{sign}(p^0) f_{FD}((p^0-\mu_a))\right]\ , \tag{5.111a}$$
$$i S^{>}_{l,a}(p) = P_L\left[+2\pi\delta(p^2)\ \not{p}\ \mathrm{sign}(p^0) f_{FD}(-(p^0-\mu_a))\right]\ , \tag{5.111b}$$

$$i\Delta_H^<(q) = -2\pi\delta(q^2)\ \mathrm{sign}(q^0) f_{BE}((q^0-\mu_\phi))\ , \tag{5.112a}$$
$$i\Delta_H^>(q) = +2\pi\delta(q^2)\ \mathrm{sign}(q^0) f_{BE}(-(q^0-\mu_\phi))\ . \tag{5.112b}$$

Note that now the lepton propagators depend on flavor *via* their chemical potential. These propagators satisfy a modified KMS relation

$$iS_{l,a}^>(p) = -e^{(p^0-\mu_a)/T} iS_{l,a}^<(p)\ , \tag{5.113a}$$
$$i\Delta_H^>(q) = e^{(q^0-\mu_a)/T} i\Delta_H^<(q)\ . \tag{5.113b}$$

For small chemical potentials $\mu_a, \mu_\phi \ll T$, the propagators can be expanded,

$$iS_{l,a}^{<,>} \simeq iS_{l,\mathrm{eq}}^{<,>} - \frac{\mu_a}{T}\ P_L\left[2\pi\delta(p^2)\ \not{p}\ \mathrm{sign}(p^0) f_{FD}(p_0) f_{FD}(-p^0)\right]\ , \tag{5.114}$$

$$i\Delta_H^{<,>} \simeq i\Delta_{H,\mathrm{eq}}^{<,>} + \frac{\mu_\phi}{T}\ 2\pi\delta(q^2)\ \mathrm{sign}(q^0) f_{BE}(q^0) f_{BE}(-q^0)\ . \tag{5.115}$$

Their properties under charge conjugation are changed compared to (5.106),

$$CiS_{l,a}^<(-p)^T C^{-1} = iP_R S_{\mathrm{eq}}^>(p) + \frac{\mu_a}{T}\ P_R\left[2\pi\delta(p^2)\ \not{p}\ \mathrm{sign}(p^0) f_{FD}(p_0)(1-f_{FD}(p^0))\right]\ , \tag{5.116a}$$
$$i\Delta_H^<(-q) = i\Delta_{H,\mathrm{eq}}^>(q) - \frac{\mu_\phi}{T}\ 2\pi\delta(q^2)\ \mathrm{sign}(q^0) f_{BE}(q^0) f_{BE}(-q^0)\ . \tag{5.116b}$$

Note how the sign of the extra term is flipped in both cases. The self-energy will have terms proportional to $\mu_a, \mu_\phi/T$, at lowest order, relating to our previous notations,

$$\begin{aligned} i\Sigma_{IJ}^{<,>}(k) &\simeq\ i\Sigma_{IJ,\mathrm{eq}}^{<,>}(k) + \sum_a g_W\left[Y_{Ia}Y_{Ja}^* P_L - Y_{Ia}^* Y_{Ja} P_R\right] i\delta_a\hat{\Sigma}^{<,>}(k) \\ &\equiv i\Sigma_{IJ,\mathrm{eq}}^{<,>}(k) + \sum_a i\delta_a\Sigma_{IJ}^{<,>}(k)\ , \end{aligned} \tag{5.117}$$

where the small deviation from chemical potentials is found to be

$$\begin{aligned} i\delta_a\hat{\Sigma}^<(k) = \int \frac{\mathrm{d}^4p}{(2\pi)^4}(2\pi)^2\delta(p^2)\delta((k-p)^2)\ \mathrm{sign}(p^0)\ \mathrm{sign}((k-p)^0)\ \not{p} \\ \times f_{FD}(p^0) f_{BE}((k-p)^0)\left[\frac{\mu_a}{T} f_{FD}(-p^0) - \frac{\mu_\phi}{T} f_{BE}(-(k-p)^0)\right] \end{aligned} \tag{5.118}$$

$$\begin{aligned} i\delta_a\hat{\Sigma}^>(k) = \int \frac{\mathrm{d}^4p}{(2\pi)^4}(2\pi)^2\delta(p^2)\delta((k-p)^2)\ \mathrm{sign}(p^0)\ \mathrm{sign}((k-p)^0)\ \not{p} \\ \times f_{FD}(-p^0) f_{BE}(-(k-p)^0)\left[-\frac{\mu_a}{T} f_{FD}(p^0) + \frac{\mu_\phi}{T} f_{BE}((k-p)^0)\right]\ . \end{aligned} \tag{5.119}$$

Using the fact that $f_{BE}(q^0) + f_{BE}(-q_0) = -1$ and $f_{FD}(p^0) + f_{FD}(-p^0) = 1$, we have the relation

$$i\delta_a\hat{\Sigma}^< = \frac{\mu_a+\mu_\phi}{T} i\hat{\Sigma}_{\mathrm{eq}}^< - e^{-k^0/T} i\delta_a\hat{\Sigma}^>\ . \tag{5.120}$$

This is simply a consequence of the (linearized version of) KMS relation (5.113). We note that it relates the deviation $\delta_a\hat{\Sigma}$ to the equilibrium $\hat{\Sigma}_{\mathrm{eq}}$.

5.4.2 Self-energy beyond one-loop

We gave a derivation of the self-energy calculated at one-loop, in interaction with a thermal bath. This one-loop estimate is valid for Non-Relativistic (NR) regimes. In the Ultra-Relativistic (UR) regime, thermal corrections are important and more processes need to be included, leading to significant corrections. Incorporating both regimes was done in [139], which we follow, in order to write an estimate for the self-energy in all regimes.

Let us focus on the equilibrium spectral self-energy $\Sigma^{\rho}_{\text{eq}}$. Extracting the flavor structure of the interaction with lepton and Higgs fields, the sterile neutrino's self-energy at equilibrium (in all regimes of masses) can be written

$$\Sigma^{\rho}_{\text{eq},IJ}(k) = g_W \left[\left(YY^\dagger\right)_{IJ} P_L + \left(Y^* Y^T\right)_{IJ} P_R \right] \hat{\Sigma}^{\rho}_{\text{eq}}(k) \ , \tag{5.121}$$

where $\hat{\Sigma}^{\rho}_{\text{eq}}$ is a reduced self-energy that doesn't carry any flavor index. This reduced self-energy will be computed for different regimes of masses in the following.

NR regime

The first estimate for the self-energy is to use the (bare) one-loop self-energy corresponding to $1 \to 2$ processes; this is what was done in section 5.4.1. It describes well the decays and inverse decays, which are central in thermal and resonant leptogenesis, in the NR regime. From the expression (5.110) found previously, this first estimate is calculated to be

$$\hat{\Sigma}^{\rho,1\to2}_{\text{eq}}(k) = a_0^{1\to2}\gamma^0 + b_0^{1\to2}\boldsymbol{\gamma}\cdot\hat{\mathbf{k}} \ , \tag{5.122}$$

with the functions $a_0^{1\to2}$ and $b_0^{1\to2}$ computed for example in [167, 183] and given by

$$a_0^{1\to2} \equiv \frac{T^2}{8\pi|\mathbf{k}|} I_1(k^0/T, |\mathbf{k}|/T) \ , \tag{5.123}$$

$$b_0^{1\to2} \equiv \frac{T^2}{8\pi|\mathbf{k}|} \left[\frac{k^0}{|\mathbf{k}|} I_1(k^0/T, |\mathbf{k}|/T) - \frac{(k^0)^2 - |\mathbf{k}|^2}{2|\mathbf{k}|T} I_0(k^0/T, |\mathbf{k}|/T) \right] \ , \tag{5.124}$$

with

$$I_n(y_0, y) \equiv \int_{y_-}^{y_+} \mathrm{d}x \ x^n \left(\tilde{f}_{FD}(-x) + \tilde{f}_{BE}(y_0 - x) \right) \ , \tag{5.125}$$

where

$$y_\pm \equiv \frac{y_0 \pm y}{2} \ , \ \tilde{f}_{FD}(x) = \frac{1}{e^x + 1} \ , \tilde{f}_{BE}(x) = \frac{1}{e^x - 1} \ . \tag{5.126}$$

Analytical expressions are known for these integrals (see [183] Eq (78a-b)), leading to

$$I_0(y_0, y) = \ln\left(\frac{e^{y_0+y} - 1}{e^{y_0-y} - 1} \right) - y \ , \tag{5.127}$$

$$I_1(y_0,y) = \frac{y_0+y}{2}\ln\left(\frac{1+e^{(y_0+y)/2}}{1-e^{(-y_0+y)/2}}\right) - \frac{y_0-y}{2}\ln\left(\frac{1+e^{(-y_0+y)/2}}{1-e^{(-y_0-y)/2}}\right) + \mathrm{Li}_2\left(-e^{(y_0+y)/2}\right) + \mathrm{Li}_2\left(e^{(-y_0-y)/2}\right) - \mathrm{Li}_2\left(e^{(-y_0+y)/2}\right) - \mathrm{Li}_2\left(-e^{(y_0-y)/2}\right) \ . \quad (5.128)$$

The expression we found for the self-energy describes $1 \to 2$ processes for all regimes of masses. However, while it is enough for the NR regime, it is too naive for the UR regime, as we will argue.

UR regime

The $1 \to 2$ processes do not capture all the relevant physics in the UR regime. Indeed, it is known [184–186] that when the temperature is much larger than the mass, thermal corrections cannot be neglected. In particular, gauge interactions in the plasma induce a thermal mass for the Higgs and the lepton fields (the so called Landau-Pomeranchuk-Migdal effect [187,188]) and $1+n \to 2+n$ processes should be included. The change in the self-energy is significant in the UR regime, and collision terms are enhanced by several orders of magnitude compared to the first estimate.

The price to pay for better treatment of the relativistic regime is that the coefficients are calculated numerically. Data for the collision terms were given in [185, 186] for exactly massless sterile neutrinos, and for a certain range of momenta $\frac{|\mathbf{k}|}{T} \in [0.01, 12]$ and temperature $T \in [10^2, 10^7]$GeV. In these studies, numerical values were provided for some functions $Q_\pm(|\mathbf{k}|/T)$ that are related to the self-energy. In terms of the reduced self-energy,

$$\hat{\Sigma}^{\rho,\mathrm{UR}}_{\mathrm{eq},IJ}(k) = a_0^{\mathrm{UR}}\gamma^0 + b_0^{\mathrm{UR}}\boldsymbol{\gamma}\cdot\hat{\mathbf{k}} \ , \quad (5.129)$$

in the UR regime, the functions calculated in [185,186] are related to a_0^{UR} and b_0^{UR},

$$a_0^{\mathrm{UR}}(k,T) = \frac{1}{4}\left(Q_+ + \frac{4|\mathbf{k}|^2}{T^2}Q_-\right)T \ , \ b_0^{\mathrm{UR}}(k,T) = \frac{1}{4}\left(Q_+ - \frac{4|\mathbf{k}|^2}{T^2}Q_-\right)T \ . \quad (5.130)$$

We note that there is no dependency in the sterile neutrino masses, as their masses are negligible and thermal contributions dominate.

Interpolation between both regimes

We now have an understanding of the form of the spectral self-energy in both extreme regimes of masses. Exact results are not known in the intermediate regimes and are hard to estimate. Following a previous work [139] that tackled leptogenesis over different mass regimes, we will adopt the procedure that we explain here. The total self-energy is estimated as the sum of the self-energy used in the UR regime and the $1 \to 2$ self-energy used in the NR regime. The $1 \to 2$ self-energy should only contribute if the sterile neutrino mass can decay into other particles, so

the threshold separating the two regimes is estimated at the thermal mass of the Higgs field. In summary, we consider a total (reduced) self-energy

$$\hat{\Sigma}^{\rho,\mathrm{tot}}_{\mathrm{eq}}(k;M,T) \equiv \hat{\Sigma}^{\rho,\mathrm{UR}}_{\mathrm{eq}}(k;0,T) + \theta\left(M - m_H(T)\right)\hat{\Sigma}^{\rho,1\to 2}_{\mathrm{eq}}(k;M,T)\ . \tag{5.131}$$

The thermal mass of the Higgs field is $m_H(T) \approx 0.3\ T$. This self-energy interpolates the two regimes of interest for our study. We note that a somehow similar estimate was used in a study of ARS leptogenesis [189] in a regime of relatively large masses. The collision rates were given as the product of a fixed term (related to the self-energy) and a phase space factor which changes as the mass is taken to be larger.

5.4.3 Discussion on the temperature dependence

Our study focuses on relativistic as well as non-relativistic regimes. The ratio M/T determines which regime is relevant, and we want to know how the interactions are affected as temperature evolves. A key observation, from the expression for the self-energies that we just derived, is that in both regimes, we could write the self-energy as temperature times a function of $\kappa^0 \equiv k^0/T$ and $\kappa \equiv |\mathbf{k}|/T$,

$$\Sigma(k;T) = T\ \sigma(k^0/T, |\mathbf{k}|/T) = T\sigma(\kappa^0,\kappa)\ . \tag{5.132}$$

Once the on-shell condition is imposed,

$$\frac{k^0}{T} \to \frac{\sqrt{|\mathbf{k}|^2+M^2}}{T} = \sqrt{\frac{|\mathbf{k}|^2}{T^2}+\frac{M^2}{T^2}} \equiv \sqrt{\kappa^2+x_M^2}\ , \tag{5.133}$$

which will be a function of κ and $x_M \equiv M/T$ only. This observation applies to the interpolated self-energy (5.131) as well, as $\theta(M - m_H(T)) \simeq \theta(0.3\ x_M - 1)$.

5.5 General kinetic equations

Now that we derived expressions for the self-energies, we give the general equations for the mass- and coherence-shell distributions, derived from the propagator's equation (5.102). We explain in Appendix E that the term $\left(\delta_a\mathbf{\Sigma}^R_{\mathbf{k}} * \mathcal{S}^<_{\mathrm{ad},\mathbf{k}} + \delta_a\mathbf{\Sigma}^<_{\mathbf{k}} * \mathcal{S}^A_{\mathrm{ad},\mathbf{k}}\right)(t,t) + \mathrm{h.c.}$ in this equation can be replaced, considering small deviations coming from the chemical potentials, such that

$$\begin{aligned}\partial_t\left(\delta\mathcal{S}^<_{\mathbf{k},IJ}\right)(t,t) \simeq &-i\left[\mathbf{H}_0,\delta\mathcal{S}^<_{\mathbf{k}}(t,t)\right]_{IJ} - \partial_t\mathcal{S}^<_{\mathrm{ad},\mathbf{k},IJ}\\ &-i\left[\mathbf{\Sigma}^{\mathrm{eff},R}_{\mathrm{eq},\mathbf{k}}(t,t)\delta\mathcal{S}^<_{\mathbf{k}}(t,t) + \mathrm{h.c.}\right]_{IJ}\\ &+i\sum_a \frac{\mu_a+\mu_\phi}{T} g_W\left(Y_{Ia}Y^*_{Ja}P_L - Y^*_{Ia}Y_{Ja}P_R\right)\sum_{\eta=\pm}\{\mathbf{F}^{\rho,\eta}_J, \mathbf{P}^\eta_J\}\ ,\end{aligned} \tag{5.134}$$

where

$$\mathbf{F}^{\rho,\eta}_J \equiv f_{FD}(\omega_J)(1-f_{FD}(\omega_J))\tilde{\hat{\mathbf{\Sigma}}}^\rho_{\mathrm{eq}}(\eta\omega_J,\mathbf{k})\ . \tag{5.135}$$

We will express this equation in terms of the mass- and coherence-shell distribution functions, defined by

$$f^{ss'}_{h,IJ} \equiv -i\mathrm{Tr}\left[\mathcal{P}^{ss'}_{h\ JI}\mathcal{S}^{<}_{\mathbf{k},IJ}(t,t)\right] = -i\mathrm{Tr}\left[\mathcal{P}^{ss'}_{h\ JI}\left(\mathcal{S}^{<}_{\mathrm{ad},\mathbf{k},IJ}(t,t) + \delta\mathcal{S}^{<}_{\mathbf{k},IJ}(t,t)\right)\right] \ . \tag{5.136}$$

The adiabatic background $S^{<}_{\mathrm{ad},\mathbf{k}}$ is diagonal in flavor and leads to the decomposition of the mass- and coherence-shell functions into an equilibrium and a deviation part,

$$f^{ss'}_{h,IJ} \equiv \delta f^{ss'}_{h,IJ} + s\delta_{s,s'}\delta_{IJ}\ f_{FD}(s\omega_I) \ . \tag{5.137}$$

5.5.1 Sterile neutrino evolution

Decomposing the (local) propagator into the various projectors $\mathcal{P}^{ss'}_{h,IJ}$ defined previously and injecting it in Equation (5.102) leads to

$$\begin{aligned}\frac{\mathrm{d}}{\mathrm{d}t}\delta f^{ss'}_{h,IJ} = &-i(s\omega_I(t) - s'\omega_J(t))\ \delta f^{ss'}_{h,IJ} - s\delta_{ss'}\delta_{IJ}\partial_t f_{FD}(s\omega_I(t)) \\ &+ ss'\frac{|\mathbf{k}|}{2}\left(\frac{\partial_t M_I}{\omega_I(t)^2}f^{-ss'}_{h,IJ} + \frac{\partial_t M_J}{\omega_J(t)^2}f^{s-s'}_{h,IJ}\right) \\ &- \sum_{L,\eta} C^{s\eta s'}_{h,ILJ}\delta f^{\eta s'}_{h,LJ} + \left(C^{s'\eta s}_{h,JLI}\right)^*\delta f^{s\eta}_{h,IL} \\ &+ \sum_a B^{ss'}_{h,a,IJ}\frac{\mu_a + \mu_\phi}{T} \ .\end{aligned} \tag{5.138}$$

The first two lines can be recognized as the flavor-full version of the (free) equations described in section 5.2.5. The third line represents interactions among sterile neutrinos, with coefficients derived from the (effective) retarded self-energy,

$$C^{s\eta s'}_{h,ILJ}(t) \equiv i\mathrm{Tr}\left[\mathcal{P}^{s's}_{h,JI}\mathbf{\Sigma}^{\mathrm{eff},R}_{\mathbf{k},\mathrm{eq},IL}(t,t)\mathcal{P}^{\eta s'}_{h,LJ}\right] \ . \tag{5.139}$$

The fourth line is the backreaction of the lepton asymmetry on the sterile neutrinos, coming from deviation of the lepton distribution in the self-energy of the sterile neutrinos,

$$B^{ss'}_{h,a,IJ}(t) \equiv g_W\mathrm{Tr}\left[\mathcal{P}^{s's}_{h,JI}\left(Y_{Ia}Y^*_{Ja}P_L - Y^*_{Ia}Y_{Ja}P_R\right)\sum_{\eta=\pm}\{\mathbf{F}^{\rho,\eta}_J, \mathbf{P}^{\eta}_J\}\right] \ . \tag{5.140}$$

Note that this last term was originally not explicitly written down in [167], because the authors were mainly concerned with resonant leptogenesis in which the backreaction of the lepton asymmetry plays only a minor role. Indeed, because $\mathbf{F}^{\rho,\eta}_{a,J} \propto f_{FD}(\omega_J)(1 - f_{FD}(\omega_J)$, it can be thought of as coming from inverse decays, converting the lepton asymmetry back into sterile neutrinos. They are suppressed if the sterile neutrino mass is large and $f_{FD} \sim \exp(-M/T)$. This term is however important to us as we will apply these equations to regimes similar to ARS leptogenesis.

Including the expansion of the Universe relates to the discussion on kinetic Boltzmann equations in section 2.3. Here we have *quantum* kinetic Boltzmann equations because $\delta f_{h,IJ}$ is a matrix but the same reasoning applies. If we consider δf as a function of the rescaled momentum

$$\boldsymbol{\kappa} \equiv \frac{\mathbf{k}}{T} \ , \ \delta f_{h,IJ}(\mathbf{k},t) \to \delta f^{\rm resc}_{h,IJ}(\boldsymbol{\kappa},t) \ , \tag{5.141}$$

the equations (5.138) with the replacement above automatically include the Universe's expansion. For simplicity in the following, we drop the "resc" superscript, and we will make clear which quantity is considered when needed. This rescaling of the momentum is natural for the various coefficients appearing in the equation. Indeed, the temperature dependence of the self-energies tells us that the collision and backreaction can be written as

$$C^{s\eta s'}_{h,ILJ} \equiv T \ c^{s\eta s'}_{h,ILJ}(\kappa, \{x^I_M\}) \ , \tag{5.142}$$

$$B^{ss'}_{h,a,IJ} \equiv T \ b^{ss'}_{h,a,IJ}(\kappa, \{x^I_M\}) \ , \tag{5.143}$$

where the lower case letter are only function of $\kappa = |\mathbf{k}|/T$ and $x^I_M = M_I/T$.

5.5.2 Lepton asymmetry evolution

We also give the equation for the asymmetry in the leptons, which can be found derived in [138, 167, 190] and whose derivation is sketched in Appendix F,

$$T^3 \frac{{\rm d}\Delta_a}{{\rm d}t} = W_a \ \frac{\mu_a + \mu_\phi}{T} - S_a \ . \tag{5.144}$$

We introduced $\Delta_a \equiv n_{B/3} - n_{L_a}$, the (rescaled) number density for the lepton number $B/3 - L_a$, for which the Boltzmann equation in an expanding Universe is written with a T^3 pre-factor (see the relations (2.45)). It is directly connected to the chemical potentials of the SM particles when SM interactions are assumed at equilibrium, as we mentioned in section 3.1. We recall the relation

$$\frac{\mu_a + \mu_\phi}{T} \equiv \sum_b \mathcal{A}_{ab} \Delta_b \ . \tag{5.145}$$

We gave the values of $\mathcal{A}$ for different regimes of temperatures in section 3.1. The first term in (5.144) is a washout term, *i.e.* it tends to reduce the asymmetry in leptons. It is given by

$$W_a = \sum_{I,s} |Y_{Ia}|^2 \int \frac{{\rm d}^3\mathbf{k}}{(2\pi)^3} f_{FD}(\omega_I)(1 - f_{FD}(\omega_I)) {\rm Tr}\left[P_R \left\{\tilde{\hat{\boldsymbol{\Sigma}}}^\rho_{\rm eq}(s\omega_I, \mathbf{k}), \mathbf{P}^s_I\right\}\right] \ . \tag{5.146}$$

The second term S_a in (5.144) is a source term corresponding to the decays of sterile neutrinos producing leptons. It is proportional to the sterile neutrinos densities and is given by

$$S_a = \sum_{h,s,s'} \sum_{I,J} \int \frac{{\rm d}^3\mathbf{k}}{(2\pi)^3} \ {\rm Tr}\left[\left(P_R \boldsymbol{\Sigma}^{{\rm eff},\rho}_{{\rm eq},\mathbf{k},a,JI} + \left(\boldsymbol{\Sigma}^{{\rm eff},\rho}_{{\rm eq},\mathbf{k},a,IJ}\right)^\dagger P_R\right) \mathcal{P}^{ss'}_{h,IJ}\right] \ \delta f^{ss'}_{h,IJ}(\mathbf{k},t) \ . \tag{5.147}$$

From the above discussions, δf is understood as a function of $\boldsymbol{\kappa} = \mathbf{k}/T$ and the self-energies are of the form $\boldsymbol{\Sigma} = T\ \boldsymbol{\sigma}$, so the integrals can be re-written in terms of rescaled quantities

$$W_a = T^4 \sum_I |Y_{Ia}|^2 \int \frac{\mathrm{d}^3\boldsymbol{\kappa}}{(2\pi)^3} \mathrm{Tr}\left[\tilde{f}_{FD}(1-\tilde{f}_{FD}) P_R \left\{\tilde{\tilde{\boldsymbol{\sigma}}}^{\rho}_{\mathrm{eq}}, \mathbf{P}^s_I\right\}\right] \equiv T^4 w_a \ , \tag{5.148}$$

$$S_a = T^4 \sum_{h,s,s'} \sum_{I,J} \int \frac{\mathrm{d}^3\boldsymbol{\kappa}}{(2\pi)^3}\ \mathrm{Tr}\left[\left(P_R \boldsymbol{\sigma}^{\mathrm{eff},\rho}_{\mathrm{eq},\boldsymbol{\kappa},a,JI} + \left(\boldsymbol{\sigma}^{\mathrm{eff},\rho}_{\mathrm{eq},\boldsymbol{\kappa},a,IJ}\right)^\dagger P_R\right) \mathcal{P}^{ss'}_{h,IJ}\right]\ \delta f^{ss'}_{h,IJ}(\boldsymbol{\kappa},t) \equiv T^4 s_a \ . \tag{5.149}$$

The equation for the lepton asymmetry can then be written in terms of the rescaled quantity Δ_a

$$\frac{\mathrm{d}\Delta_a}{\mathrm{d}t} = T\ w_a \sum_b \mathcal{A}_{ab}\Delta_b - T\ s_a \ . \tag{5.150}$$

This equation is equivalent to a maybe more familiar expression in the context of ARS leptogenesis in terms of a variable $z \equiv T_{\mathrm{ref}}/T$,

$$\frac{\mathrm{d}\Delta_a}{\mathrm{d}z} = \frac{a_R}{T_{\mathrm{ref}}}\ w_a \sum_b \mathcal{A}_{ab}\Delta_b - \frac{a_R}{T_{\mathrm{ref}}}\ s_a \ . \tag{5.151}$$

Both formulations are equivalent, but as we will see, it is sometimes useful to switch from a time dependence to a z dependence.

Part III

Numerical and analytical results

This third and final part presents the results of our analysis of leptogenesis with a First-Order Phase Transition. We consider two regimes: on the one hand, in Chapter 6, large sterile neutrino masses $M > T_n$, which recover the so-called Mass Gain mechanism that resembles thermal and resonant leptogenesis; and on the other hand, in Chapter 7 low masses $M < T_n$ which recovers a regime similar to ARS leptogenesis.

Chapter 6

Mass Gain mechanism

In this chapter, we use our general equations (5.138), (5.144) to describe sterile neutrinos whose masses are larger than the temperature T_n of the FOPT. They are massless before the FOPT but become (almost) instantaneously massive and non-relativistic. In a FOPT with relativistic bubble expansion, the change is sudden enough so that the sterile neutrino distribution cannot stay at equilibrium. They can then decay efficiently and produce a lepton asymmetry. It is a discontinuous process, contrarily to thermal leptogenesis where the deviation from equilibrium happens due to the adiabatic expansion of the Universe. Depending on the ratio M/T_n, the production of asymmetry can be fast compared to the expansion of the Universe.

This scenario was first presented, in the context of baryogenesis, in [32] and called "Mass Gain" (MG) scenario. In the context of leptogenesis, several studies [28–31] used this mechanism with sterile neutrinos. Our goal is to extend these studies by working with kinetic equations instead of equations for number densities, which will allow us to recover resonant as well as non-resonant regimes for the production of the lepton asymmetry.

This chapter is organized as follows: we first introduce and describe the mechanism in section 6.1, which will lead us to consider relevant assumptions for simplifying the kinetic equations, as shown in section 6.2. The equations are then solved and the results presented in section 6.3. These results are interpreted in section 6.4 in terms of sterile neutrino out-of-equilibrium decays, which may or may not be resonantly enhanced. We then conclude in section 6.5 with a comparison to previous studies and a discussion on the similarities and differences with the present work. Our general conclusions on the Mass Gain mechanism are wrapped up in section 6.6.

6.1 Leptogenesis in the Mass Gain scenario

Originally, the Mass Gain (MG) scenario [32] is a way to achieve baryogenesis through decays of an $SU(3)$-triplet scalar Δ that is made massive by a FOPT. The sudden mass gain makes the equilibrium distribution suppressed by a Boltzmann factor $\exp(-M_\Delta/T)$, while the actual distribution is initially a massless distribution. If the change is fast enough compared to the typical time of interaction, it results in a scalar population well out of equilibrium that decays efficiently. Such a rapid transition is typically obtained for supercooled phase transitions, where the bubbles are expanding at a velocity $v_w \simeq 1$.

We consider the same situation with sterile neutrinos instead of the scalar, as was studied in [28–31]. We therefore expect them to decay shortly after the FOPT. This can be estimated by comparing the typical time of decay $t_\Gamma \equiv \Gamma^{-1}$, where Γ is the decay rate for the massive sterile neutrino, and $t_n \equiv H^{-1}(T_n)$ which is the Hubble time at temperature T_n,

$$\Gamma = \mathrm{Tr}\left[YY^\dagger\right]\frac{M}{8\pi}\ , \tag{6.1}$$

$$H(T_n) = \frac{T_n^2}{a_R}\ , \tag{6.2}$$

such that the ratio between the two time scales is

$$\frac{t_\Gamma}{t_n} = \frac{T_n^2}{a_R}\frac{8\pi}{\mathrm{Tr}\left[YY^\dagger\right]M} \approx \frac{T_n^2}{a_R}\frac{8\pi v^2}{m_\nu M} = \left(\frac{T_n}{M}\right)^2\frac{8\pi v^2}{m_\nu a_R}\ , \tag{6.3}$$

where we used the estimate from the Casas-Ibarra (3.41) parametrization, with order one coefficients in the R matrix. The parameter m_ν is the scale of the active neutrino masses; if we take it around $m_\nu \simeq 0.05$ eV,

$$\frac{t_\Gamma}{t_n} \approx 4\times 10^{-2}\ \left(\frac{T_n}{M}\right)^2\ . \tag{6.4}$$

In the MG scenario, the ratio M/T_n is typically $O(10)$, larger than one at least, because we consider a supercooled FOPT that allows such large ratios, as argued in section 3.5. This ensures that the typical decay time is smaller by (at least) two orders of magnitude than the Hubble time. Most of the decays therefore happen very fast, before the Universe has time to expand too much and reduce the temperature. Indeed, considering time scales after the FOPT such that $\Delta t \equiv t - t_{\mathrm{nucl}} \sim t_\Gamma \ll t_n$; recalling the time dependence (2.25) of temperature

$$T(t) = \left(\frac{a_R}{2}\right)^{1/2} t^{1/2} = \left(\frac{a_R}{2}\right)^{1/2}(t_{\mathrm{nucl}} + \Delta t)^{1/2} = \left(\frac{a_R}{2}\right)^{1/2}(t_n/2 + \Delta t)^{1/2}\ , \tag{6.5}$$

temperature is approximately constant $T \sim T_n$ during the period of interest. This statement can be made clear by plotting the asymmetry produced as a function of time, as in Figure 6.1, for different set of parameters. On the left, the temperature is relatively low ($T_n = 10^6$ GeV) with a certain mass degeneracy ($\Delta M/M = 10^{-3}$), while on the right the masses are less degenerate ($\Delta M/M = 1$) but the temperature ($T_n = 10^8$ GeV) is higher. In both cases, a

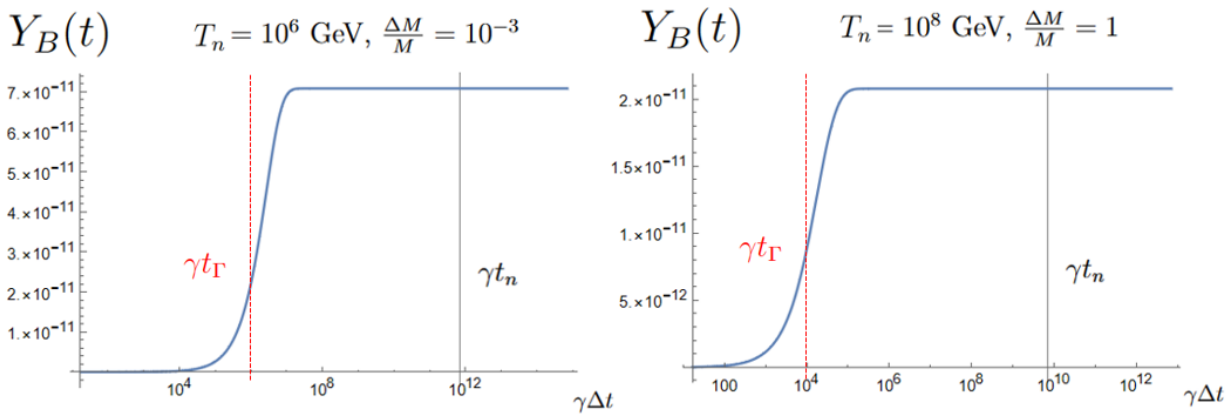

Figure 6.1: Baryon asymmetry produced during the MG scenario as a function of time. In both plots, the mass-to-temperature ratio is fixed at $M/T_n = 50$, and the angle of the matrix R is $z_R = \frac{3\pi}{4} + i$.

plateau at large times signifies that the asymmetry is freezed-out, it is no longer created nor washed-out after a certain time. We summarize our description of the MG regime in Figure 6.2. Our conclusion is the following: in the MG scenario, at the time of the sterile neutrino decays, the temperature is approximately constant. For numerical purposes, we will fix the temperature to be constant, so that we can solve efficiently the kinetic equations.

6.2 Kinetic equations

In this section, we present the assumptions made for solving the kinetic equations for leptogenesis. The original MG scenario relies on the fact that the particles are already present in the plasma and at thermal equilibrium, with zero mass, before the transition. We will therefore consider an initial thermal distribution of (massless) sterile neutrinos,

$$[\text{MG}] \quad f_{\mathbf{k}}^{m,s}(t = t_{\text{in}}) = s f_{FD}^{M=0}(|\mathbf{k}|) = s \, \frac{1}{e^{|\mathbf{k}|/T} + 1} \, , \tag{6.6}$$

$$[\text{MG}] \quad f_{\mathbf{k}}^{c,s}(t = t_{\text{in}}) = 0 \, , \tag{6.7}$$

and a vanishing initial lepton asymmetry

$$[\text{MG}] \quad \Delta_a(t = t_{\text{in}}) = 0 \, . \tag{6.8}$$

Numerically, the initial time is taken to be $\gamma \Delta t_{\text{in}} = \gamma(t_{\text{in}} - t_{\text{nucl}}) = -15$, starting a bit before the bubble totally expands. The time dependence of the mass can also be simplified. Given the hyperbolic tangent profile we assumed,

$$M(t) = M_0 \frac{1 + \tanh(\gamma \Delta t)}{2} \overset{\text{Assumption 3.78}}{=} M_0 \frac{1 + \tanh(T_n \Delta t)}{2} \, , \tag{6.9}$$

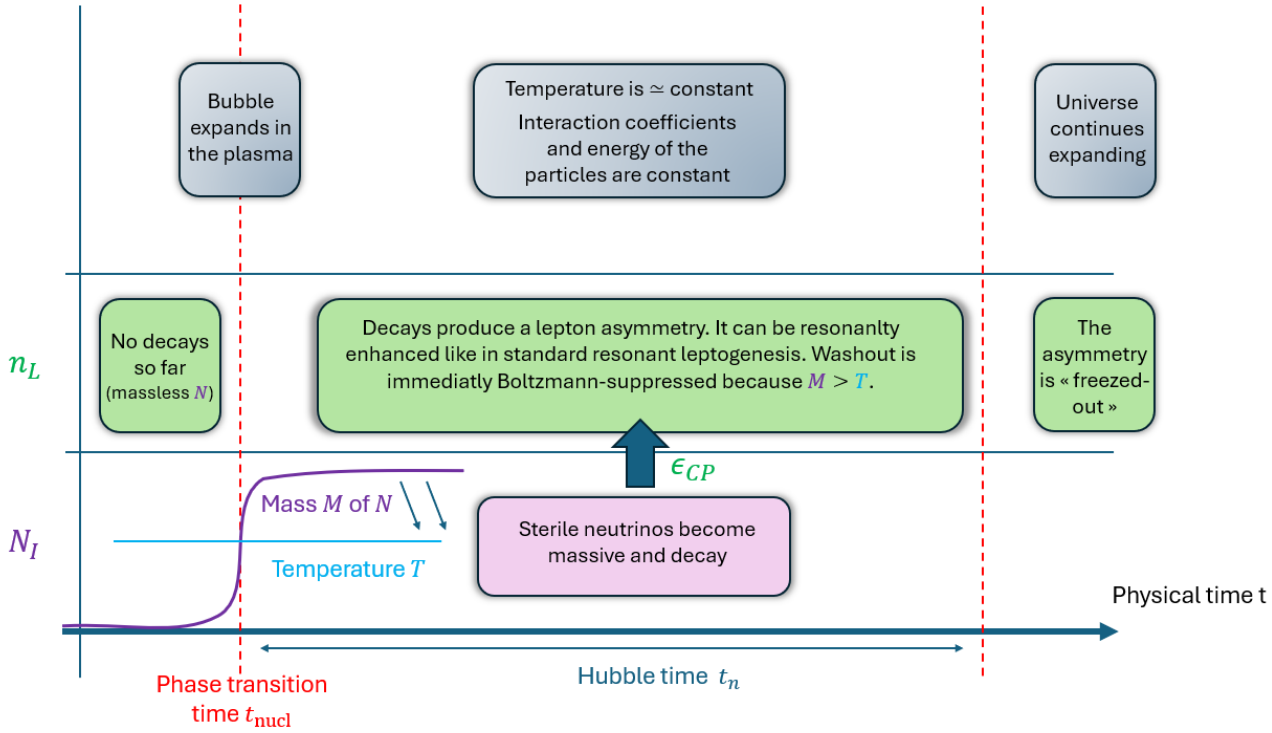

Figure 6.2: Schematic description of the MG scenario. The top row presents the different steps of the cosmological context, in which the sterile neutrinos (bottom row) decay to give the lepton asymmetry (middle row).

the mass should theoretically be dependent for all values of time. However, it approaches its final value exponentially fast, so that most of the variation happens during a small period around our reference time $\Delta t = 0$. For $|\Delta t| \lesssim$ few T_n^{-1}, the variation can be important, but for longer times, the mass is close to its final value. Numerically, it is a very good approximation to take $M(t) \approx M_0$ once Δt is large enough,

$$M(t) = M_0 \text{ for } \gamma \Delta t = T_n \Delta t > 15. \tag{6.10}$$

Moreover, sterile neutrinos are very massive ($M > T_n$) during the period of interest where the asymmetry is produced. Inverse decays will then be suppressed by a Boltzmann factor coming from $f_{FD}(\omega) \sim \exp(-M/T_n)$. This means that the backreaction of the asymmetry on sterile neutrinos is negligible, as well as inverse decays responsible for asymmetry washout. Neglecting the B_a-factor in the equations (5.138) for the sterile neutrinos and W_a-term in the lepton asymmetry equation (5.144), leads to

$$\begin{aligned}\frac{\mathrm{d}}{\mathrm{d}t}\delta f^{ss'}_{h,IJ} = &-i(s\omega_I(t) - s'\omega_J(t))\ \delta f^{ss'}_{h,IJ} - s\delta_{ss'}\delta_{IJ}\partial_t f_{FD}(s\omega_I(t)) \\ &+ ss'\frac{|\mathbf{k}|}{2}\left(\frac{\partial_t M_I}{\omega_I(t)^2} f^{-ss'}_{h,IJ} + \frac{\partial_t M_J}{\omega_J(t)^2} f^{s-s'}_{h,IJ}\right) \\ &- \sum_{L,\eta} C^{s\eta s'}_{h,ILJ}\delta f^{\eta s'}_{h,LJ} + \left(C^{s'\eta s}_{h,JLI}\right)^* \delta f^{s\eta}_{h,IL}\ ,\end{aligned} \tag{6.11}$$

$$\frac{\mathrm{d}\Delta_a}{\mathrm{d}t} = -S_a(t) \ . \tag{6.12}$$

The source term is computed from the sterile neutrino distributions

$$S_a = \sum_{h,s,s'} \sum_{I,J} \int \frac{\mathrm{d}^3\mathbf{k}}{(2\pi)^3} \ \mathrm{Tr}\left[\left(P_R \mathbf{\Sigma}^{\mathrm{eff},\rho}_{\mathrm{eq},\mathbf{k},a,JI} + \left(\mathbf{\Sigma}^{\mathrm{eff},\rho}_{\mathrm{eq},\mathbf{k},a,IJ}\right)^\dagger P_R\right) \mathcal{P}^{ss'}_{h,IJ}\right] \ \delta f^{ss'}_{h,IJ}(\mathbf{k},t) \ . \tag{6.13}$$

Our justified simplifications allow us to keep the momentum dependence while solving our equations for mass- and coherence-shell in a reasonable amount of computational time. Our equations are momentum-dependent. In order to solve them efficiently, we restrain ourselves to a certain range of momenta, and take a discrete set of them. Following the discussion of section 5.4, we only consider momenta $k \in [0.01, 12] \times T$ for which we have a numerical expression for the self-energy in the relativistic regime. We have checked that, in the non-relativistic regime where we have expression for all momenta, contributions of higher or lower momenta to the asymmetry are negligible. Once the equations are solved for all momenta in the sterile sector, we use them to compute the lepton asymmetry. Finally we obtain the yield

$$Y_B = \frac{28}{79} \frac{\sum_a \Delta_a}{\frac{2\pi^2}{45}} \ , \tag{6.14}$$

and compare it to the (central value of the) observed [3] $Y_B^{\mathrm{obs}} = 8.75 \times 10^{-11}$.

6.3 MG Results

We recall that we have 4 parameters that are of interest, the temperature T_n, the ratio between the mass scale and the temperature M/T_n, the mass degeneracy $\Delta M/M$ and the imaginary part z_i of the complex angle. We summarize in Table 6.1 which relevant parameters are being fixed and which ones are being varied, from the discussions in Chapter 3.

	FOPT sector	neutrino sector
Fixed	$\gamma = T_n$	$\delta = 3\pi/2$, $\alpha_1 = \alpha_2 = 0$, $z_r = 3\pi/4$
Free	T_n	M, $\Delta M/M$, z_i

Table 6.1: Summary of all parameters of interest. In the scalar sector, the FOPT happens at a temperature T_n, which (we assumed) is fixing the scale for the relevant parameters of the FOPT. In the neutrino sector, most low-energy PMNS matrix-elements are determined by experiments; for the CP and Majorana phases that remain uncertain, we make a choice. The sterile neutrinos have their own degrees of freedom, their masses and the angle in the R matrix.

We find successful regions for leptogenesis. Plotting the produced asymmetry as a function of M/T_n and $\Delta M/M$ in Figure 6.3a allowed us to verify that the masses needed to be greater by

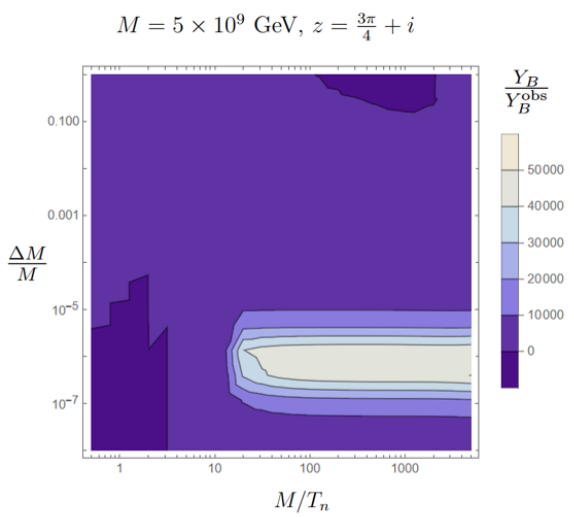

(a) Normalized baryon asymmetry as a function of M/T_n and $\Delta M/M$. The mass of the sterile neutrinos should be a factor $\simeq 10$ over the temperature in order to obtain a large asymmetry. The mass degeneracy exhibits a resonance when it reaches $\Delta M/M \simeq 10^{-6}$.

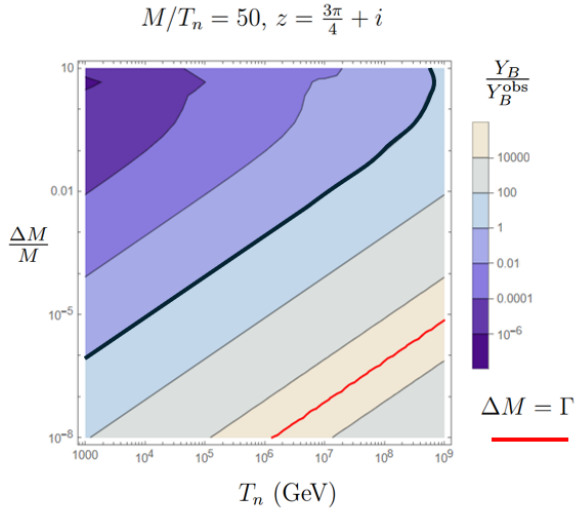

(b) Normalized baryon asymmetry as a function of T_n and $\Delta M/M$. The thick-black contour delimits the region of successful leptogenesis. The isocurves in the lower part of the panel are straight lines in a log-log scale. We plotted in red the curve corresponding to $\Delta M = \Gamma$.

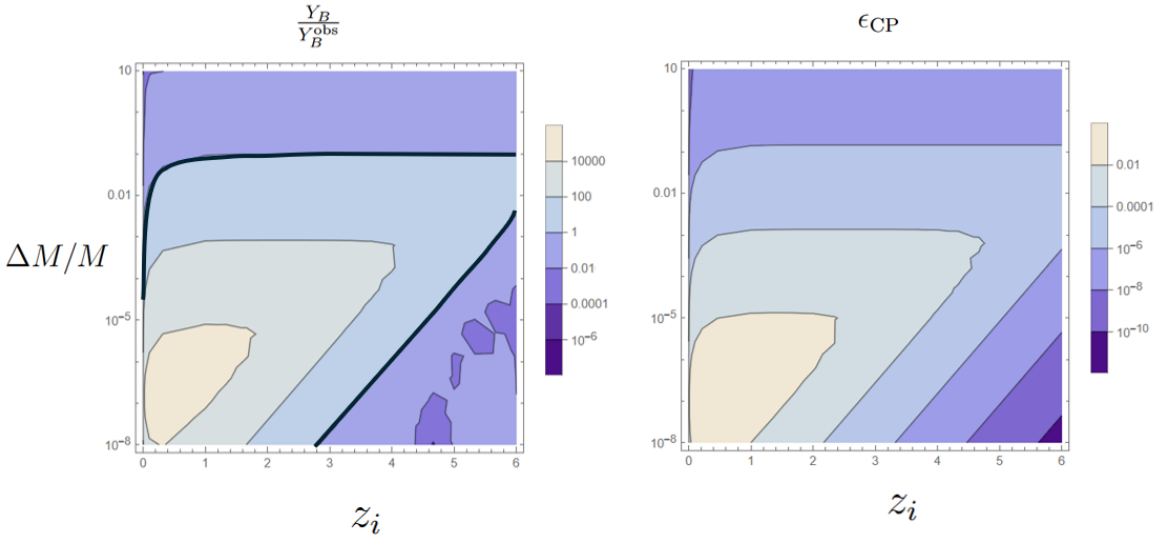

(c) Comparison of the normalized baryon asymmetry (on the left) and the CP asymmetry $\epsilon_{\rm CP}$ (on the right) as a function of z_i and $\Delta M/M$. The ratio M/T_n was fixed at 50, and the temperature of the FOPT is $T_n = 10^8$ GeV. The region of successful leptogenesis is delimited by a thick-black contour.

Figure 6.3: Numerical results in the MG scenario

some factor ten compared to the temperature in order to produce enough asymmetry. For M too close to T_n, the washout is not suppressed enough by the Boltzmann factor to avoid significant washout. However, at fixed $\Delta M/M$, the baryon asymmetry does not increase indefinitely

as M/T_n is increased. Once the washout is suppressed enough to let the asymmetry survive, it does not help much to suppress it further.

In the $(\Delta M/M, T_n)$ plane in Figure 6.3b, we may see that the baryon asymmetry produced is maximal along a certain line $\Delta M/M \propto T_n$, which can be seen with the isocurves that are straight lines of slope 1 (in the log-log scale). We have checked that the maximum corresponds to $M_2 - M_1 \approx (\Gamma_1 + \Gamma_2)/2 \equiv \Gamma$, with Γ the decay rates for the sterile neutrinos in the non-relativistic regime.

For non-degenerate sterile neutrinos, the region where leptogenesis is successful is for temperatures $T_n \gtrsim 10^8$ GeV, *i.e.* $M \gtrsim 5 \times 10^9$ GeV in the upper-right region of the plot. Lower temperatures (and therefore lower masses because M/T_n is fixed in this case) are successful only to the price of stronger mass degeneracy (around $\Delta M/M \sim 10^{-6}$ for $M \sim 5 \times 10^5$ GeV). This is reminiscent of thermal and resonant leptogenesis; with hierarchical masses, leptogenesis works only above the Davidson-Ibarra bound. For lower masses, the resonant regime is needed to create enough asymmetry. We make in the next section the connection with resonant leptogenesis for the interpretation of our results.

6.4 CP asymmetry in decays

We wish to compare and interpret our results in terms of thermal leptogenesis, in which the asymmetry is also generated by decays. The general kinetic equations (6.11) that we started with (and solved numerically) are equations for density matrices, that contain flavor-mixing between sterile neutrinos (the off-diagonal elements $\delta f^{ss'}_{h,12}$). This type of matrix equations are known [139,143] to lead to the classical Boltzmann equations used in thermal and resonant leptogenesis, once kinetic equilibrium is assumed and that the off-diagonal elements are integrated out of the dynamics. Recall that in thermal leptogenesis, the equations are

$$\frac{\mathrm{d}N_{N_I}}{\mathrm{d}t} + 3HN_I = -\gamma_I \left(\frac{N_{N_I}}{N^{\mathrm{eq}}_{N_I}} - 1 \right) \tag{6.15}$$

$$\frac{\mathrm{d}N_L}{\mathrm{d}t} + 3HN_L = -\sum_I \left[\gamma_I \frac{N_L}{2N^{\mathrm{eq}}_l} - \epsilon^I_{\mathrm{CP}} \gamma_I \left(\frac{N_{N_I}}{N^{\mathrm{eq}}_{N_I}} - 1 \right) \right] \ , \tag{6.16}$$

where γ_I is the decay rate, and ϵ^I_{CP} is the CP asymmetry. We discussed this quantity in 3.3; it contains contributions from vertex and wave-function corrections. In resonant leptogenesis, the wave-function contribution dominates, as $\Delta M \ll M$. We will therefore neglect the vertex contribution and work with $\epsilon^I_{\mathrm{CP,wave}}$ only, with a regulated expression compared to our original definition (3.56),

$$\epsilon^I_{\mathrm{CP}} \simeq \epsilon^{I,\mathrm{reg}}_{\mathrm{CP,wave}} \equiv \frac{\mathrm{Im}\left[\left(YY^\dagger \right)^2_{12} \right]}{\left(YY^\dagger \right)_{11} \left(YY^\dagger \right)_{22}} \frac{\left(M_2^2 - M_1^2 \right) M_I \Gamma_J}{\left(M_2^2 - M_1^2 \right)^2 + \left(R_{IJ} \right)^2} \ , \ I \neq J \ . \tag{6.17}$$

We introduced the decay rates (in the non-relativistic regime) $\Gamma_I \equiv \left(YY^\dagger\right)_{II} M_I/(8\pi)$. R_{IJ} is a regulator, preventing the expression to blow up as $M_1 \to M_2$. In resonant leptogenesis, $\epsilon_{\rm CP,wave}$ is an input, so there is some arbitrariness in the choice of R_{IJ}. There is indeed no consensus on what value to take for R_{IJ}; several possibilities have approximately the same behaviour for the resonance. Options are [131, 132, 135, 143]

$$R_{IJ} = M_I\Gamma_J \ , \ M_I\Gamma_I - M_J\Gamma_J \ , \ M_I\Gamma_I + M_J\Gamma_J \ , \ (M_I\Gamma_I + M_J\Gamma_J)\,\frac{\left|\mathrm{Im}\left[\left(YY^\dagger\right)^2_{IJ}\right]\right|}{\left(YY^\dagger\right)_{II}\left(YY^\dagger\right)_{JJ}} \ . \quad (6.18)$$

We fixed $R_{IJ} = M_I\Gamma_I + M_J\Gamma_J$, for concreteness, and computed $\epsilon_{\rm CP} \equiv \epsilon^1_{\rm CP} + \epsilon^2_{\rm CP}$. In this case, the asymmetry is resonantly enhanced when $M_2 - M_1 \approx \Gamma \equiv (\Gamma_1 + \Gamma_2)/2$, For degenerate sterile neutrinos, using the Casas-Ibarra parametrization (3.41)

$$\begin{aligned} M_2 - M_1 = \Gamma \Leftrightarrow M_2 - M_1 &= \frac{(YY^\dagger)_{11} + (YY^\dagger)_{22}}{16\pi} M \\ \Leftrightarrow \frac{\Delta M}{M} &= M\frac{\sum_{i,I} m_i |R_{Ii}|^2}{16\pi} = T_n \frac{M}{T_n}\frac{\sum_{i,I} m_i |R_{Ii}|^2}{16\pi} \ . \end{aligned} \quad (6.19)$$

The resonance corresponds to a linear relation between $\Delta M/M$ and T_n, at fixed M/T_n and fixed z. This explains the isocurves that are straight lines in this plane, corresponding to equal values of $\epsilon_{\rm CP}$.

Using the expression for $\epsilon_{\rm CP}$, we can further compare the baryon asymmetry obtained numerically with the one expected from sterile neutrino decays. In the $(z_i, \Delta M/M)$ plane plotted in Figure 6.3c, the shape of the isocurves of the (numerical) asymmetry are similar to the shape of ϵ_{CP} values isocurves. The imaginary part z_i affects the value of $|R_{Ii}|^2$, so that the mass gap at the resonance, from the expression above, is changed. This reflects the fact that, for different z_i's, the maximum baryon asymmetry produced is obtained for different $\Delta M/M$.

6.5 Comparison to previous studies

In this section, we compare our approach to previous studies. In previous works [28,31], the final baryon asymmetry was estimated from semi-analytical results in the strong washout regime. The asymmetry Y_B is written as the product of different factors

$$Y_B = \kappa_{\rm pen}\kappa_{\rm dep}\kappa_w \left(\frac{T_n}{T_{\rm reh}}\right)^3 \kappa_{\rm sph}\epsilon_{\rm CP} Y^0_N \ . \quad (6.20)$$

Transmission inside the bubble The penetration rate $\kappa_{\rm pen}$ captures how efficiently the sterile neutrinos enter the bubble. In practice, for a relativistic bubble wall, the penetration rate is close to 1, $\kappa_{\rm pen} \simeq 1$.

Washout The factors $\kappa_{\rm dep}$ and κ_w are numerically determined by the Boltzmann equations and capture the reduction of the asymmetry from two channels. First, the factor κ_w corresponds to the usual washout in thermal leptogenesis. Second, the depletion rate $\kappa_{\rm dep}$ includes the reduction of the sterile neutrino distribution by their annihilation into the scalar field $NN \to S$ (and also into the gauge boson of the $B-L$ symmetry in [28, 31]).

Dilution After the FOPT and the entropy injection in the plasma, the asymmetry is diluted by a factor $\left(\frac{T_n}{T_{\rm reh}}\right)^3$.

Sterile neutrino decays Finally, $\kappa_{\rm sph}\epsilon_{\rm CP}Y_N^0$ is the naive estimate of the asymmetry produced by the decay of an initial sterile neutrino distribution Y_N^0, with a CP-asymmetry $\epsilon_{\rm CP}$ creating a lepton asymmetry, converted into a baryon asymmetry by the sphalerons by a factor $\kappa_{\rm sph} = \frac{28}{79}$. In the Mass Gain mechanism, the sterile neutrinos are initially massless, such that $Y_N^0 = \frac{135\zeta(3)}{4\pi^4 g_*}$.

These different factors were plotted as a function of the phase transition strength α_n. We recall its definition from (2.71)

$$\alpha_n \equiv \frac{\Delta V_S(T_n)}{\rho_{\rm SM}(T_n)} \ , \tag{6.21}$$

which is the ratio between the potential energy released by the phase transition and the energy density of the SM plasma at the nucleation. The phase transition will have a significant impact on the plasma energy density if $\alpha_n > 1$. The effect of the energy released is to reheat the plasma to a temperature $T_{\rm reh}$ such that

$$\rho_{\rm SM}(T_{\rm reh}) = \rho_{\rm SM}(T_n) + \Delta V \tag{6.22}$$

which can be rewritten in terms of α_n, using $\rho_{\rm SM}(T) \propto T^4$,

$$\frac{\rho_{\rm SM}(T_n)}{\rho_{\rm SM}(T_{\rm reh})} = \left(\frac{T_n}{T_{\rm reh}}\right)^4 = (1+\alpha_n)^{-1} \ . \tag{6.23}$$

We obtain a direct relation between the dilution factor $(T_n/T_{\rm reh})^3$ and the strength α_n.

In general, several factors depend on the strength α_n. In [31], the authors conclude that a strong FOPT with large values of α_n reduces the asymmetry because of the dilution factor from reheating $(T_n/T_{\rm reh})^3$, while lower values of α_n imply less deviation from equilibrium and a stronger washout and depletion effect from the Boltzmann equations (smaller values of κ_w and $\kappa_{\rm dep}$). The optimal case, for the mass and coupling values they considered, was found to be around $\alpha_n \approx 5$. This corresponds to values of the parameters (see Figure 2 in [31])

$$\underline{\alpha_n = 5}: \ \kappa_{\rm pen} = 1 \ , \ \kappa_{\rm dep} \approx 0.5 \ , \ \kappa_{\rm w} \approx 0.8 \ , \ \left(\frac{T_n}{T_{\rm reh}}\right)^3 \approx 0.26 \ . \tag{6.24}$$

A reasonable estimate of the reheating for refining our study would then be to add a factor $(T_n/T_{\rm reh})^3 \sim 1/4$ in our numerical results. We would still obtain large regions of successful leptogenesis.

These previous approaches did not include particle production during the phase transition. From section 4, for an initial number density of massless sterile neutrinos, distributed thermally, we can compute the number density obtained after the passage of the bubble, which is larger due to production. Integrating over all momenta, we describe the production in terms of a factor $\kappa_{\rm PT}$ defined by

$$\kappa_{\rm PT} = \frac{N_{\rm PT}}{N_{\rm eq}^{M=0}(T_n)} = \frac{4\pi^2}{3\zeta(3)T_n^3} \int \frac{{\rm d}^3\mathbf{k}}{(2\pi)^3} \, f_{\mathbf{PT}} \ , \tag{6.25}$$

where $f_{\mathbf{PT}}$ was obtained from hypergeometric functions in section 4. Its effect on the baryon asymmetry produced is simply that it enhances the number of particles able to decay after the FOPT,

$$Y_N^{\rm in} = \kappa_{\rm PT} Y_N^0 \ , \tag{6.26}$$

$$Y_B = \kappa_{\rm PT}\kappa_{\rm pen}\kappa_{\rm dep}\kappa_w \left(\frac{T_n}{T_{\rm reh}}\right)^3 \kappa_{\rm sph}\epsilon_{\rm CP} Y_N^0 \ . \tag{6.27}$$

The behaviour of $\kappa_{\rm PT}$ as a function of α_n is plotted in Figure 6.4a, assuming we fix

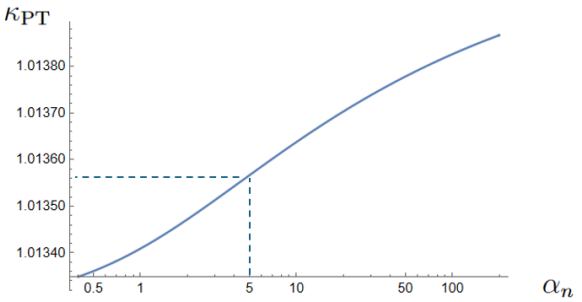

(a) $\kappa_{\rm PT}$ as function of the phase transition strength α_n, at fixed $M/T_{\rm reh} = 10$. The value $\alpha_n = 5$ is indicated.

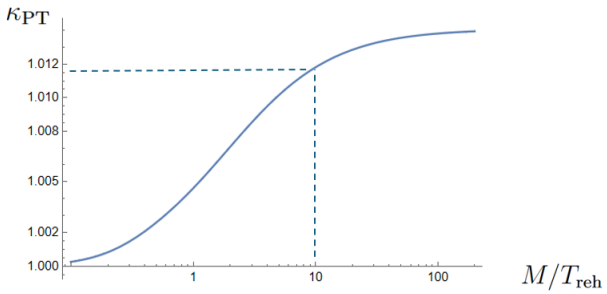

(b) $\kappa_{\rm PT}$ as function of the $M/T_{\rm reh}$, at fixed $\alpha_n = 5$. The value $M/T_{\rm reh} = 10$ is indicated.

$M/T_{\rm reh} = (1+\alpha_n)^{-1/4} M/T_n = 10$. The stronger the phase transition, the more particle will be produced, as one can expect. In [31], the optimal enhancement of the asymmetry was found for $\alpha_n \simeq 5$. For this strength, the factor $\kappa_{\rm PT}$ gives only an O(1%) enhancement of the asymmetry. Augmenting the mass ratio $M/T_{\rm reh}$ improves this factor slightly, but a plateau is reached at large masses, as seen in Figure 6.4b. The particle production at the phase transition for the MG scenario has therefore a sub-leading effect on the asymmetry.

In addition to particle production, our approach also included the full dynamics of the mass- and coherence-shell functions, as function of momentum. We did not assume kinetic equilibrium, and moreover, we kept sterile flavor correlations (*i.e.* off-diagonal terms in the matrices

$\delta f_{12}^{ss'}$) dynamical. In particular, the resonant behaviour of the decays was not put by hand; it came automatically from the resolution of the equations. No regulator was needed to make the CP-asymmetry finite when $\Delta M \ll M, \Gamma$.

6.6 Conclusion for the MG scenario

Working with sterile neutrinos that become very massive during a first-order phase transition, we found successful regions for leptogenesis. We were able to interpret the results clearly in terms of sterile neutrino decays, happening shortly after the FOPT. Our equations also included particle production due to the FOPT, but we estimated its effect to be only a minor O(1%) improvement. For hierarchical sterile neutrinos, we need $M \gtrsim 5 \times 10^9$ GeV in order to successfully reproduce the baryon asymmetry, consistent with the Davidson-Ibarra bound. For degenerate sterile neutrinos, the asymmetry exhibits a resonant behaviour at $\Delta M \sim \Gamma$, like in resonant leptogenesis. Note that we did not need to put by hand a regulator R_{IJ} in a resonant CP-asymmetry $\epsilon^I_{\text{CP,wave}}$, because we solved for the complete kinetic equations for mass- and coherence-shell functions, including flavor mixing (from off-diagonal terms $\delta f_h^{ss'}{}_{12}$). We never needed the expression for ϵ^I_{CP}, the asymmetry is automatically regulated, coming out of the equations.

Chapter 7

ARS-like leptogenesis

In this chapter, we describe the impact of a FOPT on a regime similar to ARS leptogenesis, in which the asymmetry is created while the sterile neutrinos are produced from the plasma. We first show that, starting from our kinetic equations (5.138),(5.144), we recover similar equations to the ones presented in section 3.4 for ARS leptogenesis. We then explain how an extra scalar S and its FOPT modify them, and what are the physical consequences of this modification. In particular, the vacuum masses, crucial for flavor oscillations in ARS leptogenesis, are no longer present since the beginning; they only appear after the FOPT. It is however possible, as we will see, that thermal masses coming from the scalar S contributed to oscillations before the FOPT.

We then distinguish three scenarios, that we designate with roman numbers: (I) standard ARS leptogenesis (without a FOPT); (II) ARS-like leptogenesis with a FOPT and no thermal masses from S (no oscillations before the FOPT); (III) ARS-like leptogenesis with a FOPT and with thermal masses from S (oscillations before and/or after the FOPT). Scenario (I) is well known, so we will only briefly re-derive some known analytical estimates of the asymmetry in this case, in order to compare them to the other scenarios. Scenario (II) is one of the main focuses of this thesis and is an original work. We detail the associated numerical and analytical studies, and compare them to standard ARS leptogenesis. Scenario (III) extends prior studies [37, 39] on the effect of thermal masses by developing analytical estimates and completes our description of ARS leptogenesis with a phase transition.

This chapter is organized around the presentation of these scenarios. We start by discussing in section 7.1 the qualitative differences that we expect between ARS with and without a phase transition. In both cases, we consider the flavor oscillations of relativistic sterile neutrinos, for which we derive in section 7.2 equations that are common to all scenarios. The difference between the scenarios is then concretely given in terms of the coefficients of the equations in section 7.3. Each scenario is treated separately: section 7.4 presents analytical estimates for standard ARS leptogenesis, while sections 7.5 and 7.6 present the second scenario numerically and analytically, respectively. Section 7.7 gives the analytical estimates found in the third sce-

nario, before we compare all three cases in section 7.8 and conclude on the advantages of each scenario.

7.1 Qualitative discussion

Before getting started, let us insist on why we expect scenario (II) (ARS-like scenario with a phase transition) to be qualitatively different from scenario (I) (standard ARS leptogenesis). In our equations (and in ARS scenarios in general), we expect flavor oscillations in the sterile sector to be the origin of CP-violation, and eventually of asymmetry generation. Usually, in standard ARS leptogenesis, sterile neutrinos are massive from the beginning of the evolution, and as we saw in section 3.4, oscillations start around a typical temperature given by

$$T_{\rm osc}^{\rm ARS} \equiv \left[a_R \left(M_2^2 - M_1^2\right)\right]^{1/3} \ . \tag{7.1}$$

However, in scenario (II), oscillations could not have been started by vacuum masses before the FOPT because they were exactly zero. At the temperature T_n of the FOPT, we may already be past the oscillation temperature. This brings us to consider two extreme cases, $T_n \gg T_{\rm osc}^{\rm ARS}$ or $T_n \ll T_{\rm osc}^{\rm ARS}$:

If $T_n \gg T_{\rm osc}^{\rm ARS}$, the FOPT happens long before the oscillations, and sterile neutrinos have acquired their vacuum masses by then. In this regime, the evolution will be the same as in ARS leptogenesis, with potentially a different initial condition for the sterile neutrino density, coming from the particle production at the FOPT.

We are more interested in the second case, where $T_n \ll T_{\rm osc}^{\rm ARS}$. Here, the oscillations were frustrated because the vacuum masses were still zero at $T = T_{\rm osc}^{\rm ARS}$, so no flavor oscillations were permitted. Once the FOPT is complete, the oscillations can start. They will occur at a lower temperature than what is standard. Lower temperatures imply a slower expansion of the Universe, so we expect the oscillations to happen more rapidly than the evolution of the temperature. To make this precise, we compare the typical time $t_{\rm osc}$ of one sterile flavor oscillation (at fixed temperature T_n) to the time for which temperature varies, $t_n \equiv H^{-1}(T_n)$. For a generic particle of momentum $|\mathbf{k}| \approx T_n \gg M_1, M_2$ in the plasma, the energy difference between the flavors (thus the frequency of flavor oscillations) is

$$\omega_{12} = \omega_2 - \omega_1 \simeq \frac{M_2^2 - M_1^2}{2|\mathbf{k}|} \approx \frac{M_2^2 - M_1^2}{2T_n} \ . \tag{7.2}$$

The corresponding time we want to consider is

$$t_{\rm osc} \equiv \left(\frac{M_2^2 - M_1^2}{2T_n}\right)^{-1} \quad \text{compared to} \quad t_n \equiv \frac{a_R}{T_n^2} \ , \tag{7.3}$$

$$\frac{t_{\rm osc}}{t_n} = 2\frac{T_n}{a_R}\frac{T_n^2}{M_2^2 - M_1^2} \stackrel{!}{=} 2\left[\frac{T_n}{T_{\rm osc}^{\rm ARS}}\right]^3 \ . \tag{7.4}$$

Remarkably, the time ratio is directly related to the ratio of the relevant temperatures. This is not too surprising; given the power-law dependence in temperature of the time, if the temperature T_n is lower than the typical temperature for which one oscillation occurs (in standard ARS), then there is enough room, in one Hubble time at temperature T_n, for oscillations to happen.

We summarize this description in Figure 7.1. The domain we want to explore is the non-standard scenario in which oscillations happen at (approximately) *constant temperature*, with $t_{\rm osc} \ll t_n$. The flavor oscillations then have time to produce an asymmetry in the different flavors and then average out, their contribution to the total lepton asymmetry becoming negligible. Since washout processes are flavor-dependent, they will produce a non-zero total asymmetry. Eventually, washout will erase this asymmetry; it is then crucial that sphaleron decoupling occurs before this happens, such that a net baryon asymmetry is produced.

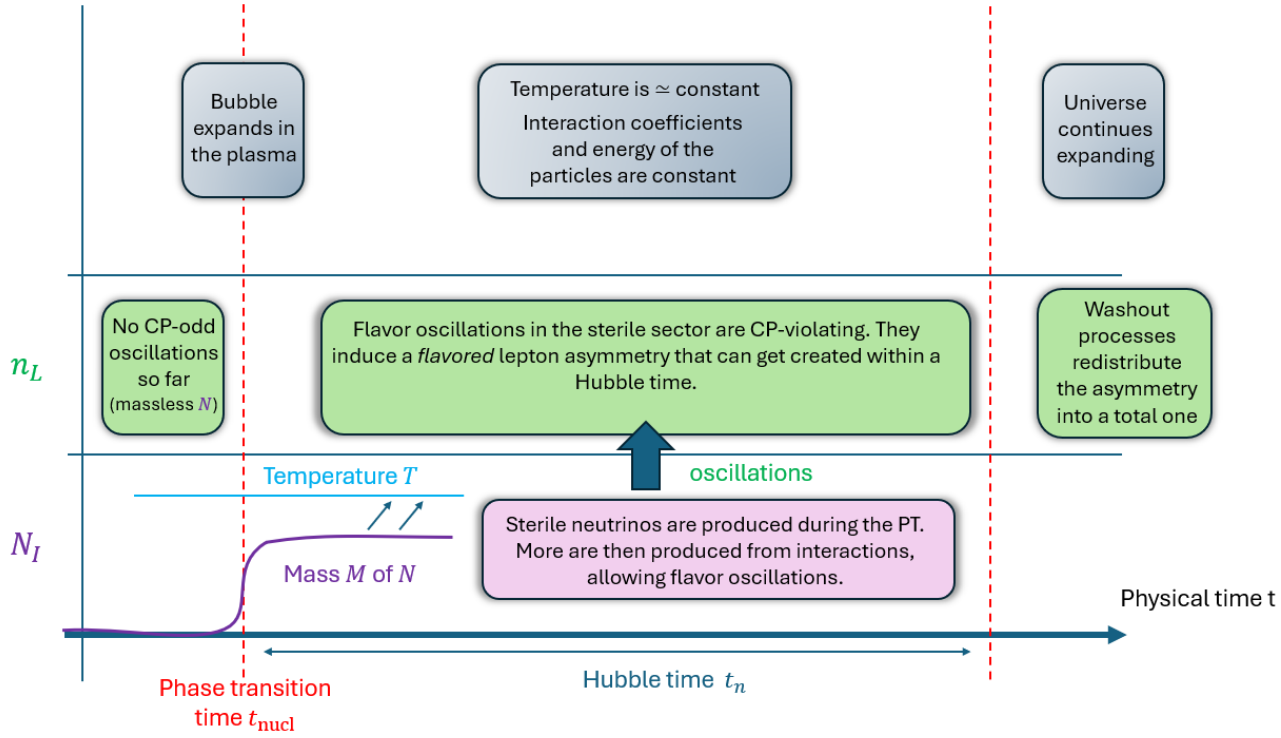

Figure 7.1: Schematic description of scenario (II) (an ARS-like regime with a FOPT).

7.2 ARS-like equations

ARS leptogenesis relies on flavor oscillations in the sterile sector. The quantum nature of the density matrix should be present in our evolution equations, but we are mainly concerned with flavor oscillations, which are the (relatively) slow oscillations between states of different masses, therefore of different vacuum energy. They correspond to the mass-shell functions, oscillating

at a rate $\approx \omega_I - \omega_J$. The coherence-shell functions, as mentioned earlier, oscillate much faster and are interpreted as particle-antiparticle oscillations.

Consider for instance a typical particle in the plasma, of momentum $|\mathbf{k}| \simeq T$. In ARS leptogenesis, masses are much smaller than the temperature, so the energy of such a particle would be

$$\omega_I = \sqrt{|\mathbf{k}|^2 + M_I^2} \approx T + \frac{M_I^2}{2T} \ . \tag{7.5}$$

Then, frequency of mass- and coherence-shell functions are

$$\Omega_m = \omega_I - \omega_J \approx \frac{M_I^2 - M_J^2}{2T} \ , \ \Omega_c = \omega_I + \omega_J \approx 2T \ . \tag{7.6}$$

The low values of the masses $M_I \ll T$ ensure that $\Omega_m \ll \Omega_c$. This means that the coherence-shell functions can be quickly averaged out if we consider evolution over larger scales than $1/T$. Going back to the equations for the sterile neutrino distributions, putting all the coherence-shell terms to zero leaves only

$$\begin{aligned}\frac{\mathrm{d}}{\mathrm{d}t}\delta f^{m,s}_{h,IJ} = &- is\left(\omega_I - \omega_J\right)\delta f^{m,s}_{h,IJ} - s\delta_{IJ}\,\frac{\mathrm{d}f_{FD}(s\omega_I)}{\mathrm{d}t} \\ &- \sum_L \left[C^{sss}_{h,ILJ}\delta f^{m,s}_{h,LJ} + \left(C^{sss}_{h,JLI}\right)^* \delta f^{m,s}_{h,IL}\right] + \sum_a B^{ss}_{h,a,IJ}\frac{\mu_a + \mu_\phi}{T} \ .\end{aligned} \tag{7.7}$$

Because $\delta f^{m,-}_{h,IJ} = -\delta f^{m,+}_{h,JI}$, (see 5.2.6), we might as well focus only on $\delta f^{m,+}_{h,IJ}$. The equations now only involve one collision term given by $C^{+++}_{h,ILJ}$, and one backreaction per flavor $B^{++}_{a,IJ}$, whose definitions we recall

$$C^{+++}_{h,ILJ} \equiv i\mathrm{Tr}\left[\mathcal{P}^{++}_{h,JI}\boldsymbol{\Sigma}^{\mathrm{eff},R}_{\mathbf{k},\mathrm{eq},IL}\mathcal{P}^{++}_{h,LJ}\right] = i\mathrm{Tr}\left[\mathcal{P}^{++}_{h,JI}\left(\boldsymbol{\Sigma}^{\mathrm{eff},\mathcal{H}}_{\mathbf{k},\mathrm{eq},IL} - i\boldsymbol{\Sigma}^{\mathrm{eff},\rho}_{\mathbf{k},\mathrm{eq},IL}\right)\mathcal{P}^{++}_{h,LJ}\right] \ , \tag{7.8}$$

$$B^{++}_{h,a,IJ}(t) \equiv g_W\mathrm{Tr}\left[\mathcal{P}^{++}_{h,JI}\left(Y_{Ia}Y^*_{Ja}P_L - Y^*_{Ia}Y_{Ja}P_R\right)\sum_{\eta=\pm}\{\mathbf{F}^{\rho,\eta}_J, \mathbf{P}^\eta_J\}\right] \ . \tag{7.9}$$

With the assumption that the sterile neutrino masses are sufficiently degenerate ($\omega_I \approx \omega$ in the computation of the self-energies) and relativistic, the projectors appearing in the definition of the C and B coefficients can be simplified (see Appendix G). Using the expression for the self-energies from section 5.4, computing the various coefficients leads to

$$\begin{aligned}C^{+++}_{h,ILJ} &= g_W\left[\left(YY^\dagger\right)_{h,IL}\frac{k+\tilde{k}}{2\omega} + \left(Y^*Y^T\right)_{h,IL}\frac{k-\tilde{k}}{2\omega}\right]\cdot\left(\hat{\Sigma}^\rho_{\mathrm{eq}} + i\hat{\Sigma}^{\mathcal{H}}_{\mathrm{eq}}\right)(k) \\ &= \frac{T}{2}\left(\left(YY^\dagger\right)_{h,IL}(\gamma_+ + ih_+) + \left(Y^*Y^T\right)_{h,IL}(\gamma_- + ih_-)\right) \ ,\end{aligned} \tag{7.10}$$

$$\begin{aligned}B^{++}_{h,a,IJ} &= h\ g_W f_{FD}\left(1 - f_{FD}\right)\left[\left(Y_{\cdot a}Y^\dagger_{a\cdot}\right)_{h,IJ}\frac{k+\tilde{k}}{2\omega} - \left(Y^*_{\cdot a}Y^T_{a\cdot}\right)_{h,IJ}\frac{k-\tilde{k}}{2\omega}\right]\cdot\hat{\Sigma}^\rho_{\mathrm{eq}}(k) \\ &= \frac{hT}{2}f_{FD}\left(1 - f_{FD}\right)\left(\left(Y_{\cdot a}Y^\dagger_{a\cdot}\right)_{h,IJ}\gamma_+ - \left(Y^*_{\cdot a}Y^T_{a\cdot}\right)_{h,IJ}\gamma_-\right) \ ,\end{aligned} \tag{7.11}$$

$$k = (\omega, \mathbf{k}) \ , \ \tilde{k} = (|\mathbf{k}|, \omega \ \hat{\mathbf{k}}), \tag{7.12}$$

where we defined, for the matrix $A = YY^\dagger$ or Y^*Y^T,

$$A_h = A \text{ if } h = +1 \ , \ A_h = A^* \text{ if } h = -1 \ . \tag{7.13}$$

We introduced more standard notation from ARS leptogenesis (for instance used in [137–139])

$$\gamma_+ \equiv \frac{1}{T} \frac{g_W \left(k + \tilde{k}\right) \cdot \hat{\Sigma}^\rho_{\rm eq}(k)}{\omega} \ , \ \gamma_- \equiv \frac{1}{T} \frac{g_W \left(k - \tilde{k}\right) \cdot \hat{\Sigma}^\rho_{\rm eq}(k)}{\omega} \ , \tag{7.14}$$

$$h_+ \equiv \frac{1}{T} \frac{g_W \left(k + \tilde{k}\right) \cdot \hat{\Sigma}^{\mathcal{H}}_{\rm eq}(k)}{\omega} \ , \ h_- \equiv \frac{1}{T} \frac{g_W \left(k - \tilde{k}\right) \cdot \hat{\Sigma}^{\mathcal{H}}_{\rm eq}(k)}{\omega} \ , \tag{7.15}$$

where we recall that at thermal equilibrium, the self-energies with a "hat" correspond to the self-energies from which we extracted the flavor indices,

$$\Sigma^{\rho/\mathcal{H}}_{{\rm eq},IJ}(k) \equiv g_W \left(Y_{Ia} Y^*_{Ja} P_L + Y^*_{Ia} Y_{Ja} P_R\right) \hat{\Sigma}^{\rho/\mathcal{H}}_{\rm eq}(k) \ . \tag{7.16}$$

The Minkowski scalar product in $k \cdot \hat{\Sigma} = k^\mu \hat{\Sigma}_\mu$ is implicitly defined with respect to the 4-vector associated with the hatted self-energies, $\hat{\Sigma} \equiv \hat{\Sigma}_\mu \gamma^\mu$. These coefficients were derived from the spectral (γ) and hermitian (h) parts of the self-energy. Equation (7.7) now takes the form

$$\begin{aligned} \frac{\mathrm{d}}{\mathrm{d}t} \delta f^{m,s}_h = & - is \left[H_0 + H^h_{th}, \delta f^{m,s}_h\right] - \frac{\mathrm{d} f_{FD}}{\mathrm{d}t} \\ & - \frac{1}{2} \left\{\Gamma_h, \delta f^{m,s}_h\right\} + f_{FD} \left(1 - f_{FD}\right) \sum_a \tilde{\Gamma}_{h,a} \frac{\mu_a + \mu_\phi}{T} \ , \end{aligned} \tag{7.17}$$

$$\left(H_0\right)_{IJ} \equiv \omega_I \delta_{IJ} \ , \ \left(H^h_{th}\right)_{IJ} \equiv T \left[\frac{h_+}{2} \left(YY^\dagger\right)_{h,IJ} + \frac{h_-}{2} \left(Y^*Y^T\right)_{h,IJ}\right] \ , \tag{7.18}$$

$$\left(\Gamma_h\right)_{IJ} \equiv T \left[\gamma_+ \left(YY^\dagger\right)_{h,IJ} + \gamma_- \left(Y^*Y^T\right)_{h,IJ}\right] \ , \tag{7.19}$$

$$\left(\tilde{\Gamma}_{h,a}\right)_{IJ} \equiv \frac{hT}{2} \left[\gamma_+ \left(Y_{\cdot a} Y^\dagger_{a\cdot}\right)_{h,IJ} - \gamma_- \left(Y^*_{\cdot a} Y^T_{a\cdot}\right)_{h,IJ}\right] \ . \tag{7.20}$$

The hermitian self-energy contributed to a Hamiltonian interpreted as thermal sterile neutrino masses coming from the Yukawa couplings. The spectral self-energy gave us the collision terms Γ, $\tilde{\Gamma}$. So far, we have kept the momentum dependence explicit. In most ARS studies, the momentum dependence is removed by making the assumption of kinetic equilibrium. It assumes that the momentum distribution is proportional to the Fermi-Dirac distribution. In this case, one can integrate over momentum to get an equation involving the number density

$$\delta N_h \equiv \int \frac{\mathrm{d}^3 \mathbf{k}}{(2\pi)^3} \ \delta f^{m,+}_h \ . \tag{7.21}$$

As δf is a function of the normalized momentum $\boldsymbol{\kappa} = \mathbf{k}/T$, the number density goes like T^3,

$$\delta N_h = T^3 \int \frac{\mathrm{d}^3 \boldsymbol{\kappa}}{(2\pi)^3} \ \delta f^{m,+}_h \ . \tag{7.22}$$

This T^3-factor is responsible for the dilution of the number density as the Universe expands. It is therefore convenient to work with a normalized number density

$$\delta n_h \equiv \frac{\delta N_h}{T^3} \ . \tag{7.23}$$

Kinetic equilibrium assumes that the momentum distribution is a Fermi-Dirac distribution multiplied by a momentum-independent amplitude,

$$\delta f_h^{+,s} = \delta n_h \frac{\tilde{f}_{FD}(\boldsymbol{\kappa})}{n_{\rm eq}} \ , \tag{7.24}$$

with

$$\tilde{f}_{FD}(\boldsymbol{\kappa}) \equiv \frac{1}{e^{|\boldsymbol{\kappa}|}+1} \ , \ n_{\rm eq} = \int \frac{\mathrm{d}^3\boldsymbol{\kappa}}{(2\pi)^3} \ f_{FD} = \frac{3\zeta(3)}{4\pi} \ . \tag{7.25}$$

We took the Fermi-Dirac distribution for a relativistic particle, which is a good approximation in our case ($M \ll T$ during the whole evolution). In particular, the equilibrium distribution is no longer time dependent. The equation (7.17) can then be integrated over momentum,

$$\frac{\mathrm{d}}{\mathrm{d}t}\delta n_h = -i\left[\left\langle H_0 + H_{th}^h \right\rangle, \delta n_h\right] - \frac{1}{2}\left\{\left\langle \Gamma_h \right\rangle, \delta n_h\right\} + n_{\rm eq} \sum_a \left\langle \tilde{\Gamma}_{h,a} \right\rangle^{(1)} \frac{\mu_a + \mu_\phi}{T} \ . \tag{7.26}$$

We recover the equation (3.58) from section 3.4. The momentum averages are defined by

$$\langle X \rangle \equiv \frac{1}{n_{eq}} \int \frac{\mathrm{d}^3\mathbf{k}}{(2\pi)^3} \ X(\mathbf{k}) \ f_{FD} \ , \tag{7.27}$$

$$\langle X \rangle^{(1)} \equiv \int \frac{\mathrm{d}^3\mathbf{k}}{(2\pi)^3} \ X(\mathbf{k}) \ f_{FD}\left(1 - f_{FD}\right) \ , \tag{7.28}$$

for all quantities X. The lepton asymmetry equation can also be simplified in the relativistic regime and once kinetic equilibrium is assumed. In the end, we recover the standard equations used in ARS leptogenesis

$$\frac{\mathrm{d}}{\mathrm{d}t}\delta n_h = -i\left[\left\langle H_0 + H_{th}^h \right\rangle, \delta n_h\right] - \frac{1}{2}\left\{\left\langle \Gamma_h \right\rangle, \delta n_h\right\} + n_{\rm eq} \sum_a \left\langle \tilde{\Gamma}_{h,a} \right\rangle^{(1)} \frac{\mu_a + \mu_\phi}{T} \ , \tag{7.29}$$

$$\frac{\mathrm{d}\Delta_a}{\mathrm{d}t} = \mathrm{Tr}\left[\langle \Gamma_{h,a} \rangle^{(1)}\right] \frac{\mu_a + \mu_\phi}{T} - \sum_{I,J,h} \left\langle \tilde{\Gamma}_{h,a} \right\rangle_{JI} (\delta n_h)_{IJ} \ . \tag{7.30}$$

$\Gamma_{h,a}$ is the contribution of the decay matrix Γ_h to the flavor a, meaning we replace $\left(YY^\dagger\right)$ by $\left(Y_{\cdot a}Y_{\cdot a}^\dagger\right)_{IJ}$ in equation (7.19).

7.3 Different ARS-like regimes

Now that our equations are set, we can describe concretely the differences between each of the three scenarios we want to consider. The main difference will have to do with the Hamiltonian H_0, responsible for the vacuum flavor oscillations of our sterile neutrinos. In scenario (I) (standard ARS), the Hamiltonian is simply given by the energy of the particles, of constant mass matrix M,

$$H_{0,IJ}^{(\mathrm{I})} \equiv \sqrt{|\mathbf{k}|^2 + M_I^2}\delta_{IJ} \simeq |\mathbf{k}|\delta_{IJ} + \frac{M_I^2}{2|\mathbf{k}|}\delta_{IJ} \ . \tag{7.31}$$

The first term is proportional to identity in flavor space, so its commutator will always vanish. Abusing of our notations, we will identify the Hamiltonian to the part that depends on flavor

$$H_{0,IJ}^{(\mathrm{I})} \to H_{0,IJ}^{(\mathrm{I})} = \frac{M_I^2}{2|\mathbf{k}|}\delta_{IJ} \ . \tag{7.32}$$

The momentum average of this quantity can be calculated

$$\left\langle H_{0,IJ}^{(\mathrm{I})} \right\rangle = \frac{\pi^2}{36\zeta(3)}\frac{M_I^2}{T}\delta_{IJ} \ . \tag{7.33}$$

In the last line, we used the fact that in the UR limit, $\left\langle \frac{1}{|\mathbf{k}|} \right\rangle = \frac{\pi^2}{18\zeta(3)}\frac{1}{T}$ (see for example [8]). The averaged Hamiltonian therefore goes like $1/T$ in scenario (I).

The situation is different in scenarios with a FOPT, because the mass matrix M_N is vanishing before the phase transition. One should use a time-dependent mass,

$$M_I = M_{I0}\frac{1+\tanh(\gamma\Delta t)}{2} \ , \ \Delta t \equiv t - t_{\mathrm{nucl}} = t - \frac{a_R}{2T_n^2} \ . \tag{7.34}$$

We studied the impact of such a profile *during* the phase transition in chapter 4, with a creation of particles. Here, we will be interested in a cosmological evolution, so over longer periods of time. We took $\gamma = T_n$, as argued in section 3.5.1. This means that over time scales $\Delta t \sim H^{-1}(T_n) = \frac{a_R}{T_n^2} \gg T_n^{-1}$, the mass profile can be well approximated by a step function at time t_{nucl} (or temperature T_n),

$$M_I \simeq \theta(t - t_{\mathrm{nucl}})M_{I0} = \theta(T - T_n)M_{I0} \ . \tag{7.35}$$

The vacuum Hamiltonian is then simply

$$H_0^{(\mathrm{II})} = \theta(T - T_n)H_0^{(\mathrm{I})} = \theta(T - T_n)\frac{M^2}{2|\mathbf{k}|} \ , \tag{7.36}$$

$$\left\langle H_0^{(\mathrm{II})} \right\rangle = \theta(T - T_n)\frac{\pi^2}{36\zeta(3)}\frac{M^2}{T} \ . \tag{7.37}$$

As we mentioned in the introduction of this chapter, this change can make a qualitative difference, because oscillations can get frustrated and will happen differently than in the standard

case.

Sterile neutrinos were considered masssless before the FOPT, in this scenario (II). They could however have a *thermal* mass, from their interaction with the scalar field, as we briefly described in section 3.5.3. This is only possible if the scalar field S is present and has thermalized with the SM plasma. If that's the case, they contribute to an additional term for the squared mass

$$M_I^2 \to M_I^2 + \frac{\lambda_I^2}{12} T^2 \ , \tag{7.38}$$

where λ_I is the coupling of the sterile neutrino to the scalar field S. In particular, we have $M_{I0} \equiv \lambda_I v_S$. The Hamiltonian H_0 is consequently given by two terms, one from the vacuum mass and one from the thermal mass,

$$H_0^{(\mathrm{III})} = \frac{\lambda_I^2}{2|\mathbf{k}|} \frac{T^2}{12} + \theta(T - T_n) \frac{M^2}{2|\mathbf{k}|} \ , \tag{7.39}$$

$$\left\langle H_0^{(\mathrm{III})} \right\rangle = \frac{\pi^2}{36\zeta(3)} \left[\frac{\lambda_I^2}{12} T + \theta(T - T_n) \frac{M^2}{T} \right] \ . \tag{7.40}$$

Note the interesting temperature-dependence. First, before the FOPT, the vacuum Hamiltonian goes like T, then after the FOPT it goes like $aT + b/T$.

Another complementary difference between standard ARS and ARS with a FOPT is the creation of particles from the phase transition. The initial condition can no longer be vacuum, but a non-zero population of sterile neutrinos. The effect on our analytical study is the inclusion of the factor κ. According to the procedure of section 4, one can compute κ from the parameters T_n and M_I. It should be present in both scenario (II) and III.

We summarize the three scenarios considered in this work by giving their characteristic vacuum Hamiltonian and the typical temperature at which oscillation occur. We anticipate the discussions in section 7.7 about scenario (III) and give directly its oscillation temperature, which will be explained later. We will present the three scenarios and compare their conclusions.

Scenario	Temperature of oscillation	Vacuum Hamiltonian
(I)	$T_{\mathrm{osc}}^{\mathrm{ARS}} \equiv \left(a_R \left(M_2^2 - M_1^2\right)\right)^{1/3}$	$H_0^{(\mathrm{I})} = c \ \frac{M^2}{T}$
(II)	T_n	$H_0^{(\mathrm{II})} = c \ \theta(T_n - T) \frac{M^2}{T}$
(III)	$T_{\mathrm{osc}}^{(\mathrm{III})} \equiv 12 \ a_R \left(\lambda_2^2 - \lambda_1^2\right)^{-1}$	$H_0^{(\mathrm{III})} = c \left[\lambda^2 T/12 + \theta(T_n - T) \frac{M^2}{T}\right]$

Table 7.1: Summary of the different ARS-like scenarios. We pose $c \equiv \frac{\pi^2}{36\zeta(3)}$.

7.4 Scenario (I): standard ARS leptogenesis

In standard scenarios, without a phase transition, the sterile neutrinos evolve and oscillate due to their vacuum mass since the first instants of the Universe, at large temperatures $T \to +\infty$ corresponding to $z = T_{\rm ref}/T \to 0$. It is then more convenient to work with the variable z instead of time t as the variable. Sterile neutrinos are assumed to be absent of the plasma initially,

$$\delta n_h(z=0) = -n_{\rm eq}\delta_{IJ} \ , \tag{7.41}$$

with $n_{\rm eq} = (3\zeta(3))/(4\pi^2)$ the rescaled number density for one helicity of relativistic sterile neutrinos. The equation for the density matrix (7.29), written in terms of the variable z thanks to the relation (2.43), give

$$\begin{aligned}\frac{\mathrm{d}}{\mathrm{d}z}\delta n_h =& -i\frac{a_R}{2T_{\rm ref}}\left[\left\langle \frac{\pi^2}{18\zeta(3)}\frac{M^2}{T_{\rm ref}}z^2 + \langle h_+\rangle \left(YY^\dagger\right)_h + \langle h_-\rangle \left(Y^*Y^T\right)_h \right\rangle, \delta n_h\right] \\ & - \frac{a_R}{2T_{\rm ref}}\left\{\left\langle \langle\gamma_+\rangle \left(YY^\dagger\right)_h + \langle\gamma_-\rangle \left(Y^*Y^T\right)_h \right\rangle, \delta n_h\right\} \\ & + h\ n_{\rm eq}\frac{a_R}{2T_{\rm ref}}\sum_a \left(\langle\gamma_+\rangle^{(1)}\left(Y_{\cdot a}Y_{\cdot a}^\dagger\right)_h - \langle\gamma_-\rangle^{(1)}\left(Y_{\cdot a}^*Y_{\cdot a}^T\right)_h\right)\frac{\mu_a+\mu_\phi}{T} \ . \end{aligned} \tag{7.42}$$

So far, we kept all collision terms, but for our analytical approach, we will neglect the terms $\langle\gamma_-\rangle$, $\langle h_-\rangle$. Indeed, in ARS-like leptogenesis, the sterile neutrinos are relativistic, and $\langle\gamma_-\rangle$ and $\langle h_-\rangle$ are proportional to

$$\left\langle \frac{k-\tilde{k}}{\omega}\right\rangle \propto \frac{M^2}{T^2} \ . \tag{7.43}$$

They are therefore suppressed by a M^2/T^2 factor, which for $M = 1$ GeV would give a factor at least 10^{-4}. γ_- and h_- are usually interpreted as helicity-changing terms, that come from the non-zero Majorana mass of the sterile neutrinos. For small masses, they correspond to a small correction.

Under these assumptions, the equation for the lepton asymmetries Δ_a is given by

$$\frac{\mathrm{d}\Delta_a}{\mathrm{d}z} = \frac{a_R\langle\gamma_+\rangle^{(1)}}{T_{\rm ref}}\sum_{b,I}|Y_{Ia}|^2\mathcal{A}_{ab}\Delta_b - \frac{a_R}{T_{\rm ref}}S_a \ , \tag{7.44}$$

$$S_a \equiv \frac{\langle\gamma_+\rangle}{2}\sum_{I\leq J}\left(\mathrm{Re}\left[Y_{Ia}Y_{Ja}^*\right]\mathrm{Re}\left[\delta n_+ - \delta n_-\right]_{IJ} + \mathrm{Im}\left[Y_{Ia}Y_{Ja}^*\right]\mathrm{Re}\left[\delta n_+ + \delta n_-\right]_{IJ}\right) \tag{7.45}$$

There are two extreme regimes where ARS leptogenesis can be approached analytically. The two regimes can be understood from the comparison of two scales in the problem. On one hand, there is the time at which the sterile neutrinos reach equilibrium, $z_{\rm eq}^I$. It is related to the strength of the Yukawa couplings, that tend to bring the sterile neutrinos to equilibrium.

It corresponds to the temperature $T_{\rm eq}^I$ at which the decay rate Γ_I of the sterile neutrino is of similar magnitude as the Hubble function. We obtain

$$z_{\rm eq}^I = \frac{T_{\rm ref}}{T_{\rm eq}^I} = \frac{T_{\rm ref}}{a_R} \frac{1}{\langle \gamma_+ \rangle \left(YY^\dagger\right)_{II}} \ . \tag{7.46}$$

On the other hand, sterile neutrinos undergo oscillations due to their vacuum masses. The typical time over which the oscillations develop is given by the vacuum Hamiltonian and depends on the mass gap between the two flavors of sterile neutrinos. We give

$$z_{\rm osc}^{\rm ARS} = \left[\frac{T_{\rm ref}^3}{a_R \left(M_2^2 - M_1^2\right)} \right]^{1/3} \ . \tag{7.47}$$

There is a competition between both scales. The sterile neutrinos are trying to reach equilibrium, and doing so they experience oscillations. A race engages, where if the equilibration is faster, $z_{\rm eq}^I \ll z_{\rm osc}^{\rm ARS}$, then only a few oscillations can occur. This regime is dubbed the **over-damped** regime. If oscillations are faster, $z_{\rm osc}^{\rm ARS} \ll z_{\rm eq}^I$, they have time to occur many times, and can average out the off-diagonal part of the sterile neutrino density matrix before equilibrium is approached. This is simply called the **oscillation** regime.

Comparing both scales directly,

$$\begin{aligned} \frac{z_{\rm osc}^{\rm ARS}}{z_{\rm eq}^I} = \langle \gamma_+ \rangle \left(YY^\dagger\right)_{II} \left[\frac{a_R^2}{M_2^2 - M_1^2} \right]^{1/3} &\sim \langle \gamma_+ \rangle \frac{M m_\nu}{v^2} \left[\frac{a_R^2}{M_2^2 - M_1^2} \right]^{1/3} \\ &\simeq 5 \times 10^{-4} \left(\frac{M}{1 \text{ GeV}} \right)^{2/3} \left(\frac{\Delta M/M}{10^{-6}} \right)^{-1/3} \ , \end{aligned} \tag{7.48}$$

where we used the Casas-Ibarra parametrization with order 1 coefficients for the R matrix. We took $m_\nu = 0.05$ eV and $\langle \gamma_+ \rangle = 0.012$ [185, 186]. We then see that in general, the oscillations happen long before the equilibration. One way to obtain the overdamped regime is by using the R matrix to make at least one sterile neutrino flavor more coupled than the standard estimate. We will only be interested here in the oscillation regime $z_{\rm osc}^{\rm ARS} \ll z_{\rm eq}^I$, but refer the reader to [137, 138, 189, 191] for details on the over-damped regime.

7.4.1 Analytical expansion in Yukawa couplings

One way to approach the solution to the equations above analytically is by an expansion in the Yukawa couplings. In the relativistic regime, the sterile neutrino masses are low and the Yukawa couplings are typically small. Using again an estimate where the R matrix coefficients are order one and $m_\nu = 0.05$ eV for the active neutrino mass scale, we have

$$YY^\dagger \sim \frac{M m_\nu}{v^2} \simeq 8 \times 10^{-16} \left(\frac{M}{1 \text{ GeV}} \right) \ . \tag{7.49}$$

We will therefore consider in this section (and in the analytical approaches in the other scenarios) an expansion in powers of the Yukawa couplings. This approach is found in many studies [138, 189–192]. Our approach in this section follows closely [138]. We note

$$\delta n_h = \delta n_h^{(0)} + \delta n_h^{(1)} + \delta n_h^{(2)} + ... \tag{7.50}$$

where $\delta n_h^{(n)}$ is of order $\left(YY^\dagger\right)^n$. We do the same for the lepton asymmetry Δ_a,

$$\Delta_a = \Delta_a^{(0)} + \Delta_a^{(1)} + \Delta_a^{(2)} + ... \tag{7.51}$$

7.4.2 Zeroth and first orders

Initially, the sterile neutrinos are out-of-equilibrium, and no mixing exists between the sterile flavors, $\delta n_h^{(0)}$ is only diagonal. For $M_I \ll T$, the initial conditions are the same for both flavors and $n_{\mathrm{eq},1} \approx n_{\mathrm{eq},2} = n_{\mathrm{eq}}$. It is convenient to consider the equation for $\delta n_{h,11} + \delta n_{h,22}$; keeping the lowest order in the Yukawa couplings (except for homogeneous terms), we obtain

$$\frac{\mathrm{d}\left(\delta n_{h,11}^{(0)} + \delta n_{h,22}^{(0)}\right)}{\mathrm{d}z} \simeq -\frac{a_R}{T_{\mathrm{ref}}} \langle\gamma_+\rangle \left[\frac{\left(YY^\dagger\right)_{11} + \left(YY^\dagger\right)_{22}}{2}\right] \left(\delta n_{h,11}^{(0)} + \delta n_{h,22}^{(0)}\right) . \tag{7.52}$$

The solution to this equation is simply a decaying exponential,

$$\left(\delta n_{h,11}^{(0)} + \delta n_{h,22}^{(0)}\right)(z) = -2n_{\mathrm{eq}}\, e^{-\frac{a_R}{T_{\mathrm{ref}}}\langle\gamma_+\rangle\left[\frac{\left(YY^\dagger\right)_{11}+\left(YY^\dagger\right)_{22}}{2}\right]z} \equiv -2n_{\mathrm{eq}}\, e^{-\frac{a_R}{T_{\mathrm{ref}}}\gamma_0 z} . \tag{7.53}$$

The zeroth order describes how the initial deviation from equilibrium evolves, getting closer to equilibrium at a rate $\gamma_0 \equiv \langle\gamma_+\rangle \frac{\left(YY^\dagger\right)_{11}+\left(YY^\dagger\right)_{22}}{2}$. At zeroth-order, the off-diagonal term $\delta n_{h,12}^{(2)}$ remains zero.

The off-diagonal term only starts being interesting at first-order in $YY^\dagger$. Its equations is

$$\begin{aligned}
\frac{\mathrm{d}\delta n_{h,12}^{(1)}}{\mathrm{d}z} &= -i\frac{a_R}{T_{\mathrm{ref}}^3}\frac{\pi^2}{36\zeta(3)}\left(M_1^2 - M_2^2\right) z^2 \delta n_{h,12}^{(1)} - \frac{a_R}{2T_{\mathrm{ref}}}\langle\gamma_+\rangle\left\{\left(YY^\dagger\right), \delta n_h\right\}_{12} \\
&\approx -i\frac{a_R}{T_{\mathrm{ref}}}\frac{\pi^2}{36\zeta(3)}\left(M_1^2 - M_2^2\right) z^2 \delta n_{h,12}^{(1)} - \frac{a_R}{T_{\mathrm{ref}}}\gamma_0 \delta n_{h,12}^{(1)} \\
&\quad - \frac{a_R}{T_{\mathrm{ref}}}\langle\gamma_+\rangle\left(YY^\dagger\right)_{h,12}\left[\frac{\delta n_{h,11}^{(0)}(t) + \delta n_{h,22}^{(0)}(z)}{2}\right] .
\end{aligned} \tag{7.54}$$

It contains an oscillation part given by the vacuum masses M_I and proportional to z^2, in addition to a damping term $\propto \gamma_0$. It also receives contribution from the zeroth order, that acts as a source. The solution to the equation is

$$\delta n_{h,12}^{(1)} = \frac{a_R\langle\gamma_+\rangle}{T_{\mathrm{ref}}}\left(YY^\dagger\right)_{h,12} e^{-\frac{a_R}{T_{\mathrm{ref}}}\gamma_0 z} e^{-i\frac{a_R}{T_{\mathrm{ref}}}\frac{\pi^2}{108\pi^2}\left(M_1^2-M_2^2\right)z^3} \int_0^z \mathrm{d}z'\; n_{\mathrm{eq}} e^{+i\frac{a_R}{T_{\mathrm{ref}}}\frac{\pi^2}{108\zeta(3)}\left(M_1^2-M_2^2\right)z'^3} . \tag{7.55}$$

As long as we are far from equilibration, $\frac{a_R}{T_{\rm ref}}\gamma_0 z \ll 1$ and the damping is reasonably neglected. This allows us to obtain a compact solution

$$\begin{aligned}\delta n^{(1)}_{h,12} &\simeq n_{\rm eq}\frac{a_R\langle\gamma_+\rangle}{T_{\rm ref}}\left(YY^\dagger\right)_{h,12} e^{-ibz^3}\int_0^z \mathrm{d}z'\; e^{+ibz'^3} \\ &= n_{\rm eq}\frac{a_R\langle\gamma_+\rangle}{T_{\rm ref}}\left(YY^\dagger\right)_{h,12}\left[C-\frac{z}{3}E_{2/3}(-ibz^3)\right]e^{-ibz^3}\;, \end{aligned} \tag{7.56}$$

where

$$E_n(x)\equiv\int_1^{+\infty}\mathrm{d}t\;\frac{e^{-xt}}{t^n} \tag{7.57}$$

is the exponential integral function. We also defined some constants

$$b\equiv\frac{a_R}{T_{\rm ref}}\frac{\pi^2}{108\zeta(3)}\left(M_1^2-M_2^2\right)\;, \tag{7.58}$$

$$C=\lim_{z\to0}\frac{z}{3}E_{2/3}(-ibz^3)=\frac{\Gamma(1/3)}{3b^{1/3}}\;, \tag{7.59}$$

with Γ the gamma function. At first-order, the lepton asymmetries Δ_a remain zero. It could in principle be sourced by the zeroth-order, but $\delta n^{(0)}_h$ is helicity symmetric and no asymmetry is produced. $\delta n^{(1)}_h$, however, has an helicity dependence,

$$\mathrm{Re}\left[\delta n^{(1)}_{+,12}-\delta n^{(1)}_{-,12}\right]=-2n_{\rm eq}\frac{a_R\langle\gamma_+\rangle}{T_{\rm ref}}\mathrm{Im}\left[\left(YY^\dagger\right)_{12}\right]\mathrm{Im}\left(\left[C-\frac{z}{3}E_{2/3}(-ibz^3)\right]e^{-ibz^3}\right)\;, \tag{7.60}$$

$$\mathrm{Im}\left[\delta n^{(1)}_{+,12}+\delta n^{(1)}_{-,12}\right]=+2n_{\rm eq}\frac{a_R\langle\gamma_+\rangle}{T_{\rm ref}}\mathrm{Re}\left[\left(YY^\dagger\right)_{12}\right]\mathrm{Im}\left(\left[C-\frac{z}{3}E_{2/3}(-ibz^3)\right]e^{-ibz^3}\right)\;. \tag{7.61}$$

7.4.3 Second order and lepton asymmetry

It is then only at second order that the lepton asymmetry starts being interesting. Plugging $\delta n^{(1)}_h$ in the equation (7.44) for Δ_a, we get

$$\begin{aligned}\frac{\mathrm{d}\Delta^{(2)}_a}{\mathrm{d}z} = -2n_{\rm eq}\left(\frac{a_R\langle\gamma_+\rangle}{T_{\rm ref}}\right)^2 &\left(-\mathrm{Re}\left[Y_{1a}Y^*_{2a}\right]\mathrm{Im}\left[\left(YY^\dagger\right)_{12}\right]+\mathrm{Im}\left[Y_{1a}Y^*_{2a}\right]\mathrm{Re}\left[\left(YY^\dagger\right)_{12}\right]\right) \\ &\times\mathrm{Im}\left(\left[C-\frac{z}{3}E_{2/3}(-ibz^3)\right]e^{-ibz^3}\right)\;. \end{aligned} \tag{7.62}$$

The asymmetry is simply found by integrating the source over z. An analytical expression [138] exists for this integral of $E_{2/3}$, given in terms of a hypergeometric function,

$$\int_0^z\mathrm{d}z'\;\mathrm{Im}\left(\left[C-\frac{z'}{3}E_{2/3}(-ibz'^3)\right]e^{-ibz'^3}\right)=-\frac{z^2}{2}\mathrm{Im}\,{}_2F_2\left(\left\{\frac{2}{3},1\right\},\left\{\frac{4}{3},\frac{5}{3}\right\},-i|b|z^3\right)\;. \tag{7.63}$$

It is instructive to consider the limit of $\Delta_a^{(2)}$ at late times, *i.e.* for $z \to 1$, divided by the entropy s

$$\left(\frac{\Delta_{a,\infty}^{(2)}}{s}\right)_{\text{(I)}} = 2n_{\text{eq}}\frac{45}{2\pi^2 g_*}\left(\frac{a_R\langle\gamma_+\rangle}{T_{\text{ref}}}\right)^2\frac{\pi^{1/2}\Gamma(1/6)}{2^{2/3}9|b|^{2/3}}\text{Im}\left[Y_{1a}^* Y_{2a}\left(YY^\dagger\right)_{12}\right]$$
$$= 5n_{\text{eq}}\frac{108^{2/3}\zeta(3)^{2/3}\Gamma(1/6)}{2^{2/3}\pi^{17/6}g_*}\langle\gamma_+\rangle^2\,\text{Im}\left[Y_{1a}^* Y_{2a}\left(YY^\dagger\right)_{12}\right]\left(\frac{a_R^2}{M_2^2-M_1^2}\right)^{2/3}. \quad (7.64)$$

This result should be compared to the flavored asymmetries derived in [190] (Eq. (4.77)) or in [141] (Eq. (28)). We have obtained a finite asymmetry, at second order in the Yukawa couplings.

The estimated lepton asymmetry in flavor a is proportional to a CP-violating imaginary part $\text{Im}\left[Y_{1a}^* Y_{2a}\left(YY^\dagger\right)_{12}\right]$, coming from the Yukawa couplings. One can note that it is only flavored; indeed $\sum_a \Delta_a^{(2)} = 0$. The asymmetry depends on the mass degeneracy $M_2 - M_1$ and is enhanced for degenerate sterile neutrinos. This is due to the oscillations, which would have a higher frequency for a smaller mass gap.

The factor $\langle\gamma_+\rangle$ coming from collisions is computed from the self-energy. Numerical estimates [186] give $\langle\gamma_+\rangle \simeq 0.012$. Computing the pre-factor's numerical value in the lepton asymmetry, we keep only the dependence on the parameters

$$\left(\frac{\Delta_{a,\infty}^{(2)}}{s}\right)_{\text{(I)}} \simeq 2.4\times10^{-5}\; n_{\text{eq}}\text{Im}\left[Y_{1a}^* Y_{2a}\left(YY^\dagger\right)_{12}\right]\left(\frac{a_R^2}{M_2^2-M_1^2}\right)^{2/3}. \quad (7.65)$$

The flavored asymmetry was produced after flavor oscillations in the sterile sector induced an helicity asymmetry. The Hamiltonian $H_0 \propto z^2$ led to oscillations $\delta n_{h,12} \propto \exp(-ibz^3)$ and ultimately to a dependence of the flavored asymmetry $\Delta_a^{(2)} \propto \left(\frac{a_R^2}{M_2^2-M_1^2}\right)^{2/3}$. In the scenarios (II) and (III), the dependence in z (or time) of the Hamiltonian is different and leads to qualitatively different results.

7.5 Scenario (II): a numerical study

Scenario (II) is one of the main object of this thesis. Contrarily to ARS leptogenesis that has been extensively studied, this case has been less explored. In this scenario, a phase transition happens at a certain temperature T_n and gives their vacuum masses to the sterile neutrinos. We solve numerically the equation for δn_h coupled to the lepton asymmetry Δ_a. We first present some of the underlying assumptions specific to our numerical approach, before detailing the results of the parameter scan.

7.5.1 Numerical assumptions

In the ARS-like case, we try to realize leptogenesis by oscillations of low-scale sterile neutrinos as they are being produced. In scenarios with a phase transition, however, the oscillations will only occur after the sterile neutrinos obtain their vacuum masses at the FOPT. We therefore start our numerical analysis at a time $t_{\rm in}$ close to the time $t_{\rm nucl}$ of the phase transition. Before that time, for higher temperatures $T > T_n$, no asymmetry is produced, and only production of the sterile neutrinos is relevant. Using the analytical estimate from the previous section for the zeroth order of the sterile neutrino density (7.53), we assume an initial distribution, for sterile neutrinos,

$$\text{[ARS-like]}\ \ \delta n_{h,IJ}(t = t_{\rm in}) = -n_{\rm eq}\ e^{-\frac{a_R}{T_{\rm ref}}\gamma_0 z_n}\delta_{IJ} = -n_{\rm eq}\ e^{-\frac{a_R}{T_n}\gamma_0}\delta_{IJ}\ , \tag{7.66}$$

$$\text{[ARS-like]}\ \ \Delta_a(t = t_{\rm in}) = 0\ , \tag{7.67}$$

where $z_n \equiv T_{\rm ref}/T_n$ and $T_n\,(t_{\rm in} - t_{\rm nucl}) = -15$. The sterile neutrinos, before the FOPT *i.e.* until we reach the temperature T_n, only approach equilibrium and no asymmetry is produced yet. We assumed that sterile neutrinos are only produced in the diagonal population $\delta n_{h,11} = \delta n_{h,22}$, neglecting flavor effects that would be of higher order in the Yukawa couplings.

Moreover, numerically, the mass of the sterile neutrinos will be constant shortly after the FOPT, like we assumed in the Mass Gain mechanism, for $T_n\,(t - t_{\rm nucl}) > 15$.

Finally, recalling our discussion in section 7.1, the domain we want to explore is the non-standard scenario in which oscillations happen before the Universe expands significantly, with $t_{\rm osc} \ll t_n \equiv H^{-1}(T_n)$. We will assume this is reasonable as long as

$$\text{[ARS-like]}\ \ t_{\rm osc} < 10^{-2} \times t_n\ . \tag{7.68}$$

Oscillations therefore happen within a single Hubble time. Because it is numerically expensive to keep track of the oscillatory parts, we manually turn them off after a Hubble time; but when the above condition is satisfied, a significant number of oscillations already occurred by then, and their contribution to the asymmetry averages out. We have checked the final asymmetry is not sensitive to the particular choice of this cut-off time, for the region of parameter space explored.

7.5.2 ARS-like results

We recall our parameters of interest are, like in the Mass Gain scenario, the temperature of the phase transition T_n, the sterile neutrino mass scale M, the mass degeneracy ΔM and the (imaginary part of the) complex angle z_i in the R matrix (see Figure 6.1). In all plots in terms of the parameters, we exclude the regions where the condition (7.68) is not satisfied.

The ARS-like scenario typically requires a certain level of mass degeneracy. The masses are

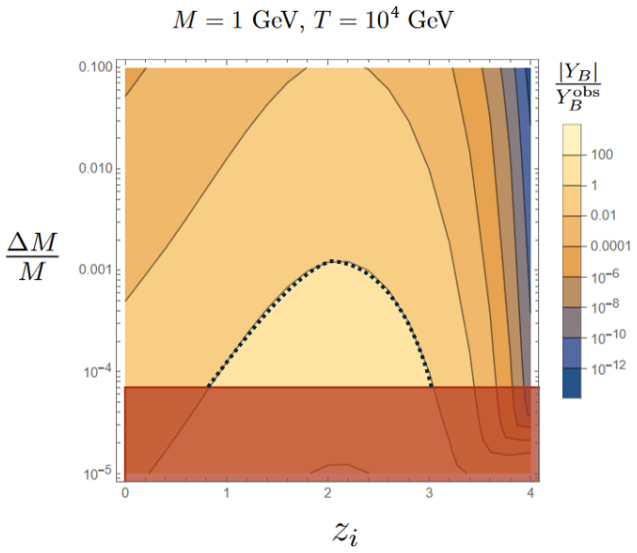

Figure 7.2: Baryon asymmetry in the ARS-like scenario as a function of z_i and $\Delta M/M$, at fixed $M = 1$ GeV and $T = 10^4$ GeV. The dotted-black contour shows the region of successful leptogenesis within the validity domain of our assumptions. The dark-red area corresponds to the region $t_{\rm osc} \geq 10^{-2} t_n$.

much smaller, around the GeV scale and Yukawa couplings are therefore small too. They can be increased by a large value of the imaginary part of the angle z_i. This increases both the CP-asymmetries from the Yukawa couplings and the washout. There is therefore an interplay between a higher asymmetry created and a low-enough washout such that the asymmetry survives until the electroweak scale and the sphaleron decoupling at $T_{\rm sph}$. This can be seen explicitly in the $(z_i, \Delta M/M)$ plot in Figure 7.2; at fixed $M = 1$ GeV and $T_n = 10^4$ GeV, a degeneracy of at least $\Delta M/M \approx 10^{-3}$ is needed, and at this value the (imaginary part of the) angle should be around 2, not too small but not too large either. At fixed nucleation temperature, we do not want the asymmetry to be erased between the time of the FOPT and the decoupling of sphalerons. If the imaginary part z_i is large, even a large asymmetry that would have been created is washed out. This is particularly visible in the upper-right corner of Figure 7.2, where the angle is large and the masses not degenerate enough to compensate.

In the following, we stick to this value of $z_i = 2$. For $\Delta M/M = 10^{-6}$, we had successful leptogenesis with sterile neutrinos of mass $M = 1$ GeV. We investigated masses around the GeV-scale in Figure 7.3a with the baryon asymmetry plotted as function of mass and temperature of the FOPT. Greater masses give larger Yukawa couplings, at fixed $z_i = 2$, and therefore a larger asymmetry. However, if the couplings become too important and the starting temperature is too close to sphaleron decoupling, the washout suppresses the asymmetry before it reaches the electroweak scale, so the masses should not be too large either. The values compatible with leptogenesis are around the .5 to almost 10 GeV, for temperatures T_n up to 10 TeV.

Trying to reduce the mass degeneracy, we looked at $(T_n, \Delta M/M)$ plot of Figure 7.3b. We

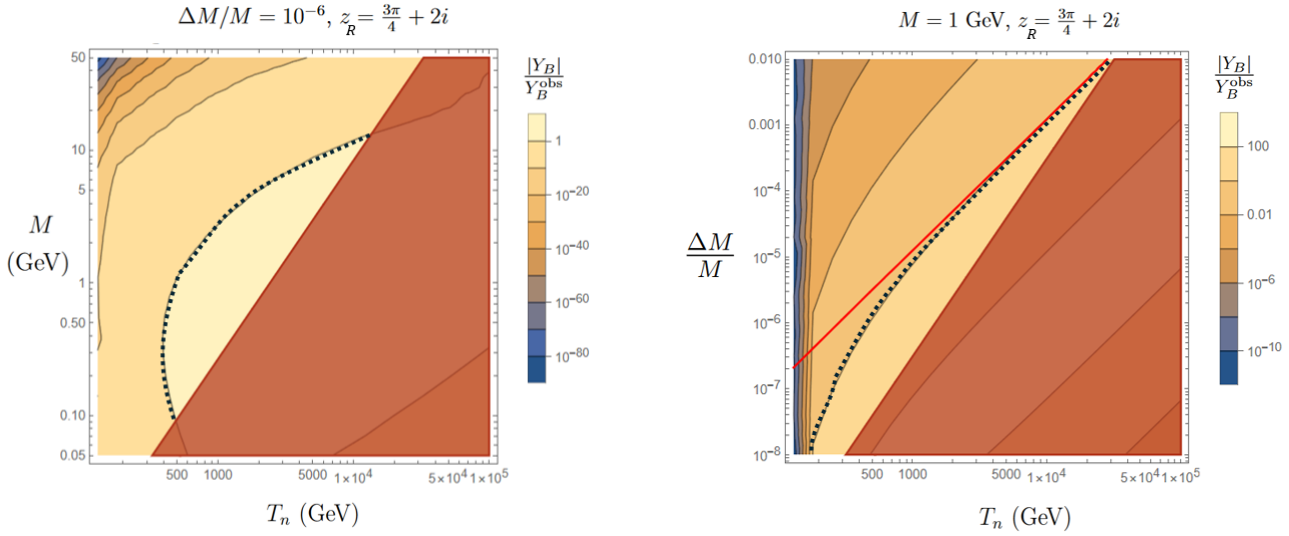

(a) Normalized baryon asymmetry as a function of T_n and M.

(b) Normalized baryon asymmetry as a function of T_n and $\Delta M/M$. The red line is purely indicative, and has a slope of 2.

Figure 7.3: Numerical results in the ARS-like scenario. The dotted-black contour shows the region of successful leptogenesis within the validity domain of our assumptions. The dark-red area corresponds to $t_{\rm osc} \geq 10^{-2} t_n$. The temperatures are plotted from $T_{\rm sph}$ to 10^5 GeV.

find that larger values of T_n up to 10 TeV can accommodate successful baryogenesis with larger values of $\Delta M/M$. The figure tells us that lower temperature are less favorable, as they leave less time before the electroweak temperature and sphaleron decoupling. Higher temperature can be favorable, but we cannot conclude in the shaded region, where our assumption [ARS-like] (7.68) (that oscillations happen during one Hubble time) is no longer satisfied.

In Figure 7.3b, we find that, for large values of T_n, the isocurves have a slope 2 in log-log scale, corresponding to a $\frac{T_n^2}{\Delta M/M}$ dependency. At fixed $M = 1$ GeV, consistently with the analytical estimate (7.81) of the next section, this is equivalent to having the baryon asymmetry proportional to

$$Y_B \propto \frac{T_n^2}{M_2^2 - M_1^2} = \frac{T_n^2}{2M^2 \Delta M/M} \ . \tag{7.69}$$

This dependency however does not hold anymore once T_n is too close to $T_{\rm sph}$, *i.e.* when there is less time before the electroweak phase transition to produce the asymmetry. We explain how we obtain the above dependency by analytical estimates of the asymmetry in this scenario (II).

7.6 Scenario (II): analytical estimates

We will adopt the same procedure as in section 7.4: the solutions to the equations are expanded in powers of $YY^\dagger$, and we only keep the helicity-preserving factor γ_+ in the collision terms.

In scenario (II), the interesting dynamics happens shortly after the FOPT. This corresponds to small values of $\Delta t \equiv t - t_{\rm nucl}$ compared to the Hubble time t_n. Recalling the time dependence (2.25) of temperature

$$T(t) = \left(\frac{a_R}{2}\right)^{1/2} t^{1/2} = \left(\frac{a_R}{2}\right)^{1/2} (t_{\rm nucl} + \Delta t)^{1/2} = \left(\frac{a_R}{2}\right)^{1/2} (t_n/2 + \Delta t)^{1/2} \ , \tag{7.70}$$

temperature may be considered constant, $T(t) \simeq T_n$ as long as $\Delta t \ll t_n$. In our numerical analysis, we kept the time dependence of temperature exact, but for our analytical study, we will simply assume the temperature is constant during sterile neutrino oscillations.

Initially, the population of sterile neutrinos is assumed to have only been produced diagonally

$$\delta n_{h,IJ}(t = t_{\rm in}) = -n_{\rm eq}\, e^{-\frac{a_R}{T_n}\gamma_0} \delta_{IJ} \ . \tag{7.71}$$

Including the effect of the FOPT, we know from Chapter 4 that an extra amount of sterile neutrinos is produced, reducing the deviation to equilibrium. Calculating the production by the procedure detailed in Chapter 4, for $f_0(|\mathbf{k}|) = f_{FD}(|\mathbf{k}|)\left(1 - e^{-\frac{a_R}{T_n}\gamma_0}\right)$, integrating over momentum, we obtain a total sterile neutrino density $n_{\rm PT}$ once the phase transition is completed, from which we define the deviation from equilibrium

$$\delta n_{h,IJ}(\Delta t \approx 0) = (n_{\rm PT} - n_{\rm eq})\, \delta_{IJ} \equiv -\kappa\ n_{\rm eq}\ \delta_{IJ} \ . \tag{7.72}$$

Note that it is helicity symmetric. The factor $\kappa < 1$ signals how the particle production before and at the FOPT reduced the deviation from equilibrium usually assumed initially in ARS leptogenesis.

Taking the above initial condition, we can proceed to the expansion in powers of Yukawa couplings. If we neglect the lepton asymmetry and the off-diagonal term, the lowest order equation for the total number of sterile neutrinos gives, similarly to the ARS case (Scenario (I)),

$$\frac{{\rm d}\left(\delta n^{(0)}_{h,11} + \delta n^{(0)}_{h,22}\right)}{{\rm d}t} \simeq -\left\langle \gamma_+ \right\rangle T_n \left[\frac{\left(YY^\dagger\right)_{11} + \left(YY^\dagger\right)_{22}}{2}\right] \left(\delta n^{(0)}_{h,11} + \delta n^{(0)}_{h,22}\right) \ . \tag{7.73}$$

Recall that we assume the temperature is constant during the time of oscillations, $T = T_n$. The solution to this equation is

$$\left(\delta n^{(0)}_{h,11} + \delta n^{(0)}_{h,22}\right)(t) = -2\kappa\ n_{\rm eq}\ e^{-\langle\gamma_+\rangle T_n \left[\frac{\left(YY^\dagger\right)_{11} + \left(YY^\dagger\right)_{22}}{2}\right] t} \equiv 2\kappa\ n_{\rm eq}\ e^{-\gamma_0 T_n t} \ . \tag{7.74}$$

Note that it is a decaying exponential as a function of t, and not z as in scenario (I). At first, the off-diagonal term in the sterile neutrino density matrix is zero. The equation for this off-diagonal term $\delta n_{h,12}$ is, at first-order in $YY^\dagger$,

$$\begin{aligned}\frac{\mathrm{d}\delta n^{(1)}_{h,12}}{\mathrm{d}t} &= -i\frac{\pi^2}{36\zeta(3)}\left(\frac{M_1^2-M_2^2}{T_n}\right)\delta n^{(1)}_{h,12} - \frac{1}{2}\left\{\langle\Gamma_h\rangle, \delta n_h\right\}_{12} \\ &\approx -i\frac{\pi^2}{36\zeta(3)}\left(\frac{M_1^2-M_2^2}{T_n}\right)\delta n^{(1)}_{h,12} - \gamma_0 T_n \delta n^{(1)}_{h,12} - \langle\gamma_+\rangle\left(YY^\dagger\right)_{h,12}\left[\frac{\delta n^{(0)}_{h,11}(t)+\delta n^{(0)}_{h,22}(t)}{2}\right] .\end{aligned} \tag{7.75}$$

The solution to the equation is

$$\begin{aligned}\delta n^{(1)}_{h,12} &= e^{-\gamma_0 T_n t} e^{-i\frac{\pi^2}{36\zeta(3)}\left(\frac{M_1^2-M_2^2}{T_n}\right)t}\int_0^t \mathrm{d}t'\ \langle\gamma_+\rangle\left(YY^\dagger\right)_{h,12}\kappa\ n_{\mathrm{eq}}\ e^{+i\frac{\pi^2}{36\zeta(3)}\left(\frac{M_1^2-M_2^2}{T_n}\right)t'} \\ &= i\langle\gamma_+\rangle\left(YY^\dagger\right)_{h,12}\kappa\ n_{\mathrm{eq}}\ e^{-\gamma_0 T_n t}\frac{36\zeta(3)}{\pi^2}\frac{T_n}{M_2^2-M_1^2}\left(1-e^{-i\frac{\pi^2}{36\zeta(3)}\left(\frac{M_1^2-M_2^2}{T_n}\right)t}\right) .\end{aligned} \tag{7.76}$$

Note how we easily integrated the complex exponentials: in our regime the temperature is constant for the period of interest, the time dependence is simple. We compare the expression to numerical results in Figure 7.4a and find very good agreement with the analytical estimate. The only part dependent on helicity is the $\left(YY^\dagger\right)_{h,12}$. The source of lepton asymmetry depends on two quantities,

$$\begin{aligned}\mathrm{Re}\left[\delta n^{(1)}_{+,12}-\delta n^{(1)}_{-,12}\right] &= -2\langle\gamma_+\rangle\,\mathrm{Im}\left[\left(YY^\dagger\right)_{12}\right]\frac{36\zeta(3)}{\pi^2}\frac{T_n}{M_2^2-M_1^2}\kappa\ n_{\mathrm{eq}} \\ &\quad\times\left[1-\cos\left(\frac{\pi^2}{36\zeta(3)}\left(\frac{M_1^2-M_2^2}{T_n}\right)t\right)\right]e^{-\gamma_0 T_n t} ,\end{aligned} \tag{7.77}$$

$$\begin{aligned}\mathrm{Im}\left[\delta n^{(1)}_{+,12}+\delta n^{(1)}_{-,12}\right] &= 2\langle\gamma_+\rangle\,\mathrm{Re}\left[\left(YY^\dagger\right)_{12}\right]\frac{36\zeta(3)}{\pi^2}\frac{T_n}{M_2^2-M_1^2}\kappa\ n_{\mathrm{eq}} \\ &\quad\times\left[1-\cos\left(\frac{\pi^2}{36\zeta(3)}\left(\frac{M_1^2-M_2^2}{T_n}\right)t\right)\right]e^{-\gamma_0 T_n t} .\end{aligned} \tag{7.78}$$

The asymmetry at this stage is obtained by integrating the source over time, like in section 7.4

$$\Delta^{(2)}_a = -\int_0^t \mathrm{d}t'\ \langle\gamma_+\rangle T_n\left[\mathrm{Re}\left[Y_{1a}Y^*_{2a}\right]\mathrm{Re}\left[\delta n^{(1)}_{+,12}-\delta n^{(1)}_{-,12}\right]+\mathrm{Im}\left[Y_{1a}Y^*_{2a}\right]\mathrm{Im}\left[\delta n^{(1)}_{+,12}+\delta n^{(1)}_{-,12}\right]\right] . \tag{7.79}$$

We can then use the expressions obtained for the δn's, and integrate over time. We are interested in the asymptotic limit $t\to+\infty$, such that we obtain

$$\Delta^{(2)}_{a,\infty} = \frac{36\zeta(3)}{\pi^2}\langle\gamma_+\rangle^2\kappa\ n_{\mathrm{eq}}\mathrm{Im}\left[Y^*_{1a}Y_{2a}\left(YY^\dagger\right)_{12}\right]\frac{T_n^2}{M_2^2-M_1^2}\frac{1}{\gamma_0}\frac{\left(\frac{\pi^2}{36\zeta(3)}\left(\frac{M_1^2-M_2^2}{T_n}\right)\right)^2}{\gamma_0^2T_n^2+\left(\frac{\pi^2}{36\zeta(3)}\left(\frac{M_1^2-M_2^2}{T_n}\right)\right)^2} . \tag{7.80}$$

In the parameter space considered in our study, we systematically have $(M_2^2 - M_1^2)/T_n \gg \gamma_0 T_n$. As an example, for $M = 1$ GeV, $\Delta M = 10^{-6} M$, $T_n = 10^3$ GeV and $z_i = 2$, we obtain $\gamma_0 \sim 10^{-13}$ while $(M_2^2 - M_1^2)/T_n^2 \sim 10^{-9}$. This simplifies a bit the above estimate for the asymmetry, leading to

$$\left(\frac{\Delta^{(2)}_{a,\infty}}{s}\right)_{\text{(II)}} = \frac{45}{2\pi^2 g_*}\frac{36\zeta(3)}{\pi^2}\langle\gamma_+\rangle\,\kappa n_{\text{eq}}\frac{\text{Im}\left[Y^*_{1a}Y_{2a}\left(YY^\dagger\right)_{12}\right]}{\left(YY^\dagger\right)_{11}+\left(YY^\dagger\right)_{22}}\frac{T_n^2}{M_2^2-M_1^2}$$
$$\simeq 1.1\times 10^{-3}\;\kappa\; n_{\text{eq}}\frac{\text{Im}\left[Y^*_{1a}Y_{2a}\left(YY^\dagger\right)_{12}\right]}{\left(YY^\dagger\right)_{11}+\left(YY^\dagger\right)_{22}}\frac{T_n^2}{M_2^2-M_1^2}\;. \tag{7.81}$$

The parametric dependency is different from scenario (I), where we found

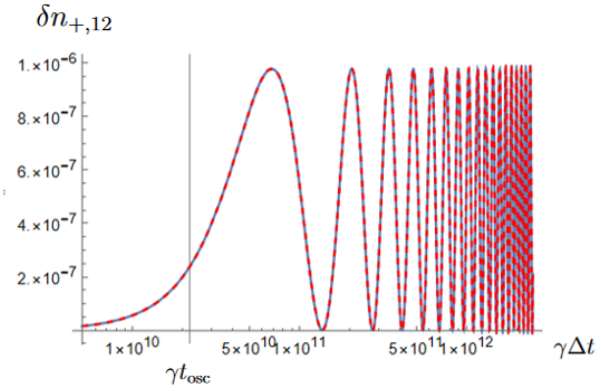

(a) Off-diagonal term of the sterile neutrino density matrix, as a function of time. In thick-blue, the numerical oscillations are compared to the dashed-red analytical estimate. They start after a typical time $\Delta t \simeq t_{\text{osc}}$, represented by a gray vertical line.

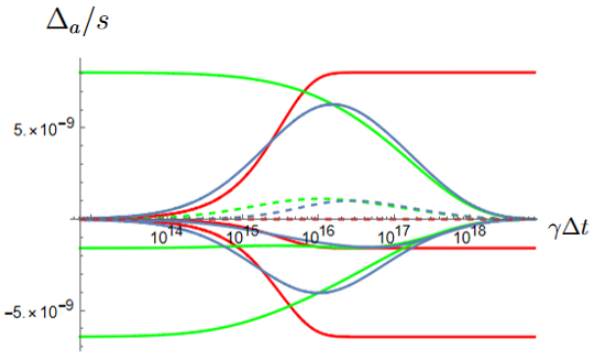

(b) Evolution of the asymmetry in the three flavors (thick line for each color) and the total asymmetry (dashed), as a function of time. The numerical result is plotted in blue, the analytical results from late washout are plotted in green, with initial conditions given by the flavored asymmetry produced by sterile neutrino oscillations, shown in red.

Figure 7.4: Comparison of numerical and analytical results in the ARS-like regime. The mass scale is taken at $M = 1$ GeV, with a mass degeneracy $\Delta M/M = 10^{-6}$, at a temperature $T_n = 10^3$ GeV. The angle of the R matrix is fixed at $\frac{3\pi}{4} + 2i$.

$$\left(\frac{\Delta^{(2)}_{a,\infty}}{s}\right)_{\text{(I)}} \propto \text{Im}\left[Y^*_{1a}Y_{2a}\left(YY^\dagger\right)_{12}\right]\left(\frac{a_R^2}{M_2^2-M_1^2}\right)^{2/3}\;. \tag{7.82}$$

In both cases, this is so far only a flavored lepton asymmetry. One can check that $\sum_a \Delta^{(2)}_a = 0$. The final total asymmetry is created after washout effects redistribute the asymmetry between the active flavors and the sterile sector. Because washout is flavor dependent, a total lepton asymmetry gets created. The flavored asymmetry calculated above can be understood as an

initial condition before these washout effects dominate. The larger they are, the more total asymmetry we expect.

This late washout effect is described by a set of equations for the asymmetries in the active sector Δ_a and the diagonal asymmetries in the sterile sector $q_I \equiv n_{+\,II} - n_{-\,II}$. Similarly to [138], neglecting the contribution of off-diagonal entries in the sterile neutrino density matrix to the asymmetry,

$$\frac{\mathrm{d}\Delta_a}{\mathrm{d}t} = \langle\gamma_+\rangle^{(1)} T(t) \sum_I |Y_{Ia}|^2 \left(\sum_b \mathcal{A}_{ab}\Delta_b - q_I \right) \ , \tag{7.83}$$

$$\frac{\mathrm{d}q_I}{\mathrm{d}t} = \langle\gamma_+\rangle^{(1)} T(t) \sum_a |Y_{Ia}|^2 \left(\sum_b \mathcal{A}_{ab}\Delta_b - q_I \right) \ . \tag{7.84}$$

The analytical approximation consists in taking the initial condition for this system as given by Equation (7.81) since $\Delta t = 0$. This approximation amounts to saying that the flavored asymmetry was instantaneously created by flavor oscillations, and was then converted into a total asymmetry by the washout. The comparison to the numerical solution is given in Figure 7.4b. At early times, when washout is negligible, the red curve corresponding to the creation of a flavored lepton asymmetry reproduces well the numerical result. However, when the effect of washout becomes important, the numerical curve is better reproduced by the green curve which is the solution to the late washout system.

7.7 Scenario (III): oscillations before the FOPT

In the case where thermal masses coming from the scalar field S are present since the beginning ($z \approx 0$), we should start our equations before the phase transition. z is, just as it was in scenario (I), the relevant variable instead of time t. Initially, the sterile neutrinos are absent,

$$\delta n_{h,IJ}(z=0) = -n_{\mathrm{eq}}\delta_{IJ} \ . \tag{7.85}$$

The Yukawa couplings produce the sterile neutrinos and drive the population towards equilibrium,

$$\frac{\mathrm{d}\left(\delta n^{(0)}_{h,11} + \delta n^{(0)}_{h,22}\right)}{\mathrm{d}z} \simeq -\frac{a_R}{T_{\mathrm{ref}}}\gamma_0 \left(\delta n^{(0)}_{h,11} + \delta n^{(0)}_{h,22}\right) \ . \tag{7.86}$$

The solution to this equation is

$$\left(\delta n^{(0)}_{h,11} + \delta n^{(0)}_{h,22}\right)(z) = -2n_{\mathrm{eq}}\, e^{-\frac{a_R}{T_{\mathrm{ref}}}\gamma_0 z} \ . \tag{7.87}$$

We directly give the expression for the off-diagonal term at first-order

$$\delta n^{(1)}_{h,12} = i\,\langle\gamma_+\rangle \left(YY^\dagger\right)_{h,12} e^{-\frac{a_R}{T_{\mathrm{ref}}}\gamma_0 z} n_{\mathrm{eq}} \frac{36\zeta(3)}{\pi^2} \frac{12}{\lambda_2^2 - \lambda_1^2} \left(1 - e^{-i\frac{a_R}{T_{\mathrm{ref}}}\frac{\pi^2}{36\zeta(3)}\frac{\lambda_1^2-\lambda_2^2}{12}z}\right) \ . \tag{7.88}$$

We observe from the argument of the complex exponential that the oscillations take place once z reaches a certain value $z_{\rm osc}^{\rm (III)}$

$$z_{\rm osc}^{\rm (III)} \equiv \frac{T_{\rm ref}}{a_R}\frac{12}{\lambda_2^2-\lambda_1^2}\ , \tag{7.89}$$

corresponding to a temperature

$$T_{\rm osc}^{\rm (III)} \equiv a_R\frac{\lambda_2^2-\lambda_1^2}{12} = \frac{a_R}{12}\frac{M_2^2-M_1^2}{v_S^2}\ . \tag{7.90}$$

It is interesting to compare this oscillation temperature, coming from the thermal masses, to the temperature of the phase transition T_n,

$$\frac{T_n}{T_{\rm osc}^{\rm (III)}} = 12\frac{T_n}{a_R}\frac{v_S^2}{M_2^2-M_1^2} = 12\ \frac{v_S^2}{T_n^2}\frac{T_n}{a_R}\frac{T_n^2}{M_2^2-M_1^2} = 12\ \frac{v_S^2}{T_n^2}\left[\frac{T_n}{T_{\rm osc}^{\rm ARS}}\right]^3\ . \tag{7.91}$$

In the discussion without thermal masses, we discussed only the ratio $T_n/T_{\rm osc}^{\rm ARS}$; if it was large, then the FOPT happened early, and standard ARS oscillations can happen at $T_{\rm osc}^{\rm ARS}$. However, if the ratio was small, the FOPT happened late enough so that all oscillations happen during a Hubble time, fast compared to the expansion of the Universe.

From the estimate (7.91), we now have a third temperature scale, the temperature at which oscillations from thermal masses happen. If these oscillations happen before the FOPT, we can obtain an asymmetry from thermal masses only. If however the temperature of oscillations is smaller than the temperature T_n, vacuum mass will change our estimate by modifying the oscillation frequency. In scenario (III), we will assume that oscillations occur before the FOPT happens, that is

$$\frac{T_n}{T_{\rm osc}^{\rm (III)}} = 12\ \frac{v_S^2}{T_n^2}\left[\frac{T_n}{T_{\rm osc}^{\rm ARS}}\right]^3 < 1\ . \tag{7.92}$$

We can compare it to the condition for scenario (II), which was

$$\frac{T_n}{T_{\rm osc}^{\rm ARS}} < 1\ . \tag{7.93}$$

Depending on the ratio v_S/T_n, the two conditions can be related or not. We recall that for a strong FOPT, that we consider in this work, $v_S > T_c > T_n$. For a supercooled FOPT, we even have $T_c \gg T_n$, so v_S can be much larger than T_n.

Going back to our analytical study, we obtained in equation (7.88) the first-order contribution to the off-diagonal element $\delta n_{h,12}^{(1)}$. Plugging it in the source S_a, we can compute the asymmetry Δ_a. Taking the limit $z \to +\infty$ (and dividing by s) like in the previous sections gives

$$\left(\frac{\Delta_{a,\infty}^{(2)}}{s}\right)_{\rm (III)} = \frac{9720\zeta(3)}{\pi^4 g_*}\left\langle\gamma_+\right\rangle n_{\rm eq}\frac{{\rm Im}\left[Y_{1a}^* Y_{2a}\left(YY^\dagger\right)_{12}\right]}{\left(YY^\dagger\right)_{11}+\left(YY^\dagger\right)_{22}}\frac{1}{\lambda_2^2-\lambda_1^2}\ . \tag{7.94}$$

Now, recall that the sterile neutrino mass is given by its coupling λ to the scalar field times the *vev* v_S, $M_I = \lambda_I v_S$, such that

$$\left(\frac{\Delta^{(2)}_{a,\infty}}{s}\right)_{\text{(III)}} \simeq 1.3\times 10^{-2}\; n_{\text{eq}} \frac{\text{Im}\left[Y^*_{1a}Y_{2a}\left(YY^\dagger\right)_{12}\right]}{\left(YY^\dagger\right)_{11}+\left(YY^\dagger\right)_{22}} \frac{T_n^2}{M_2^2-M_1^2}\left(\frac{v_S}{T_n}\right)^2 . \tag{7.95}$$

7.8 Comparison of the three scenarios

Following our discussions, we can now summarize and compare the results in each case. We recall that we considered three scenarios, where (I) is standard ARS leptogenesis, while (II) and (III) consider a phase transition. The sterile neutrino vacuum masses, in (II) and (III), only come into play when $T < T_n$, after the transition. In scenario (II), dynamics are assumed to start from then, producing an asymmetry shortly after the transition. In scenario (III), we include thermal masses coming from the scalar field, that induce oscillations even before the transition, at $T > T_n$.

Our goal is to find the regions of parameter space where each scenario produces the most asymmetry. We were able to derive analytical estimates (7.4), (7.81) and (7.95) for the flavored asymmetries (before washout) that we recall here

$$\left(\frac{\Delta^{(2)}_{a,\infty}}{s}\right)_{\text{(I)}} \simeq 2.4\times 10^{-5}\; n_{\text{eq}} \text{Im}\left[Y^*_{1a}Y_{2a}\left(YY^\dagger\right)_{12}\right]\left(\frac{a_R^2}{M_2^2-M_1^2}\right)^{2/3} , \tag{7.96a}$$

$$\left(\frac{\Delta^{(2)}_{a,\infty}}{s}\right)_{\text{(II)}} \simeq 1.1\times 10^{-3}\; \kappa\; n_{\text{eq}} \frac{\text{Im}\left[Y^*_{1a}Y_{2a}\left(YY^\dagger\right)_{12}\right]}{\left(YY^\dagger\right)_{11}+\left(YY^\dagger\right)_{22}} \frac{T_n^2}{M_2^2-M_1^2} , \tag{7.96b}$$

$$\left(\frac{\Delta^{(2)}_{a,\infty}}{s}\right)_{\text{(III)}} \simeq 1.3\times 10^{-2}\; n_{\text{eq}} \frac{\text{Im}\left[Y^*_{1a}Y_{2a}\left(YY^\dagger\right)_{12}\right]}{\left(YY^\dagger\right)_{11}+\left(YY^\dagger\right)_{22}} \frac{T_n^2}{M_2^2-M_1^2}\left(\frac{v_S}{T_n}\right)^2 . \tag{7.96c}$$

Remember that κ, appearing in (7.96b), was estimating the deficit, due to the production of sterile neutrinos before and during the FOPT in scenario (II), of the deviation from equilibrium,

$$\kappa \equiv \frac{n_{\text{PT}}}{n_{\text{eq}}} - 1 . \tag{7.97}$$

We estimated that the production during the FOPT only represented up to an order O(1 %) correction. Neglecting it in this discussion, the production of sterile neutrinos before the FOPT gives

$$n_{\text{PT}} \simeq n_{\text{eq}} + \delta n_h(t = t_{\text{in}}) = n_{\text{eq}}\left(1 - e^{-\frac{a_R}{T_n}\gamma_0}\right) , \tag{7.98}$$

$$\kappa \simeq e^{-\frac{a_R}{T_n}\gamma_0} . \tag{7.99}$$

As we emphasized in the previous sections, the estimates (7.96) are *not* the final asymmetries because washout effects are crucial in ARS-like leptogenesis. However, here we only wish to

compare the different scenarios among them. We will therefore only focus on the flavored asymmetries produced by the oscillations, in order to work with analytical expressions. We immediately note that the expressions for (II) and (III) have a similar form,

$$\left(\frac{\Delta^{(2)}_{a,\infty}}{s}\right)_{\text{(III)}} \simeq 12\kappa^{-1}\left(\frac{v_S}{T_n}\right)^2\left(\frac{\Delta^{(2)}_{a,\infty}}{s}\right)_{\text{(II)}} . \tag{7.100}$$

Their physical origins are quite different, as (II) comes from oscillations due to vacuum masses in a short time after the FOPT, in less than a Hubble time, while (III) comes from oscillations going along with temperature evolution and that are caused by thermal masses. Let us also remind ourselves our discussion in section 7.7 about the different regimes where scenarios (II) and (III) are relevant. For scenario (II), we want the temperature of nucleation T_n to be low enough such that standard oscillations are frustrated, so

$$\text{scenario (II)} \;\Rightarrow \frac{T_n}{T^{\text{ARS}}_{\text{osc}}} < 1 . \tag{7.101}$$

For scenario (III), we want oscillations to happen from the thermal masses to happen before the FOPT, so the temperature T_n should also be low enough. As we described in the previous section from Equation (7.91),

$$\text{scenario (III)} \;\Rightarrow \frac{T_n}{T^{\text{III}}_{\text{osc}}} = 12\left(\frac{v_S}{T_n}\right)^2\left(\frac{T_n}{T^{\text{ARS}}_{\text{osc}}}\right)^3 < 1 . \tag{7.102}$$

In particular, there is an overlapping region where both scenarios could be considered, because for $v_S > T_n$, we always have $\frac{T_n}{T^{\text{III}}_{\text{osc}}} > \frac{T_n}{T^{\text{ARS}}_{\text{osc}}}$. This means that whenever scenario (III) is possible, so is scenario (II). But because of the pre-factor $12\left(\frac{v_S}{T_n}\right)^2$, there are regions where scenario (II) would be possible but not scenario (III).

We can consider two different cases: first, the case $v_S = T_n$ where the scenarios (II) and (III) correspond roughly to the same region and produce a similar asymmetry. We compare the amount of asymmetry produced by oscillations in scenario (II) and (III) with the one produced in standard ARS,

$$\begin{aligned}
\frac{\left(\Delta^{(2)}_{a,\infty}/s\right)_{\text{(II)}}}{\left(\Delta^{(2)}_{a,\infty}/s\right)_{\text{(I)}}} \simeq \frac{\kappa}{12}\,\frac{\left(\Delta^{(2)}_{a,\infty}/s\right)_{\text{(III)}}}{\left(\Delta^{(2)}_{a,\infty}/s\right)_{\text{(I)}}} &\simeq 46\;\kappa\;\left(\frac{T_n^2}{M_2^2-M_1^2}\right)\left(\frac{M_2^2-M_1^2}{a_R^2}\right)^{2/3}\frac{1}{\text{Tr}\left[YY^\dagger\right]} \\
&= 46\;\kappa\left(\frac{T_n}{\left(a_R\left(M_2^2-M_1^2\right)\right)^{1/3}}\right)\left(\frac{T_n}{a_R}\right)\frac{1}{\text{Tr}\left[YY^\dagger\right]} \\
&= 46\,\langle\gamma_+\rangle\;\kappa\;\left(\frac{T_n}{T^{\text{ARS}}_{\text{osc}}}\right)\left(\frac{T_n}{a_R\,\langle\gamma_+\rangle\,\text{Tr}\left[YY^\dagger\right]}\right) \\
&\simeq \frac{1}{2}\;e^{-\frac{1}{2}(T_{\text{eq}}/T_n)}\left(\frac{T_n}{T^{\text{ARS}}_{\text{osc}}}\right)\left(\frac{T_n}{T_{\text{eq}}}\right) ,
\end{aligned} \tag{7.103}$$

where we defined

$$T_{\rm eq} \equiv a_R \langle \gamma_+ \rangle \, {\rm Tr}\left[YY^\dagger\right] \tag{7.104}$$

and used the expression of κ in terms of γ_0 defined previously in (7.53)

$$\kappa \simeq e^{-\frac{a_R}{T_{\rm ref}}\gamma_0} = e^{-\frac{a_R}{T_{\rm ref}}\langle\gamma_+\rangle \frac{\left(YY^\dagger\right)_{11}+\left(YY^\dagger\right)_{22}}{2}} = e^{-\frac{1}{2}(T_{\rm eq}/T_n)} \ . \tag{7.105}$$

We recognize two temperature scales appearing: the oscillation temperature for standard ARS leptogenesis $T_{\rm osc}^{\rm ARS}$, and the equilibration temperature $T_{\rm eq}$. Their value relative to the temperature T_n of the FOPT will determine which scenario produces the most (flavored) asymmetry. We define

$$x \equiv \frac{T_n}{T_{\rm osc}^{\rm ARS}} \ , \ y \equiv \frac{T_{\rm eq}}{T_n} \ . \tag{7.106}$$

The domains of dominance for each scenario can be summarized in the comparative diagram 7.5a, drawn in the plane (x, y) . The value of $x = T_n/T_{\rm osc}^{\rm ARS}$ determines when scenarios (II) ($x < 1$) and (III) ($x < (1/12)^{1/3} (T_n/v_S)^{2/3} = (1/12)^{1/3}$) can be used. The value of $y = T_{\rm eq}/T_n$ then fixes if the scenarios with a phase transition ((II) or (III)) are better than standard ARS leptogenesis.

We colored three regions corresponding to the three possible dominating scenarios. The red color corresponds to the region where standard ARS leptogenesis, which we called scenario (I), produces more flavored asymmetry, the blue one corresponds to scenario (II) and the green one to scenario (III). The blue and green zones are restricted to certain values of x from our discussion above. Because they correspond to different physical scenarios (one in which the scalar field isn't thermalized and doesn't contribute to a thermal mass and one in which it does), we also show the overlapping region where both scenarios are possible, and both produce more flavored asymmetry than standard ARS. Note however (from (7.100)) that scenario (III) always produces more asymmetry than scenario (II).

The boundaries between scenario (I) and the other scenarios are fixed by the relations (7.103). The asymmetry in scenario (II) has an extra $\exp\left(-T_{\rm eq}/(2T_n)\right) = \exp\left(-y/2\right)$ factor compared to scenario (III), which explains its suppression at larger values of y. We note that scenarios with a phase transition ((II) and (III)) produce more flavored asymmetry than standard ARS leptogenesis for low values of the parameters ($x \lesssim 1$, $y \lesssim 1$). The condition $x \lesssim 1$ makes sense because it is the condition for which our phase-transition-based scenarios are relevant. The second condition $y \lesssim 1$ corresponds to an equilibration temperature happening later than the temperature of the FOPT; this is desired if we want our sterile neutrinos to still be out of equilibrium at the time of the FOPT. The region ($x \lesssim 1$, $y \lesssim 1$) imposes that our phase transition should happen at a temperature T_n such that

$$T_{\rm eq} < T_n < T_{\rm osc}^{\rm ARS} \tag{7.107}$$

in order to have an enhancement of the phase transition scenarios compared to the standard case.

Note that the colors in the diagram only represent relative comparison between the scenarios, but do not tell us if leptogenesis is successful or not. In order to estimate this, we represented (with black dots) the values of x and y for which leptogenesis was indeed successful in our numerical study in section 7.5. This study was conducted within scenario (II); points that end up in the blue sector indicate that scenario (II) was successful and even provides a better estimate than standard ARS leptogenesis.

Finally, it is worth looking at what changes for a stronger FOPT, for which we could have $v_S \gg T_n$. In that case, the asymmetry in scenario (III) can be quite larger than the one in scenario (II), due to the v_S^2/T_n^2 factor in the comparison (7.100). At the same time, the temperature of oscillations in scenario (III) is affected, looking at relation (7.91),

$$\frac{T_n}{T_{\rm osc}^{\rm (III)}} = 12\ \frac{v_s^2}{T_n^2}\left[\frac{T_n}{T_{\rm osc}^{\rm ARS}}\right]^3 \ . \tag{7.108}$$

Scenario (III) becomes relevant for $\frac{v_s^2}{T_n^2}\left[\frac{T_n}{T_{\rm osc}^{\rm ARS}}\right]^3 = \frac{v_s^2}{T_n^2}\ x^3 < 1$. The boundary between scenarios (II) and (III) will then be shifted in the phase diagram. This is what we observe in the diagram 7.5b, fixing $v_S/T_n = 10$. For stronger FOPT, scenario (III) produces more asymmetry and competes with ARS for higher values of y, but it is only relevant for smaller values of x.

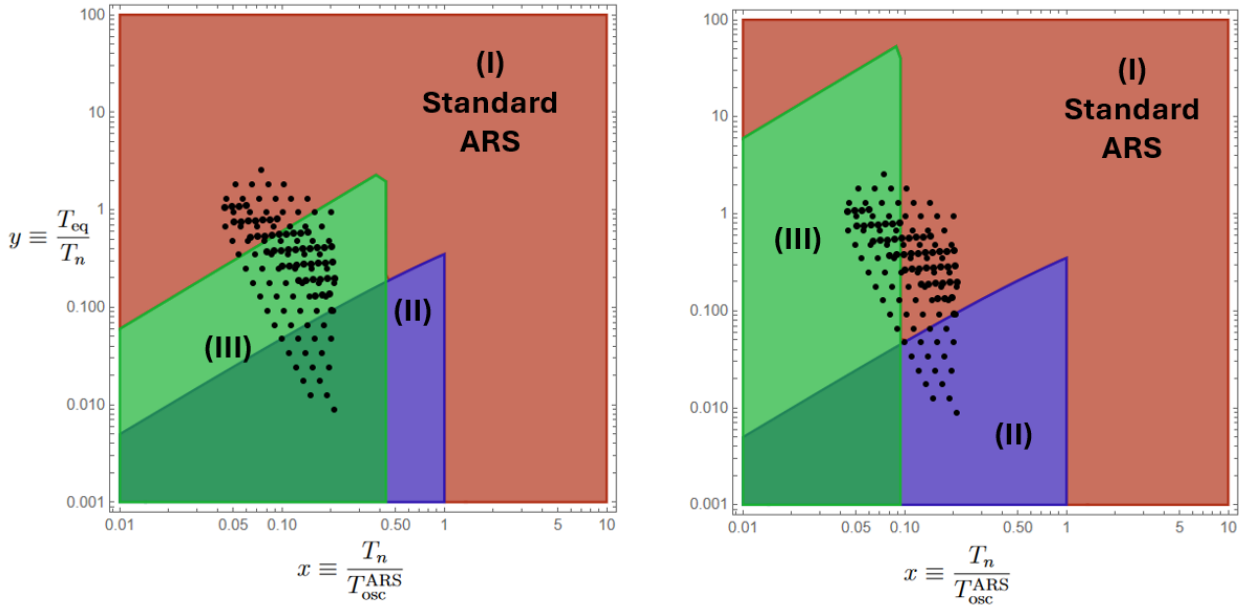

(a) $v_S = T_n$. (b) $v_S = 10\ T_n$.

Figure 7.5: Comparative diagram of the different scenarios, for two values of v_S/T_n. The black dots represent points of successful baryogenesis in our numerical study. Each color delimits the region in the (x, y) plane where a given scenario produces more flavored asymmetry than the others. The red color represents scenario (I), which is just standard ARS leptogenesis, the blue one represents scenario (II) and the green one represents scenario (III).

7.9 Conclusion for ARS-like leptogenesis

In this chapter, we studied the effect of a phase transition on ARS leptogenesis, which involves relativistic sterile neutrinos. The mechanism that produces the lepton asymmetry is based on flavor oscillations in the sterile sector that are usually driven by the vacuum masses of these sterile neutrinos. In a scenario with a phase transition, these vacuum masses only exist after the transition. If it happens late enough ($T_n < T_{\rm osc}^{\rm ARS}$), the oscillations are "frustrated" and happen differently and at a different time than in the standard case.

We studied ARS-like leptogenesis with a phase transition and found successful regions for leptogenesis. Compared to previous studies [37, 39], we also gave detailed analytical estimates and were able to compare standard ARS leptogenesis to ARS-like leptogenesis with a phase transition. We determined which region of parameter space allows an enhancement of the produced lepton asymmetry thanks to a phase transition.

Chapter 8

Discussion and conclusion

We studied a scenario of leptogenesis with sterile neutrinos involved in a cosmological phase transition. Provided it is first-order, bubbles are nucleated at a certain nucleation temperature T_n and expand in the early Universe plasma. These bubbles render the masses of the sterile neutrinos time dependent, and can make them deviate from equilibrium. We first described the sterile neutrino dynamics analytically, following previous work [159], in the single flavor case and concluded that sterile neutrinos were produced during the phase transition. Adding interactions with the Standard Model plasma required that we use out-of-equilibrium Quantum Field Theory. Using the Closed-Time Path formalism, we provided kinetic equations that allow us to describe sterile neutrinos interacting with the Standard Model plasma and experiencing a time dependent mass. The formalism involved the so-called local approximation [167, 168], and we used an estimate [139] for the sterile neutrino self-energy such that we can describe all regimes of masses for the sterile neutrinos. In the context of a phase transition, we focused in particular on two scenarios corresponding to two distinct mechanisms of asymmetry creation. The first one, called Mass Gain scenario, considers heavy sterile neutrinos decaying after the phase transition, while the second one, called ARS-like leptogenesis, considers the production of low-scale sterile neutrinos.

8.1 Mass Gain scenario

In the Mass Gain (MG) regime, we found leptogenesis was indeed successful, and studied the dependence of the produced asymmetry in terms of our parameters. Similar to previous results [28–31] and as expected, the asymmetry is best produced for large ratios $M/T_n \gtrsim O(10)$, in order to avoid washout effects. Such a large ratio can be obtained considering a supercooled phase transition, for which the nucleation temperature T_n can be significantly smaller than the critical temperature T_c of the phase transition, which relates to the *vev* v_S and the masses $M = \lambda v_S$.

We find that the baryon asymmetry can be reproduced for a large range of sterile neutrino mass scales M between 50 TeV up to 10^{10} GeV, provided we allow a sufficiently strong mass degeneracy. While for $M \gtrsim 5 \times 10^9$ GeV no mass degeneracy is needed, the mass degeneracy needs to be increasingly strong for lower masses, around $\Delta M \simeq 10^{-6} M$ for $M \lesssim 5 \times 10^5$ GeV. These lower values of the mass correspond to nucleation temperature just above the TeV scale, which will be tested in future Gravitational Wave (GW) detection experiments. For all masses, we observe a resonance for a mass degeneracy $\Delta M \sim \Gamma$ of the same order than the decay rate. We showed it is consistent with an interpretation in terms of decays (that might be resonantly enhanced or not) of the sterile neutrinos, as they are brought out of equilibrium by the First-Order Phase Transition (FOPT). We also studied the particle production, coming from the change in mass during the transition. We estimated its effect to be sub-leading.

We used, in this regime, a description of the sterile neutrinos in terms of kinetic equations for mass- and coherence-shell matrices. This differs from previous studies of the MG and in particular all mass degeneracies are treated the same, without the need of a regulator for $\Delta M \ll \Gamma$. The asymmetry produced is shown to be proportional to the resonant CP-asymmetry $\epsilon_{\text{CP,wave}}$ in the degenerate case.

8.2 ARS-like leptogenesis

In ARS-like scenarios, with low-scale sterile neutrinos, an interesting scenario can be considered for the production of the sterile neutrinos, as in ARS leptogenesis. Usually, they undergo flavor oscillations, due to their vacuum mass, as they are being produced. When this vacuum mass is originating from a phase transition, the oscillations can be frustrated until the moment of the transition at temperature T_n. Once vacuum masses are present, flavor oscillations are then completed within a single Hubble time, that is, before temperature has time to evolve too much. This is different from standard ARS, where the oscillations occur as temperature evolves. Leptogenesis is still successful in the region we studied, for masses M between .1 and 10 GeV. The mass degeneracy is needed to be as strong as $\Delta M \simeq 10^{-7} M$ for nucleation temperatures close to the electroweak scale $T_n \lesssim 1$ TeV, but the degeneracy can be relatively mild $\Delta M \simeq 10^{-2} M$ for higher nucleation temperatures $T_n \simeq 10$ TeV. We found a different parametric dependence, compared to the standard scenario, of the produced asymmetry on the parameters. In particular, ARS-like leptogenesis is sensible to the mass degeneracy; in standard ARS, one expects $Y_B \propto (\Delta M/M)^{-2/3}$ while with a phase transition, we found (analytically and numerically) a dependence $Y_B \propto (\Delta M/M)^{-1}$. The asymmetry obtained in the scenario with a phase transition can thus be greater than the one obtained in standard ARS scenarios, as $\Delta M \ll M$.

A distinction can also be made depending on whether the scalar field S provides a thermal mass for the sterile neutrinos or not. If it does, oscillations can happen before the phase transition because of the misalignment between the thermal masses (diagonal in the mass eigenbasis) and the Yukawa couplings. We studied each possibility analytically and compared their esti-

mates for the produced asymmetry. Scenarios with a phase transition were found to be more favorable than standard ARS leptogenesis for a temperature T_n of the phase transition such that $T_{\rm eq} < T_n < T_{\rm osc}^{\rm ARS}$, where $T_{\rm eq}$ is the typical temperature at which sterile neutrinos equilibrate, and $T_{\rm osc}^{\rm ARS}$ is the temperature at which they would oscillate, in standard ARS leptogenesis.

8.3 Outlook

Our work in this thesis relied on a number of assumptions that could be relaxed for future work. For instance, we would like to investigate more the effect on the dynamics of the additional scalar field S. In this work, we assumed it was weakly coupled to the Standard Model, and only considered (in the ARS-like scenario) its contribution to sterile neutrino thermal masses. If we consider a stronger coupling to the Standard Model, especially in the ARS-like regime, we expect it can have an influence on the lepton asymmetry produced, by opening new decay or production channels for the sterile neutrinos.

Moreover, the FOPT itself contains more complex dynamics that we exposed here. During the nucleation and expansion of bubbles, reflection R and transmission T coefficients at the bubble wall may affect the densities recovered inside the bubble. In the present work, we assumed all particles entered the bubble, hence $R = 0$, $T = 1$. A more ambitious goal would be to consider realistic bubble expansion, that would be inhomogeneous in space. The "post-FOPT" sterile neutrino distribution would be more complicated, being a combination of a produced distribution as was studied in this paper, and the reflection and transmission of the pre-existing distribution.

More generally, a complete first-principle approach to the dynamics during the phase transition is lacking. Non-local effects together with the explicit time dependence are usually not included in practice but could be relevant for describing all the physical processes. This might involve equations more intricate than Boltzmann equations, keeping the non-local parts of the propagators dynamical.

Finally, studies of phase transitions are interesting because of their close connection to Gravitational Waves (GW). In an era where GW detection becomes more and more precise, over a wider range of frequencies, phenomenological studies of early Universe phenomenon could soon start using GW constraints. In the context of baryogenesis with a phase transition, the ultimate goal is to find close correlations between the parameters of the phase transition (its temperature and strength, for instance) and the baryon asymmetry produced. This participates in the interplay between theory and experiments; GW experiments define parameter regions of phenomenological interest, where interesting theories can be developed.

Part IV

Appendices

Appendix A

Active neutrino parameters

In this thesis, we worked the preferred value of combined fits provided by the NuFIT collaboration (without including atmospheric data from Super-Kamiokande). We assumed Normal Ordering (NO) as well as $m_1 = 0$, such that $m_3 = \sqrt{|\Delta m^2_{31}|}$ and $m_2 = \sqrt{|\Delta m^2_{21}|}$. We fixed the CP-violating phase $\delta = \frac{3\pi}{2}$ for simplicity, and both Majorana phases were taken to be zero $\alpha_1 = \alpha_2 = 0$. Otherwise, we used the central values of the parameters given in Table A.1.

NuFIT 5.2 (2022)

		Normal Ordering (best fit)		Inverted Ordering ($\Delta\chi^2 = 2.3$)	
		bfp $\pm 1\sigma$	3σ range	bfp $\pm 1\sigma$	3σ range
without SK atmospheric data	$\sin^2\theta_{12}$	$0.303^{+0.012}_{-0.011}$	$0.270 \to 0.341$	$0.303^{+0.012}_{-0.011}$	$0.270 \to 0.341$
	$\theta_{12}/^\circ$	$33.41^{+0.75}_{-0.72}$	$31.31 \to 35.74$	$33.41^{+0.75}_{-0.72}$	$31.31 \to 35.74$
	$\sin^2\theta_{23}$	$0.572^{+0.018}_{-0.023}$	$0.406 \to 0.620$	$0.578^{+0.016}_{-0.021}$	$0.412 \to 0.623$
	$\theta_{23}/^\circ$	$49.1^{+1.0}_{-1.3}$	$39.6 \to 51.9$	$49.5^{+0.9}_{-1.2}$	$39.9 \to 52.1$
	$\sin^2\theta_{13}$	$0.02203^{+0.00056}_{-0.00059}$	$0.02029 \to 0.02391$	$0.02219^{+0.00060}_{-0.00057}$	$0.02047 \to 0.02396$
	$\theta_{13}/^\circ$	$8.54^{+0.11}_{-0.12}$	$8.19 \to 8.89$	$8.57^{+0.12}_{-0.11}$	$8.23 \to 8.90$
	$\delta_{\rm CP}/^\circ$	197^{+42}_{-25}	$108 \to 404$	286^{+27}_{-32}	$192 \to 360$
	$\frac{\Delta m^2_{21}}{10^{-5}\ \mathrm{eV}^2}$	$7.41^{+0.21}_{-0.20}$	$6.82 \to 8.03$	$7.41^{+0.21}_{-0.20}$	$6.82 \to 8.03$
	$\frac{\Delta m^2_{3\ell}}{10^{-3}\ \mathrm{eV}^2}$	$+2.511^{+0.028}_{-0.027}$	$+2.428 \to +2.597$	$-2.498^{+0.032}_{-0.025}$	$-2.581 \to -2.408$

Figure A.1: Table of the values taken in our analysis for the parameters in the neutrino sector.

Appendix B

Helicity eigenvectors

In the field decomposition (4.2), we introduced the helicity eigenvectors $\xi_h^{\mathbf{k}}$ that satisfy the eigenvector equation

$$\mathbf{k} \cdot \boldsymbol{\sigma} \xi_h^{\mathbf{k}} = h|\mathbf{k}|\xi_h^{\mathbf{k}} \ . \tag{B.1}$$

Using the coordinates of $\mathbf{k}$ in spherical coordinates

$$k_x = |\mathbf{k}| \cos(\varphi_{\mathbf{k}}) \sin(\theta_{\mathbf{k}}) \tag{B.2}$$

$$k_y = |\mathbf{k}| \sin(\varphi_{\mathbf{k}}) \sin(\theta_{\mathbf{k}}) \tag{B.3}$$

$$k_z = |\mathbf{k}| \cos(\theta_{\mathbf{k}}) \ , \tag{B.4}$$

we can write the helicity eigenvectors

$$\xi_+^{\mathbf{k}} = \begin{pmatrix} \cos(\theta_{\mathbf{k}}/2) \\ e^{i\varphi_{\mathbf{k}}} \sin(\theta_{\mathbf{k}}/2) \end{pmatrix} \ , \tag{B.5}$$

$$\xi_-^{\mathbf{k}} = \begin{pmatrix} e^{-i\varphi_{\mathbf{k}}} \sin(\theta_{\mathbf{k}}/2) \\ -\cos(\theta_{\mathbf{k}}/2) \end{pmatrix} \ . \tag{B.6}$$

It can be easily checked that these eigenvectors are normalized such that

$$\xi_h^{\mathbf{k}\dagger} \cdot \xi_r^{\mathbf{k}} = \delta_{h,r} \ , \tag{B.7}$$

and the phase has been fixed in order to obtain the additional relation

$$\xi_h^{\mathbf{k}} = -h \ i\sigma_2 \xi_{-h}^{\mathbf{k}*} \ , \tag{B.8}$$

useful for computing the charge-conjugation of the fields. Once the helicity eigenvectors are written this way, we can check that for $\mathbf{k} \to -\mathbf{k}$,

$$\theta_{\mathbf{k}} \to \pi - \theta_{\mathbf{k}} \tag{B.9}$$

$$\varphi_{\mathbf{k}} \to \pi + \varphi_{\mathbf{k}} \tag{B.10}$$

and

$$\xi_h^{-\mathbf{k}} = e^{ih\varphi_{\mathbf{k}}} \xi_{-h}^{\mathbf{k}} \ . \tag{B.11}$$

Appendix C

Mode normalization

We detail in this Appendix the steps needed in order to determine the constants $A_{h\pm}$ appearing in section 4 in the functions

$$u_{h\pm} = A_{h\pm} Z^{\alpha}(1-Z)^{\beta}\, {}_2F_1(a_{\pm}, b_{\pm}, c, Z)\ . \tag{C.1}$$

Following [159], we start by the Dirac equation (4.17) written in terms of u's,

$$\begin{aligned}[2i\gamma Z(1-Z)\partial_Z - M_0 Z] A_{h+} Z^{\alpha}(1-Z)^{\beta}\, {}_2F_1(a_+, b_+, c, Z) \\ = -h|\mathbf{k}| A_{h-} Z^{\alpha}(1-Z)^{\beta}\, {}_2F_1(b_+ + 1, a_+ - 1, c, Z)\ ,\end{aligned} \tag{C.2}$$

where we used $a_- = b_+ + 1$, $b_- = a_+ - 1$. The left-hand term will involve the derivative of the hypergeometric function,

$$\begin{aligned}&[2i\gamma Z(1-Z)\partial_Z - M_0 Z]\, A_{h+} Z^{\alpha}(1-Z)^{\beta}\, {}_2F_1(a_+, b_+, c, Z) \\ &\quad = A_{h+} Z^{\alpha}(1-Z)^{\beta} \left[2i\gamma Z(1-Z)\partial_Z + \alpha 2i\gamma(1-Z) - \beta 2i\gamma Z - M_0 Z\right] {}_2F_1(a_+, b_+, c, Z)\ .\end{aligned} \tag{C.3}$$

We can now use the relations

$$\partial_Z \left[{}_2F_1(a_+, b_+, c, Z)\right] = \frac{a_+ b_+}{c}\ {}_2F_1(a_+ + 1, b_+ + 1, c + 1, Z)\ , \tag{C.4}$$

$$\frac{a_+ b_+}{c}\ Z\ {}_2F_1(a_+ + 1, b_+ + 1, c + 1, Z) = (c-1)\left[{}_2F_1(a_+, b_+, c-1, Z) - {}_2F_1(a_+, b_+, c, Z)\right]\ , \tag{C.5}$$

in order to simplify further more the term involving the derivative

$$\begin{aligned}&[2i\gamma Z(1-Z)\partial_Z + \alpha 2i\gamma(1-Z) - \beta 2i\gamma Z - M_0 Z]\, {}_2F_1(a_+, b_+, c, Z) \\ &= 2i\gamma \left[(c-1)(1-Z)\left[{}_2F_1(a_+, b_+, c-1, Z) - {}_2F_1(a_+, b_+, c, Z)\right]\right. \\ &\quad \left. + \left(\alpha - \left(\alpha + \beta - i\frac{M_0}{2\gamma}\right) Z\right) {}_2F_1(a_+, b_+, c, Z)\right] \\ &= 2i\gamma \left[(c-1)(1-Z)\, {}_2F_1(a_+, b_+, c-1, Z) - (\alpha - (c - 1 - b_+)Z)\, {}_2F_1(a_+, b_+, c, Z)\right]\ .\end{aligned} \tag{C.6}$$

We need to transform the arguments of the hypergeometric function in order to match the one on the right-hand part of Equation (C.2). Hypergeometric funcitons satisfy

$$(c-1)\,{}_2F_1(a_+,b_+,c-1,Z) = b_+\,{}_2F_1(a_+,b_++1,c,Z) + (c-1-b_+)\,{}_2F_1(a_+,b_+,c,Z)\ , \quad \text{(C.7)}$$

$$(1-Z)b_+\,{}_2F_1(a_+,b_++1,c,Z) = \alpha\,{}_2F_1(a_+-1,b_++1,c,Z) + (b_+-\alpha)\,{}_2F_1(a_+,b_+,c,Z)\ . \quad \text{(C.8)}$$

We can regroup all hypergeometric functions with same arguments,

$$\begin{aligned} &2i\gamma\left[(c-1)(1-Z)\,{}_2F_1(a_+,b_+,c-1,Z) - (\alpha-(c-1-b_+)Z)\,{}_2F_1(a_+,b_+,c,Z)\right] \\ &= 2i\gamma\left[(1-Z)b_+\,{}_2F_1(a_+,b_++1,c,Z) - (\alpha-(c-b_+-1))\,{}_2F_1(a_+,b_+,c,Z)\right] \\ &= 2i\gamma\alpha\,{}_2F_1(a_+-1,b_++1,c,Z) = |\mathbf{k}|\,{}_2F_1(a_+-1,b_++1,c,Z)\ . \end{aligned} \quad \text{(C.9)}$$

Going back to the equation (C.2), after the simplifications presented above, one finds

$$A_{h+}\ |\mathbf{k}|\,{}_2F_1(a_+-1,b_++1,c,Z) = -A_{h-}\ h|\mathbf{k}|\,{}_2F_1(a_+-1,b_++1,c,Z) \quad \text{(C.10)}$$

which gives the simple condition that $A_{h+} = -hA_{h-}$. Note that our final expression is much simpler that what is derived in [159], because we considered the sterile neutrinos as massless before the FOPT.

The constants can be totally fixed if we add the requirement that the modes are normalized, meaning

$$|L_h|^2 + |R_h|^2 = 1 = 2 \times \left(|u_{h+}| + |u_{h-}|^2\ .\right) \quad \text{(C.11)}$$

Because $h^2 = 1$, we have $|A_{h+}|^2 = |A_{h-}|^2$ and, noting that $Z^\alpha(1-Z)^\beta$ has norm 1 because α and β are purely imaginary, the above normalization condition gives

$$|A_{h+}|^2 \times \left[|\,{}_2F_1(a_+,b_+,c,Z)|^2 + |\,{}_2F_1(a_+-1,b_++1,c,Z)|^2\right] = \frac{1}{2}\ . \quad \text{(C.12)}$$

We can use successively the property of complex-conjugation

$${}_2F_1(a,b,c,Z)^* = {}_2F_1(a^*,b^*,c^*,Z)\ ,\ \text{with}\ a_+^* = 2-a_+\ ,\ b_+^* = -b_+\ ,\ c^* = 2-c\ , \quad \text{(C.13)}$$

and the properties relating a hypergeometric function to its "adjacent" functions, whose argument are shifted by one, as in

$$\begin{aligned} (1-a)\times&\left[{}_2F_1(2-a,-b,c,Z) - {}_2F_1(1-a,-b,c,Z)\right] \\ &= -b\left[{}_2F_1(1-a,1-b,c,Z) - {}_2F_1(1-a,-b,c,Z)\right]\ , \end{aligned} \quad \text{(C.14)}$$

$$\begin{aligned} (a-1)\times&\left[{}_2F_1(a,b,c,Z) - {}_2F_1(a-1,b,c,Z)\right] \\ &= b\left[{}_2F_1(a-1,b+1,c,Z) - {}_2F_1(a-1,b,c,Z)\right]\ . \end{aligned} \quad \text{(C.15)}$$

The complex norms of the two functions appearing in Equation (C.12) can then be manipulated into

$$\begin{aligned} &|\,{}_2F_1(a,b,c,Z)|^2 + |\,{}_2F_1(a-1,b+1,c,Z)|^2 \\ &= {}_2F_1(a,b,c,Z)\,{}_2F_1(2-a,-b,2-c,Z) + {}_2F_1(a-1,b+1,c,Z)\,{}_2F_1(1-a,1-b,2-c,Z) \\ &= {}_2F_1(a,b,c,Z)\left[{}_2F_1(2-a,-b,2-c,Z) - {}_2F_1(1-a,-b,2-c,Z)\right] \\ &+ {}_2F_1(a,b,c,Z)\,{}_2F_1(1-a,-b,2-c,Z) + {}_2F_1(a-1,b+1,c,Z)\,{}_2F_1(1-a,1-b,2-c,Z)\ . \end{aligned} \quad \text{(C.16)}$$

From the previous derivation, due to the equation (4.17) between u_{h+} and u_{h-}, we know

$$|\mathbf{k}|\,{}_2F_1(a_+-1,b_++1,c,Z) = [2i\gamma Z(1-Z)\partial_Z + 2i\gamma\alpha - 2i\gamma Z b_+]\,{}_2F_1(a_+,b_+,c,Z) \tag{C.17}$$

which is given in terms of the constants a_+, b_+, c

$${}_2F_1(a_+-1,b_++1,c,Z) = \frac{2}{c-1}\left[Z(1-Z)\partial_Z + \frac{c-1}{2} - Zb_+\right]{}_2F_1(a_+,b_+,c,Z)\ . \tag{C.18}$$

A similar relation is found for different arguments ($a_+ \to 1-b_+$, $b_+ \to 1-a_+$, $c \to 2-c$),

$${}_2F_1(2-a_+,-b_+,2-c,Z) = \frac{2}{1-c}\left[Z(1-Z)\partial_Z + \frac{1-c}{2} - Z(1-a_+)\right]{}_2F_1(1-b_+,1-a_+,2-c,Z)\ , \tag{C.19}$$

which allows to write the write the sums of the squared norms in terms of derivatives

$$\begin{aligned}
&|\,{}_2F_1(a_+,b_+,c,Z)|^2 + |\,{}_2F_1(a_+-1,b_++1,c,Z)|^2 \\
&= {}_2F_1(a_+,b_+,c,Z)\,{}_2F_1(2-a_+,-b_+,2-c,Z) \\
&\qquad + {}_2F_1(a_+-1,b_++1,c,Z)\,{}_2F_1(1-a_+,1-b_+,2-c,Z) \\
&= {}_2F_1(a_+,b_+,c,Z)\ \frac{2}{1-c}\left[Z(1-Z)\partial_Z + \frac{1-c}{2} - Z(1-a_+)\right]{}_2F_1(1-b_+,1-a_+,2-c,Z) \\
&\qquad + \frac{2}{c-1}\left[Z(1-Z)\partial_Z + \frac{c-1}{2} - Zb_+\right]{}_2F_1(a_+,b_+,c,Z)\ \ {}_2F_1(1-a_+,1-b_+,2-c,Z) \\
&= \frac{2Z(1-Z)}{1-c} W[{}_2F_1(a_+,b_+,c,Z), {}_2F_1(1-b_+,1-a_+,2-c,Z)] \\
&\qquad + {}_2F_1(a_+,b_+,c,Z)\,{}_2F_1(1-b_+,1-a_+,2-c,Z)\left(2 - 2Z\frac{1-a_+-b_+}{1-c}\right)
\end{aligned} \tag{C.20}$$

In the process, we introduced the Wronskian W of two functions defined as $W[f,g] \equiv fg' - f'g$. For two independent solutions to the hypergeometric equations, the Wronskian is known and is given by

$$W[{}_2F_1(a_+,b_+,c,Z), z^{1-c}\,{}_2F_1(1+a_+-c,1+b_+-c,2-c,Z)] = (1-c)z^{-c}(1-z)^{c-a_+-b_+-1} \tag{C.21}$$

Using a Pfaff transformation [193], the second function can be turned into one of our functions of interest,

$$W[{}_2F_1(a_+,b_+,c,Z), z^{1-c}(1-z)^{c-a_+-b_+}\,{}_2F_1(1-a_+,1-b_+,2-c,Z)] = (1-c)z^{-c}(1-z)^{c-a_+-b_+-1}\ . \tag{C.22}$$

Deriving the Wronskian explicitly,

$$\begin{aligned}
&W[{}_2F_1(a_+,b_+,c,Z), {}_2F_1(1-a_+,1-b_+,2-c,Z)] \\
&+ {}_2F_1(a_+,b_+,c,Z)\,{}_2F_1(1-a_+,1-b_+,2-c,Z)\left(\frac{1-c}{Z} - \frac{c-a_+-b_+}{1-Z}\right) = (1-c)z^{-1}(1-z)^{-1}\ .
\end{aligned} \tag{C.23}$$

This directly relates to the equation we found above, leading to

$$|u_{h+}|^2 + |u_{h-}|^2 = |A_{h+}|^2 \times \left[|\,{}_2F_1(a_+, b_+, c, Z)|^2 + |\,{}_2F_1(a_+ - 1, b_+ + 1, c, Z)|^2 \right] = 2|A_{h+}|^2 = \frac{1}{2} \ . \tag{C.24}$$

We can then simply choose $A_{h+} = 1/2 = -hA_{h-}$ and

$$u_{h+} = \frac{1}{2} Z^\alpha (1-Z)^\beta \,{}_2F_1(a_+, b_+, c, Z) \ , \ u_{h-} = -\frac{h}{2} Z^\alpha (1-Z)^\beta \,{}_2F_1(a_-, b_-, c, Z) \ , \tag{C.25}$$

$$L_h = \frac{1}{2} Z^\alpha (1-Z)^\beta \left[{}_2F_1(a_+, b_+, c, Z) - h\,{}_2F_1(a_-, b_-, c, Z) \right] \ , \ R_h = L_{-h} \ . \tag{C.26}$$

Appendix D

Particle production with flavor

In the main text, we derived an analytical estimate of the sterile neutrino production when the mass is time-dependent. The results were obtained for a single flavor, without interactions. If we want to add flavor and interactions with the Standard Model plasma, additional terms will appear in the Dirac equation for the fields N_I. An analytical approach is then more complicated; we give in this section a description of how we could estimate the production in the flavored case.

D.1 Dirac equation in the flavored case

Let us consider the lepton l_a and Higgs ϕ fields interacting with the sterile neutrinos. First, we write down the full Dirac equations, including the ones for the lepton field now including Yukawa couplings,

$$i\partial\!\!\!/ N_I - M_I N_I = P_L Y_{Ia} l_a \phi^\dagger + P_R Y^*_{Ia} l^c_a \phi^T \ , \tag{D.1}$$

$$i\partial\!\!\!/ l_a = P_R Y^*_{Ja} N_J \phi \ , \ i\partial\!\!\!/ l^c_a = P_L Y_{Ja} N_J \phi^* \ . \tag{D.2}$$

Differentiating (D.1) leads to a second-order differential equation

$$-\partial^2 N_I - i\partial\!\!\!/ \left(M_I N_I\right) = P_R Y_{Ia} Y^*_{Ja} N_J \phi^\dagger \phi + P_L Y^*_{Ia} Y_{Ja} N_J \phi^T \phi^* + P_R Y_{Ia} \gamma^\mu l_a \partial_\mu \phi^\dagger + P_L Y^*_{Ia} \gamma^\mu l^c_a \partial_\mu \phi^T \ . \tag{D.3}$$

As before, the derivative acts on the mass, and we can use the Dirac equation (D.1) to get

$$\begin{aligned} \partial^2 N_I + & i\partial_t \left(M_I\right) \gamma^0 N_I + M_I^2 N_I + P_R Y_{Ia} Y^*_{Ja} N_J \phi^\dagger \phi + P_L Y^*_{Ia} Y_{Ja} N_J \phi^T \phi^* \\ & = -P_L M_I Y_{Ia} l_a \phi^\dagger - P_R M_I Y^*_{Ia} l^c_a \phi^T - P_R Y_{Ia} \gamma^\mu l_a \partial_\mu \phi^\dagger - P_L Y^*_{Ia} \gamma^\mu l^c_a \partial_\mu \phi^T \end{aligned} \tag{D.4}$$

or equivalently, replacing N_I in the $\gamma^0 N_I$ factor,

$$\begin{aligned}\partial^2 N_I - \frac{\partial_t M_I}{M_I}\gamma^0\gamma^\mu\partial_\mu N_I + M_I^2 N_I + P_R Y_{Ia} Y_{Ja}^* N_J \phi^\dagger \phi + P_L Y_{Ia}^* Y_{Ja} N_J \phi^T \phi^* \\ = i\frac{\partial_t M_I}{M_I}\gamma^0 \left[P_L Y_{Ia} l_a \phi^\dagger + P_R Y_{Ia}^* l_a^c \phi^T\right] \\ - P_L M_I Y_{Ia} l_a \phi^\dagger - P_R M_I Y_{Ia}^* l_a^c \phi^T - P_R Y_{Ia}\gamma^\mu l_a \partial_\mu \phi^\dagger - P_L Y_{Ia}^* \gamma^\mu l_a^c \partial_\mu \phi^T \end{aligned} \tag{D.5}$$

This equation involves a number of undesirable terms. To deal with them, we will assume thermal equilibrium for both lepton and Higgs fields for the entirety of the phase-transition, meaning in particular that the quantum state for the SM particles factors out of the total wave-function and is equal to a thermal state of temperature $T \equiv 1/\beta_T$,

$$|\psi\rangle = |\psi_N\rangle \otimes |\beta_T\rangle \ . \tag{D.6}$$

The wave-function $|\beta_T\rangle$ contains the thermal fluctuations of the lepton and Higgs fields. By averaging over these fluctuations, we can largely simplify our previous equation, using

$$\langle\beta_T|l_a|\beta_T\rangle = 0 \ , \ \langle\beta_T|\phi|\beta_T\rangle = 0 \ , \ \langle\beta_T|\partial_\mu\phi|\beta_T\rangle = 0 \ , \ \text{etc.} \tag{D.7}$$

while the only non-zero average (for two-point functions) is for the norm-squared of the Higgs field (an $SU(2)$-doublet scalar) [194]

$$\langle\beta_T|\phi^\dagger\phi|\beta_T\rangle = \frac{T^2}{6} = \langle\beta_T|\phi^T\phi^*|\beta_T\rangle \ . \tag{D.8}$$

Averaging (D.3) over the thermal state, we get an equation that only involves the sterile neutrino field, however including corrections from the thermal bath. It takes the same form as in the flavorless case, but with an additional term,

$$\partial^2 N_I + i\gamma^0 \left(\partial_t M_I\right) N_I + \left[\left(M_I\right)^2 \delta_{IJ} + P_R Y_{Ia} Y_{Ja}^* \frac{T^2}{6} + P_L Y_{Ia}^* Y_{Ja} \frac{T^2}{6}\right] N_J = 0 \ . \tag{D.9}$$

The vacuum mass squared M_I^2 has been added a thermal mass squared $M_{\text{th},IJ}^2 \equiv \left[P_R Y_{Ia} Y_{Ja}^* + P_L Y_{Ia}^* Y_{Ja}\right] T^2/6$. Note that it is a matrix in flavor space; it couples mass eigenstates N_I of different flavors.

Let us try to repeat the procedure from section 4 in the main text, and take as our starting point a decomposition of the mass eigenstate N_I that allows mixing among flavors,

$$N_I = \sum_h \int_{\mathbf{k}} \left[e^{i\mathbf{k}\cdot\mathbf{x}} \begin{pmatrix} L_h^{IJ} \\ R_h^{IJ} \end{pmatrix} \otimes \xi_h^{\mathbf{k}} \hat{a}_{h,\mathbf{k}}^J + e^{-i\mathbf{k}\cdot\mathbf{x}} \begin{pmatrix} -hR_h^{IJ*} \\ hL_h^{IJ*} \end{pmatrix} \otimes \xi_{-h}^{\mathbf{k}} \hat{a}_{h,\mathbf{k}}^{J\dagger}\right] \ . \tag{D.10}$$

$\hat{a}_{h,\mathbf{k}}^J / \hat{a}_{h,\mathbf{k}}^{J\dagger}$ are the annihilation and creation operators for the Majorana sterile neutrino J before the phase transition. Note that the modes L_h and R_h are now matrices, as they can mix creation

(or annihilation) operators from different flavors. In terms of these modes, the thermal average of Equation (D.9) gives a second-order differential equations for each chirality mode

$$\partial_t^2 L_h^{IJ} - \frac{\partial_t M_I}{M_I}\partial_t L_h^{IJ} + \left(|\mathbf{k}|^2 + (M_I)^2 + ih|\mathbf{k}|\frac{\partial_t M_I}{M_I}\right) L_h^{IJ} + (Y^* Y^T)_{IK}\frac{T^2}{6} L_h^{KJ} = 0 \ , \tag{D.11}$$

$$\partial_t^2 R_h^{IJ} - \frac{\partial_t M_I}{M_I}\partial_t R_h^{IJ} + \left(|\mathbf{k}|^2 + (M_I)^2 - ih|\mathbf{k}|\frac{\partial_t M_I}{M_I}\right) R_h^{IJ} + (Y Y^\dagger)_{IK}\frac{T^2}{6} R_h^{KJ} = 0 \ . \tag{D.12}$$

Note how the thermal masses are different for L_h and R_h. This logically comes from the chiral Yukawa interaction, coupling the sterile neutrinos to the left-handed lepton. This is interesting in order to create an asymmetry; recall how in the single flavor case, we had $R_h = L_{-h}$ because they obeyed the same equation (and boundary condition) up to the sign of the $ih|\mathbf{k}|\partial_t M/M$. Now there is another discrepancy, which is the thermal mass matrix which is either Y^*Y^T or $YY^\dagger$. We may expect that the CP-violating Yukawa couplings, mixing the different flavors, will allow an asymmetry in the sterile sector, between the two helicities.

D.2 Flavored Bogoliubov transformation

The flavored Hamiltonian is calculated as before, starting with

$$H = \sum_I \int \mathrm{d}^3\mathbf{x}\ \frac{1}{2}\left[i\overline{N_I}\boldsymbol{\gamma}\cdot\boldsymbol{\nabla} N_I + M(t)\overline{N}_I^c N_I\right] \ , \tag{D.13}$$

and using the decomposition (D.10), we arrive at

$$H = \frac{1}{2}\sum_h \sum_{K,J} \int \frac{\mathrm{d}^3\mathbf{k}}{(2\pi)^3}\left[\Omega^h_{\mathbf{k},KJ}\hat{a}^{K\dagger}_{h,\mathbf{k}}\hat{a}^J_{h,\mathbf{k}} - \Omega^{h*}_{\mathbf{k},KJ}\hat{a}^K_{h,\mathbf{k}}\hat{a}^{J\dagger}_{h,\mathbf{k}} + \left(\Lambda^h_{\mathbf{k},KJ}e^{-ih\varphi_{\mathbf{k}}}\ \hat{a}^K_{h,-\mathbf{k}}\hat{a}^J_{h,\mathbf{k}} + \text{h.c.}\right)\right] \ , \tag{D.14}$$

where the coefficients $\Omega^h_{\mathbf{k},KJ}$ and $\Lambda^h_{\mathbf{k},KJ}$ are now matrices with sterile flavor indices, defined as

$$\Omega^h_{\mathbf{k}} \equiv h|\mathbf{k}|\left(L_h^\dagger L_h - R_h^\dagger R_h\right) + L_h^\dagger M_N R_h + R_h^\dagger M_N L_h \ , \tag{D.15}$$

$$\Lambda^h_{\mathbf{k}} \equiv 2|\mathbf{k}|\left(L_h^T R_h + R_h^T L_h\right) + hL_h^T M_N L_h - hR_h^T M_N R_h \ , \tag{D.16}$$

where $(M_N)_{IJ} = M_I\ \delta_{IJ}$ is the diagonal mass matrix. Similarly to before, this Hamiltonian can be diagonalized, this time by a flavored Bogoliubov transformation, given by a change of annihilation and creation operators

$$\hat{A}^I_{h,\mathbf{k}} \equiv \alpha^{IJ}_{h,\mathbf{k}}\hat{a}^J_{h,\mathbf{k}} + \beta^{IJ}_{h,\mathbf{k}}e^{ih\varphi_{\mathbf{k}}}\hat{a}^{J\dagger}_{h,\mathbf{k}} \tag{D.17a}$$

$$\hat{A}^{I\dagger}_{h,\mathbf{k}} \equiv \alpha^{IK*}_{h,\mathbf{k}}\hat{a}^{K\dagger}_{h,\mathbf{k}} + \beta^{IK*}_{h,\mathbf{k}}e^{-ih\varphi_{\mathbf{k}}}\hat{a}^{K\dagger}_{h,\mathbf{k}} \ . \tag{D.17b}$$

The matrices α and β are found to be the generalization of the flavorless expressions (4.59),

$$\alpha_{h,\mathbf{k}} = \frac{1}{\sqrt{2}}\left[\left(1+\frac{h|\mathbf{k}|}{\omega_{\mathbf{k},N}}\right)^{1/2} L_h + \left(1-\frac{h|\mathbf{k}|}{\omega_{\mathbf{k},N}}\right)^{1/2} R_h\right] , \tag{D.18a}$$

$$\beta_{h,\mathbf{k}} = \frac{h}{\sqrt{2}}\left[\left(1-\frac{h|\mathbf{k}|}{\omega_{\mathbf{k},N}}\right)^{1/2} L_h^* - \left(1+\frac{h|\mathbf{k}|}{\omega_{\mathbf{k},N}}\right)^{1/2} R_h^*\right] . \tag{D.18b}$$

where now $\omega_{\mathbf{k},N} \equiv (|\mathbf{k}|^2 + M_N^2)^{1/2}$ is a diagonal matrix, with the square-root taken in the mass eigenbasis where M_N is diagonal so that it is well-defined. L_h and R_h are also matrices in the above expressions.

The Bogoliubov transformation is only valid if it preserves the anti-commutators of the annihilation and creation operators. Imposing

$$\left\{\hat{A}^I_{h,\mathbf{k}} \ , \ \hat{A}^{J\dagger}_{r,\mathbf{k}'}\right\} = \delta^{(3)}(\mathbf{k}-\mathbf{k'})\ \delta_{hr}\delta_{IJ} \ , \tag{D.19}$$

$$\left\{\hat{A}^I_{h,\mathbf{k}} \ , \ \hat{A}^{J}_{r,\mathbf{k}'}\right\} = \left\{\hat{A}^{I\dagger}_{h,\mathbf{k}} \ , \ \hat{A}^{J\dagger}_{r,\mathbf{k}'}\right\} = 0 \tag{D.20}$$

leads to two conditions in terms of the matrices α and β. The first one is

$$\alpha_{h,\mathbf{k}}\alpha^\dagger_{h,\mathbf{k}} + \beta_{h,\mathbf{k}}\beta^\dagger_{h,\mathbf{k}} = \mathbb{I} \ , \tag{D.21}$$

which is the flavored version of the condition $|\alpha_{h,\mathbf{k}}|^2 + |\beta_{h,\mathbf{k}}|^2 = 1$ imposed in the previous section. The second one is

$$\beta_{h,\mathbf{k}}\alpha^T_{h,\mathbf{k}} - \alpha_{h,\mathbf{k}}\beta^T_{h,\mathbf{k}} = 0 \ , \tag{D.22}$$

which is automatically satisfied in the flavorless case, but is non-trivial for matrices.

The mixing of different flavors is however an issue for solving the equations. The equations (D.11), (D.12) are equations for matrices, with couplings between the various matrix elements. Moreover, if we want to diagonalize the Hamiltonian, we should also satisfy the conditions (D.21) and (D.22). The matrix structure of the equations and of the normalization conditions makes this problem much harder than the single flavor case.

We may think of two ways to address this issue and get an estimate of the sterile neutrino dynamics. The first one involves a perturbative expansion in the Yukawa couplings, the second one is an attempt to diagonalize the mass term.

D.3 Expansion in Yukawa couplings

One attempt would be to consider an expansion for small Yukawa couplings. More precisely, it would mean consider the thermal mass as a small correction to the vacuum mass,

$$\mathrm{Tr}\left[M^2_{\mathrm{th}}\right] = \mathrm{Tr}\left[YY^\dagger\right]\frac{T^2}{6} \ll M_I^2 \ . \tag{D.23}$$

Depending on the regime of masses, this may or may not be relevant. For instance, a naive estimate from the Seesaw condition (considering the matrix R in the Casas-Ibarra parametrization (3.41) to be of order 1), we have

$$\frac{\mathrm{Tr}\left[M_{\mathrm{th}}^2\right]}{M^2} \sim \frac{M m_\nu}{v^2}\frac{T^2}{M^2} \simeq 8\times 10^{-9}\left(\frac{M}{10^9\ \mathrm{GeV}}\right)\left(\frac{10}{M/T}\right)^2 = 8\times 10^{-9}\left(\frac{M}{10\ \mathrm{GeV}}\right)\left(\frac{10^{-3}}{M/T}\right)^2 . \tag{D.24}$$

In the estimate, we took the scale of active neutrino masses $m_\nu = 0.05$ eV for concreteness. We gave the numerical estimates for two scenarios of interest in this thesis, both for a heavy sterile neutrino mass $M \sim 10^9$ GeV in a non-relativistic scenario $M \sim 10T$, and for a low-scale relativistic sterile neutrino $M \sim 10$ GeV and $M \sim 10^{-3}T$. In both cases, the thermal mass constitutes a small correction.

The equations (D.11) and (D.12) can then be approximately solved by considering an expansion of L_h and R_h in terms of the Yukawa couplings,

$$L_h = L_h^{(0)} + L_h^{(1)} + \dots\ ,\ \ R_h = R_h^{(0)} + R_h^{(1)} + \dots \tag{D.25}$$

where $L_h(0)$ is the zeroth-order, $L_h^{(1)}$ is of order $YY^\dagger/Y^*Y^T$, etc. We can then use our results from the single flavor case because the equation for $L_h^{(0)}$ for example is

$$\partial_t^2 L_h^{(0)IJ} - \frac{\partial_t M_I}{M_I}\partial_t L_h^{(0)IJ} + \left(|\mathbf{k}|^2 + (M_I)^2 + ih|\mathbf{k}|\frac{\partial_t M_I}{M_I}\right) L_h^{(0)IJ} = 0\ . \tag{D.26}$$

This is the same equation as in the previous sections, with M_I instead of M. We know its solutions, given in terms of hypergeometric functions. The first order contribution $L_h^{(1)}$ is then computed from (D.11),

$$\partial_t^2 L_h^{(1)IJ} - \frac{\partial_t M_I}{M_I}\partial_t L_h^{(1)IJ} + \left(|\mathbf{k}|^2 + (M_I)^2 + ih|\mathbf{k}|\frac{\partial_t M_I}{M_I}\right) L_h^{(1)IJ} = -(Y^*Y^T)_{IK}\frac{T^2}{6}L_h^{(0)KJ}\ . \tag{D.27}$$

The zeroth-order plays the role of a source for the first-order. The resolution becomes a bit more involved as there is now an inhomogeneous term in the equation for $L_h^{(1)}$. The perturbative expansion starts with the equations (D.11), (D.12) for L_h and R_h including a thermal mass,

$$\partial_t^2 L_h^{IJ} - \frac{\partial_t M_I}{M_I}\partial_t L_h^{IJ} + \left(|\mathbf{k}|^2 + (M_I)^2 + ih|\mathbf{k}|\frac{\partial_t M_I}{M_I}\right) L_h^{IJ} + (Y^*Y^T)_{IK}\frac{T^2}{6}L_h^{KJ} = 0\ , \tag{D.28}$$

$$\partial_t^2 R_h^{IJ} - \frac{\partial_t M_I}{M_I}\partial_t R_h^{IJ} + \left(|\mathbf{k}|^2 + (M_I)^2 - ih|\mathbf{k}|\frac{\partial_t M_I}{M_I}\right) R_h^{IJ} + (YY^\dagger)_{IK}\frac{T^2}{6}R_h^{KJ} = 0\ . \tag{D.29}$$

It is, as in the free case, convenient to write these in terms of $u_{h\pm} \equiv (L_h \pm R_h)/2$, such that

$$\partial_t^2 u_{h\pm}^{IJ} \pm i\left(\partial_t M_I\right) u_{h\pm}^{IJ} + \left(k^2 + (M_I)^2\right) u_{h\pm}^{IJ} + \mathrm{Re}\left[(YY^\dagger)_{IK}\right]\frac{T^2}{6}u_{h\pm}^{KJ} - i\mathrm{Im}\left[(YY^\dagger)_{IK}\right]\frac{T^2}{6}u_{h\mp}^{KJ} = 0\ . \tag{D.30}$$

Contrary to the flavorless case, the second-order differential equations for the $u_{h\pm}$ are not decoupled. Recall that we were able to find solutions when the interactions were off, $Y = 0$. Now, more terms are involved and an analytical direct solution is not available. However, for small Yukawa couplings, we can find an approximate solution by expanding in power of Y. Indeed, let us rewrite Equation (D.30) as an homogeneous term and a source term,

$$\mathcal{L}^I_\pm u^{IJ}_{h\pm} = -\mathrm{Re}\left[(YY^\dagger)_{IK}\right]\frac{T^2}{6}u^{KJ}_{h\pm} + i\mathrm{Im}\left[(YY^\dagger)_{IK}\right]\frac{T^2}{6}u^{KJ}_{h\mp}\ , \tag{D.31}$$

$$\mathcal{L}^I_\pm \equiv \partial_t^2 \pm i\left(\partial_t M_I\right) + |\mathbf{k}|^2 + M_I(t)^2\ . \tag{D.32}$$

The operator $\mathcal{L}^I_\pm$ has already been solved for in the flavorless case, for $M = M_I$. We know the basis of solutions is made of hypergeometric equations times powers of Z and $1-Z$, with coefficients that may now depend on flavor,

$$f^I_{A\pm} \equiv Z^\alpha(1-Z)^{\beta_I}\,{}_2F_1(a^I_\pm, b^I_\pm, c, Z)\ , \tag{D.33a}$$
$$f^I_{B\pm} \equiv Z^{\alpha+1-c}(1-Z)^{\beta_I}\,{}_2F_1(a^I_\pm + 1 - c, b^I_\pm + 1 - c, 2 - c, Z)\ , \tag{D.33b}$$

$$\mathcal{L}^I_\pm\left[f^I_{A\pm}/f^I_{B\pm}\right] = 0\ . \tag{D.34}$$

Expanding the flavored functions $u^{IJ}_{h\pm}$ in powers of $\left(YY^\dagger\right)$ / $\left(Y^*Y^T\right)$, we define

$$u^{IJ}_{h\pm} \equiv u^{IJ(0)}_{h\pm} + u^{IJ(1)}_{h\pm} + O(Y^4)\ , \tag{D.35}$$

where $u^{IJ(0)}_{h\pm}$ is of order 0, $u^{IJ(1)}_{h\pm}$ is of order 1. The zeroth-order should be a solution of the homogeneous equation $\mathcal{L}^I_\pm u^{IJ(0)}_{h\pm} = 0$ so it is given in terms of the hypergeometric functions of flavor I described above (see (C.25) for the single flavor case),

$$u^{IJ(0)}_{h\pm} = A^{IJ(0)}_{h,\pm} f^I_{A\pm} + B^{IJ(0)}_{h,\pm} f^I_{B\pm}\ . \tag{D.36}$$

Moreover, the first-order equation is found by plugging the zeroth-order solution in the right-hand term of Equation (D.31),

$$\mathcal{L}^I_\pm u^{IJ(1)}_{h\pm} = -\mathrm{Re}\left[(YY^\dagger)_{IK}\right]\frac{T^2}{6}u^{KJ(0)}_{h\pm} + i\mathrm{Im}\left[(YY^\dagger)_{IK}\right]\frac{T^2}{6}u^{KJ(0)}_{h\mp} \equiv S^{IJ}_{h\pm}\ . \tag{D.37}$$

Here, the right-hand term is fixed and acts as a source term for the first order. The homogeneous part of the equation is known and has two linearly-independent solutions. A particular solution can be constructed generically from the homogeneous solutions (D.33) for a second-order differential equations,

$$u^{IJ(1)}_{h\pm} = f^{IJ}_{\mathrm{part},\pm} = f^I_{A\pm}(Z)\int_0^Z \mathrm{d}U\ \frac{f^I_{B\pm}(U)S^{IJ}_{h\pm}(U)}{W[f^I_{A\pm}, f^I_{B\pm}](U)} - f^I_{B\pm}(Z)\int_0^Z \mathrm{d}U\ \frac{f^I_{A\pm}(U)S^{IJ}_{h\pm}(U)}{W[f^I_{A\pm}, f^I_{B\pm}](U)} \tag{D.38}$$

where W is the Wronskian of the two functions, defined as

$$W[f_1, f_2](U) \equiv \left(f_1 f_2' - f_1' f_2\right)(U)\ . \tag{D.39}$$

The Wronskian for two solution of the hypergeometric equation is known (see Appendix C, (C.22)) and leads to

$$W[f^I_{A\pm}, f^I_{B\pm}](U) = (1-c)U^{-1-\alpha}(1-U)^{-\beta_I} \ . \tag{D.40}$$

The first-order is then determined by the zeroth-order. Imposing the normalization conditions to hold at all orders would impose a series of conditions on the integration constants $A^{IJ(0)}_{h\pm}/B^{IJ(0)}_{h\pm}$, but we did not attempt to solving this system.

D.4 Degenerate sterile neutrinos

The perturbative expansion in Yukawa couplings we just showed presents the advantage of being straightforward and general, as long as the thermal masses are small. It is however hard to fix all the integration constants and check all the normalization conditions. A non-perturbative attempt at solving (D.11) and (D.12) could be to try to diagonalize the mass term, in order to find decoupled equations for the elements in the diagonal basis, *i.e.* we want to diagonalize

$$M^2_{\text{tot},IJ}(t) \equiv M_I(t)^2\delta_{IJ} + \left(Y^*Y^T\right)_{IJ}\frac{T^2}{6} \tag{D.41}$$

For instance, we can already diagonalize the matrix $\mathcal{Y} \equiv \left(Y^*Y^T\right)T^2/6$ which is constant once we fixed our parameters. A more detailed discussion on how the diagonalization is done and how it relates to the parameters of interest is presented in Appendix D.5. We will here simply state that $\mathcal{Y}_L$ is a hermitian matrix, which means it has positive real eigenvalues and that it can be diagonalized by a unitary matrix U_0

$$\mathcal{Y}_L = U_0 D_0^2 U_0^\dagger \ , \tag{D.42}$$

where D_0^2 is a diagonal matrix of positive real elements. Another combination of the Yukawa couplings appears in the equations, namely $\mathcal{Y}_R \equiv \left(YY^\dagger\right)T^2/6$ which has the same eigenvalues but is diagonalized by U_0^*

$$\mathcal{Y}_R = \mathcal{Y}_L^* = U_0^* D_0^2 U_0^T \ . \tag{D.43}$$

We want to diagonalize the total mass $M^2_{\text{tot},IJ}$, which is also a hermitian matrix. It can be diagonalized but in a basis that is time-dependent, in principle,

$$M^2_{\text{tot}}(t) = U(t)D^2(t)U(t)^\dagger \ . \tag{D.44}$$

This still leaves the problem quite complicated, because even if we change the flavor basis to go in the diagonal eigenbasis, new terms coming from the derivatives of U would appear in the equations.

A limit in which we can derive simpler results is the case where sterile neutrinos are perfectly degenerate,$M_1 = M_2 = M$ for two flavors. This amounts to taking the mass matrix $(M_N)_{IJ} = M_I\delta_{IJ} = M\delta_{IJ}$ proportional to identity in flavor space. In this case,

$$\left(M^2_{\text{tot}}\right) = M^2(t)\mathbb{I} + (Y^*Y^T)\frac{T^2}{6} = U_0\left(M^2(t) + D_0^2\right)U_0^\dagger \ . \tag{D.45}$$

We diagonalized the mass term in a fixed basis (U_0 is time-independent). We then just have to rotate the mode matrices L_h on the left by U_0, and R_h by U_0^*,

$$\tilde{L}_h \equiv U_0 L_h \ , \ \tilde{R}_h \equiv U_0^* R_h \ , \tag{D.46}$$

so that the rotated matrices satisfy

$$\partial_t^2 \left(\tilde{L}_h^{\tilde{I}J}\right) - \frac{\partial_t M}{M}\partial_t \left(\tilde{L}_h^{\tilde{I}J}\right) + \left(|\mathbf{k}|^2 + M^2(t) + \left(D_0^2\right)_{\tilde{I}\tilde{I}} + ih|\mathbf{k}|\frac{\partial_t M}{M}\right)\tilde{L}_h^{\tilde{I}J} = 0 \ , \tag{D.47a}$$

$$\partial_t^2 \left(\tilde{R}_h^{\tilde{I}J}\right) - \frac{\partial_t M}{M}\partial_t \left(\tilde{R}_h^{\tilde{I}J}\right) + \left(|\mathbf{k}|^2 + M^2(t) + \left(D_0^2\right)_{\tilde{I}\tilde{I}} - ih|\mathbf{k}|\frac{\partial_t M}{M}\right)\tilde{R}_h^{\tilde{I}J} = 0 \ . \tag{D.47b}$$

We recover similar equations compared the flavorless case, except for an additional (constant) $\left(D_0^2\right)_{II}$ term. Following the same procedure as before, (change the variable to $Z \equiv (1 + \tanh(\gamma t))/2$, such that $M(t) = M_0 Z(t)$, divide by $4\gamma^2 Z(1-Z)$, look for poles in $1/Z$ or $1/(1-Z)$), this term will contribute to both types of poles in $1/Z$ and $1/(1-Z)$. These poles are absorbed by the powers of the scaling $Z^\alpha(1-Z)^\beta$, which will now be found to be

$$\alpha_{\tilde{I}}^2 = -\frac{|\mathbf{k}|^2 + \left(D_0^2\right)_{\tilde{I}\tilde{I}}}{4\gamma^2} \ \Leftrightarrow \ \alpha_{\tilde{I}} = \pm i\frac{\sqrt{|\mathbf{k}|^2 + \left(D_0^2\right)_{\tilde{I}\tilde{I}}}}{2\gamma} \ , \tag{D.48}$$

$$\beta_{\tilde{I}}^2 = -\frac{|\mathbf{k}|^2 + M_0^2 + \left(D_0^2\right)_{\tilde{I}\tilde{I}}}{4\gamma^2} \ \Leftrightarrow \ \beta_{\tilde{I}} = \pm i\frac{\sqrt{|\mathbf{k}|^2 + M_0^2 + \left(D_0^2\right)_{\tilde{I}\tilde{I}}}}{2\gamma} \ . \tag{D.49}$$

In particular, they now dependent on flavor. The solutions for $\tilde{L}$ are therefore given by hypergeometric functions, similarly to the flavorless case.

$$\tilde{L}_-^{IJ}(Z) = Z^{\alpha_I}(1-Z)^{\beta_I}\left[A_{L,+}^{IJ}{}_2F_1(a_+^I, b_+^I, c) + A_{L,-}^{IJ}{}_2F_1(a_-^I, b_-^I, c)\right] \ , \tag{D.50a}$$

$$\tilde{R}_-^{IJ}(Z) = Z^{\alpha_I}(1-Z)^{\beta_I}\left[A_{R,+}^{IJ}{}_2F_1(a_+^I, b_+^I, c) + A_{R,-}^{IJ}{}_2F_1(a_-^I, b_-^I, c)\right] \ . \tag{D.50b}$$

The determination of the constants remains to be done, using the normalization conditions.

D.5 Diagonalization of the thermal mass matrix

The matrix $\mathcal{Y}_L \equiv \left(Y^*Y^T\right)T^2/6$ can be diagonalized analytically, rather simply in the case of two flavours. Indeed, for two flavors, a hermitian matrix like the one we have here M_{th}^2 can be written as a linear combination of Pauli matrices $\sigma_{x/y/z}$ and the identity $\sigma_0 \equiv \mathbb{I}_2$,

$$\mathcal{Y}_L \equiv \frac{T^2}{6}\left(m_0\sigma_0 + \mathbf{m}\cdot\boldsymbol{\sigma}\right) \ , \tag{D.51}$$

with

$$m_0 = \frac{1}{2}\left(\left(Y^*Y^T\right)_{11} + \left(Y^*Y^T\right)_{22}\right) \ , \tag{D.52}$$

$$m_z = \frac{1}{2}\left(\left(Y^*Y^T\right)_{11} - \left(Y^*Y^T\right)_{22}\right) \ , \tag{D.53}$$

$$m_x = \mathrm{Re}\left[\left(Y^* Y^T\right)_{12}\right] \ , \tag{D.54}$$

$$m_y = -\mathrm{Im}\left[\left(Y^* Y^T\right)_{12}\right] \ . \tag{D.55}$$

A diagonal matrix in this case is only a linear combination of σ_0 and σ_z. The unitary matrix that realizes the diagonalization by conjugation can only affect the σ's coordinates, and therefore should be seen as a rotation of $\mathbf{m}$. Indeed, it can be shown that

$$e^{-i\theta\sigma_\alpha/2}\mathbf{m}\cdot\boldsymbol{\sigma}e^{i\theta\sigma_\alpha/2} = \mathcal{R}_\alpha(\theta)(\mathbf{m})\cdot\boldsymbol{\sigma} \ , \tag{D.56}$$

where $\mathcal{R}_\alpha(\theta)(\mathbf{m})$ is the vector $\mathbf{m}$ rotated by an angle θ around the $\alpha = x/y/z$-axis. Finding the unitary that diagonalizes our matrix amounts to rotating $\mathbf{m}$ along the axis z (because σ_z is diagonal). Very generically, we can define the angles η and φ such that

$$e^{-i\eta\sigma_y/2}\left(e^{-i\varphi\sigma_z/2}\mathbf{m}\cdot\boldsymbol{\sigma}e^{i\varphi\sigma_z/2}\right)e^{i\eta\sigma_y/2} = \tilde{m}_z\sigma_z \ , \tag{D.57}$$

$$\varphi = \arctan\left(\frac{m_y}{m_x}\right) \ , \ \eta = \arctan\left(\frac{\sqrt{m_x^2+m_y^2}}{m_z}\right) \ . \tag{D.58}$$

Basically, we first rotate $\mathbf{m}$ in the (x,y) plane until its component in this plane is aligned along the x-axis. Then, in the (x,z) plane, we rotate until it is only aligned along the z-axis. All these operations preserve the norm of the spatial vector $\mathbf{m}$, thus $\tilde{m}_z = \sqrt{m_x^2+m_y^2+m_z^2}$.

For our specific matrix, in the two-flavor case,

$$\tilde{m}_z = \frac{1}{2}\left(4|\left(Y^* Y^T\right)_{12}|^2 + \left(\left(Y^* Y^T\right)_{11} - \left(Y^* Y^T\right)_{22}\right)^2\right)^{1/2} \ , \tag{D.59}$$

$$\varphi = -\arctan\left(\frac{\mathrm{Im}\left[\left(Y^* Y^T\right)_{12}\right]}{\mathrm{Re}\left[\left(Y^* Y^T\right)_{12}\right]}\right) \ , \tag{D.60}$$

$$\eta = \arctan\left(2\frac{|\left(Y^* Y^T\right)_{12}}{\left(Y^* Y^T\right)_{11} - \left(Y^* Y^T\right)_{22}}\right) \ . \tag{D.61}$$

We note that φ is only non-zero when the Yukawa couplings are complex, *i.e.* when there is CP-violation. The diagonalization of $\mathcal{Y}_L$ is then realized by

$$\mathcal{Y}_L = U_0 D_0^2 U_0^\dagger \tag{D.62}$$

with

$$U_0 \equiv e^{-i\eta\sigma_y/2}e^{-i\varphi\sigma_z/2} \tag{D.63}$$

$$D_0^2 \equiv \frac{T^2}{6}\tilde{m}_z\begin{pmatrix}1 & 0\\ 0 & -1\end{pmatrix} \ . \tag{D.64}$$

Appendix E

Backreaction of the lepton asymmetry

In this Appendix, we detail some of the steps needed to arrive at the master equations from the Kadanoff-Baym equation (5.77). In particular, the backreaction of the lepton asymmetry on the sterile neutrinos was computed and encapsulated in the deviations $\delta\mathbf{\Sigma}$. It appeared in a combination of retarded and advanced propagators. We will use the definitions of these propagators, namely

$$\delta\mathbf{\Sigma}^R_{\mathbf{k}} = \delta\mathbf{\Sigma}^{\mathcal{H}}_{\mathbf{k}} - i\delta\mathbf{\Sigma}^{\rho}_{\mathbf{k}} \ , \ \mathcal{S}^A_{\mathrm{ad},\mathbf{k}} = \mathcal{S}^{\mathcal{H}}_{\mathrm{ad},\mathbf{k}} + i\mathcal{S}^{\rho}_{\mathrm{ad},\mathbf{k}} \ . \tag{E.1}$$

This allows us to re-write the right-hand side of Equation (5.77)

$$\begin{aligned}
&\delta\mathbf{\Sigma}^R_{\mathbf{k}} * \mathcal{S}^<_{\mathrm{ad},\mathbf{k}} + \delta\mathbf{\Sigma}^<_{\mathbf{k}} * \mathcal{S}^A_{\mathrm{ad},\mathbf{k}} \\
&\qquad = \left(\delta\mathbf{\Sigma}^{\mathcal{H}}_{\mathbf{k}} - i\delta\mathbf{\Sigma}^{\rho}_{\mathbf{k}}\right) * \mathcal{S}^<_{\mathrm{ad},\mathbf{k}} + \delta\mathbf{\Sigma}^<_{\mathbf{k}} * \left(\mathcal{S}^{\mathcal{H}}_{\mathrm{ad},\mathbf{k}} + i\mathcal{S}^{\rho}_{\mathrm{ad},\mathbf{k}}\right) \\
&\qquad = \delta\mathbf{\Sigma}^{\mathcal{H}}_{\mathbf{k}} * \mathcal{S}^<_{\mathrm{ad},\mathbf{k}} + \delta\mathbf{\Sigma}^<_{\mathbf{k}} * \mathcal{S}^{\mathcal{H}}_{\mathrm{ad},\mathbf{k}} + i\delta\mathbf{\Sigma}^<_{\mathbf{k}} * \mathcal{S}^{\rho}_{\mathrm{ad},\mathbf{k}} - i\delta\mathbf{\Sigma}^{\rho}_{\mathbf{k}} * \mathcal{S}^<_{\mathrm{ad},\mathbf{k}} \\
&\qquad = \delta\mathbf{\Sigma}^{\mathcal{H}}_{\mathbf{k}} * \mathcal{S}^<_{\mathrm{ad},\mathbf{k}} + \delta\mathbf{\Sigma}^<_{\mathbf{k}} * \mathcal{S}^{\mathcal{H}}_{\mathrm{ad},\mathbf{k}} + \frac{1}{2}\left(\delta\mathbf{\Sigma}^<_{\mathbf{k}} * \left(\mathcal{S}^<_{\mathrm{ad},\mathbf{k}} - \mathcal{S}^>_{\mathrm{ad},\mathbf{k}}\right) - \left(\delta\mathbf{\Sigma}^<_{\mathbf{k}} - \delta\mathbf{\Sigma}^>_{\mathbf{k}}\right) * \mathcal{S}^<_{\mathrm{ad},\mathbf{k}}\right) \\
&\qquad = \delta\mathbf{\Sigma}^{\mathcal{H}}_{\mathbf{k}} * \mathcal{S}^<_{\mathrm{ad},\mathbf{k}} + \delta\mathbf{\Sigma}^<_{\mathbf{k}} * \mathcal{S}^{\mathcal{H}}_{\mathrm{ad},\mathbf{k}} + \frac{1}{2}\left(\delta\mathbf{\Sigma}^>_{\mathbf{k}} * \mathcal{S}^<_{\mathrm{ad},\mathbf{k}} - \delta\mathbf{\Sigma}^<_{\mathbf{k}} * \mathcal{S}^>_{\mathrm{ad},\mathbf{k}}\right) \ .
\end{aligned} \tag{E.2}$$

Following [138], once we take the hermitian part of the expression above, we get

$$\delta\mathbf{\Sigma}^R_{\mathbf{k}} * \mathcal{S}^<_{\mathrm{ad},\mathbf{k}} + \delta\mathbf{\Sigma}^<_{\mathbf{k}} * \mathcal{S}^A_{\mathrm{ad},\mathbf{k}} + \text{ h.c.} = \left[\delta\mathbf{\Sigma}^{\mathcal{H}}_{\mathbf{k}}, \mathcal{S}^<_{\mathrm{ad},\mathbf{k}}\right] + \left[\delta\mathbf{\Sigma}^<_{\mathbf{k}}, \mathcal{S}^{\mathcal{H}}_{\mathrm{ad},\mathbf{k}}\right] + \frac{1}{2}\left(\left\{\delta\mathbf{\Sigma}^>_{\mathbf{k}}, \mathcal{S}^<_{\mathrm{ad},\mathbf{k}}\right\} - \left\{\delta\mathbf{\Sigma}^<_{\mathbf{k}}, \mathcal{S}^>_{\mathrm{ad},\mathbf{k}}\right\}\right) \ . \tag{E.3}$$

We introduced commutators (and anti-commutators) that should be understood as commutators with respect to the convolution product. Hence for example

$$\left[\delta\mathbf{\Sigma}_{\mathbf{k}}, \mathcal{S}_{\mathbf{k}}\right] \equiv \delta\mathbf{\Sigma}_{\mathbf{k}} * \mathcal{S}_{\mathbf{k}} - \mathcal{S}_{\mathbf{k}} * \delta\mathbf{\Sigma}_{\mathbf{k}} \ . \tag{E.4}$$

For $T \gg M_I$ or $M_I \approx M_J$, $\mathcal{S}^<_{\mathrm{ad},\mathbf{k}}$ and $\mathcal{S}^{\mathcal{H}}_{\mathrm{ad},\mathbf{k}}$ are proportional to identity in flavor space, so the commutator with them will vanish, at leading order [138]. The contribution of these terms is then sub-leading. What is left are the anti-commutators, such that

$$\delta\mathbf{\Sigma}^R_{\mathbf{k}} * \mathcal{S}^<_{\mathrm{ad},\mathbf{k}} + \delta\mathbf{\Sigma}^<_{\mathbf{k}} * \mathcal{S}^A_{\mathrm{ad},\mathbf{k}} + \text{ h.c.} \simeq \frac{1}{2}\left(\left\{\delta\mathbf{\Sigma}^>_{\mathbf{k}}, \mathcal{S}^<_{\mathrm{ad},\mathbf{k}}\right\} - \left\{\delta\mathbf{\Sigma}^<_{\mathbf{k}}, \mathcal{S}^>_{\mathrm{ad},\mathbf{k}}\right\}\right) \ . \tag{E.5}$$

In the main text, we described how the convolution product at equal time can be related to the Wigner representation of the propagators. At lowest order in the gradient expansion, we have

$$\left(\delta\mathbf{\Sigma}^{>}_{\mathbf{k}} * \mathcal{S}^{<}_{\mathrm{ad},\mathbf{k}}\right)(t,t) \simeq \int \frac{\mathrm{d}k^0}{2\pi}\, \delta\tilde{\mathbf{\Sigma}}^{>}(k,t)\tilde{\mathcal{S}}^{<}_{\mathrm{ad}}(k,t) \tag{E.6}$$

such that the anti-commutators above give

$$\left\{\delta\mathbf{\Sigma}^{>}_{\mathbf{k}}, \mathcal{S}^{<}_{\mathrm{ad},\mathbf{k}}\right\}(t,t) \simeq \int \frac{\mathrm{d}k^0}{2\pi}\, \left\{\delta\tilde{\mathbf{\Sigma}}^{>}(k,t), \tilde{\mathcal{S}}^{<}_{\mathrm{ad}}(k,t)\right\} \tag{E.7}$$

We can then use the KMS relation (5.97) satisfied by the adiabatic propagator,

$$\tilde{\mathcal{S}}^{>}_{\mathrm{ad}}(k,t) = -e^{k^0/T}\tilde{\mathcal{S}}^{<}_{\mathrm{ad}}(k,t) \tag{E.8}$$

and the (linearized) KMS relation (5.120) for the self-energy deviation

$$\delta_a\tilde{\hat{\mathbf{\Sigma}}}^{<}(k,t) = \frac{\mu_a+\mu_\phi}{T}\tilde{\hat{\mathbf{\Sigma}}}^{<}_{\mathrm{eq}}(k) - e^{-k^0/T}\delta_a\tilde{\hat{\mathbf{\Sigma}}}^{>}(k,t) \tag{E.9}$$

where

$$\delta\mathbf{\Sigma}^{<,>}_{IJ} = \sum_a \delta_a\mathbf{\Sigma}_{IJ} = g_W\sum_a \left(Y_{Ia}Y^*_{Ja}P_L - Y^*_{Ia}Y_{Ja}P_R\right)\hat{\mathbf{\Sigma}}^{<,>} \tag{E.10}$$

We then write the difference between the anti-commutators in (E.5) as a single anti-commutator

$$\begin{aligned}
&\frac{1}{2}\left(\left\{\delta_a\mathbf{\Sigma}^{>}_{\mathbf{k}}, \mathcal{S}^{<}_{\mathrm{ad},\mathbf{k}}\right\} - \left\{\delta_a\mathbf{\Sigma}^{<}_{\mathbf{k}}, \mathcal{S}^{>}_{\mathrm{ad},\mathbf{k}}\right\}\right)_{IJ} \\
&\quad\simeq \frac{1}{2}\int \frac{\mathrm{d}k^0}{2\pi}\, \left\{\left(\delta_a\tilde{\mathbf{\Sigma}}^{>}(k,t) + e^{k^0/T}\delta_a\tilde{\mathbf{\Sigma}}^{<}(k,t)\right), \tilde{\mathcal{S}}^{<}_{\mathrm{ad}}(k,t)\right\}_{IJ} \\
&\quad= \frac{g_W}{2}\frac{\mu_a+\mu_\phi}{T}\left(Y_{Ia}Y^*_{Ja}P_L - Y^*_{Ia}Y_{Ja}P_R\right)\int \frac{\mathrm{d}k^0}{2\pi}\, \left\{e^{k^0/T}\tilde{\hat{\mathbf{\Sigma}}}^{<}_{\mathrm{eq}}(k), \tilde{\mathcal{S}}^{<}_{\mathrm{ad},JJ}(k,t)\right\} \\
&\quad= g_W\frac{\mu_a+\mu_\phi}{T}\left(Y_{Ia}Y^*_{Ja}P_L - Y^*_{Ia}Y_{Ja}P_R\right)\int \frac{\mathrm{d}k^0}{2\pi}\, \left(1-f_{FD}(k^0)\right)\left\{\tilde{\hat{\mathbf{\Sigma}}}^{\rho}_{\mathrm{eq}}(k), i\tilde{\mathcal{S}}^{<}_{\mathrm{ad},JJ}(k,t)\right\} \\
&\quad\simeq -g_W\frac{\mu_a+\mu_\phi}{T}\left(Y_{Ia}Y^*_{Ja}P_L - Y^*_{Ia}Y_{Ja}P_R\right)\sum_s f_{FD}(s\omega_J)\left(1-f_{FD}(s\omega_J)\right)\left\{\tilde{\hat{\mathbf{\Sigma}}}^{\rho}_{\mathrm{eq}}(s\omega_J,\mathbf{k}), \mathbf{P}^s_J\right\}\ .
\end{aligned} \tag{E.11}$$

In the first line we used the gradient expansion to write the convolution product as a product of Wigner transforms. In the last line, we computed the residue at the poles $k^0 = \pm\omega_I$ coming from the adiabatic background. The chirality projectors could be extracted as they commute with $\hat{\mathbf{\Sigma}}^{\rho} \equiv \hat{\Sigma}^{\rho}\gamma^0$ and $\mathcal{S}^{<}_{\mathrm{ad}}$. We can also make one final observation that $f_{FD}(-\omega) = (1-f_{FD}(\omega)$, such that

$$\begin{aligned}
&\frac{1}{2}\left(\left\{\delta_a\mathbf{\Sigma}^{>}_{\mathbf{k}}, \mathcal{S}^{<}_{\mathrm{ad},\mathbf{k}}\right\} - \left\{\delta_a\mathbf{\Sigma}^{<}_{\mathbf{k}}, \mathcal{S}^{>}_{\mathrm{ad},\mathbf{k}}\right\}\right)_{IJ} \\
&\quad\simeq -g_W\frac{\mu_a+\mu_\phi}{T}\left(Y_{Ia}Y^*_{Ja}P_L - Y^*_{Ia}Y_{Ja}P_R\right)f_{FD}(\omega_J)(1-f_{FD}(\omega_J))\sum_s \left\{\tilde{\hat{\mathbf{\Sigma}}}^{\rho}_{\mathrm{eq}}(s\omega_J,\mathbf{k}), \mathbf{P}^s_J\right\}\ .
\end{aligned} \tag{E.12}$$

Appendix F

Lepton asymmetry evolution

In this Appendix, we sketch the derivation of the equation for the lepton asymmetry. It is convenient to work with the four-current for the lepton asymmetry in the flavor a, defined as

$$J^{\mu}_{l,a}(x) \equiv i\mathrm{Tr}\left[\gamma^{\mu} S^{<}_{l,a}(x,x)\right] \ . \tag{F.1}$$

If we focus on the (spatial integral of the) zeroth-component of this vector, $N_{l,a} - \overline{N}_{l,a} \equiv N_{L_a} = \int \mathrm{d}^3\mathbf{x}\ J^0_{l,a}$, we obtain the asymmetry in lepton number a. For now, we do not consider spectator effects, such that only the sterile neutrino Yukawa couplings are changing the lepton number. We also don't consider the expansion of the Universe yet. Using the Kadanoff-Baym equation for the lepton field (see [143, 167]), we derive

$$\begin{aligned}
\frac{\mathrm{d}}{\mathrm{d}t} N_{L_a} &= \int \mathrm{d}^3\mathbf{x}\ \mathrm{Tr}\left[i\gamma^0\partial_t S^{<}_{l,a}(x,x)\right] \\
&= \int \mathrm{d}^3\mathbf{x}\ \mathrm{Tr}\left[i\gamma^j\partial_j S_{l,a} + \frac{1}{2}\int \mathrm{d}t' \left(\Sigma^{<}_{l,a}(x,x')S^{>}_{l,a}(x',x) - \Sigma^{>}_{l,a}(x,x')S^{<}_{l,a}(x',x) + \mathrm{h.c.}\right)\right] \\
&\simeq \frac{1}{2}\int \frac{\mathrm{d}^4k}{(2\pi)^4}\left(\tilde{\Sigma}^{<}_{l,a}(k,t)\tilde{S}^{>}_{l,a}(k,t) - \tilde{\Sigma}^{>}_{l,a}(k,t)\tilde{S}^{<}_{l,a}(k,t) + \mathrm{h.c.}\right) \ .
\end{aligned} \tag{F.2}$$

$\Sigma_{l,a}$ is the self-energy of the lepton field. The first term on the right-hand side on the second line is the integral of a space-derivative, it therefore vanishes for vanishing (spatial) boundary conditions. In the last line, we applied inverse Fourier and Wigner transforms and used the gradient expansion to relate the convolution product to the Wigner transforms.

The lepton self-energy can be related to the sterile neutrino self-energy, allowing us to write the equations above in terms of the sterile neutrino self-energy and propagator. Its one-loop expression involves a loop of sterile neutrino (of propagator S_N where we restore an explicit N subscript for clarity) and Higgs propagators,

$$i\tilde{\Sigma}^{<,>}_{l,a}(p) = g_W \int \frac{\mathrm{d}^4k}{(2\pi)^4} Y^*_{Ia}Y_{Ja}P_R\ i\tilde{S}^{<,>}_{N,IJ}(k) i\Delta^{<,>}_{H}(-(k-p)) \ , \tag{F.3}$$

where the indices I, J are implicitly summed over. In the equation for the lepton asymmetry, it appears multiplied by a lepton propagator in the combination

$$\begin{aligned}\int \frac{\mathrm{d}^4p}{(2\pi)^4}\, i\tilde{\Sigma}^<_{l,a}(p) i\tilde{S}^>_{l,a}(p) &= g_W Y^*_{Ia} Y_{Ja} \int \frac{\mathrm{d}^4p}{(2\pi)^4}\frac{\mathrm{d}^4k}{(2\pi)^4}\, P_R i\tilde{S}^<_{N,IJ}(k) i\Delta^<_H(-(k-p)) iS^>_{l,a}(p) \\ &= g_W Y^*_{Ia} Y_{Ja} P_R \int \frac{\mathrm{d}^4k}{(2\pi)^4} i\tilde{S}^<_{N,IJ}(k) \left[\int \frac{\mathrm{d}^4p}{(2\pi)^4}\, i\Delta^>_H(k-p) i\tilde{S}^>_{l,a}(p)\right] \\ &= P_R \int \frac{\mathrm{d}^4k}{(2\pi)^4} i\tilde{S}^<_{N,IJ}(k) P_L i\tilde{\Sigma}^>_{JI;a}(k)\ . \end{aligned} \tag{F.4}$$

We defined

$$\begin{aligned} i\tilde{\Sigma}^{<,>}_{JI;a}(k) = g_W \int \frac{\mathrm{d}^4p}{(2\pi)^4} \Big[& Y_{Ja} Y^*_{Ia} P_L\ i\tilde{S}^{<,>}_{l,a}(p) i\Delta^{<,>}_H(k-p) \\ & + Y^*_{Ja} Y_{Ia} P_R\ C i\tilde{S}^{>,<}_{l,a}(-p)^T C^{-1} i\Delta^{>,<}_H(-k+p)\Big]\ . \end{aligned} \tag{F.5}$$

keeping simply the flavor a contribution to the total sterile neutrino self-energy $i\Sigma^{<,>}_{JI}(k)$. The right-hand term of (F.2) is then expressed in terms of the sterile neutrino self-energy $i\Sigma^{<,>}_{JI}$ and propagator $iS^{<,>}_N$. They both contain an equilibrium part and a small deviation; keeping only first-order terms in the deviations, the equation for the lepton asymmetry becomes [143, 167]

$$\begin{aligned}\frac{\mathrm{d}N_{L_a}}{\mathrm{d}t} &= \frac{i}{2}\int \frac{\mathrm{d}^4k}{(2\pi)^4} \mathrm{Tr}\left[P_R \tilde{\Sigma}^>_a P_L \tilde{S}^>_N - P_R \tilde{S}^<_N P_L \tilde{\Sigma}^<_a\right] + \text{ h.c.} \\ &\simeq \frac{1}{2}\int \frac{\mathrm{d}^4k}{(2\pi)^4} \mathrm{Tr}\left[P_R\left\{\delta_a\tilde{\mathbf{\Sigma}}^<, i\tilde{\mathcal{S}}^>_{\mathrm{ad}}\right\} - P_R\left\{\delta_a\tilde{\mathbf{\Sigma}}^>, i\tilde{\mathcal{S}}^<_{\mathrm{ad}}\right\}\right] \\ &\quad + \frac{1}{2}\int \frac{\mathrm{d}^4k}{(2\pi)^4} \mathrm{Tr}\left[P_R \tilde{\mathbf{\Sigma}}^<_{\mathrm{eq},a} i\delta\tilde{\mathcal{S}}^> - P_R \tilde{\mathbf{\Sigma}}^>_{\mathrm{eq},a} i\delta\tilde{\mathcal{S}}^<\right] + \text{ h.c.} \end{aligned} \tag{F.6}$$

where we extracted the contribution $\tilde{\mathbf{\Sigma}}^<_{\mathrm{eq},a}$ to the flavor a of the total (equilibrium) self-energy, replacing $\left(YY^\dagger\right)_{IJ}$ by $Y_{Ia}Y^*_{Ja}$,

$$\left(\tilde{\mathbf{\Sigma}}_{\mathrm{eq},a}\right)_{IJ} \equiv g_W \left[Y_{Ia}Y^*_{Ja}P_L + Y^*_{Ia}Y_{Ja}P_R\right] \tilde{\hat{\mathbf{\Sigma}}}_{\mathrm{eq}}\ . \tag{F.7}$$

This leads to

$$\frac{\mathrm{d}N_{L_a}}{\mathrm{d}t} = \mathcal{W} + S_a\ , \tag{F.8}$$

where

$$\mathcal{W} \equiv \frac{1}{2}\int \frac{\mathrm{d}^4k}{(2\pi)^4} \mathrm{Tr}\left[P_R\left\{\delta_a\tilde{\mathbf{\Sigma}}^<, i\tilde{\mathcal{S}}^>_{\mathrm{ad}}\right\} - P_R\left\{\delta_a\tilde{\mathbf{\Sigma}}^>, i\tilde{\mathcal{S}}^<_{\mathrm{ad}}\right\}\right]\ , \tag{F.9}$$

$$S_a \equiv \frac{1}{2}\int \frac{\mathrm{d}^4k}{(2\pi)^4} \mathrm{Tr}\left[P_R \tilde{\mathbf{\Sigma}}^<_{\mathrm{eq},a} i\delta\tilde{\mathcal{S}}^> - P_R \tilde{\mathbf{\Sigma}}^>_{\mathrm{eq},a} i\delta\tilde{\mathcal{S}}^<\right] + \text{ h.c.}\ . \tag{F.10}$$

Both expressions can be manipulated into clear and simpler forms. Let us start with the washout term $\mathcal{W}$. We can use the equation (E.12) for relating the anti-commutator in $\mathcal{W}$ to

the chemical potentials

$$\mathcal{W} = -\frac{\mu_a + \mu_\phi}{T} g_W \sum_{I,s} |Y_{Ia}|^2 \int \frac{\mathrm{d}^3\mathbf{k}}{(2\pi)^3} f_{FD}(\omega_I)(1 - f_{FD}(\omega_I)) \mathrm{Tr}\left[P_R \left\{\tilde{\tilde{\mathbf{\Sigma}}}^{\rho}_{\mathrm{eq}}(s\omega_I, \mathbf{k}), \mathbf{P}^s_I\right\}\right]$$
$$\equiv -W_a \frac{\mu_a + \mu_\phi}{T} \ , \tag{F.11}$$

$$W_a \equiv \sum_I \sum_s |Y_{Ia}|^2 \int \frac{\mathrm{d}^3\mathbf{k}}{(2\pi)^3} f_{FD}(\omega_I)(1 - f_{FD}(\omega_I)) \mathrm{Tr}\left[P_R \left\{\tilde{\tilde{\mathbf{\Sigma}}}^{\rho}_{\mathrm{eq}}(s\omega_I, \mathbf{k}), \mathbf{P}^s_I\right\}\right] \tag{F.12}$$
$$= \sum_I \sum_s |Y_{Ia}|^2 \int \frac{\mathrm{d}^3\mathbf{k}}{(2\pi)^3} \mathrm{Tr}\left[P_R \{\mathbf{F}^{\rho,s}_I, \mathbf{P}^s_I\}\right] \ . \tag{F.13}$$

The source term S_a can be simplified by recalling that the sterile neutrino propagators, at equal time, satisfy the spectral (or sum) rule (5.41)

$$i\delta\mathcal{S}^{>} = i\delta\mathcal{S}^{<} \ , \tag{F.14}$$

such that

$$S_a = -\frac{1}{2} \int \frac{\mathrm{d}^4k}{(2\pi)^4} \mathrm{Tr}\left[P_R \left(\tilde{\mathbf{\Sigma}}^{<}_{\mathrm{eq},a} - \tilde{\mathbf{\Sigma}}^{>}_{\mathrm{eq},a}\right) i\delta\tilde{\mathcal{S}}^{<}\right] + \text{ h.c.} \tag{F.15}$$
$$= \int \frac{\mathrm{d}^3\mathbf{k}}{(2\pi)^3} \mathrm{Tr}\left[P_R \left(\mathbf{\Sigma}^{\rho}_{\mathrm{eq},\mathbf{k},a} * \delta\mathcal{S}^{<}_{\mathbf{k}}\right)(t,t) + \text{ h.c.}\right] \tag{F.16}$$

where we recovered the convolution product by integrating over k^0, and used the gradient expansion. The convolution product with the function $\delta\mathcal{S}_{\mathbf{k}}$ makes the effective self-energy appear. Together with the projection of the propagator in terms of mass- and coherence-shell, we obtain an S_a term given in terms of the $\delta f^{ss'}_{h,IJ}$, like in [167],

$$S_a = \sum_{h,s,s'} \sum_{I,J} \int \frac{\mathrm{d}^3\mathbf{k}}{(2\pi)^3} \ \mathrm{Tr}\left[\left(P_R \mathbf{\Sigma}^{\mathrm{eff},\rho}_{\mathrm{eq},\mathbf{k},a,JI} + \left(\mathbf{\Sigma}^{\mathrm{eff},\rho}_{\mathrm{eq},\mathbf{k},a,IJ}\right)^\dagger P_R\right) \mathcal{P}^{ss'}_{h,IJ}\right] \ \delta f^{ss'}_{h,IJ} \ . \tag{F.17}$$

The change in lepton charge is thus given by the equation

$$\frac{\mathrm{d}N_{L_a}}{\mathrm{d}t} = -W_a \frac{\mu_a + \mu_\phi}{T} + S_a \ . \tag{F.18}$$

This equation was derived without considering the spectator effects. If we add them, there are actually other interactions that would modify a lepton asymmetry. The number Δ_a corresponding to the quantum number $B/3 - L_a$ is better suited than N_{L_a}, as it can only receive a source from the sterile sector and the lepton number violating Yukawa couplings. What we computed should actually be the evolution of the charge Δ_a, with a minus sign (because of the minus sign in front of L_a in the definition of Δ_a).

Moreover, including the expansion of the Universe and recalling that Δ_a is a rescaled quantity, we get the final equation used in the text

$$T^3 \frac{\mathrm{d}\Delta_a}{\mathrm{d}t} = W_a \frac{\mu_a + \mu_\phi}{T} - S_a \ . \tag{F.19}$$

Appendix G

Relativistic and non-relativistic projectors

The different coefficients in the master equations (5.138) were derived from a self-energy valid for all values of the masses. It has a quite complicated form in general. In order to get a better physical understanding, we give here expressions in two extreme regimes of interest for us, the Non-Relativistic (NR) regime $M \gg T$ and the Ultra-Relativistic (UR) one $M \ll T$.

NR regime For large values of the mass $M \gg T$, the on-shell 4-momentum on which the self-energies are evaluated is approximately

$$k_{\rm NR} \approx (M, 0, 0, 0) \ . \tag{G.1}$$

The projectors on energy $\mathcal{P}^{ss'}_{h,IJ}$ can also be simplified for a non-relativistic field,

$$\mathbf{P}^s_I = \frac{1}{2}\left(\mathbb{I} + s\frac{\mathbf{H}^I_0}{\omega_I}\right) \simeq \frac{1}{2}\left(\mathbb{I} + s\gamma_0\right) \ , \tag{G.2}$$

$$\mathcal{P}^{ss'}_{h,IJ} = P_h \frac{N^{ss'}_{IJ}\,(s+s')}{4}\left(\mathbb{I} + s\gamma^0\right) = P_h s\delta_{ss'}\frac{1}{2}\left(\mathbb{I} + s\gamma^0\right) \ , \tag{G.3}$$

where we calculated the normalization constants $N^{ss'}_{IJ}$ in the NR regime

$$N^{ss'}_{IJ} \equiv \left(\frac{2\omega_I\omega_J}{\omega_I\omega_I + ss'\left(M_IM_J - |\mathbf{k}|^2\right)}\right)^{1/2} \simeq \delta_{s,s'} + \frac{2M_IM_J}{(M_I+M_J)|\mathbf{k}|}\delta_{s,-s'} \ . \tag{G.4}$$

UR regime For lower values of the mass $M \ll T$, the on-shell four-momentum is approximately

$$k_{\rm UR} \approx (|\mathbf{k}|, \mathbf{k}) \ . \tag{G.5}$$

The various projectors give

$$\mathbf{P}^s_I \simeq \frac{1}{2}\left(\mathbb{I} + s\frac{M_I}{|\mathbf{k}|}\gamma^0 + s\gamma^0\boldsymbol{\gamma}\cdot\hat{\mathbf{k}}\right) \ , \tag{G.6}$$

$$
\begin{aligned}
\mathcal{P}^{ss'}_{h,IJ} &\simeq P_h \frac{N^{ss'}_{IJ}\,(1-ss')}{4}\left(\gamma^0 + s'\boldsymbol{\gamma}\cdot\hat{\mathbf{k}} - 2\frac{M_I+M_J}{|\mathbf{k}|}\gamma^0\boldsymbol{\gamma}\cdot\hat{\mathbf{k}} + 2s'\frac{M_I-M_J}{|\mathbf{k}|} - 2\frac{M_IM_J}{|\mathbf{k}|^2}\gamma^0\right) \\
&\quad + P_h \frac{N^{ss'}_{IJ}\,(1+ss')}{4}\frac{M_I+M_J}{2|\mathbf{k}|}\gamma^0\left(s'\gamma^0 + \boldsymbol{\gamma}\cdot\hat{\mathbf{k}} + \frac{M_IM_J}{M_I+M_J}\right) \\
&\simeq P_h \frac{\delta_{s,-s'}}{2}\left(\gamma^0 + s'\boldsymbol{\gamma}\cdot\hat{\mathbf{k}}\right) + P_h s'\frac{\delta_{s,s'}}{2}\gamma^0\left(\gamma^0 + s'\boldsymbol{\gamma}\cdot\hat{\mathbf{k}}\right) \\
&= P_h \frac{1}{2}\left(\gamma^0 + s'\boldsymbol{\gamma}\cdot\hat{\mathbf{k}}\right)\left(\delta_{s,-s'}\mathbb{I} + s'\delta_{ss'}\gamma^0\right)\ , \qquad \text{(G.7)}
\end{aligned}
$$

where the normalization constants in the UR regime give

$$
N^{ss'}_{IJ} \equiv \left(\frac{2\omega_I\omega_J}{\omega_I\omega_I + ss'\,(M_IM_J - |\mathbf{k}|^2)}\right)^{1/2} \simeq \frac{2|\mathbf{k}|}{M_I+M_J}\delta_{s,s'} + \delta_{s,-s'}\ . \qquad \text{(G.8)}
$$

Bibliography

[1] P.J.E. Peebles, *Tests of Cosmological Models Constrained by Inflation*, *Astrophys. J.* **284** (1984) 439.

[2] P.J.E. Peebles and B. Ratra, *The cosmological constant and dark energy*, *Reviews of Modern Physics* **75** (2003) 559–606 [astro-ph/0207347].

[3] N. Aghanim, Y. Akrami, M. Ashdown, J. Aumont, C. Baccigalupi, M. Ballardini et al., *Planck2018 results: VI. Cosmological parameters*, *Astronomy & Astrophysics* **641** (2020) A6 [1807.06209].

[4] B.D. Fields, K.A. Olive, T.-H. Yeh and C. Young, *Big-Bang Nucleosynthesis after Planck*, *Journal of Cosmology and Astroparticle Physics* **2020** (2020) 010–010 [1912.01132].

[5] R.H. Cyburt, B.D. Fields, K.A. Olive and T.-H. Yeh, *Big bang nucleosynthesis: Present status*, *Reviews of Modern Physics* **88** (2016) [1505.01076].

[6] G.J. Mathews, A. Kedia, N. Sasankan, M. Kusakabe, Y. Luo, T. Kajino et al., *Cosmological Solutions to the Lithium Problem*, *JPS Conf. Proc.* **31** (2020) 011033 [1909.01245].

[7] J.M. Cline, *Baryogenesis*, in *Les Houches Summer School - Session 86: Particle Physics and Cosmology: The Fabric of Spacetime*, 9, 2006 [hep-ph/0609145].

[8] E.W. Kolb and M.S. Turner, *The Early Universe*, *Nature* **294** (1981) 521.

[9] A.H. Guth, *The Inflationary Universe: A Possible Solution to the Horizon and Flatness Problems*, *Phys. Rev. D* **23** (1981) 347.

[10] A.D. Sakharov, *Violation of CP Invariance, C asymmetry, and baryon asymmetry of the universe*, *Pisma Zh. Eksp. Teor. Fiz.* **5** (1967) 32.

[11] M. Fukugita and T. Yanagida, *Baryogenesis without grand unification*, *Phys. Lett. B* **174** (1986) 45.

[12] G. Luders, *Proof of the TCP theorem*, *Annals Phys.* **2** (1957) 1.

[13] Y. Fukuda, T. Hayakawa, E. Ichihara, K. Inoue, K. Ishihara, H. Ishino et al., *Evidence for Oscillation of Atmospheric Neutrinos*, *Physical Review Letters* **81** (1998) 1562–1567 [hep-ex/9807003].

[14] SNO collaboration, *Measurement of the rate of $\nu_e + d \to p + p + e^-$ interactions produced by ^8B solar neutrinos at the Sudbury Neutrino Observatory*, *Phys. Rev. Lett.* **87** (2001) 071301 [nucl-ex/0106015].

[15] B. Dasgupta and J. Kopp, *Sterile neutrinos*, *Physics Reports* **928** (2021) 1–63 [2106.05913].

[16] E. Witten, *Cosmological consequences of a light Higgs boson*, *Nuclear Physics B* **177** (1981) 477.

[17] A.H. Guth and E.J. Weinberg, *Cosmological consequences of a first-order phase transition in the $SU(5)$ grand unified model*, *Phys. Rev. D* **23** (1981) 876.

[18] R. Hempfling, *The next-to-minimal Coleman-Weinberg model*, *Physics Letters B* **379** (1996) 153–158 [hep-ph/9604278].

[19] K.A. Meissner and H. Nicolai, *Conformal symmetry and the Standard Model*, *Physics Letters B* **648** (2007) 312–317 [hep-th/0612165].

[20] W.-F. Chang, J.N. Ng and J.M.S. Wu, *Shadow Higgs boson from a scale-invariant hidden $U(1)$ model*, *Physical Review D* **75** (2007) [hep-ph/0701254].

[21] R. Foot, A. Kobakhidze and R.R. Volkas, *Electroweak Higgs as a pseudo-Goldstone boson of broken scale invariance*, *Physics Letters B* **655** (2007) 156–161 [0704.1165].

[22] LIGO Scientific, Virgo collaboration, *Observation of Gravitational Waves from a Binary Black Hole Merger*, *Phys. Rev. Lett.* **116** (2016) 061102 [1602.03837].

[23] M. Cataldi and B. Shakya, *Leptogenesis via Bubble Collisions*, 2407.16747.

[24] J. Turner and Y.-L. Zhou, *Leptogenesis via Varying Weinberg Operator: the Closed-Time-Path Approach*, 1808.00470.

[25] S. Pascoli, J. Turner and Y.-L. Zhou, *Leptogenesis via a varying Weinberg operator: a semi-classical approach*, *Chinese Physics C* **43** (2019) 033101 [1808.00475].

[26] B. Shuve and C. Tamarit, *Phase transitions and baryogenesis from decays*, *Journal of High Energy Physics* **2017** (2017) [1704.01979].

[27] E. Fernández-Martínez, J. López-Pavón, T. Ota and S. Rosauro-Alcaraz, *ν electroweak baryogenesis*, *JHEP* **10** (2020) 063 [2007.11008].

[28] P. Huang and K.-P. Xie, *Leptogenesis triggered by a first-order phase transition*, *Journal of High Energy Physics* **2022** (2022) [2206.04691v2].

[29] A. Dasgupta, P.B. Dev, A. Ghoshal and A. Mazumdar, *Gravitational wave pathway to testable leptogenesis*, *Physical Review D* **106** (2022) [2206.07032].

[30] D. Borah, A. Dasgupta and I. Saha, *LIGO-Virgo constraints on dark matter and leptogenesis triggered by a first order phase transition at high scale*, *Phys. Rev. D* **109** (2024) 095034 [2304.08888].

[31] E.J. Chun, T.P. Dutka, T.H. Jung, X. Nagels and M. Vanvlasselaer, *Bubble-assisted leptogenesis*, *JHEP* **09** (2023) 164 [2305.10759].

[32] I. Baldes, S. Blasi, A. Mariotti, A. Sevrin and K. Turbang, *Baryogenesis via relativistic bubble expansion*, *Phys. Rev. D* **104** (2021) 115029 [2106.15602].

[33] K. Petraki and A. Kusenko, *Dark-matter sterile neutrinos in models with a gauge singlet in the Higgs sector*, *Physical Review D* **77** (2008) [0711.4646].

[34] M. Shaposhnikov and I. Tkachev, *The νMSM, inflation, and dark matter*, *Physics Letters B* **639** (2006) 414–417 [hep-ph/0604236].

[35] A. Caputo, P. Hernandez and N. Rius, *Leptogenesis from oscillations and dark matter*, *The European Physical Journal C* **79** (2019) [1807.03309v3].

[36] M. Escudero and S.J. Witte, *The Hubble tension as a hint of leptogenesis and neutrino mass generation*, *The European Physical Journal C* **81** (2021) [2103.03249].

[37] V.V. Khoze and G. Ro, *Leptogenesis and neutrino oscillations in the classically conformal standard model with the Higgs portal*, *Journal of High Energy Physics* **2013** (2013) [1307.3764].

[38] V.V. Khoze and A.D. Plascencia, *Dark matter and leptogenesis linked by classical scale invariance*, *Journal of High Energy Physics* **2016** (2016) [1605.06834].

[39] O. Fischer, M. Lindner and S. van der Woude, *Robustness of ARS leptogenesis in scalar extensions*, *Journal of High Energy Physics* **2022** (2022) [2110.14499].

[40] K.A. Olive, *The Thermodynamics of the Quark - Hadron Phase Transition in the Early Universe*, *Nucl. Phys. B* **190** (1981) 483.

[41] E. Suhonen, *The Quark - Hadron Phase Transition in the Early Universe*, *Phys. Lett. B* **119** (1982) 81.

[42] S.A. Bonometto and M. Sakellariadou, *Physical processes in the Universe at the epoch of the quark-hadron transition*, *Astrophys. J.* **282** (1984) 370.

[43] V. Kuzmin, V. Rubakov and M. Shaposhnikov, *On anomalous electroweak baryon-number non-conservation in the early universe*, *Physics Letters B* **155** (1985) 36.

[44] S. Khlebnikov and M. Shaposhnikov, *The statistical theory of anomalous fermion number non-conservation*, *Nuclear Physics B* **308** (1988) 885.

[45] M. Dine, R.G. Leigh, P. Huet, A. Linde and D. Linde, *Towards the theory of the electroweak phase transition*, *Physical Review D* **46** (1992) 550–571.

[46] C.J. Hogan, *Magnetohydrodynamic effects of a first-order cosmological phase transition*, *Phys. Rev. Lett.* **51** (1983) 1488.

[47] E. Witten, *Cosmic separation of phases*, *Phys. Rev. D* **30** (1984) 272.

[48] T. Boeckel, S. Schettler and J. Schaffner-Bielich, *The cosmological QCD phase transition revisited*, *Progress in Particle and Nuclear Physics* **66** (2011) 266–270 [1012.3342].

[49] D. Schwarz, *The first second of the universe*, *Annalen der Physik* **515** (2003) 220–270 [astro-ph/0303574].

[50] C.-W. Chiang, M.J. Ramsey-Musolf and E. Senaha, *Standard model with a complex scalar singlet: Cosmological implications and theoretical considerations*, *Physical Review D* **97** (2018) [1707.09960].

[51] A. Mégevand and S. Ramírez, *Bubble nucleation and growth in very strong cosmological phase transitions*, *Nuclear Physics B* **919** (2017) 74–109 [1611.05853].

[52] P. Athron, C. Balázs and L. Morris, *Supercool subtleties of cosmological phase transitions*, *Journal of Cosmology and Astroparticle Physics* **2023** (2023) 006 [2212.07559].

[53] S.R. Coleman, *The Fate of the False Vacuum. 1. Semiclassical Theory*, *Phys. Rev. D* **15** (1977) 2929.

[54] A. Linde, *On the vacuum instability and the Higgs meson mass*, *Physics Letters B* **70** (1977) 306.

[55] A. Linde, *Fate of the false vacuum at finite temperature: Theory and applications*, *Physics Letters B* **100** (1981) 37.

[56] A. Linde, *Decay of the false vacuum at finite temperature*, *Nuclear Physics B* **216** (1983) 421.

[57] M. Hindmarsh, M. Lüben, J. Lumma and M. Pauly, *Phase transitions in the early universe*, *SciPost Physics Lecture Notes* (2021) [2008.09136].

[58] C.L. Wainwright, *CosmoTransitions: Computing cosmological phase transition temperatures and bubble profiles with multiple fields*, *Computer Physics Communications* **183** (2012) 2006–2013 [1109.4189].

[59] A. Masoumi, K.D. Olum and B. Shlaer, *Efficient numerical solution to vacuum decay with many fields*, *Journal of Cosmology and Astroparticle Physics* **2017** (2017) 051–051 [1610.06594].

[60] P. Athron, C. Balázs, M. Bardsley, A. Fowlie, D. Harries and G. White, *Bubbleprofiler: Finding the field profile and action for cosmological phase transitions*, *Computer Physics Communications* **244** (2019) 448.

[61] K. Enqvist, J. Ignatius, K. Kajantie and K. Rummukainen, *Nucleation and bubble growth in a first-order cosmological electroweak phase transition*, *Phys. Rev. D* **45** (1992) 3415.

[62] H.-K. Guo, K. Sinha, D. Vagie and G. White, *The benefits of diligence: how precise are predicted gravitational wave spectra in models with phase transitions?*, *Journal of High Energy Physics* **2021** (2021) [2103.06933].

[63] G.D. Moore and T. Prokopec, *How fast can the wall move? A study of the electroweak phase transition dynamics*, *Physical Review D* **52** (1995) 7182–7204 [hep-ph/9506475].

[64] D. Bödeker and G.D. Moore, *Can electroweak bubble walls run away?*, *Journal of Cosmology and Astroparticle Physics* **2009** (2009) 009–009 [0903.4099].

[65] S. Höche, J. Kozaczuk, A.J. Long, J. Turner and Y. Wang, *Towards an all-orders calculation of the electroweak bubble wall velocity*, *Journal of Cosmology and Astroparticle Physics* **2021** (2021) 009 [2007.10343].

[66] A. Azatov and M. Vanvlasselaer, *Bubble wall velocity: heavy physics effects*, *Journal of Cosmology and Astroparticle Physics* **2021** (2021) 058–058 [2010.02590].

[67] X. Wang, F.P. Huang and X. Zhang, *Phase transition dynamics and gravitational wave spectra of strong first-order phase transition in supercooled universe*, *Journal of Cosmology and Astroparticle Physics* **2020** (2020) 045–045 [2003.08892].

[68] C. Badger, B. Fornal, K. Martinovic, A. Romero, K. Turbang, H.-K. Guo et al., *Probing early Universe supercooled phase transitions with gravitational wave data*, *Physical Review D* **107** (2023) [2209.14707].

[69] M. Lewicki and V. Vaskonen, *Gravitational waves from bubble collisions and fluid motion in strongly supercooled phase transitions*, *The European Physical Journal C* **83** (2023) [2208.11697].

[70] Y. Bai and M. Korwar, *Cosmological constraints on first-order phase transitions*, *Physical Review D* **105** (2022) [2109.14765].

[71] N. Christensen, *Stochastic gravitational wave backgrounds*, *Reports on Progress in Physics* **82** (2018) 016903 [1811.08797].

[72] G. Agazie, A. Anumarlapudi, A.M. Archibald, Z. Arzoumanian, P.T. Baker, B. Bécsy et al., *The NANOGrav 15 yr Data Set: Evidence for a Gravitational-wave Background*, *The Astrophysical Journal Letters* **951** (2023) L8 [2306.16213].

[73] D.J. Weir, *Gravitational waves from a first-order electroweak phase transition: a brief review*, *Philosophical Transactions of the Royal Society A: Mathematical, Physical and Engineering Sciences* **376** (2018) 20170126 [1705.01783].

[74] P. Athron, C. Balázs, A. Fowlie, L. Morris and L. Wu, *Cosmological phase transitions: From perturbative particle physics to gravitational waves*, *Progress in Particle and Nuclear Physics* **135** (2024) 104094 [2305.02357].

[75] C. Caprini, M. Hindmarsh, S. Huber, T. Konstandin, J. Kozaczuk, G. Nardini et al., *Science with the space-based interferometer eLISA. II: gravitational waves from cosmological phase transitions*, *Journal of Cosmology and Astroparticle Physics* **2016** (2016) 001–001 [1512.06239].

[76] M. Hindmarsh, S.J. Huber, K. Rummukainen and D.J. Weir, *Shape of the acoustic gravitational wave power spectrum from a first order phase transition*, *Phys. Rev. D* **96** (2017) 103520 [1704.05871].

[77] LISA Cosmology Working Group collaboration, *Gravitational waves from first-order phase transitions in LISA: reconstruction pipeline and physics interpretation*, 2403.03723.

[78] C. Caprini, M. Chala, G.C. Dorsch, M. Hindmarsh, S.J. Huber, T. Konstandin et al., *Detecting gravitational waves from cosmological phase transitions with LISA: an update*, *Journal of Cosmology and Astroparticle Physics* **2020** (2020) 024–024 [1910.13125].

[79] A. Roper Pol, A. Neronov, C. Caprini, T. Boyer and D. Semikoz, *LISA and γ-ray telescopes as multi-messenger probes of a first-order cosmological phase transition*, 2307.10744.

[80] M.B. Gavela, P. Hernandez, J. Orloff and O. Pene, *Standard model baryogenesis*, in *29th Rencontres de Moriond: Electroweak Interactions and Unified Theories*, pp. 401–410, 1994 [hep-ph/9407403].

[81] D.E. Morrissey and M.J. Ramsey-Musolf, *Electroweak baryogenesis*, *New Journal of Physics* **14** (2012) 125003 [1206.2942].

[82] V.A. Rubakov and M.E. Shaposhnikov, *Electroweak baryon number non-conservation in the early Universe and in high-energy collisions*, *Physics-Uspekhi* **39** (1996) 461–502 [hep-ph/9603208].

[83] A. Riotto, *Theories of baryogenesis*, in *ICTP Summer School in High-Energy Physics and Cosmology*, pp. 326–436, 7, 1998 [hep-ph/9807454].

[84] A.I. Bochkarev and M.E. Shaposhnikov, *Electroweak Production of Baryon Asymmetry and Upper Bounds on the Higgs and Top Masses*, *Mod. Phys. Lett. A* **2** (1987) 417.

[85] K. Kajantie, M. Laine, K. Rummukainen and M.E. Shaposhnikov, *Is there a hot electroweak phase transition at $m_H \gtrsim m_W$?*, *Phys. Rev. Lett.* **77** (1996) 2887 [hep-ph/9605288].

[86] L.s. Bento, *Sphaleron relaxation temperatures*, *Journal of Cosmology and Astroparticle Physics* **2003** (2003) 002–002 [hep-ph/0304263].

[87] M. Laine and A. Vuorinen, *Basics of Thermal Field Theory: A Tutorial on Perturbative Computations*, Springer International Publishing (2016), 10.1007/978-3-319-31933-9, [1701.01554].

[88] M.E. Carrington, *Effective potential at finite temperature in the standard model*, *Phys. Rev. D* **45** (1992) 2933.

[89] M. Dine, R.G. Leigh, P. Huet, A. Linde and D. Linde, *Comments on the electroweak phase transition*, *Physics Letters B* **283** (1992) 319–325 [hep-ph/9203201].

[90] A. Brignole, J. Espinosa, M. Quirós and F. Zwirner, *Aspects of the electroweak phase transition in the minimal supersymmetric standard model*, *Physics Letters B* **324** (1994) 181–191 [hep-ph/9312296].

[91] W. Buchmuller, Z. Fodor, T. Helbig and D. Walliser, *The weak electroweak phase transition*, *Annals of Physics* **234** (1994) 260–299 [hep-ph/9303251v1].

[92] S. Profumo, M.J. Ramsey-Musolf and G. Shaughnessy, *Singlet Higgs phenomenology and the electroweak phase transition*, *Journal of High Energy Physics* **2007** (2007) 010–010 [0705.2425].

[93] A. Ahriche, *What is the criterion for a strong first order electroweak phase transition in singlet models?*, *Physical Review D* **75** (2007) [hep-ph/0701192].

[94] A. Noble and M. Perelstein, *Higgs self-coupling as a probe of the electroweak phase transition*, *Physical Review D* **78** (2008) [0711.3018].

[95] J.M. Cline, G. Laporte, H. Yamashita and S. Kraml, *Electroweak phase transition and LHC signatures in the singlet Majoron model*, *Journal of High Energy Physics* **2009** (2009) 040–040 [0905.2559].

[96] G. 't Hooft, *Symmetry Breaking through Bell-Jackiw Anomalies*, *Phys. Rev. Lett.* **37** (1976) 8.

[97] Callan, C.G. and Dashen, R.F. and Gross, D.J., *The structure of the gauge theory vacuum*, *Physics Letters B* **63** (1976) 334.

[98] R. Jackiw and C. Rebbi, *Vacuum Periodicity in a Yang-Mills Quantum Theory*, *Phys. Rev. Lett.* **37** (1976) 172.

[99] L. McLerran, E. Mottola and M.E. Shaposhnikov, *Sphalerons and axion dynamics in high-temperature QCD*, *Phys. Rev. D* **43** (1991) 2027.

[100] R.N. Mohapatra and X. Zhang, *QCD sphalerons at high temperature and baryogenesis at the electroweak scale*, *Phys. Rev. D* **45** (1992) 2699.

[101] S.L. Adler, *Axial-vector vertex in spinor electrodynamics*, *Phys. Rev.* **177** (1969) 2426.

[102] J.A. Harvey and M.S. Turner, *Cosmological baryon and lepton number in the presence of electroweak fermion-number violation*, *Phys. Rev. D* **42** (1990) 3344.

[103] E. Nardi, Y. Nir, E. Roulet and J. Racker, *The importance of flavor in leptogenesis*, *Journal of High Energy Physics* **2006** (2006) 164–164 [hep-ph/0601084].

[104] A. Abada, S. Davidson, A. Ibarra, F.-X. Josse-Michaux, M. Losada and A. Riotto, *Flavour matters in leptogenesis*, *Journal of High Energy Physics* **2006** (2006) 010–010 [hep-ph/0605281].

[105] S. Davidson, E. Nardi and Y. Nir, *Leptogenesis*, *Physics Reports* **466** (2008) 105–177 [0802.2962].

[106] B. Garbrecht and P. Schwaller, *Spectator effects during Leptogenesis in the strong washout regime*, *Journal of Cosmology and Astroparticle Physics* **2014** (2014) 012–012 [1404.2915].

[107] I. Esteban, M. Gonzalez-Garcia, M. Maltoni, T. Schwetz and A. Zhou, *The fate of hints: updated global analysis of three-flavor neutrino oscillations*, in *NuFIT 5.3*, Mar., 2024, http://www.nu-fit.org/ [2007.14792].

[108] P. Minkowski, $\mu \to e\gamma$ *at a rate of one out of 109 muon decays?*, *Physics Letters B* **67** (1977) 421.

[109] T. Yanagida, *Horizontal gauge symmetry and masses of neutrinos*, *Conf. Proc. C* **7902131** (1979) 95.

[110] M. Gell-Mann, P. Ramond and R. Slansky, *Complex Spinors and Unified Theories*, *Conf. Proc. C* **790927** (1979) 315 [1306.4669].

[111] Mohapatra, Rabindra N. and Senjanović, Goran, *Neutrino Mass and Spontaneous Parity Nonconservation*, *Phys. Rev. Lett.* **44** (1980) 912.

[112] M. Magg and C. Wetterich, *Neutrino mass problem and gauge hierarchy*, *Physics Letters B* **94** (1980) 61.

[113] T.P. Cheng and L.-F. Li, *Neutrino masses, mixings, and oscillations in SU(2)× U(1) models of electroweak interactions*, *Phys. Rev. D* **22** (1980) 2860.

[114] G. Lazarides, Q. Shafi and C. Wetterich, *Proton lifetime and fermion masses in an SO(10) model*, *Nuclear Physics B* **181** (1981) 287.

[115] R.N. Mohapatra and G. Senjanović, *Neutrino masses and mixings in gauge models with spontaneous parity violation*, *Phys. Rev. D* **23** (1981) 165.

[116] R. Foot, H. Lew, X.G. He and G.C. Joshi, *Seesaw Neutrino Masses Induced by a Triplet of Leptons*, *Z. Phys. C* **44** (1989) 441.

[117] C.H. Albright and S.M. Barr, *Leptogenesis in the type III seesaw mechanism*, *Physical Review D* **69** (2004) [hep-ph/0312224].

[118] B. Pontecorvo, *Mesonium and anti-mesonium*, *Sov. Phys. JETP* **6** (1957) 429.

[119] B. Pontecorvo, *Inverse beta processes and nonconservation of lepton charge*, *Zh. Eksp. Teor. Fiz.* **34** (1957) 247.

[120] Z. Maki, M. Nakagawa and S. Sakata, *Remarks on the unified model of elementary particles*, *Prog. Theor. Phys.* **28** (1962) 870.

[121] J. Casas and A. Ibarra, *Oscillating neutrinos and $\mu \to e,\gamma$*, *Nuclear Physics B* **618** (2001) 171–204 [hep-ph/0103065].

[122] I. Esteban, M. Gonzalez-Garcia, M. Maltoni, T. Schwetz and A. Zhou, *The fate of hints: updated global analysis of three-flavor neutrino oscillations*, in *NuFIT 5.2*, Sept., 2020, http://www.nu-fit.org/ [2007.14792].

[123] M.A. Luty, *Baryogenesis via leptogenesis*, *Phys. Rev. D* **45** (1992) 455.

[124] M. Pluemacher, *Baryogenesis and lepton number violation*, hep-ph/9604229.

[125] W. Buchmüller, P. Di Bari and M. Plümacher, *Leptogenesis for pedestrians*, *Annals of Physics* **315** (2005) 305–351 [hep-ph/0401240].

[126] R. Barbieri, P. Creminelli, A. Strumia and N. Tetradis, *Baryogenesis through leptogenesis*, *Nuclear Physics B* **575** (2000) 61–77 [hep-ph/9911315].

[127] H. Nielsen and Y. Takanishi, *Baryogenesis via lepton number violation in Anti-GUT model*, *Physics Letters B* **507** (2001) 241–251 [hep-ph/0101307].

[128] A. Abada, H. Aissaoui and M. Losada, *A model for leptogenesis at the TeV scale*, *Nuclear Physics B* **728** (2005) 55–66 [hep-ph/0409343].

[129] O. Vives, *Flavored leptogenesis: a successful thermal leptogenesis with N_1 mass below 10^8 GeV*, *Physical Review D* **73** (2006) [hep-ph/0512160].

[130] L. Covi, E. Roulet and F. Vissani, *CP violating decays in leptogenesis scenarios*, *Physics Letters B* **384** (1996) 169–174 [hep-ph/9605319].

[131] P.S.B. Dev, M. Garny, J. Klaric, P. Millington and D. Teresi, *Resonant enhancement in leptogenesis*, *International Journal of Modern Physics A* **33** (2018) 1842003 [1711.02863].

[132] A. Pilaftsis, *CP violation and baryogenesis due to heavy Majorana neutrinos*, *Physical Review D* **56** (1997) 5431–5451 [hep-ph/9707235].

[133] J. Liu and G. Segrè, *Reexamination of generation of baryon and lepton number asymmetries in the early universe by heavy particle decay*, *Physical Review D* **48** (1993) 4609–4612 [hep-ph/9304241].

[134] S. Davidson and A. Ibarra, *A lower bound on the right-handed neutrino mass from leptogenesis*, *Physics Letters B* **535** (2002) 25–32 [hep-ph/0202239].

[135] A. Pilaftsis and T.E. Underwood, *Resonant leptogenesis*, *Nuclear Physics B* **692** (2004) 303–345 [hep-ph/0309342].

[136] E.K. Akhmedov, V.A. Rubakov and A.Y. Smirnov, *Baryogenesis via Neutrino Oscillations*, *Phys. Rev. Lett.* **81** (1998) 1359 [hep-ph/9803255].

[137] M. Drewes, B. Garbrecht, P. Hernández, M. Kekic, J. Lopez-Pavon, J. Racker et al., *ARS leptogenesis*, *International Journal of Modern Physics A* **33** (2018) 1842002 [1711.02862].

[138] M. Drewes, B. Garbrecht, D. Gueter and J. Klarić, *Leptogenesis from oscillations of heavy neutrinos with large mixing angles*, *Journal of High Energy Physics* **2016** (2016) [1606.06690].

[139] J. Klarić, M. Shaposhnikov and I. Timiryasov, *Reconciling resonant leptogenesis and baryogenesis via neutrino oscillations*, *Phys. Rev. D* **104** (2021) 055010 [2103.16545].

[140] W. Buchmüller and M. Plümacher, *CP asymmetry in Majorana neutrino decays*, *Physics Letters B* **431** (1998) 354–362 [hep-ph/9710460].

[141] M. Drewes and B. Garbrecht, *Leptogenesis from a GeV Seesaw without Mass Degeneracy*, *Journal of High Energy Physics* **2013** (2012) [1206.5537].

[142] B. Garbrecht and M. Herranen, *Effective theory of resonant leptogenesis in the closed-time-path approach*, *Nuclear Physics B* **861** (2012) 17–52 [1112.5954].

[143] M. Garny, A. Kartavtsev and A. Hohenegger, *Leptogenesis from first principles in the resonant regime*, *Annals of Physics* **328** (2013) 26–63 [1112.6428].

[144] A. Davidson, *$B-L$ as the fourth color within an $\mathrm{SU}(2)_L \times \mathrm{U}(1)_R \times \mathrm{U}(1)$ model*, *Phys. Rev. D* **20** (1979) 776.

[145] R. Marshak and R. Mohapatra, *Quark-lepton symmetry and $B-L$ as the $U(1)$ generator of the electroweak symmetry group*, *Physics Letters B* **91** (1980) 222.

[146] R.N. Mohapatra and R.E. Marshak, *Local $B-L$ Symmetry of Electroweak Interactions, Majorana Neutrinos, and Neutron Oscillations*, *Phys. Rev. Lett.* **44** (1980) 1316.

[147] A. Davidson and K.C. Wali, *Universal seesaw mechanism?*, *Phys. Rev. Lett.* **59** (1987) 393.

[148] S. Coleman and E. Weinberg, *Radiative corrections as the origin of spontaneous symmetry breaking*, *Phys. Rev. D* **7** (1973) 1888.

[149] A. Fradette and M. Pospelov, *BBN for the LHC: Constraints on lifetimes of the Higgs portal scalars*, *Physical Review D* **96** (2017) [1706.01920].

[150] G. Moore and T. Prokopec, *Bubble Wall Velocity in a First Order Electroweak Phase Transition*, *Physical Review Letters* **75** (1995) 777–780.

[151] P.B. Greene and L. Kofman, *Preheating of fermions*, *Physics Letters B* **448** (1999) 6–12 [hep-ph/9807339].

[152] D.J.H. Chung, E.W. Kolb, A. Riotto and I.I. Tkachev, *Probing planckian physics: Resonant production of particles during inflation and features in the primordial power spectrum*, *Physical Review D* **62** (2000) [hep-ph/9910437].

[153] R. Watkins and L.M. Widrow, *Aspects of reheating in first-order inflation*, *Nuclear Physics B* **374** (1992) 446.

[154] G.F. Giudice, A. Riotto and I. Tkachev, *Thermal and non-thermal production of gravitinos in the early universe*, *Journal of High Energy Physics* **1999** (1999) 036–036 [hep-ph/9911302].

[155] J. Ellis, M.A. Garcia, D.V. Nanopoulos, K.A. Olive and M. Peloso, *Post-inflationary gravitino production revisited*, *Journal of Cosmology and Astroparticle Physics* **2016** (2016) 008–008 [1512.05701].

[156] S. Cléry, Y. Mambrini, K.A. Olive and S. Verner, *Gravitational portals in the early Universe*, *Physical Review D* **105** (2022) [2112.15214].

[157] P. Adshead, A.J. Long and E.I. Sfakianakis, *Gravitational leptogenesis, reheating, and models of neutrino mass*, *Physical Review D* **97** (2018) [1711.04800].

[158] G.M. Shore, *A model of gravitational leptogenesis*, 2106.09562.

[159] T. Prokopec, M.G. Schmidt and J. Weenink, *Exact solution of the Dirac equation with CP violation*, *Physical Review D* **87** (2013) [1301.4132].

[160] A. Ayala, J. Jalilian-Marian, L. McLerran and A.P. Vischer, *Scattering in the presence of electroweak phase transition bubble walls*, *Physical Review D* **49** (1994) 5559–5570 [hep-ph/9311296].

[161] M. Peloso and L. Sorbo, *Preheating of massive fermions after inflation: analytical results*, *Journal of High Energy Physics* **2000** (2000) 016–016 [hep-ph/0003045].

[162] B. Garbrecht, T. Prokopec and M.G. Schmidt, *Particle number in kinetic theory*, *The European Physical Journal C* **38** (2004) 135–143 [hep-th/0211219].

[163] N.N. Bogoljubov, *On a new method in the theory of superconductivity*, *Il Nuovo Cimento* **7** (1958) 794.

[164] J.G. Valatin, *Comments on the theory of superconductivity*, *Il Nuovo Cimento* **7** (1958) 843.

[165] J.S. Schwinger, *Brownian motion of a quantum oscillator*, *J. Math. Phys.* **2** (1961) 407.

[166] L.V. Keldysh, *Diagram technique for nonequilibrium processes*, *Zh. Eksp. Teor. Fiz.* **47** (1964) 1515.

[167] H. Jukkala, K. Kainulainen and P.M. Rahkila, *Flavour mixing transport theory and resonant leptogenesis*, *Journal of High Energy Physics* **2021** (2021) [2104.03998].

[168] H. Jukkala, K. Kainulainen and O. Koskivaara, *Quantum transport and the phase space structure of the Wightman functions*, *JHEP* **01** (2020) 012 [1910.10979].

[169] E. Calzetta and B.L. Hu, *Nonequilibrium Quantum Fields: Closed Time Path Effective Action, Wigner Function and Boltzmann Equation*, *Phys. Rev. D* **37** (1988) 2878.

[170] F. Cooper, *Nonequilibrium problems in quantum field theory and Schwinger's closed time path formalism*, in *International Conference on Unified Symmetry In the Small and in the Large*, pp. 11–25, 2, 1995 [hep-th/9504073].

[171] B. Garbrecht, *Why is there more matter than antimatter? Calculational methods for leptogenesis and electroweak baryogenesis*, *Progress in Particle and Nuclear Physics* **110** (2020) 103727 [1812.02651].

[172] H. Jukkala, *Quantum coherence in relativistic transport theory: applications to baryogenesis*, 2211.11785.

[173] C. Itzykson and J.B. Zuber, *Quantum Field Theory*, International Series In Pure and Applied Physics, McGraw-Hill, New York (1980).

[174] H.J. Groenewold, *On the Principles of elementary quantum mechanics*, *Physica* **12** (1946) 405.

[175] Kadanoff, L.P. and Baym, G., *Quantum statistical mechanics*, Benjamin, New York (1962).

[176] R. Kubo, *Statistical mechanical theory of irreversible processes.*, *J. Phys. Soc. Jap.* **12** (1957) 570.

[177] P.C. Martin and J.S. Schwinger, *Theory of many particle systems. 1.*, *Phys. Rev.* **115** (1959) 1342.

[178] J.M. Cornwall, R. Jackiw and E. Tomboulis, *Effective action for composite operators*, *Phys. Rev. D* **10** (1974) 2428.

[179] E. Calzetta and B.L. Hu, *Nonequilibrium quantum fields: Closed-time-path effective action, Wigner function, and Boltzmann equation*, *Phys. Rev. D* **37** (1988) 2878.

[180] J. Berges, *Introduction to Nonequilibrium Quantum Field Theory*, *AIP Conference Proceedings* (2004) [hep-ph/0409233].

[181] M. Le Bellac, *Thermal Field Theory*, Cambridge Monographs on Mathematical Physics, Cambridge University Press (3, 2011), 10.1017/CBO9780511721700.

[182] A. Anisimov, W. Buchmüller, M. Drewes and S. Mendizabal, *Quantum leptogenesis I*, *Annals of Physics* **326** (2011) 1998–2038 [1012.5821].

[183] M. Beneke, B. Garbrecht, M. Herranen and P. Schwaller, *Finite number density corrections to leptogenesis*, *Nuclear Physics B* **838** (2010) 1–27 [1002.1326].

[184] A. Anisimov, D. Besak and D. Bödeker, *Thermal production of relativistic Majorana neutrinos: strong enhancement by multiple soft scattering*, *Journal of Cosmology and Astroparticle Physics* **2011** (2011) 042–042 [1012.3784].

[185] J. Ghiglieri and M. Laine, *GeV-scale hot sterile neutrino oscillations: a derivation of evolution equations*, *Journal of High Energy Physics* **2017** (2017) [1703.06087].

[186] J. Ghiglieri and M. Laine, *GeV-scale hot sterile neutrino oscillations: a numerical solution*, *Journal of High Energy Physics* **2018** (2018) [1711.08469].

[187] L.D. Landau and I. Pomeranchuk, *Limits of applicability of the theory of bremsstrahlung electrons and pair production at high-energies*, *Dokl. Akad. Nauk Ser. Fiz.* **92** (1953) 535.

[188] A.B. Migdal, *Bremsstrahlung and pair production in condensed media at high energies*, *Phys. Rev.* **103** (1956) 1811.

[189] P. Hernández, J. López-Pavón, N. Rius and S. Sandner, *Bounds on right-handed neutrino parameters from observable leptogenesis*, *Journal of High Energy Physics* **2022** (2022) [2207.01651].

[190] J. Klaric, *Right-handed Neutrinos: From the Early Universe to Experiments*, 2019.

[191] S. Sandner, P. Hernandez, J. Lopez-Pavon and N. Rius, *Predicting the baryon asymmetry with degenerate right-handed neutrinos*, *JHEP* **11** (2023) 153 [2305.14427].

[192] A. Abada, G. Arcadi, V. Domcke, M. Drewes, J. Klaric and M. Lucente, *Low-scale leptogenesis with three heavy neutrinos*, *Journal of High Energy Physics* **2019** (2019) [1810.12463].

[193] E.W. Weisstein, *Pfaff Transformation*, in *MathWorld–A Wolfram Web Resource.*, 2024, https://mathworld.wolfram.com/PfaffTransformation.html.

[194] J.I. Kapusta, *Bose-Einstein condensation, spontaneous symmetry breaking, and gauge theories*, *Phys. Rev. D* **24** (1981) 426.